AFAPL-TR-79-2015
CEEDO-TR-79-06

EVALUATION OF FUEL CHARACTER EFFECTS ON J79 ENGINE COMBUSTION SYSTEM

General Electric Company
Advanced Engineering & Technology Programs
1 Neumann Way
Cincinnati, Ohio 45215

JUNE 1979

FINAL REPORT June 1977 - August 1978

Approved for public release; distribution unlimited

Air Force Aero-Propulsion Laboratory
Air Force Wright Aeronautical Laboratories
Air Force Systems Command
Wright-Patterson Air Force Base, Ohio 45433

REPRODUCTION QUALITY NOTICE

This document is the best quality available. The copy furnished to DTIC contained pages that may have the following quality problems:

- Pages smaller or larger than normal.
- Pages with background color or light colored printing.
- Pages with small type or poor printing; and or
- Pages with continuous tone material or color photographs.

Due to various output media available these conditions may or may not cause poor legibility in the microfiche or hardcopy output you receive.

☐ If this block is checked, the copy furnished to DTIC contained pages with color printing, that when reproduced in Black and White, may change detail of the original copy.

NOTICE

When Government drawings, specifications, or other data are used for any purpose other than in connection with a definitely related Government procurement operation, the United States Government thereby incurs no responsibility nor any obligation whatsoever; and the fact that the government may have formulated, furnished, or in any way supplied the said drawings, specifications, or other data, is not to be regarded by implication or otherwise as in any manner licensing the holder or any other person or corporation, or conveying any rights or permission to manufacture, use, or sell any patented invention that may in any way be related thereto.

This report has been reviewed by the Information Office (OI) and is releasable to the National Technical Information Service (NTIS). At NTIS, it will be available to the general public, including foreign nations.

This technical report has been reviewed and is approved for publication.

Thomas A Jackson

THOMAS A. JACKSON
Fuels Branch
Fuels and Lubrication Division

Arthur V. Churchill

ARTHUR V. CHURCHILL
Chief, Fuels Branch
Fuels and Lubrication Division

FOR THE COMMANDER

Blackwell C. Dunnam

BLACKWELL C. DUNNAM, Chief
Fuels and Lubrication Division

"If your address has changed, if you wish to be removed from our mailing list, or if the addressee is no longer employed by your organization please notify AFAPL/SFF, W-PAFB, OH 45433 to help us maintain a current mailing list".

Copies of this report should not be returned unless return is required by security considerations, contractual obligations, or notice on a specific document.

AIR FORCE/56780/14 November 1979 — 350

Unclassified

SECURITY CLASSIFICATION OF THIS PAGE (When Data Entered)

REPORT DOCUMENTATION PAGE	READ INSTRUCTIONS BEFORE COMPLETING FORM
1. REPORT NUMBER: AFAPL-TR-79-2015, CEEDO-TR-79-06	2. GOVT ACCESSION NO. / 3. RECIPIENT'S CATALOG NUMBER
4. TITLE (and Subtitle): Evaluation of Fuel Character Effects on J79 Engine Combustion System	5. TYPE OF REPORT & PERIOD COVERED: Final Technical Report, 1 Jun 77-31 Aug 78
	6. PERFORMING ORG. REPORT NUMBER: R79AEG321
7. AUTHOR(s): C.C. Gleason, T.L. Oller, M.W. Shayeson, D.W. Bahr	8. CONTRACT OR GRANT NUMBER(s): F33615-77-C-2042
9. PERFORMING ORGANIZATION NAME AND ADDRESS: General Electric Company, Aircraft Engine Group, Cincinnati, Ohio 45215	10. PROGRAM ELEMENT, PROJECT, TASK AREA & WORK UNIT NUMBERS: 62203F, 3048-05-81
11. CONTROLLING OFFICE NAME AND ADDRESS: Air Force Aero Propulsion Laboratory (AFAPL/SFF), Air Force Wright Aeronautical Laboratories, Wright-Patterson AFB, Ohio 45433	12. REPORT DATE: June 1979
	13. NUMBER OF PAGES: 197
14. MONITORING AGENCY NAME & ADDRESS (if different from Controlling Office): 11) Jun 79 12) 192	15. SECURITY CLASS. (of this report): Unclassified
	15a. DECLASSIFICATION/DOWNGRADING SCHEDULE

16. DISTRIBUTION STATEMENT (of this Report)

Approved for public release; distribution unlimited.

17. DISTRIBUTION STATEMENT (of the abstract entered in Block 20, if different from Report)

18. SUPPLEMENTARY NOTES

Partial funding and technical support in the area of the measurement and analysis of gaseous emissions and smoke data were provided by the Environmental Sciences Branch of the Environics Division in the Research and Development Directorate of HQ Air Force Engineering and Services Center. (HQ AFESC/RDVC)

19. KEY WORDS (Continue on reverse side if necessary and identify by block number)

Fuels
Alternate Fuels
Gas Turbine Combustion
Exhaust Emissions
J79 Engine Combustor

20. ABSTRACT (Continue on reverse side if necessary and identify by block number)

Results of a program to determine the effects of broad variations in fuel properties on the performance, emissions, and durability of the J79-17A turbojet engine combustion system are presented. Combustor tests conducted at engine idle, takeoff, subsonic cruise, supersonic dash, cold day ground start, and altitude relight operating conditions with 13 different fuels are described. The test fuels covered a range of hydrogen contents (12.0 to 14.5 percent), aromatic type (monocyclic and bicyclic), initial boiling point (285 to 393 K), final boiling point (552 to 679 K) and viscosity

DD FORM 1 JAN 73 1473 EDITION OF 1 NOV 65 IS OBSOLETE

Unclassified

SECURITY CLASSIFICATION OF THIS PAGE (When Data Entered)

403 468

BLOCK 20 (Cont'd)

(0.83 to 3.25 mm^2/s at 300 K).

At high power operating conditions, fuel hydrogen content was found to be a very significant fuel property with respect to liner temperature, flame radiation, smoke, and NO_x emission levels. Carbon monoxide and HC emissions were very low at these conditions with all of the fuels.

At engine idle operating conditions, CO, HC, and NO_x emission levels were found to be independent of fuel hydrogen content, but a small effect of fuel volatility and/or viscosity was found.

At cold day ground start conditions (to 329 K) lightoff was obtained with all fuels, but the required fuel-air ratio increased with the more viscous fuels.

At altitude conditions, the current engine relight limits with JP-4/JP-5 fuel were essentially met or exceeded with all of the JP-4 or JP-8 based fuel blends. However, a very significant reduction in altitude relight capability was found when a No. 2 diesel fuel was tested.

Combustor liner life analyses, based on the test data, yielded relative life predictions of 1.00, 0.78, 0.52, and 0.35 for fuel hydrogen contents of 14.5, 14.0, 13.0, and 12.0 percent, respectively. Turbine life was predicted to be unaffected by any of the fuels tested.

Fuel nozzle fouling tests were also conducted with the 13 test fuels. No significant effects were noted. This was not surprising, in view of the service history of the J79 engine and the short (5-hour) test runs made.

PREFACE

This final report is submitted by the General Electric Company, Aircraft Engine Group, Evendale, Ohio. The work was conducted under Contract No. F33615-77-C-2042. Program sponsorship and guidance were provided by the Air Force Aero Propulsion Laboratory (AFAPL), Air Force Wright Aeronautical Laboratories, Air Force Systems Command, Wright-Patterson Air Force Base, Ohio under Project 3048, Task 05, and Work Unit 81. Thomas A. Jackson was the government project engineer.

Supplemental funding and technical guidance were provided in the area of gaseous emissions and smoke measurement and analysis by the Environmental Sciences Branch of the Environics Division in the Research and Development Directorate of Hq Air Force Engineering and Services Center, located at Tyndall Air Force Base, Florida. This organization has been formerly referred to as CEEDO or the Civil Engineering Center.

Test fuel analysis was provided by AFAPL, the Monsanto Research Laboratory (under contract to AFAPL), and the Air Force Logistics Command Aerospace Fuels Laboratory (SFQLA). The cooperation of these organizations is appreciated.

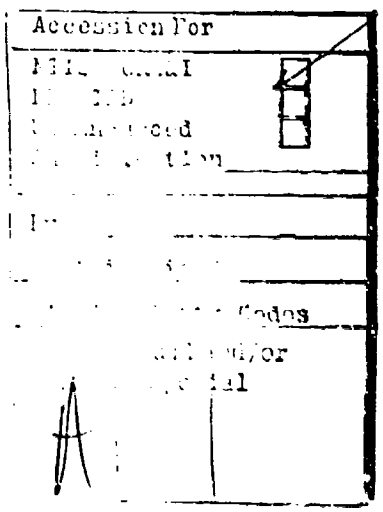

TABLE OF CONTENTS

TABLE OF CONTENTS (Continued)

LIST OF ILLUSTRATIONS

LIST OF ILLUSTRATIONS (Continued)

LIST OF ILLUSTRATIONS (Continued)

LIST OF ILLUSTRATIONS (Continued)

LIST OF ILLUSTRATIONS (Concluded)

LIST OF TABLES

LIST OF TABLES (Continued)

LIST OF TABLES (Concluded)

SECTION I

INTRODUCTION

For more than 25 years, the primary fuel for USAF gas-turbine-powered aircraft has been JP-4, a wide-cut distillate with excellent combustion characteristics and low-temperature capability. Typically, its heating value has been over 43.5 MJ/kg (18,700 BTU/lb), its freezing point below 219 K (-65° F), and its aromatic content quite low, around 11 percent by volume. A prime consideration in the definition of JP-4 was that during wartime, a large percentage of domestic crude oil could be converted into this product with minimum delay and minimum impact on other major users of petroleum products.

Conversion from high volatility JP-4 to lower volatility JP-8, which is similar to commercial Jet A-1, as the primary USAF aircraft turbine fuel has been under consideration since 1978. The strong motives for the change are NATO standardization and reduced combat vulnerability.

Domestic crude oil production peaked in 1971 and has been steadily declining since that time, while demand has continued to increase. Thus, particularly since 1973, the cost and availability of high-grade aircraft turbine fuels have drastically changed. These considerations have spurred efforts to determine the extent to which current USAF fuel specifications can be broadened to increase the yield from available petroleum crudes and, ultimately, to permit production from other sources such as coal, oil shale, and tar sands.

As a result of the current and projected fuel situation, the USAF has established an aviation turbine fuel technology program to identify JP-4 and/or JP-5 fuel specifications which:

1) Allow usage of key world-wide resources to assure availability.

2) Minimize the total cost of aircraft system operation.

3) Avoid sacrifices of engine performance, flight safety, or environmental impact.

Engine, airframe, logistic and fuel processing data are being acquired to establish these specifications. This report contributes to the needed data base by describing the effects of fuel property variations on the General Electric J79-17A engine main combustion system with respect to performance, exhaust emissions, and durability. Similar programs, based on the General Electric F101 engine and the Detroit Diesel Allison TF41 and High Mach engines, are also being conducted. Collectively, these programs will provide representative data for the engine classes that are expected to be in substantial use by the USAF in the 1980's.

This report summarizes the results of a 13-month, three-task program which was conducted to clearly identify which fuel properties are important to J79-17A engine combustor operation and quantitatively relate fuel property variations to combustor performance, emission characteristics and durability characteristics.

Thirteen test fuels provided by the USAF were utilized. Descriptions and properties of these fuels are presented in Section III. In Task I of the program, test planning and preparations were made, based on use of the J79 engine combustion system components and operating characteristics described in Section IV, and on the three test rigs and procedures described in Section V. In Task II of the program, 46 tests (14 high pressure/temperature combustor performance/emissions/durability tests, 14 low pressure/temperature combustor cold-day ground start/altitude relight tests, and 18 high temperature fuel nozzle fouling tests) were conducted. These are summarized in Section VI-A. In Task III of the program these test data were analyzed to establish the fuel property correlations also presented in Section VI-A and to establish the engine system life predictions presented in Section VI-B.

SECTION II

SUMMARY

The purpose of this program was to determine, by combustor rig tests and data analyses, the effects of fuel property variations on the performance, exhaust emission, and durability characteristics of the General Electric J79-17A turbojet engine main combustion system. Thirteen refined and blended fuels which incorporated systematic variations in hydrogen content (12.0 to 14.5 weight percent), aromatic type (monocyclic or bicyclic), initial boiling point (285 to 393 K by gas chromatograph), final boiling point (552 to 679 K, also by gas chromatograph), and viscosity (0.83 to 3.25 mm^2/s at 300 K) were evaluated in: (a) 14 high pressure/temperature combustor performance/emissions/durability tests; (b) 14 low pressure/temperature combustor cold-day ground start altitude relight tests; and, (c) 18 high temperature fuel nozzle fouling tests.

At high engine power operating conditions (takeoff, subsonic cruise, supersonic dash) fuel hydrogen content was found to be a very significant fuel property with respect to liner temperature, flame radiation, smoke and NO_x emission levels, and carbon deposition. Each of these parameters decreased with increasing fuel hydrogen content, but no discernable effect of any of the other fuel properties was found. Carbon monoxide and HC emissions were very low at each of these operating conditions with all of the fuels. Combustor exit temperature profile and pattern factor were essentially the same with all fuels, but a constant difference between the two assemblies used was noted.

At engine idle operating conditions, the same strong effects of fuel hydrogen content on smoke level, liner temperature, and flame radiation were evident. Carbon monoxide, HC, and NO_x levels were found to be independent of fuel hydrogen content, but a small effect of fuel volatility (as indicated by 10 percent recovery temperature) on CO and HC levels was found.

At cold-day ground start conditions (to 329 K) lightoff was obtained with all fuels, but the required fuel-air ratio increased with the more viscous fuels, primarily as a result of the associated increases in relative fuel spray droplet size.

At altitude relight conditions, the current engine relight limits with JP-4/JP-5 fuel were essentially met or exceeded with all of the JP-4- or JP-8-based fuel blends. However, a very significant reduction in altitude relight capability was found when a standard No. 2 diesel fuel was tested, indicating again a strong effect of fuel atomization characteristics. Improved fuel injectors and/or higher ignition energies would be needed with a diesel-type fuel.

Combustor liner life analyses, based on the test data, were conducted. These analyses resulted in relative life predictions of 1.00, 0.78, 0.52 and 0.35 for fuel hydrogen contents of 14.5 14.0, 13.0, and 12.0 percent, respectively. Turbine system life is not predicted to change for any fuels with properties within the matrix tested.

A series of short but severe fuel nozzle tests did not reveal any major problems with the fuels in the matrix. This was expected, based on service history. However, considerable additional long-time tests are needed to fully assess the effects of fuel thermal stability characteristics on fuel system performance and combustor/turbine life.

SECTION III

TEST FUEL DESCRIPTION

A. General Description

Thirteen test fuels were supplied by the USAF for combustion system evaluation in this program. These fuels included a current JP-4, a current JP-8 (which was out of specification on freeze point), five blends of the JP-4, five blends of the JP-8, and a No. 2 diesel. The blends were made up by the USAF to achieve three different levels of hydrogen content: 12, 13, and about 14 percent by weight. Two different types of aromatics were used to reduce the hydrogen content of the base fuels: a monocyclic aromatic (xylene bottoms), and a bicyclic aromatic described by the supplier as "2040 solvent" (a naphthalene concentrate) A third blend component, used to increase the final boiling point and the viscosity of two blends, is described as a Mineral Seal Oil, a predominantly (90 percent) paraffinic white oil.

The rationale for the selection of this test fuel matrix was to span systematically the possible future variations in key properties that might be dictated by availability, cost, the change from JP-4 to JP-8 as the prime USAF aviation turbine fuel, and the use of nonpetroleum sources for jet fuel production. The No. 2 diesel was selected to approximate the Experimental Referee Broad Specification (ERBS) aviation turbine fuel that evolved in the NASA-Lewis workshop on Jet Aircraft Hydrocarbon Fuel Technology (Reference 1).

B. Physical and Chemical Properties

Fuel properties shown in Tables 1, 2, and 3 were determined, for the most part, by Monsanto Research Corporation under contract to the USAF. Table 4 presents conventional fuel inspection data determined by the Aerospace Fuels Laboratory, WPAFB. These data may be useful for assessing the accuracy of test methods and comparing these fuels to those used in other investigations.

In Table 1, density, viscosity, surface tension, and vapor pressure are presented at a common temperature, together with temperature coefficients which were calculated by GE from Monsanto three-point data. Also shown in Table 1 are the fuel components, hydrogen content determined by the USAF using ASTM Method D3701 (Nuclear Magnetic Resonance), and heating value determined by Monsanto using ASTM Method D240-64. Heating value of these fuels (Q_{net}, MJ/kg) is very nearly a unique function of hydrogen content (H, %) which can be closely approximated by:

$$Q_{net} = 35.08 + 0.5849\ H \qquad (1)$$

Surface tension is virtually the same for all of the fuels. The other properties are, in general, quite dependent upon fuel components as well as on hydrogen content.

Table 2 shows hydrocarbon type analyses by mass spectroscopy (ASTM Method

Table 1. Test Fuel Chemical and Physical Properties.

Fuel No.	Fuel Components		Hydrogen Content H Weight %	Heating Value (net) MJ/kg	Density		Viscosity		Surface Tension		Vapor Pressure	
	Base Fuel	Blending Agents			$\rho_{300\ K}$ kg/m^3	$\frac{\Delta\rho}{\rho \Delta T} \times 10^4$	$\nu_{300\ K}$ mm^2/s	$b\left[\ln \ln (\nu + 0.7)\right]$ $\left[\ln T\right]$	$\sigma_{300\ K}$ mN/m	$\frac{\Delta\sigma}{\Delta T} \times 10^2$	$P_{300\ K}$ kPa	$b\left[\ln P\right]$ $\left[\ln T\right]$
1	JP-4	-	14.5	43,603	752.7	7.935	0.924	4.112	23.27	10.01	12.04	9.80
2	JP-8	-	14.0	43,210	729.5	7.363	1.849	4.009	25.85	9.53	2.15	6.19
3	JP-8	Gulf Mineral Sec1 Oil	13.8	43,189	801.2	7.330	2.071	3.995	25.92	8.78	1.97	5.84
4	JP-8	2040 Solvent	12.0	41,847	852.3	7.455	1.809	4.170	27.62	8.24	1.16	7.78
5	JP-8	Xylene Bottoms	13.0	42,724	813.4	7.525	1.428	4.051	26.38	9.50	1.48	10.84
6	JP-8	Xylene Bottoms	12.0	42,129	827.8	7.775	1.160	4.111	25.66	9.47	1.33	10.77
7	JP-8	2040	13.0	42,556	825.2	7.437	1.804	4.103	26.42	8.20	1.38	7.48
8	JP-4	2040	12.0	42,203	829.7	7.232	1.141	4.179	25.22	7.31	7.38	11.80
9	JP-4	2040	13.0	42,629	796.3	7.758	1.028	4.144	23.75	6.94	6.61	11.41
10	JP-4	Xylene	12.0	42,196	808.0	8.150	0.830	4.237	26.21	7.97	6.17	11.21
11	JP-4	Xylene	13.0	42.682	781.5	8.072	0.835	4.328	24.20	5.40	9.06	10.47
12	JP-4	Xylene & DMSO	14.0	43.366	769.8	7.513	1.057	4.027	23.45	7.20	10.26	10.57
13	S-D	-	13.1	42,881	837.2	7.041	3.245	4.315	27.95	6.35	1.59	6.43
Test Method			D3701 (NMR)	D240 (Bomb)	Dilatometer		D445		Capillary Rise		Micro-vapor Pressure Apparatus	

Table 2. Test Fuel Hydrocarbon Type Analyses (Mass Spectroscopy, ASTM Method D2789-71).

Compound Type	Volume Percent in Fuel Number												
	1	2	3	4	5	6	7	8	9	10	11	12	13
Paraffins	62.4	48.4	49.0	29.9	35.6	25.7	39.1	38.4	47.2	33.0	45.8	58.4	44.9
Cycloparaffins	21.4	32.8	31.9	26.4	30.6	21.5	34.1	20.4	25.4	11.2	15.1	20.1	32.7
Dicycloparaffins	5.3	5.4	5.5	1.7	2.3	1.9	1.5	--	--	2.4	3.4	5.0	2.5
Tricycloparaffins	--	0.9	0.8	--	--	--	--	--	--	--	--	--	--
Alkylbenzenes	8.6	7.8	7.4	11.7	28.9	49.9	9.5	12.4	10.7	53.1	34.7	14.8	8.6
Indans and Tetralins	1.5	2.7	3.0	5.7	1.0	--	3.8	4.4	3.0	--	0.6	1.1	6.1
Indenes	--[a]	0.8	0.9	--	--	--	--	--	--	--	--	--	--
Naphthalene	--[b]	0.1	0	--	--	--	--	--	--	--	--	--	--
Naphthalenes	0.8	0.9	1.0	24.6	1.6	1.0	12.0	24.4	13.7	0.3	0.4	0 6	5.2
Acenaphthenes	--	0.04	0.1	--	--	--	--	--	--	--	--	--	--
Acenaphthylenes	--	--	0.01	--	--	--	--	--	--	--	--	--	--
Tricyclicaromatics	--	0.02	0.06	--	--	--	--	--	--	--	--	--	--
Total Aromatics	10.9	12.4	12.5	42.0	31.5	50.9	25.3	41.2	27.4	53.4	35.7	16.5	19.9

(a) If present, included with indans.

(b) If present, included with general naphthalene group.

Table 3. Test Fuel Gas Chromatographic Simulated Distillation (ASTM Method D2887).

Fuel No.	Temperature (K) at Percent Recovered														
	0.5	1.0	5.0	10	20	30	40	50	60	70	80	90	95	99	99.5
1	299	-	342	362	381	392	407	426	451	472	491	510	525	-	552
2	383	-	432	446	459	472	481	494	504	515	530	547	561	-	589
3	383	-	431	443	455	472	489	498	510	526	543	566	579	-	609
4	391	-	434	446	463	475	486	499	503	512	524	542	557	-	590
5	393	-	412	418	434	443	456	469	485	501	514	534	549	-	582
6	377	-	411	413	423	433	439	444	461	480	501	526	543	-	601
7	391	403	430	442	458	470	481	493	504	515	526	539	556	579	592
8	297	306	353	368	392	422	452	471	487	503	515	530	545	569	574
9	293	303	341	360	387	406	434	456	476	492	506	526	541	570	578
10	292	300	335	356	384	406	415	430	438	452	475	502	519	545	559
11	285	292	332	353	377	399	414	431	445	465	487	509	523	548	560
12	285	292	332	354	381	404	423	447	471	495	521	565	583	611	623
13	371	393	441	460	482	500	516	531	546	563	580	601	623	658	679

Table 4. Test Fuel Conventional Inspection Data.

Fuel Number	1	2	3	4	5	6	7	8	9	10	11	12	13
Gravity, °API	54.1	43.7	43.3	32.8	40.5	37.5	38.3	37.3	44.3	41.6	46.4	50.3	35.6
Freezing Point, K	209	228	241	224	225	220	228	229	219	<215	<215	238	247(1)
Existent Gum, mg/100 ml	1.4	0.2	2.6	1.2	0.8	1.0	0.0	0.8	1.0	1.8	1.2	1.0	-
Luminometer Number	73	53	55	1	38	18	34	24	37	24	37	65	-
Viscosity, mm^2/s at 239 K	2.68	9.54	(solid)	10.18	5.90	4.09	9.62	4.39	3.59	-	-	-	-
Total Sulphur, wt %	0.04	0.06	0.07	0.05	0.06	0.05	0.07	0.02	0.04	0.03	0.04	0.04	0.18
Smoke Point, mm	32.5	26.5	-	12.5	20.5	13.5	17.0	12.0	15.0	13.0	18.0	25.0	18.0
Aromatics, volume % (D1319)	12.2	15.1	15.4	44.7	41.6	63.4	31.8	45.3	30.6	57.5	40.1	20.3	21.4
Olefins, volume %	1.1	1.6	1.2	1.8	2.7	2.2	2.1	0.5	0.7	1.1	0.8	1.1	1.2
Flashpoint, K	-	324	327	333	319	314	329	-	-	-	-	-	335
Distillation (D86)													
Initial Boiling Point, K	338	444	436	449	423	425	445	340	339	346	339	341	444
10%	375	462	460	465	441	431	462	385	379	399	389	380	488
20%	388	469	469	473	447	435	470	406	394	409	402	395	-
50%	425	487	494	494	471	450	492	472	448	425	426	435	531
90%	499	526	549	526	522	514	528	516	506	471	492	541	585
Endpoint	524	552	572	547	544	541	546	544	539	512	520	573	615

(1) Pour Point

D2789) and Figure 1 shows a comparison of total aromatics determined by mass spectroscopy (from Table 2) and by fluorescent indicator absorption (ASTM Method D1319 from Table 1). It is apparent that there is a consistent bias between the results by the two methods, with the mass spectrometer yielding the more favorable (lower aromatic) results, particularly with the JP-8-based fuels. Aromatic type (monocyclic or bicyclic) does not appear to affect this bias.

Figure 2 shows the variation in fuel aromatic content (by mass spectroscopy) with hydrogen content for these fuels. There is, of course, strong negative correlation, but it is apparent that both base fuel type and aromatic component structures affect this relationship.

Table 3 lists the Gas Chromatographic Simulated Distillation (ASTM Method D2887) data for each of the test fuels. Among the blended fuels, those containing the Mineral Seal Oil (Fuels No. 3 and No. 12) had the highest final boiling points. Figure 3 shows the complete simulated distillation curves for the three basic fuels and the variation in initial and end points for all of the blends. Points worthy of note are:

1) All of the JP-4 blends had initial boiling points (IBP's) essentially identical to that of the base JP-4 fuel (about 300 K).

2) All of the JP-8 blends and the diesel fuel had IBP's essentially identical to that of the base JP-8 fuel (about 385 K).

3) All of the JP-8 blends had final boiling points (FBP's) not greatly different from that of the base JP-8 fuel (about 590 K).

4) The JP-4 blends had a broad range of FBP's, spanning those of the JP-8 blends (about 585 $\pm$ 35 K).

5) The diesel fuel had a significantly higher FBP (about 680 K).

Figure 4 compares fuel volatility characteristics as measured by gas chromatography and conventional distillation (ASTM Method D86). It is apparent that gas chromatography significantly extends the apparent boiling range in both directions; the IBP and 10 percent recovery temperatures are lowered while the 90 percent recovery and FBP temperatures are raised. Temperature differences of up to about 70 K are obtained by the two procedures.

C. Thermal Stability Characteristics

The thermal stability of test fuels was determined by the Jet Fuel Thermal Oxidation Tester (JFTOT) described in ASTM Method D3241. The actual thermal stability is given in terms of the breakpoint, which is defined as the highest (metal) temperature at which the fuel "passes" by both filter pressure drop and tube rating. A fail on pressure drop is 25 mm Hg pressure drop or more in less than 150 minutes. A "fail" on the tube is a color code of 3 or darker as described in the ASTM procedure. In practice, the fuel is tested first at the estimated breakpoint, and then, depending upon whether it fails or passes, is rerun at a temperature 10K lower or higher until the breakpoint is established.

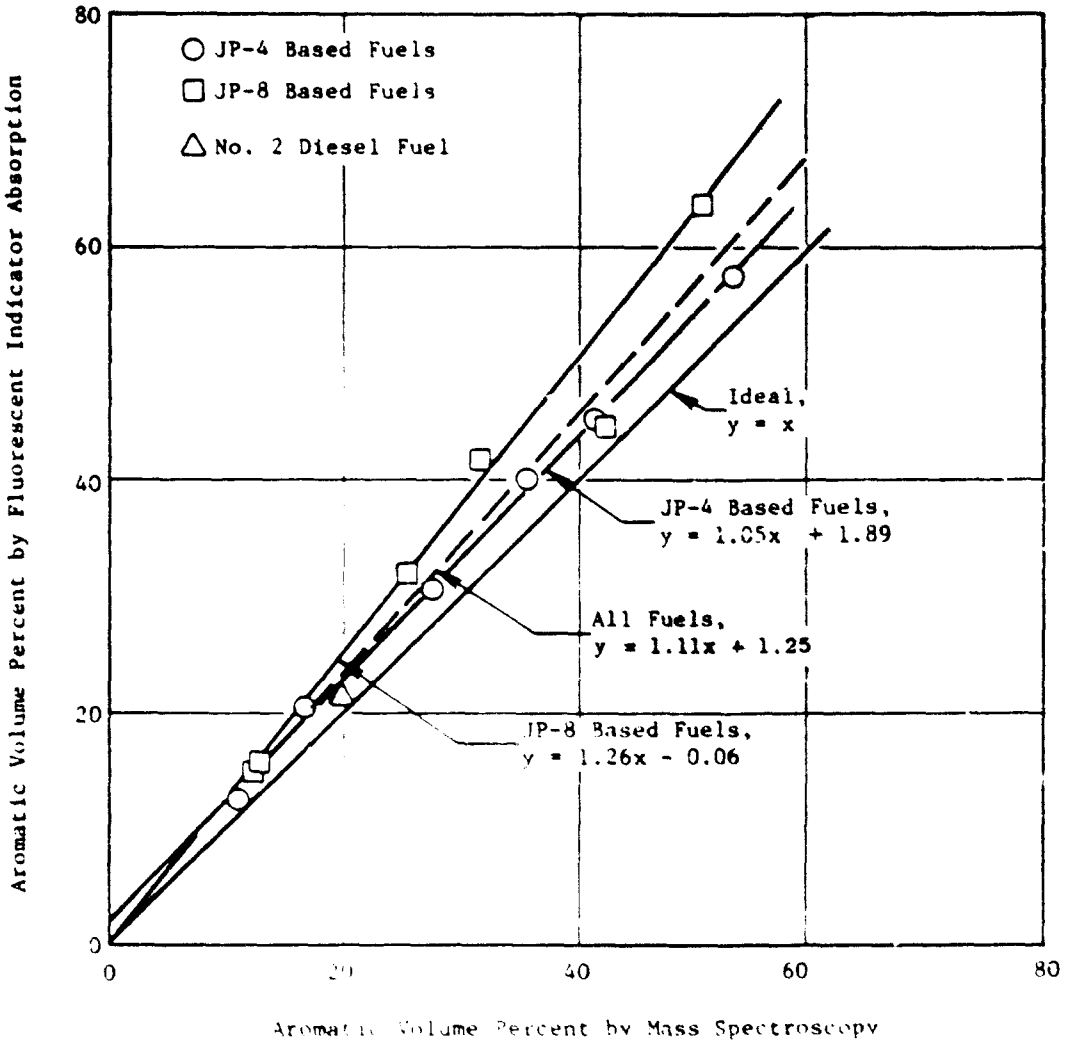

Figure 1. Comparison of Fuel Aromatic Content by Two Test Methods.

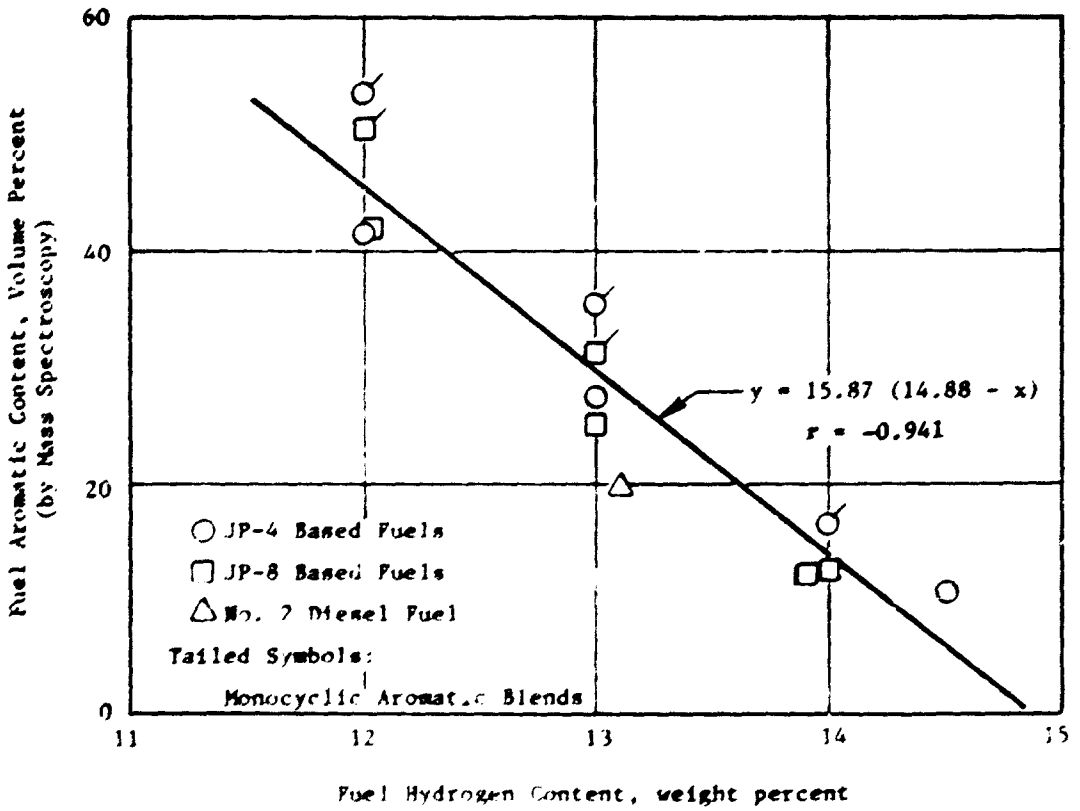

Figure 2. Variation of Fuel Aromatic Content with Hydrogen Content.

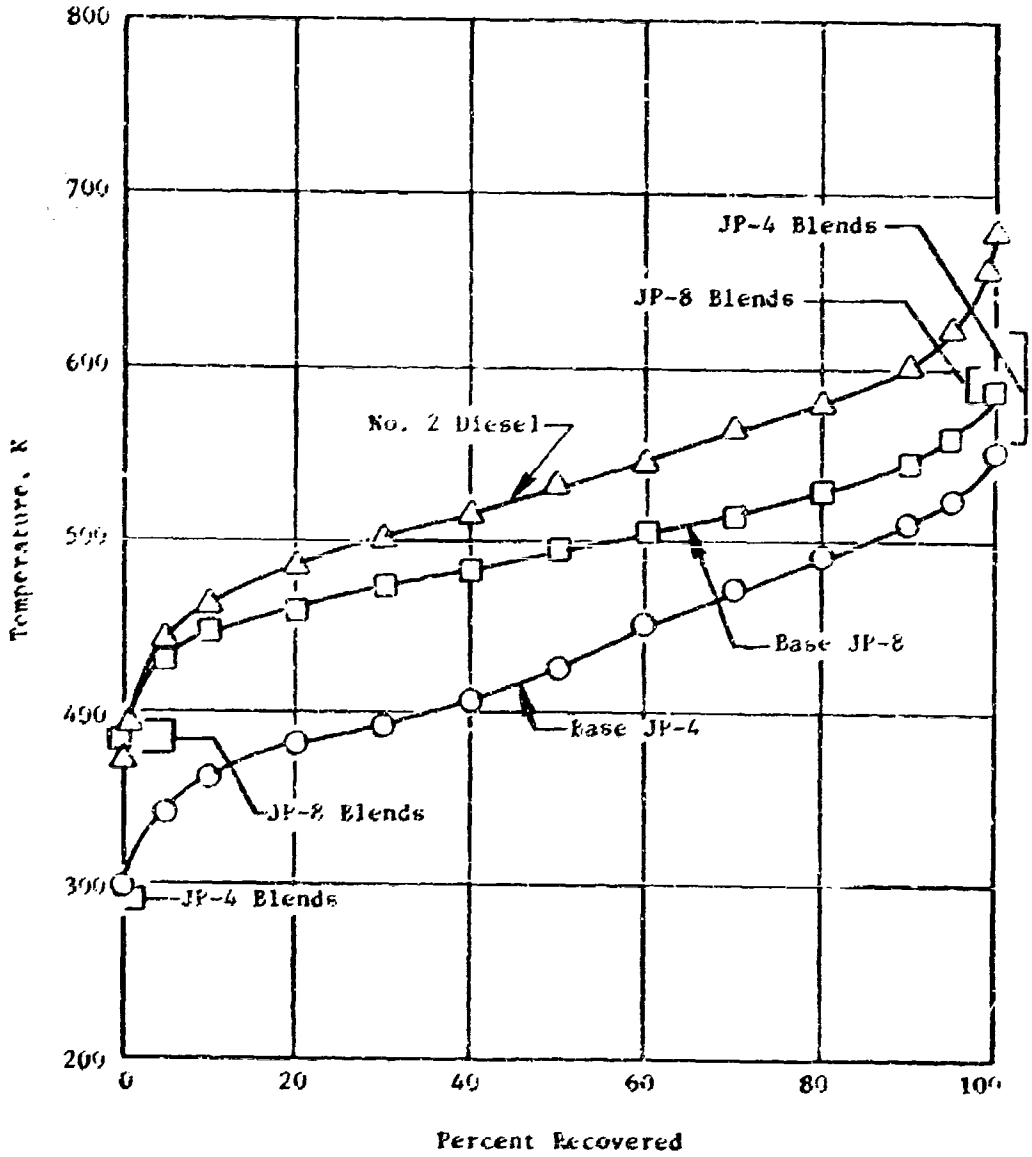

Figure 3. Comparison of Gas Chromatographic Simulated Distillation Characteristics of the Test Fuels.

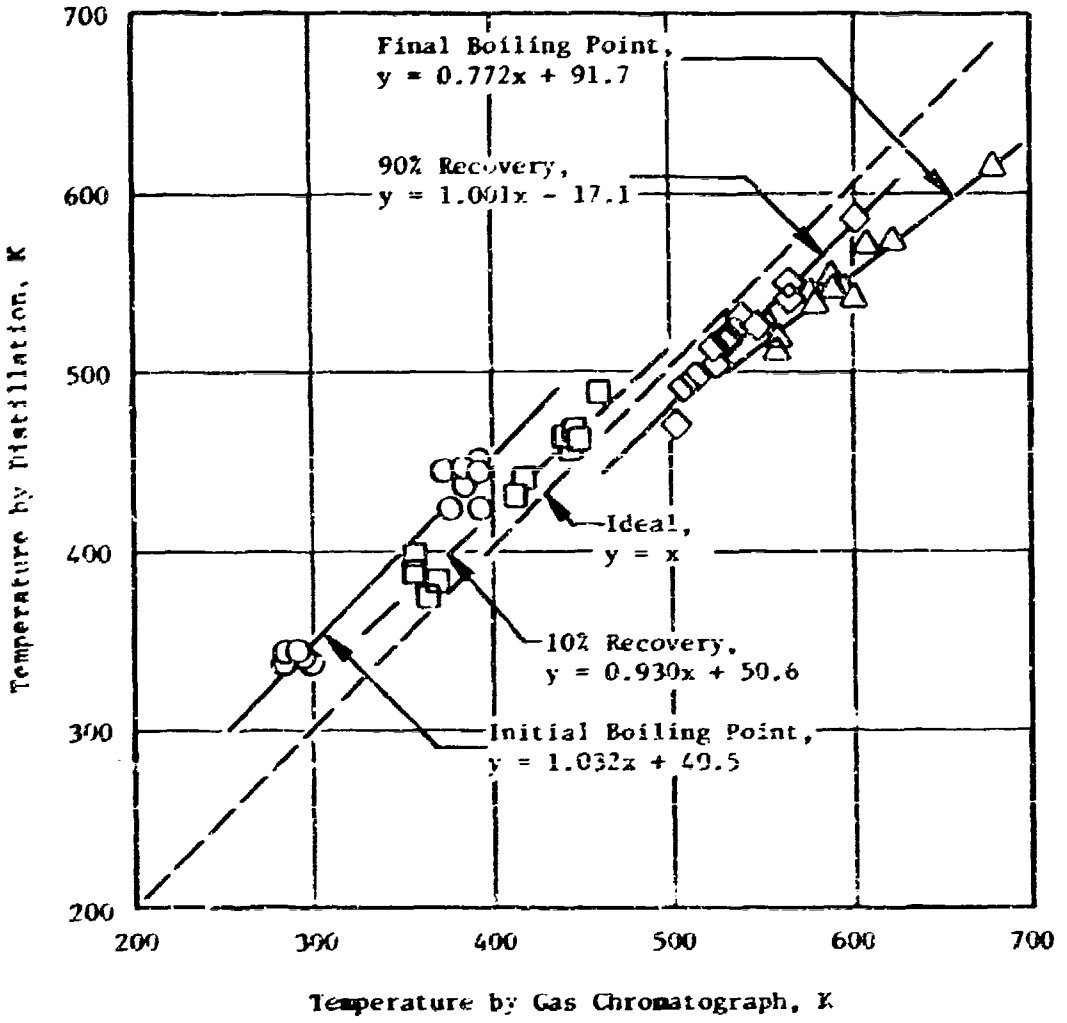

Figure 4. Comparison of Fuel Recovery Points by Distillation and Gas Chromatography.

Table 5 shows the JFTOT data that were provided by the USAF. Occasionally, anomalous or indeterminate results were obtained, and sometimes the fuel sample (one gallon) was expended before the breakpoint was determined. For these reasons, breakpoints are not shown for all of the test fuels. Anamolous results are those in which two or more tests of the same fuel at the same temperature showed both a "pass" and a "fail." Indeterminate results are those in which a fuel passes or fails by both tube color and pressure drop, but in which no additional tests were run at higher or lower temperature to determine by which criterion it would fail first. Generally, it appears that the repeatability and reproducibility of the breakpoint is greater than the difference in thermal stability of the base fuels and their blends.

Table 6 is an attempt to assign ratings to the fuels, despite some apparent lack of precision in the test results. The JP-8 base fuel appears to be significantly more stable than the JP-4 base fuel. The addition of Mineral Seal Oil has no apparent effect on the thermal stability. This would be expected, since it is a high-purity white oil, suitable for medicinal and food applications. The addition of both types of aromatics appears to have little or no adverse effect on thermal stability.

D. Computed Combustion Parameters

Table 7 shows several fuel parameters which were computed from the physical and chemical properties for use in conducting the combustion tests and analyses of the results.

Fuel hydrogen-carbon atom ratio (n) was used in the exhaust gas sample calculation. It was calculated directly from the hydrogen weight percent (H) by the relationship:

$$n = \frac{11.915\ H}{100 - H} \qquad (2)$$

and ranged from 1.625 to 2.021 as hydrogen content increased.

Stoichiometric fuel-air ratio (f_{st}) was used to calculate comparative adiabatic flame temperatures. It was calculated from the fuel hydrogen-to-carbon ratio (n) by the relationship:

$$f_{st} = \frac{0.0072324\ (1.008\ n + 12.01)}{(1 + 0.25\ n)} \qquad (3)$$

which assumes that the fuel is CH_n, that the air is 20.9495 volume-percent oxygen, and that the air has a molecular weight of 28.9666. For the test fuels the stoichiometric fuel-air ratio ranged from 67.50 to 70.19 g-fuel/kg-air as hydrogen content decreased.

Stoichiometric flame temperature was used in analyses of NO_x emissions. It was calculated at takeoff operating conditions (T_3 = 664 K, P_3 = 1.359 MPa) using a standard equilibrium-thermodynamics computer program (Reference 2) and ranged from 2494 to 2515 K as hydrogen content decreased.

Table 5. Fuel Sample Thermal Stability Test Results (ASTM Method D3241).

Fuel No.	Breakpoint, K	Mode of Failure
1	<518, 518	Tube
1	533	Tube
1	528	Tube
1	538, 543	Tube
2	<563	ΔP
2	548, 553	Tube
2	558	Tube
2	563	Tube
2	593, 603	Tube
2	603	Tube
2	553	Tube
2	573	Tube
3	568	Tube and ΔP
3	583	Tube
3	573	Tube
4	<573	Indeterminate
4	>533, <573	Indeterminate
4	573	Tube
5	<533	Indeterminate
5	<533	Tube
5	>583	Indeterminate
6	513	ΔP
6	>583	Indeterminate
6	>553, <583	Tube
7	>573	Indeterminate
8	<523	ΔP
8	553	Tube
9	>513, <533	Tube
9	533	Tube
10	553	Tube
11	543, 553	Tube and ΔP
12	543	Tube

Table 6. Estimated Thermal Stability Ratings of Test Fuels (ASTM Method D3241).

Fuel No.	Breakpoint Range, K	Estimated Rating, K
1	<518-548	533 ± 15
2	548-603	576 ± 28
3	568-583	576 ± 8
4	>533-<573	553 ± 20
5	<533->583	558 ± 25
6	513-583	548 ± 35
7	>573	573
8	<523-553	538 ± 5
9	>513-533	523 ± 10
10	553	553
11	543-553	548 ± 5
12	543	543

Table 7. Test Fuel Combustion Parameters.

Fuel Number	n, Hydrogen-to-Carbon Atom. Ratio	f_{st}, Stoichiometric Fuel-Air Ratio, g/kg	T_{st}, Stoichiometric Flame Temperature at Takeoff, K	$(W_f)/(W_f)$JP-4 Relative Required Fuel Flow Rate	(SMD)/(SMD)JP-4 Relative Fuel Spray Droplet Size
1	2.021	67.50	2494	1.0000	1.00
2	1.940	68.02	2498	1.0091	1.22
3	1.924	68.12	2499	1.0096	1.25
4	1.625	70.19	2515	1.0395	1.30
5	1.780	69.09	2506	1.0206	1.20
6	1.625	70.19	2515	1.0350	1.17
7	1.780	69.09	2506	1.0246	1.25
8	1.625	70.19	2515	1.0332	1.13
9	1.780	69.09	2506	1.0228	1.06
10	1.625	70.19	2515	1.0333	1.06
11	1.780	69.09	2506	1.0216	1.02
12	1.940	68.02	2498	1.0055	1.04
13	1.796	68.98	2505	1.0214	1.41

Relative required fuel flow rate was used in all combustion tests to adjust the JP-4 fueled engine cycle operating fuel flow rates for the reduced heating values of the other fuels. The factor is merely the ratio (Q_{JP-4}/Q) and ranged from 1.000 to 1.0395.

Relative fuel spray droplet size was used in analyses of the low-power emissions and relight performance. The J79-17A combustion system employs pressure-atomizing fuel nozzles, so Jasaja's correlation parameter for this type atomizer (Reference 3) was used to estimate the relative fuel spray droplet Sauter Mean Diameter (SMD) from the test fuel density (ρ), surface tension (σ) and viscosity (ν) by the relationship:

$$\frac{(SMD)}{(SMD)_{JP-4}} = \left(\frac{\nu}{\nu_{JP-4}}\right)^{0.16} \left(\frac{\sigma}{\sigma_{JP-4}}\right)^{0.6} \left(\frac{\rho}{\rho_{JP-4}}\right)^{0.43} \qquad (4)$$

As shown in Table 7, none of the blending agents appreciably changed the predicted relative droplet size of the base fuel. However, the JP-8-based fuels are predicted to produce mean droplet sizes about 23 percent larger than those of the JP-4 fuel. Further, the diesel fuel is expected to produce mean droplet sizes about 41 percent larger than those of the JP-4 fuel.

SECTION IV

J79 ENGINE AND COMBUSTION SYSTEM DESCRIPTION

A. Overall Engine Description

The J79 engine is a lightweight, high-thrust, axial-flow turbojet engine with variable afterburner thrust. This engine was originally qualified in 1956. Since that time various models with improved life and thrust have been developed. The model currently in use by the USAF, the J79-17A, was the reference engine for this program. An overall view of the engine is presented in Figure 5. The J79 has a 17-stage compressor in which the inlet guide vanes and the first six stator stages are variable. The compressor pressure ratio is approximately 13.4:1. The combustion system is cannular with ten louvered combusters. The turbine has an air-cooled first-stage stator and a three-stage uncooled rotor that is coupled directly to the compressor. The engine rotor is supported by three main bearings. The afterburner is fully modulating with a three-ring "V" gutter flameholder. Afterburner thrust variation is accomplished by means of fuel flow scheduling and a variable area exhaust nozzle.

B. Combustion System Description

The J79 engine employs a cannular combustion system with ten combustion cans. The ten cans are located between an inner and outer combustion casing forming an annular passage. The combustion system flowpath is illustrated in Figure 6. An exploded view of the system with the various components, including the compressor rear frame and the turbine first-stage nozzle, is shown in Figure 7. Figure 8 shows the combustor cans (one omitted) mounted in an engine transition duct. A pictorial drawing of a combustor can assembly is presented in Figure 9. Each combustor consists of three parts riveted together to form an assembly. The forward outer liner is an airflow guide to assure proper flow distribution to the inner liner. The leading edge of the outer liner has a snout which extends into the diffuser flowpath. The snout incorporates internal vanes which distribute air to the dome in the desired flow pattern. A slot in the snout permits access of the fuel nozzle to the inner liner dome. The rear liners are oval shaped and oblique at the rear to facilitate removal from the engine during overhaul or inspection. Cooling air for the inner surfaces of the inner and rear liners is admitted through punched and formed louvers. Combustion and dilution air is admitted through a series of thimbles in the inner and aft liners. These thimbles are arranged to provide flow patterns for flame stabilization in the primary zone and mixing and turbine inlet temperature profile control at the aft end. In an engine assembly, two of the cans are provided with spark igniters for starting. Adjacent cans are joined near the forward ends by cross ignition tubes to allow propagation of the flame from the cans with a spark igniter to the other cans. The flanges of adjacent cross-ignition tube bosses on the liners are held by V-band clamps which can be removed for engine disassembly or inspection. The liners are each positioned and held in place by mounting bolts at the forward ends. Axial stack-up and thermal growth are accommodated by a sliding seal between the combustor can and the transition duct. The major liner material is Hastelloy X.

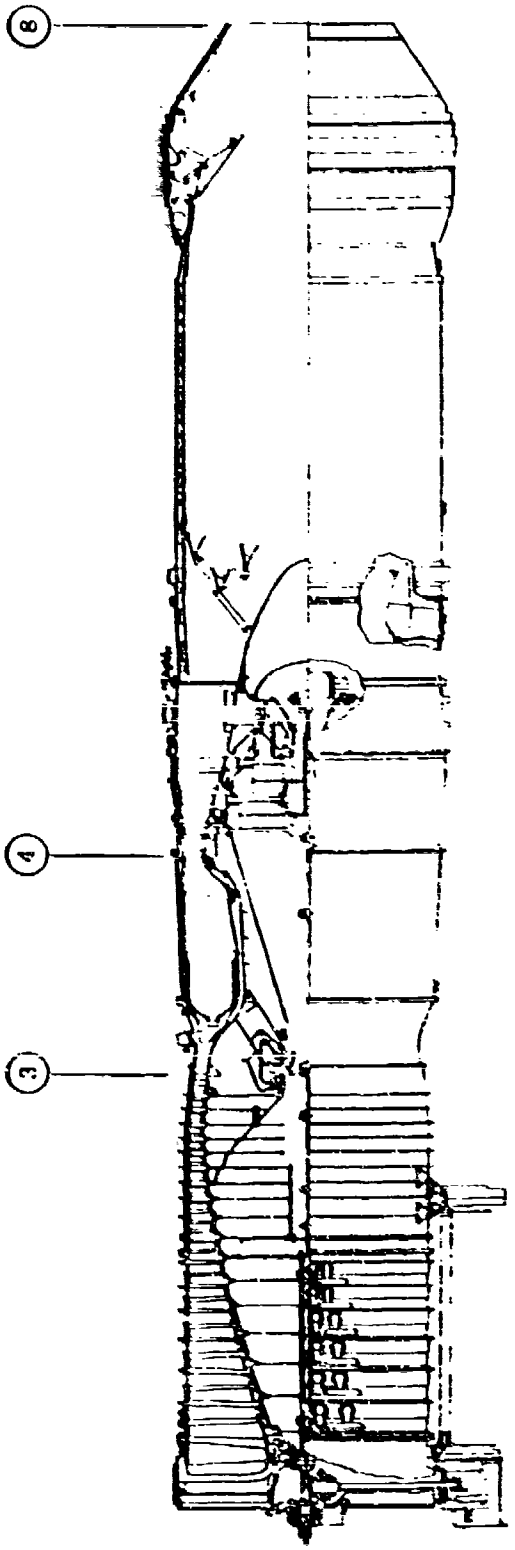

Figure 5. General Electric J79 Turbojet Engine.

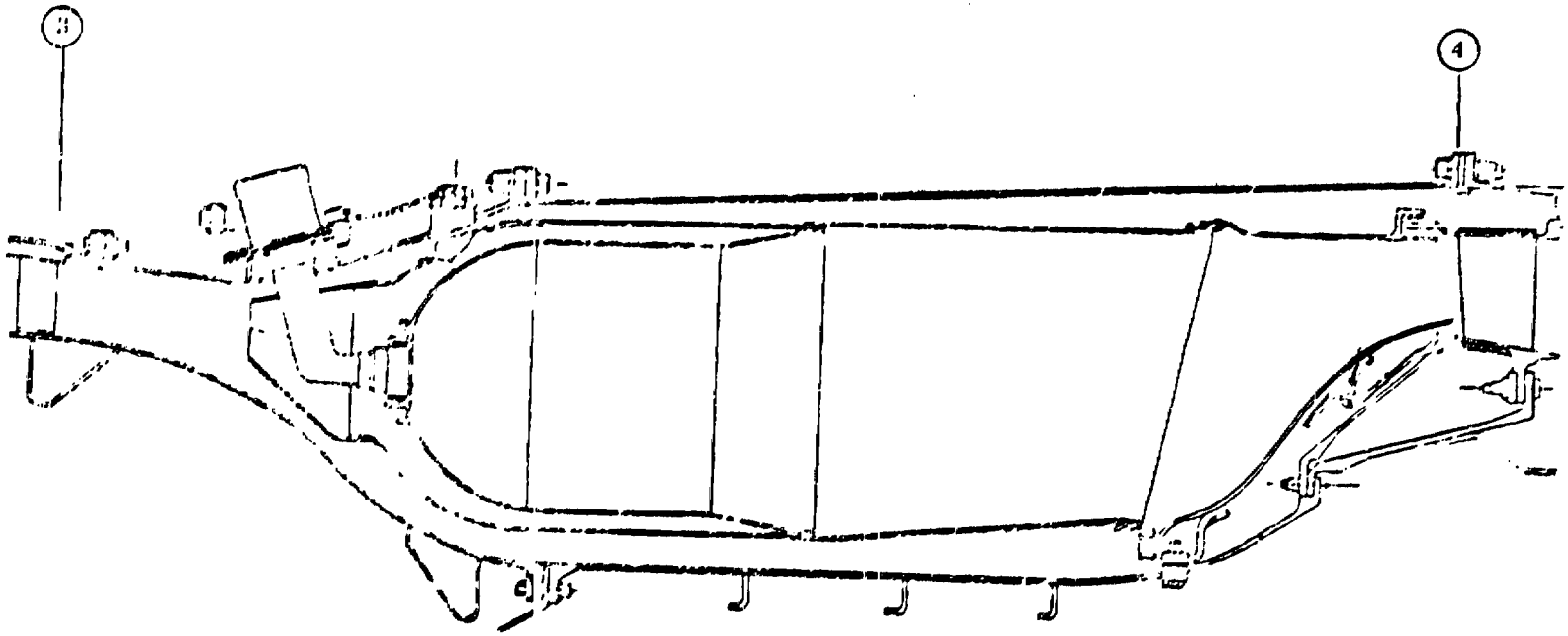

Figure 6. J79 Engine Combustion System Flowpath.

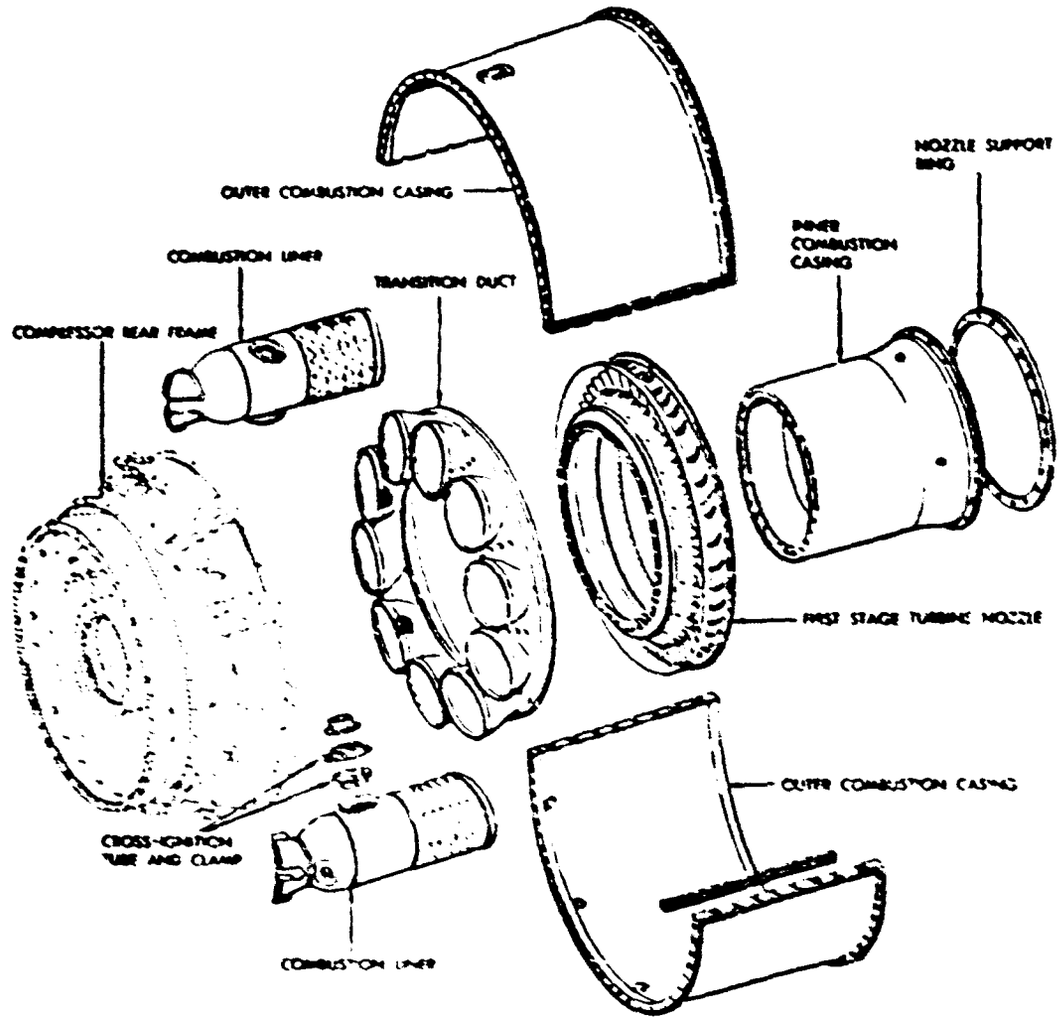

Figure 7. J79 Engine Combustion System, Exploded Pictorial View.

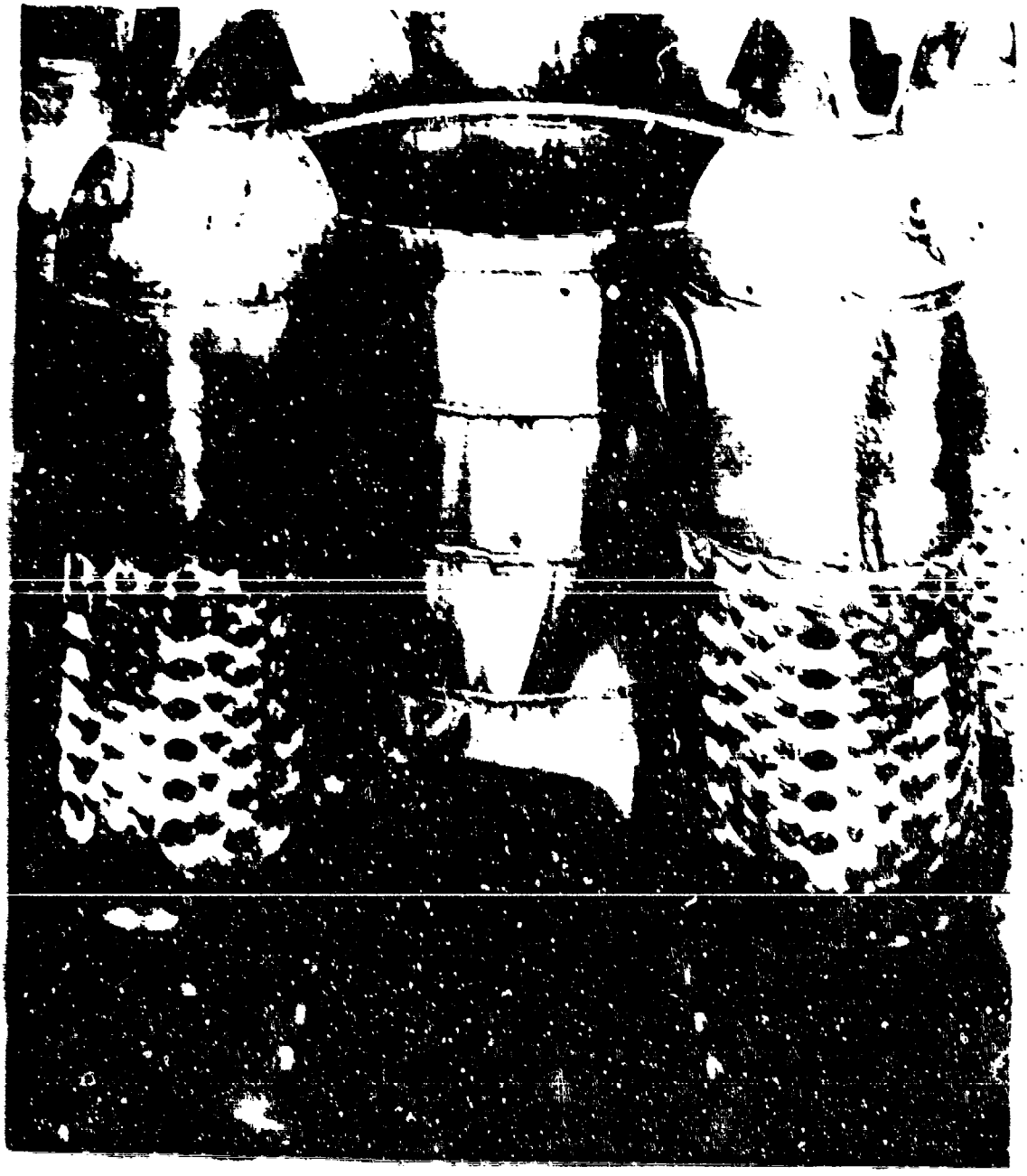

Figure 5. [illegible] Turbine Combustion System, [illegible] Assembly Photograph.

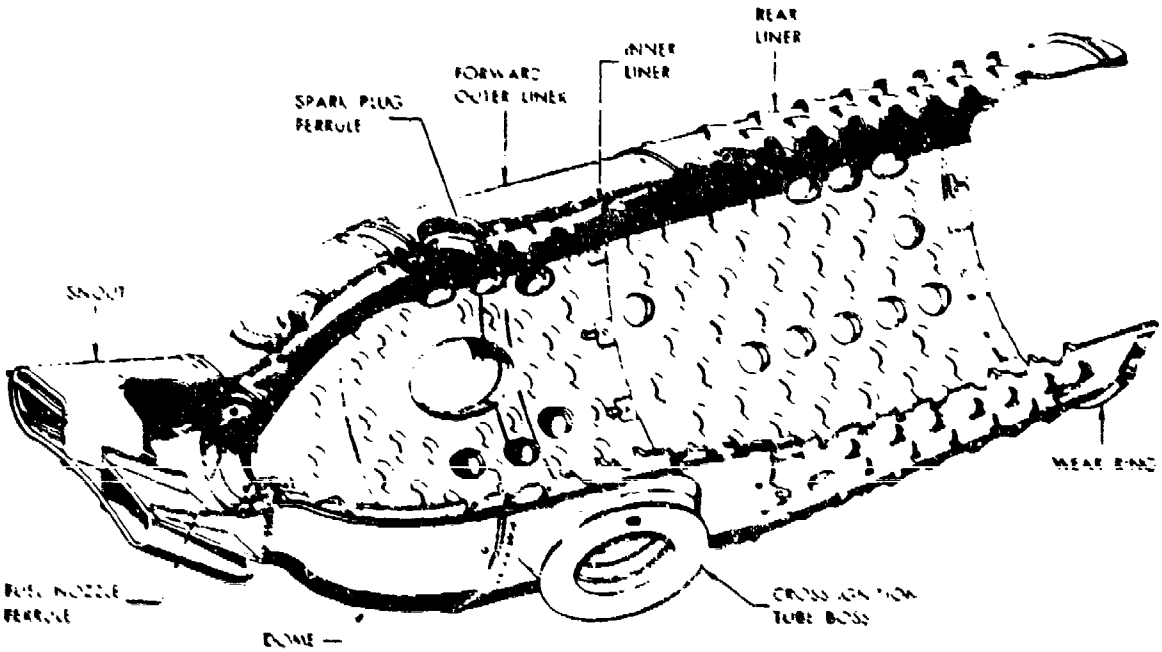

Figure 9. J79 Engine Combustor, Pictorial View.

The transition duct provides a ring of ten oval inlet ports to accept the ten combustor cans. The exit of the transition duct is annular to match up with the turbine flowpath. The transition section exit area is approximately one-half of the total exit area of the ten cans providing an accelerating flow stream into the turbine. The transition duct is mounted by five radial support pins in the inner combustion casing. These pins have a sliding fit with the transition duct, allowing for differential thermal growth, but they maintain the axial location of the duct. Sliding seals are provided with both the combustors and the turbine.

During the evolution of the J79 engine, both improved-life and low smoke combustors have been developed. For this program, however, the original design (without these low smoke and improved-life features) was employed. The life-limiting component of the combustor is the inner liner. During service use, these liners develop cracks at the louver ends due to thermal fatigue. The domes also eventually exhibit some warping and distortion. The rear liner has significantly longer life than the forward section but also eventually develops thermal fatigue cracks at the louver ends. Periodic inspections are generally conducted after 600 hours or 450 cycles with the louvered inner liner.

The ten fuel nozzles are of the dual-orifice, pressure-atomizing type. Details of the fuel nozzle are shown in Figure 10. This dual-orifice fuel nozzle consists of a single fuel inlet, a fuel-flow dividing valve external to the mounting flange, and a swirl-atomizing tip which delivers fuel to the combustor as a 90°, hollow-cone spray. Each nozzle has two fuel circuits, primary and secondary. The primary circuit is a direct connection from the fuel inlet to a small atomizing tip discharging fuel at the center of the discharge end of the fuel nozzle. The primary circuit of each nozzle has three 0.64 x 0.38 mm slots which feed the spin chamber in the tip. These are the smallest fuel flow passages within the nozzle. The primary orifice exit diameter is 1.40 mm. Protection from contaminated fuel is provided by a 20 micron low pressure filter (upstream of main engine pump), a 40 micron high pressure filter (downstream of pump), and a 100-mesh screen in the valve housing. At an engine fuel flow rate of approximately 11½ g/s, the fuel pressure causes the flow divider valve to open and admits fuel to the secondary circuit. The valve opens at 552 kPa fuel differential pressure. The secondary circuit has six 1.27 x 1.78 mm slots in the spin chamber. The orifice, which is concentric with the primary orifice, is 4.95 mm in diameter. The fuel flow schedule for a single fuel nozzle is shown in Figure 11. The tip of each fuel nozzle is provided with an air shroud which directs cooling air radially inward over the fuel nozzle tip to reduce the tendency for carbon formation.

The J79 fuel nozzle service record is generally good, with no erosion or internal gumming problems. Nozzle recalibration is currently performed at 1200 hours. Nozzles that fail to meet flow schedules (generally fewer than 10% of those tested) are overhauled. The remaining nozzles are continued in service an additional 2100 hours, at which time they are all overhauled. This is believed to be a conservative practice, as the nozzles are considered to have practically unlimited life.

C. Combustor Operating Conditions

The combustor must operate over a wide range of fuel flow, inlet airflow,

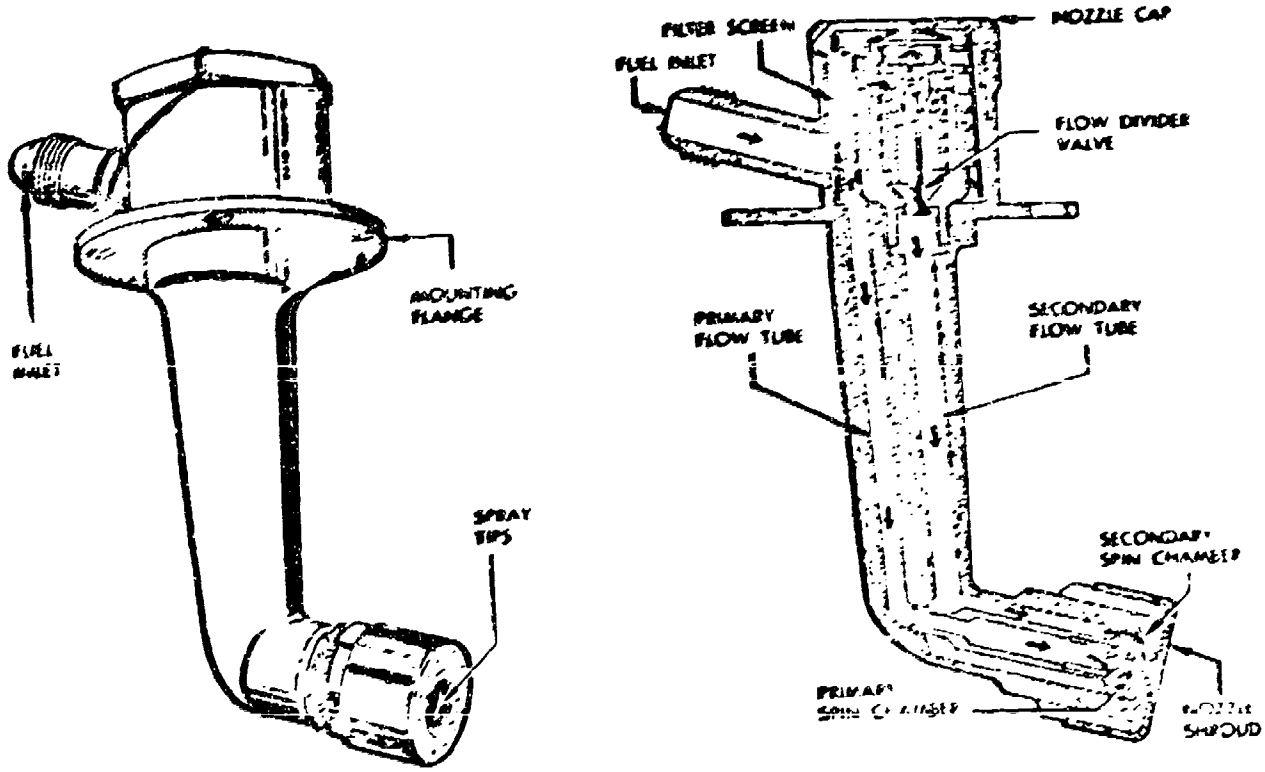

Figure 10. J75 Engine Dual Orifice Fuel Nozzle.

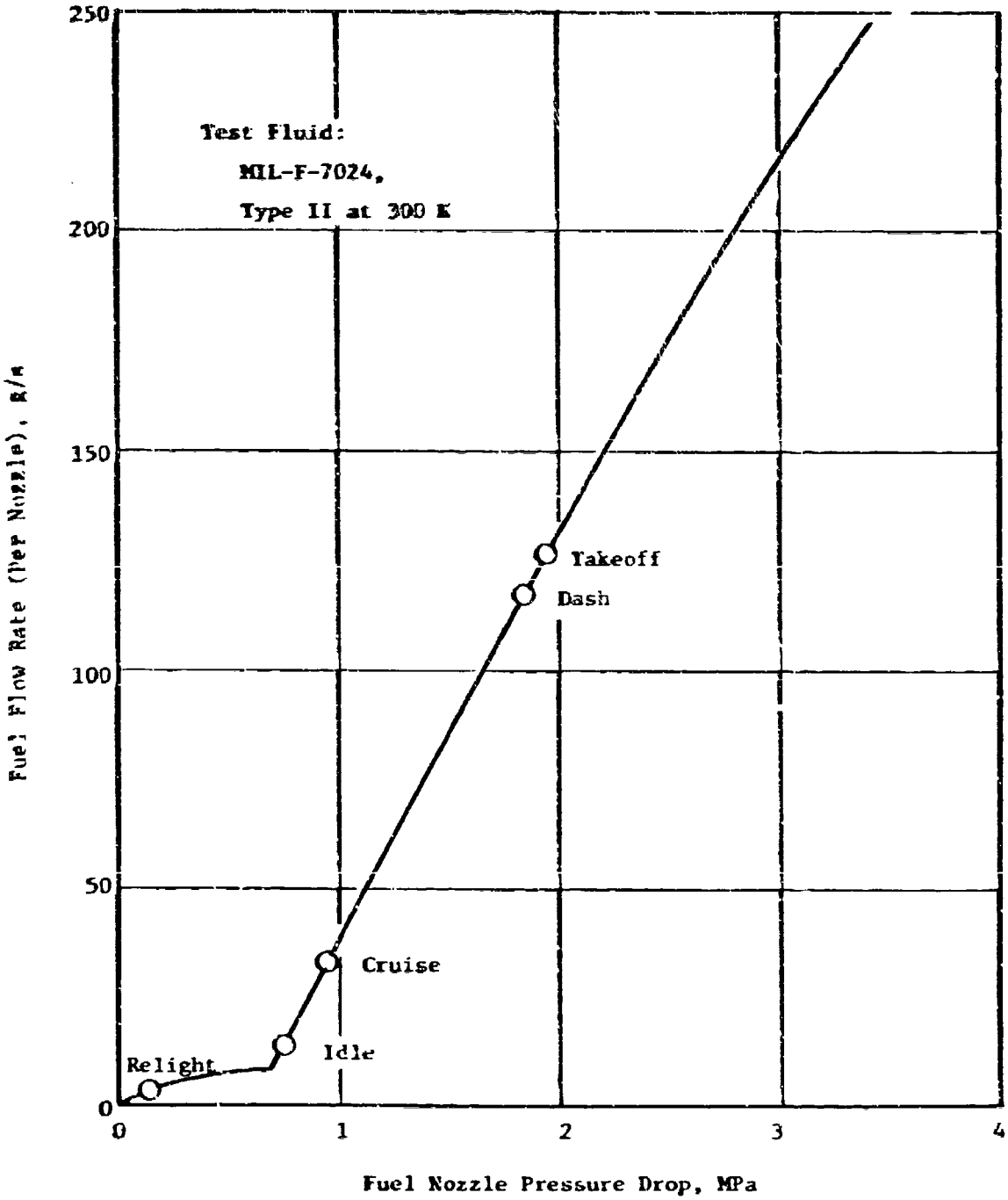

Figure 11. J79 Engine Fuel Nozzle Flow Characteristics.

temperature, and pressure. Table 8 presents the combustor operating parameters at four important steady-state engine conditions which are typically encountered. At these conditions, fuel effects on combustor performance emissions and combustor and turbine life are of particular interest.

In addition to steady-state operation, the combustion system must provide for starting over a wide range of conditions ranging from cold day ground start to relight at high altitude and high aircraft Mach number. Figure 12 presents the required J79 relight envelope.

Table 8. J79-17A Engine Combustor Operating Conditions.

	Ground Idle	Takeoff	Subsonic Cruise	Supersonic Dash	Ground Start[3]
Flight Altitude, km	0	0	10.7	10.7	0
Flight Mach Number	0	0	0.9	2.0	0
W_3[1], Total Airflow, kg/s	18.3	75.2	29.5	87.5	~3.2
W_c[1], Combustor Airflow, kg/s	15.3	62.7	24.6	73.3	~3.2
W_f[1], Fuel Flow, kg/s	0.144	1.259	0.335	1.173	0.042[4]
T_3, Inlet Total Temperature, K	421	664	559	781	≥239
P_3, Inlet Total Pressure, MPa	0.248	1.359	0.471	1.589	0.101
f_4, Fuel-Air Ratio, g/kg	9.42	20.07	13.60	16.01	~48.0
T_4, Exit Total Temperature (Ideal), K	792	1064	1362	1335	-
V_r[2], Reference Velocity, m/s	24.2	28.6	27.2	33.5	≥7.1

(1) Engine flows indicated (ten combustor cans).

(2) Based on W_3 and A_r = 3684 cm^2.

(3) 1000 rpm, typical starting speed.

(4) Minimum engine fuel flow schedule (normal).

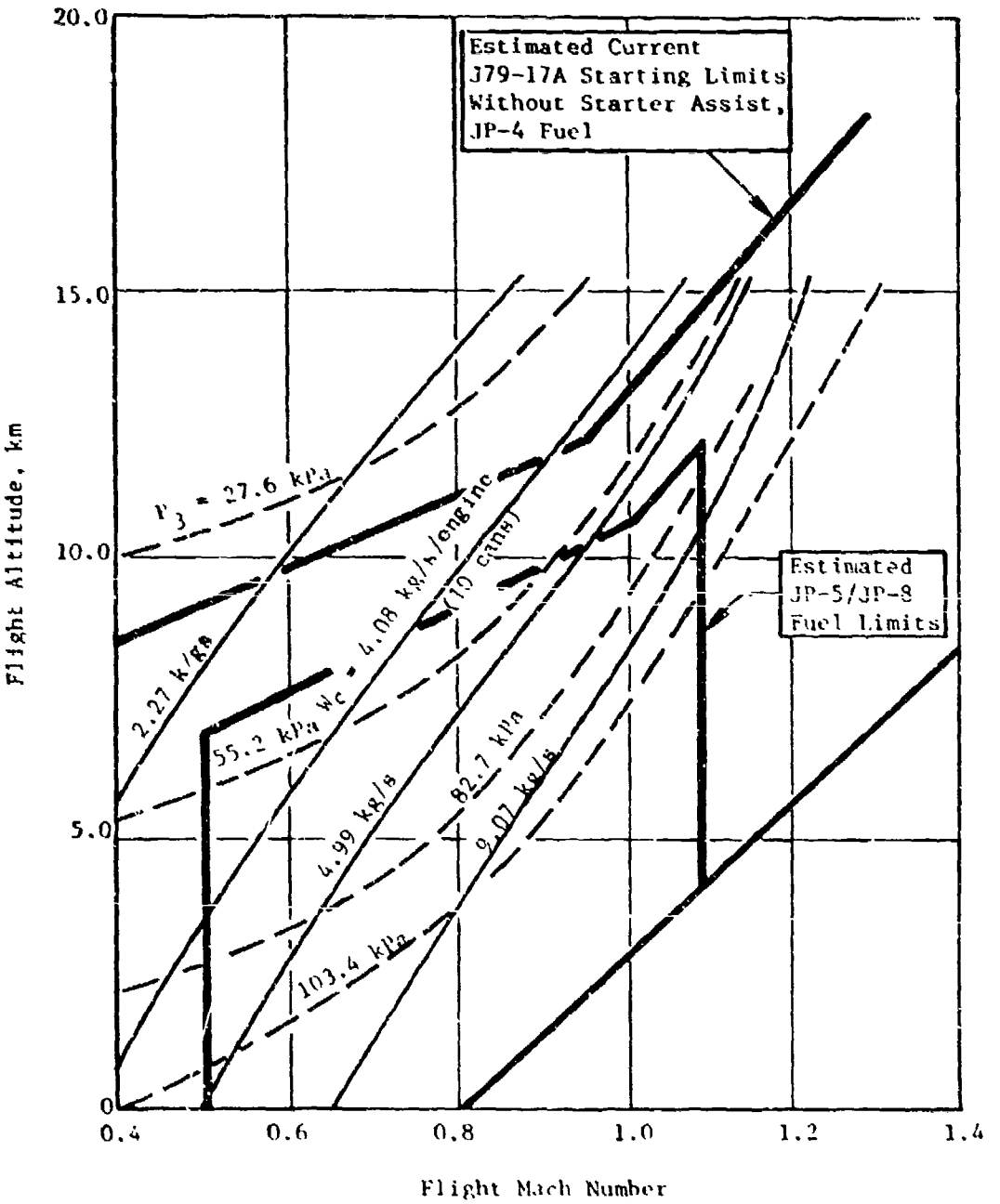

Figure 12. J79 Engine Altitude Windmilling/Relight Requirement Map.

SECTION V

APPARATUS AND PROCEDURES

All combustor and fuel nozzle testing in this program was conducted in specialized facilities at General Electric's Evendale, Ohio plant, using apparatus and procedures which are described in the following sections. Combustor performance/emissions/durability tests were conducted in a high pressure/temperature single-can combustor rig which is described in Section V-A. In parallel, combustor cold-day ground start/altitude relight tests were conducted in a low pressure/temperature single can rig which is described in Section V-B. Also in parallel, high temperature fuel nozzle fouling tests were conducted in a small specialized test rig described in Section V-C. Special fuel handling procedures used in all of these tests are described in Section V-D. Finally, procedures employed in analyses of these data are described in Section V-E.

Actual engine-quality, current-model J79-17A engine combustion system components, listed in Table 9, were provided by the USAF for use in these tests. The combustor assemblies were newly repaired units obtained from USAF stores. Four units were obtained, which visually were identical. Before testing, they were airflow calibrated; the results are listed in Table 10. Assemblies 1 and 2 were assigned to the high pressure tests because they were the most nearly alike with respect to flow calibration. Assembly 3 was used in low pressure testing.

A. Performance/Emission/Durability Tests

High pressure/temperature single-can-combustor rig tests were conducted at simulated J79 engine idle, cruise, takeoff, and dash operating conditions with each of the fuels to determine the following characteristics:

1) Gaseous emissions (CO, HC, and NO_x).

2) Smoke emissions.

3) Carbon deposition.

4) Carbon particle emissions.

5) Liner temperatures.

6) Flame radiation.

7) Combustor exit temperature profile and pattern factor.

8) Idle stability (lean blowout and ignition) limits.

Thus, a large part of the total data was obtained in these tests using apparatus and procedures described in the following sections.

Table 9. J79-17A Engine Combustor Test Parts List.

Part Name	GE Part Number	National Stock Number
Ignition Combustor Liner Assembly	106C3320G73	2840-01-004-1728-NN
Fuel Nozzle (Parker-Hannifin 1345-633327)	577C796P10	2915-00-110-5514PL
Main Ignition Unit (Bendix 10-358765-1 110VAC, 400 cps)	106C5281P3	2925-00-992-7904PL
Main Spark Plug (Champion FHE J87-2A)	696D256P02	2925-00-925-05445PL
Main Spark Plug Lead (Mfr 81482 - 59393)	517D377P2	2925-00-956-0293PL

Table 10. Test Combustor Flow Calibration Results.

	Combustor Effective Airflow Area, cm^2			
Combustor	1	2	3	4
Front Liner Assembly	23.7	24.5	23.2	24.4
Aft Thimbles	58.5	59.0	59.1	58.3
Aft Cooling Louvers and Seal	21.0	19.9	23.9	24.5
Total	103.2	103.3	106.3	107.2

1. High Pressure Test Rig Description

These tests were conducted in the Small Combustor Test Facility, Cell A5, located in Building 304 of the Evendale Plant. This test cell is equipped with all of the ducting, fuel and air supplies, controls, and instrumentation required for conducting small combustor high pressure/temperature tests. High pressure air is obtained from a central air supply system, and a gas-fired indirect air heater is located adjacent to the test cell. For the single-can-combustor rig, J79 engine idle, cruise, and takeoff operating conditions can be exactly duplicated. Dash operating conditions can be exactly duplicated with respect to temperature, velocity, and fuel-air ratio, but pressure and flow rates must be reduced about 25 percent in order to be within the facility airflow capability.

The High Pressure Combustor Test Rig, shown in Figures 13, 14 and 15, exactly duplicates a one-tenth sector of the engine flowpath from the compressor outlet guide vane (OGV) to the first-stage turbine nozzle diaphragm (TND). As shown in Figure 13, the test rig inlet flange which bolts up to a plenum chamber in the test cell, incorporates a Bellmouth transition to the simulated OGV plane. The combustor housing is a ribbed, thick-walled vessel which forms the inner flowpath contour and side walls, covered by a thick lid that forms the outer flowpath contour. Figure 14 shows a combustor installed in the pressure vessel with the lid removed. The combustor exit engages an actual segment of an engine transition duct. Immediately downstream of the transition duct is an annular sector section which contains an array of water cooled instrumentation rakes in the TND plane, indicated by an arrow in Figure 15. Additional details of the exit instrumentation rakes are shown in Figures 16 and 17. Downstream of the rakes, the combustion gases are water-quenched and the sector flowpath transitions to circular, which is bolted up to a remote-operated backpressure valve in the test cell ducting. Two other features of the test rig can be seen in Figure 15: a flame radiation pyrometer, mounted to view the combustor primary zone through a crossfire duct window; and bleed air pipes to withdraw, collect, and meter simulated turbine cooling airflow.

2. High Pressure Test Instrumentation

A summary of the important combustor operating, performance, and emission parameters which were measured or calculated in these tests is shown in Table II. Airflow rates were measured with standard ASME orifices. Fuel flow rates were measured with calibrated turbine flowmeters corrected for the density and viscosity of each test fuel at the measured supply temperature. Combustor inlet temperature and pressure were measured with plenum chamber probes.

Combustor outlet temperature, pressure, and gas samples were measured with a fixed array of seven water-cooled rakes, arranged and hooked up as shown in Figure 18. Each rake contained five capped chromel-alumel thermocouple probes, located on radial centers of area, and four impact pressure/gas sample probes, located midway between thermocouple elements. As shown in Figure 18, eight of the impact probe elements were hooked up for total-pressure measurement, and the other 20 elements were manifolded to three heated gas sample transfer lines leading out of the test cell to the gas composition measurement instruments. Transfer Lines I and II were connected through selector valves to a smoke measurement console (Figure 19) and a gas analysis console (Figure 20). Transfer

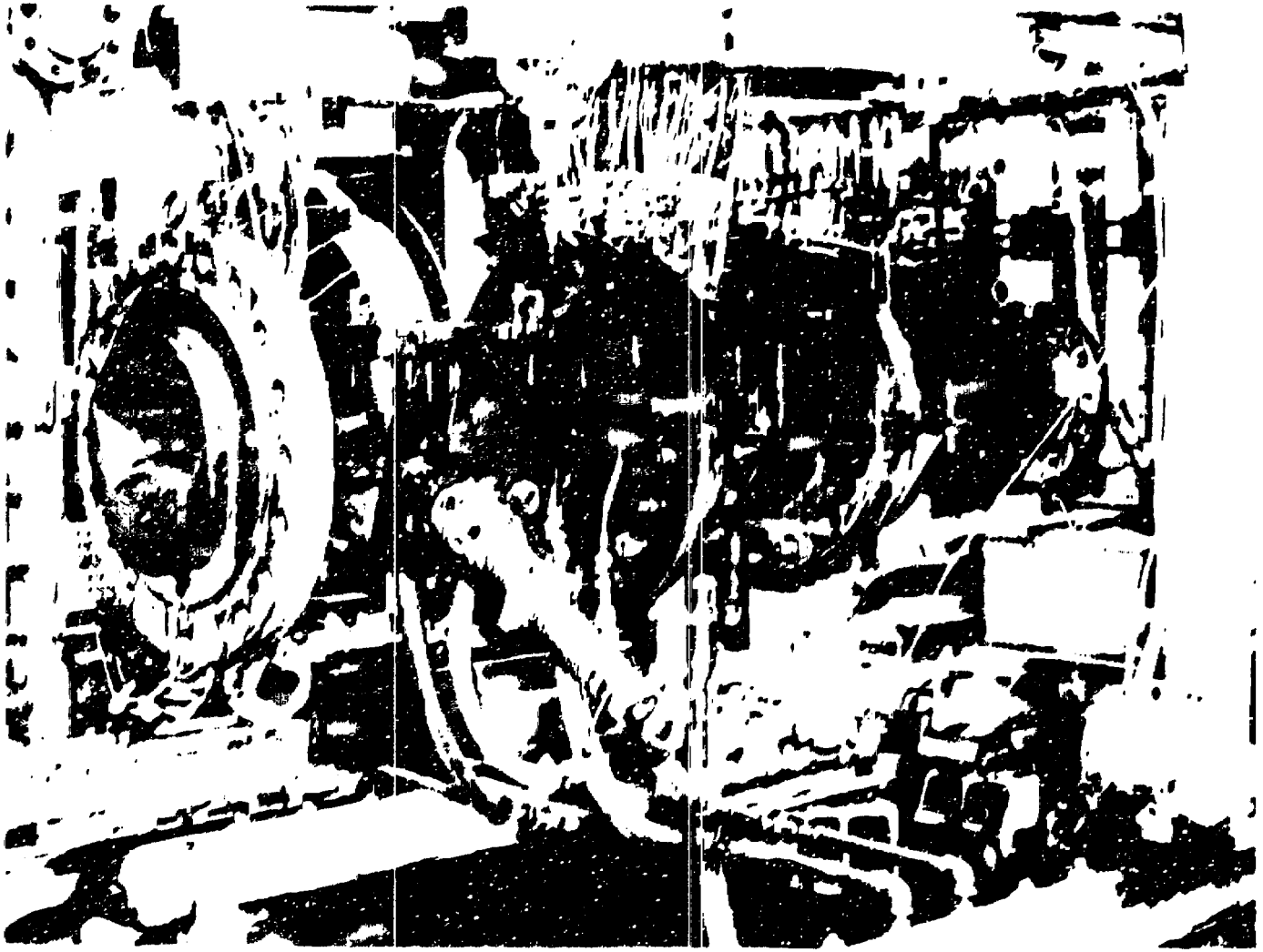

Figure 13. Inlet Quarter View of High Pressure I/A Combustor Test Rig.

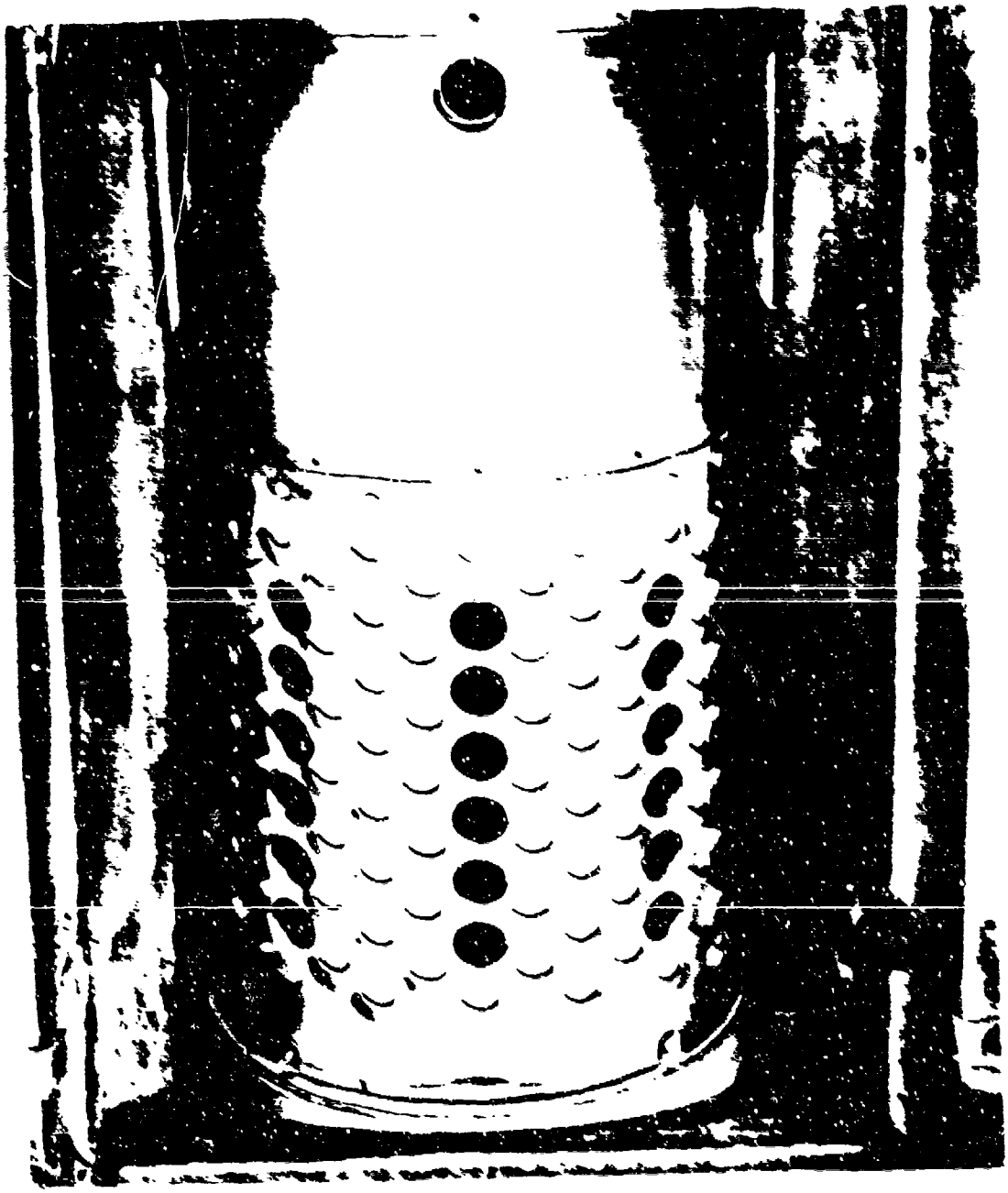

Figure 14. Combustor Installation in High Pressure J79 Test Rig.

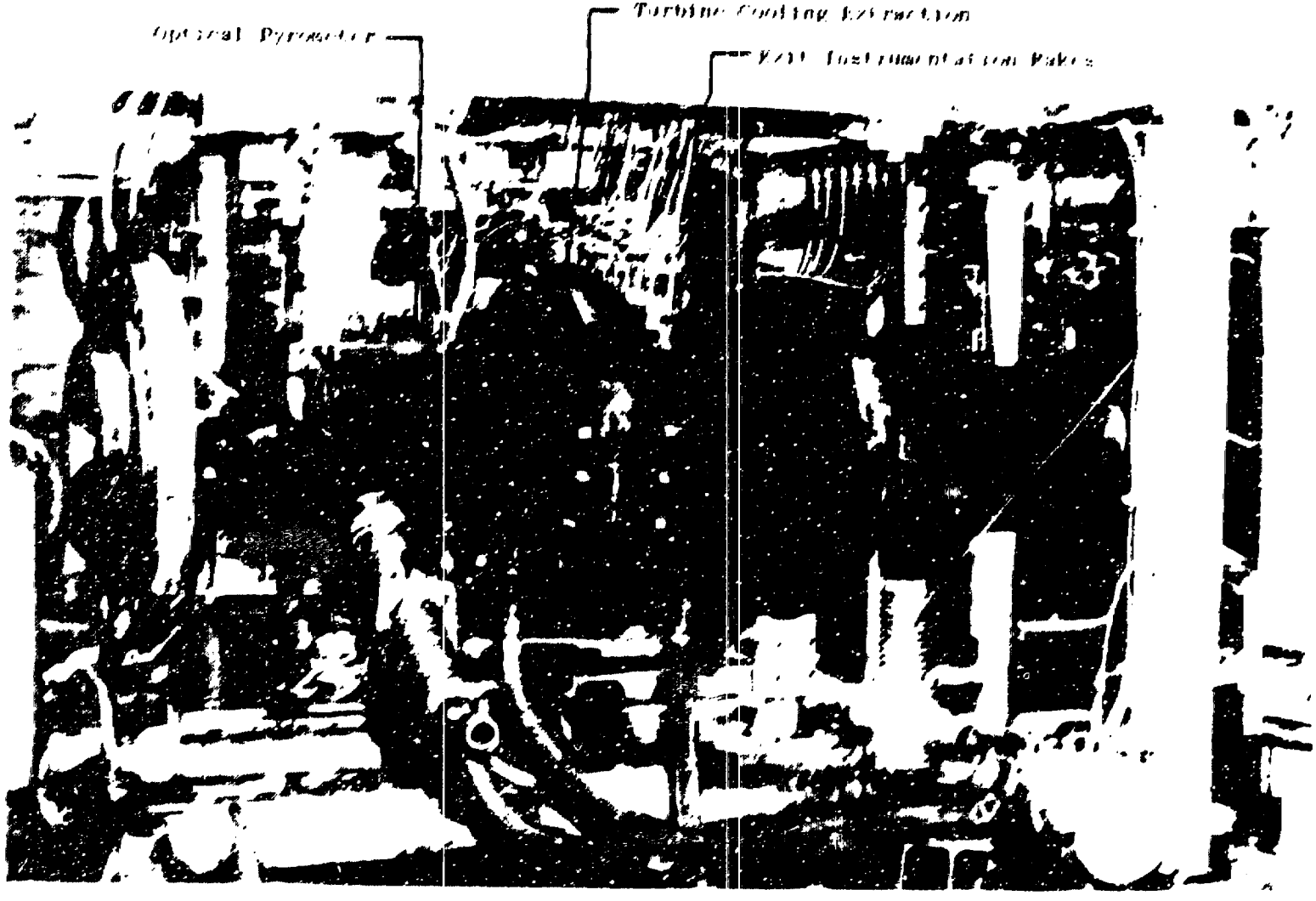

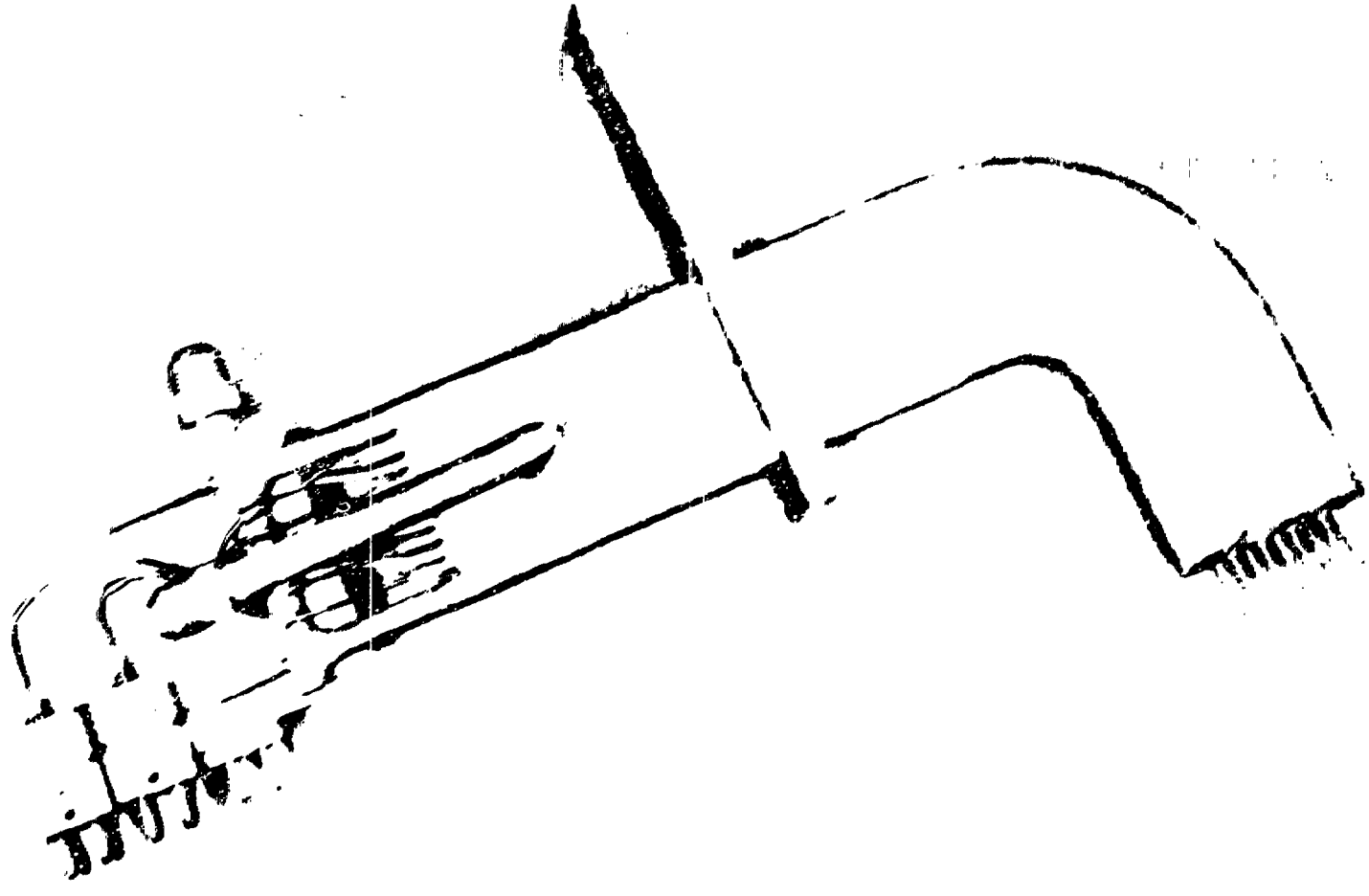

Figure 17. Tip Details, Combustor Exit Instrumentation Rake.

Table 11. Summary of Measured and Calculated Combustor Parameters in High Pressure Combustor Tests.

Parameter	Symbol	Units	Measurement/Calculation Method
Inlet Total Pressure	P_3	MPa	Average of measurements from 3 impact probes
Exit Total Pressure	P_4	MPa	Average of measurements from 8 impact probes
Total Pressure Loss	$\Delta P_T/P_3$	%	$100(P_3-P_4)/P_3$
Total Inlet Airflow	W_3	kg/s	ASME Orifice
Turbine Cooling Airflow	W_{tc}	kg/s	ASME Orifice
Combustor Airflow	W_c	kg/s	W_3-W_{tc}
Fuel Flow	W_f	g/s	Turbine flowmeters corrected for density and viscosity
Metered Fuel-Air Ratio	f_m	g/kg	W_f/W_c
Inlet Air Humidity	h_3	g/kg	Dewpoint hygrometer
Inlet Total Temperature	T_3	K	Average of measurements from 3 probes
Exit Total Temperature	T_4	K	Average of measurements from 35 probes
Pattern Factor	PF	-	$(T_{4max.}-T_{4avg})/(T_{4avg}-T_3)$
Profile Factor	PrF	-	$(T_{4[min.\ max.]}-T_3)/(T_{4avg}-T_3)$
Reference Velocity	V_r	m/s	$V_r = W_3/\rho_3 A_r = 0.0093297\ W_c T_3/P_3$
Combustor Metal Temperature	T_L	K	24 metal thermocouples
Combustor Dome Static Pressure	P_{sd}	MPa	Average of measurements from 2 wall taps
Combustor Liner Static Pressure	P_{sL}	MPa	Average of measurements from 2 wall taps
Fuel Temperature	T_f	K	Thermocouple at fuel nozzle inlet
Fuel Nozzle Pressure Drop	ΔP_f	MPa	Pressure tap at fuel nozzle inlet (P_f-P_{sd})
Fuel Nozzle Effective Area	A_{fe}	mm^2	$A_{fe} = W_f/\sqrt{2g\rho_f \Delta P_f}$
Combustor Total Flame Radiation	$\dot{q}_R$	kW/m^2	Optical pyrometer at crossfire duct
Combustor Exit Smoke Number	SN_4	-	Manifolded 12-point gas sample and ARP1179 (Ref. 4)
Smoke Emission Index	EI_s	g/kg	GE correlation at SN_4 & f_s (Appendix E)
Engine Exit Smoke Number	SN_R	-	GE correlation at EI_s (Appendix E)
Gas Sample Fuel-Air Ratio	f_s	g/kg	Manifolded 12-point gas sample & equation in ARP1256 (Ref. 5)
CO Emission Index	EI_{CO}	g/kg	Manifolded 12-point gas sample & equation in ARP1256 (Ref. 5)
HC Emission Index (as CH_n)	EI_{HC}	g/kg	Manifolded 12-point gas sample & equation in ARP1256 (Ref. 5)
NO_x Emission Index (as NO_2)	EI_{NO_x}	g/kg	Manifolded 12-point gas sample & equation in ARP1256 (Ref. 5)
Gas Sample Combustion Efficiency	η_{GS}	%	$\eta_{GS} = 100 - (EI_{HC}/10.0)+(EI_{CO}/42.8)$ (Ref. 7)
Thermocouple Combustion Efficiency	η_{TC}	%	$\eta_{TC} = 100 \left\lvert \text{ideal fuel-air ratio @ } (T_4-T_3) \right\rvert / f_m$ (Ref. 7)
Large Carbon Particle Emissions	$\bar{X}_C$	g/kg	Manifolded 8-point cumulative gas sample

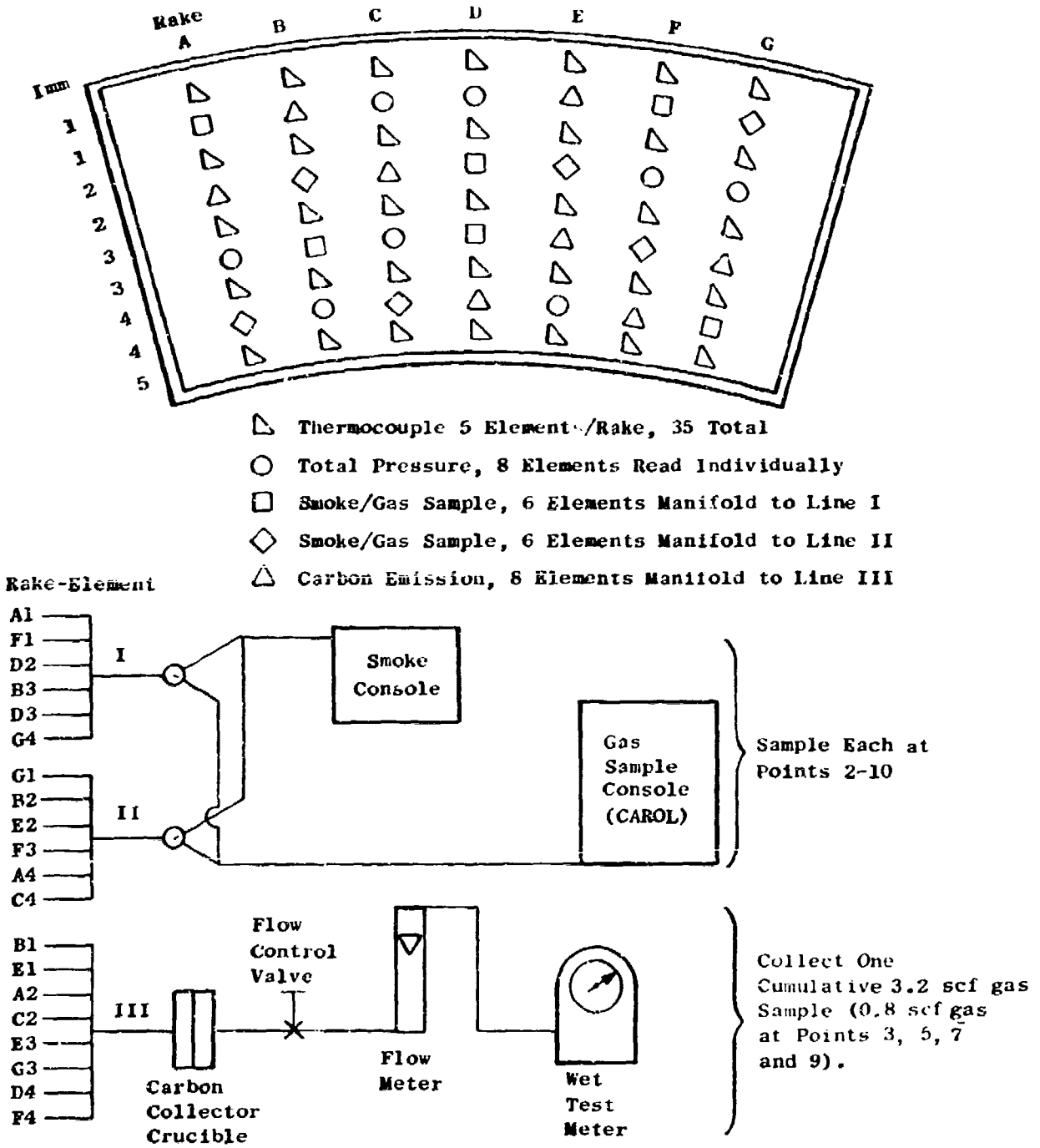

Figure 18. High Pressure Test Rig Exit Instrumentation.

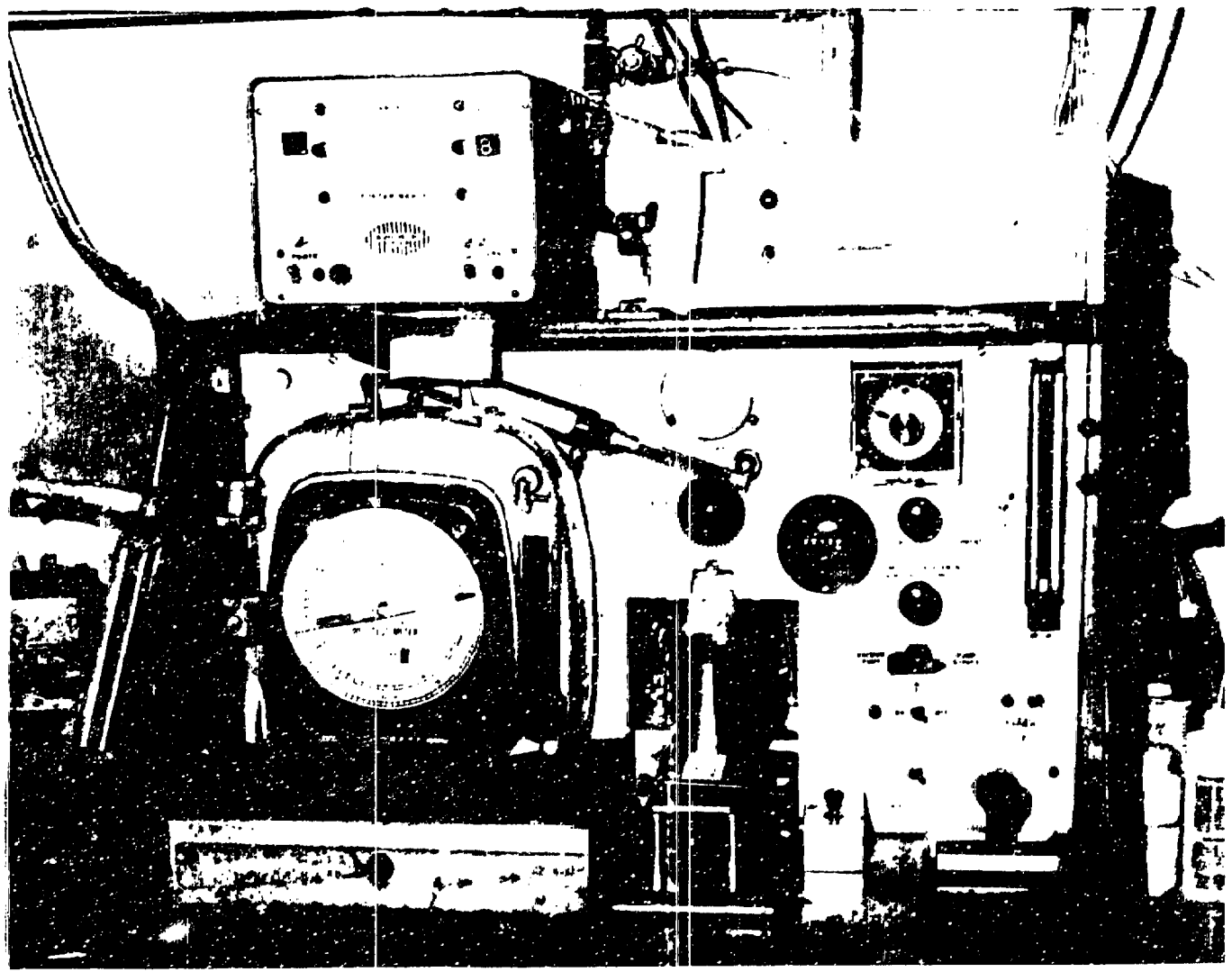

Figure 19. General Electric Smoke Measurement Console.

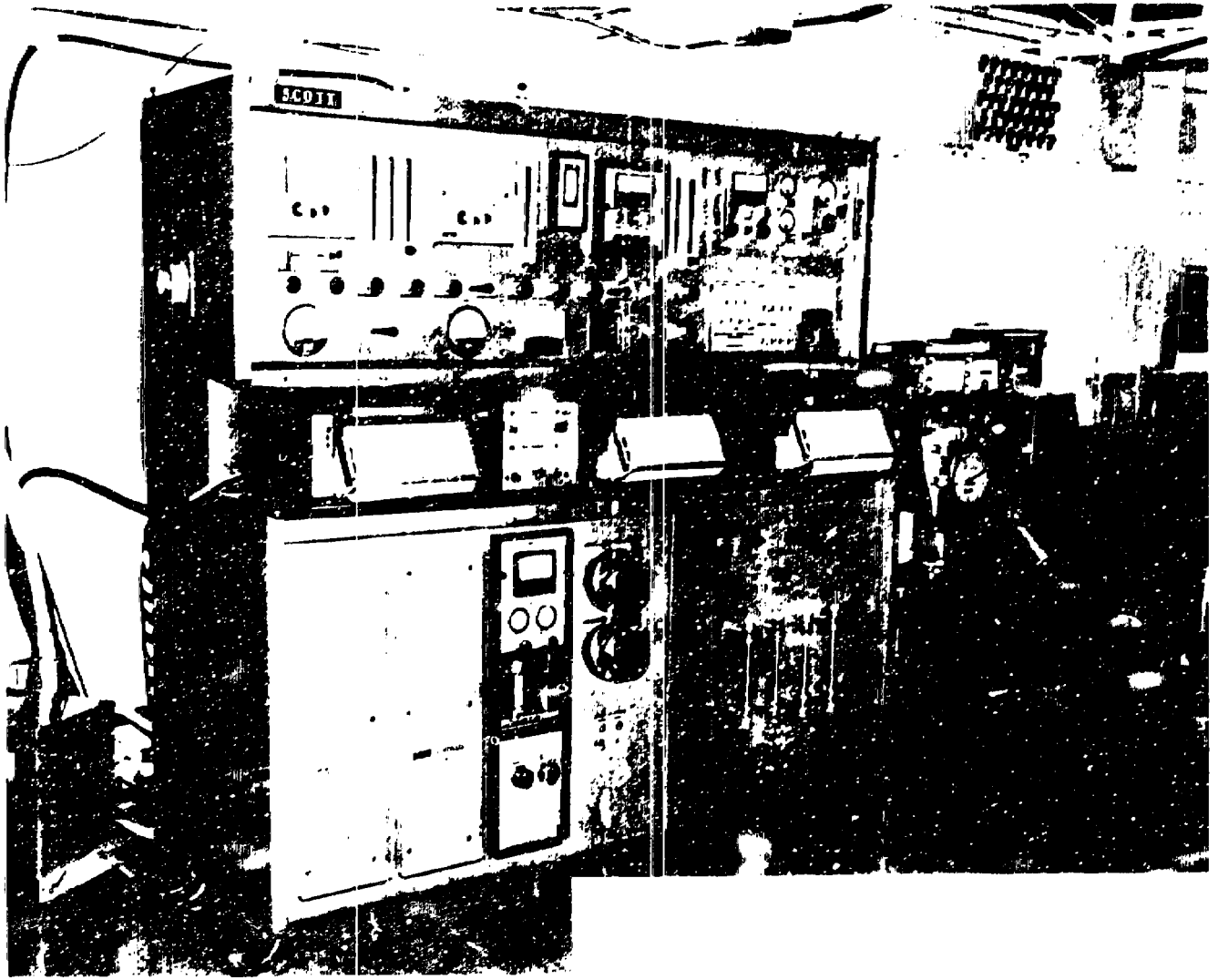

Figure 20. General Electric Emissions Measurement Console (CAROL IV).

Line III was connected to a carbon collection crucible located near the test rig, and then continues on to flow control/metering apparatus in the gas measurement area.

The General Electric smoke measurement console (Figure 19) contains standard test equipment which fully conforms to SAE ARP 1179 (Reference 4). Smoke spot samples are collected on standard filter paper at the prescribed gas flow rate and at four soiling rates spanning the specified quoted soiling rate. The spot samples are later delivered to the data processing area, where the reflectances are measured and the SAE Smoke Number is calculated.

The gaseous emission measurement console, shown in Figure 20, is one of several that were assembled to General Electric specifications for CAROL systems (Contaminants Analyzed and Recorded On-Line) and that conform, generally, to SAE ARP 1256 (Reference 5). This system consists of four basic instruments: a flame ionization detector (Beckman Model 402) to measure total hydrocarbon (HC) concentrations, two nondispersive infrared analyzers (Beckman Models 865 and 864) for measuring carbon monoxide (CO) and carbon dioxide (CO_2) concentrations, and a heating chemiluminescent analyzer (Beckman Model 951) for measuring oxides or nitrogen (NO or NO_x = NO + NO_2) concentrations. Each of the instruments are fully calibrated with certified gases before and after each test run; and periodically during testing, zero and span checks are made. Readings from the instruments are continuously recorded on strip charts and hand-logged on test and calibration points for later calculation of concentration, fuel-air ratio, and emission indices, using a computer program which incorporates the equations contained in ARP 1256. Gas sample validity was checked by comparison of sample to metered fuel-air ratios.

Carbon deposition tendencies were assessed by installing a clean combustor for each test, and inspecting it after the test, assigning it a visual rating. A cumulative carbon collection technique was also employed (Line III in Figure 18) in an attempt to quantify the amount of large carbon particles emitted directly and/or that were shed periodically from the depositions. A fixed volume of combustor exhaust gas at idle cruise, takeoff, and dash was filtered through a porous crucible. At the completion of the test, the crucible was removed for laboratory analysis to determine the total quantity of carbon collected.

Combustor liner temperature was measured by an array of 24 thermocouples located on the inner liner as shown in Figure 21. This instrumentation pattern was selected to provide detailed data in the vicinity of the known hottest regions of the combustor. There are no thermocouples downstream of the cross-fire ducts or on the aft liner, since those regions are usually at least 150 K cooler than the forward section of the inner liner (Reference 6). Figures 22 through 25 show the actual liner thermocouple installations on the inner liner.

Flame radiation in the primary burning zone of the combustor was measured by a total-radiation pyrometer (Brown Radiamatic, Type R-12), which can be seen in Figure 15. A diagram of the optical view path is shown in Figure 26. The pyrometer sensing element is a thermopile which provides a direct current voltage output. The flame radiation is focused on the thermopile with a calcium fluoride lens which is transparent to radiation of wavelengths less than three microns. The pressure seal at the test rig wall is formed by a

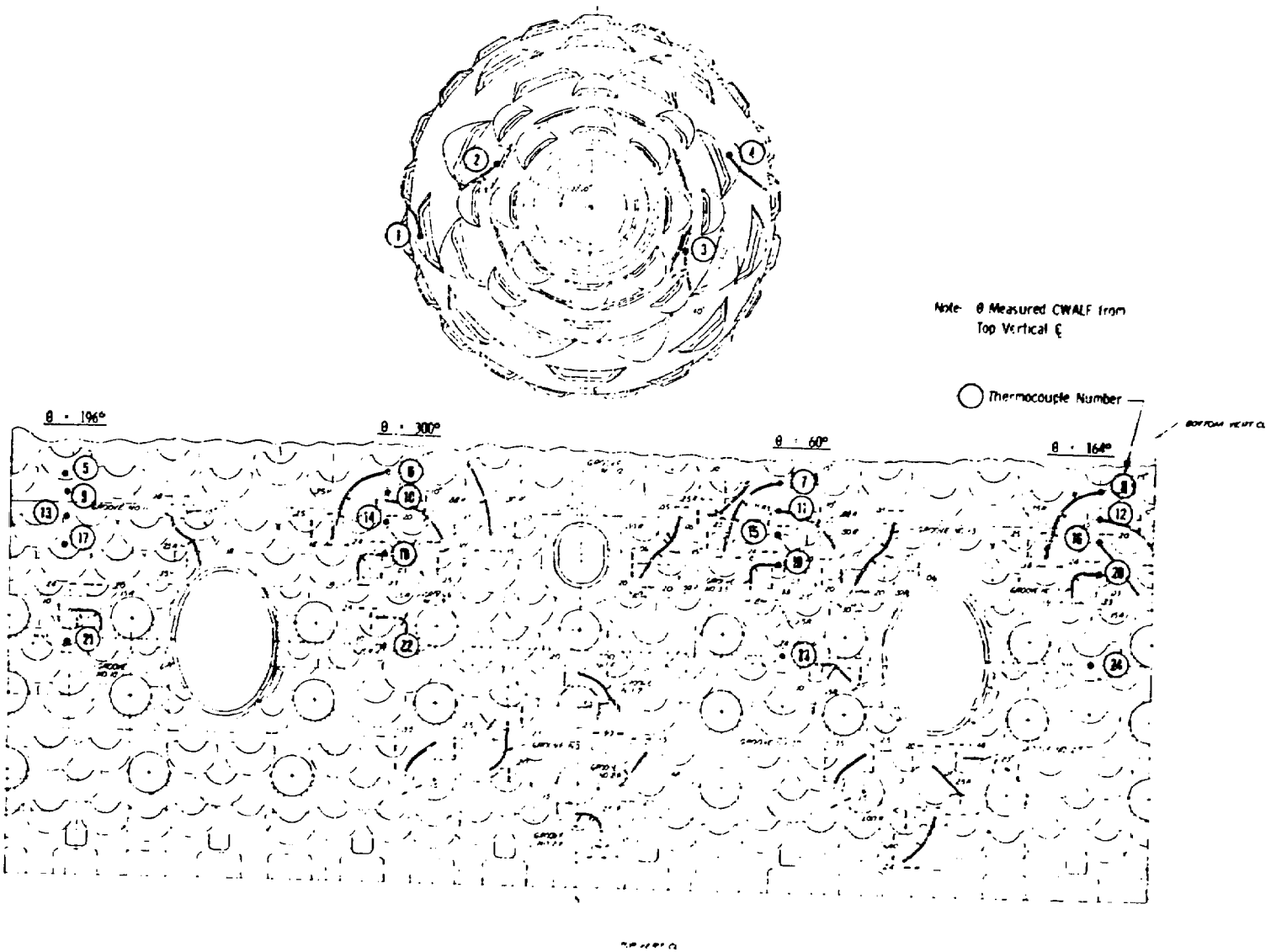

Figure 21. Combustor Liner Temperature Measurement Locations.

Figure 22. Combustor Liner Instrumentation at 60 Degrees, CWAIF.

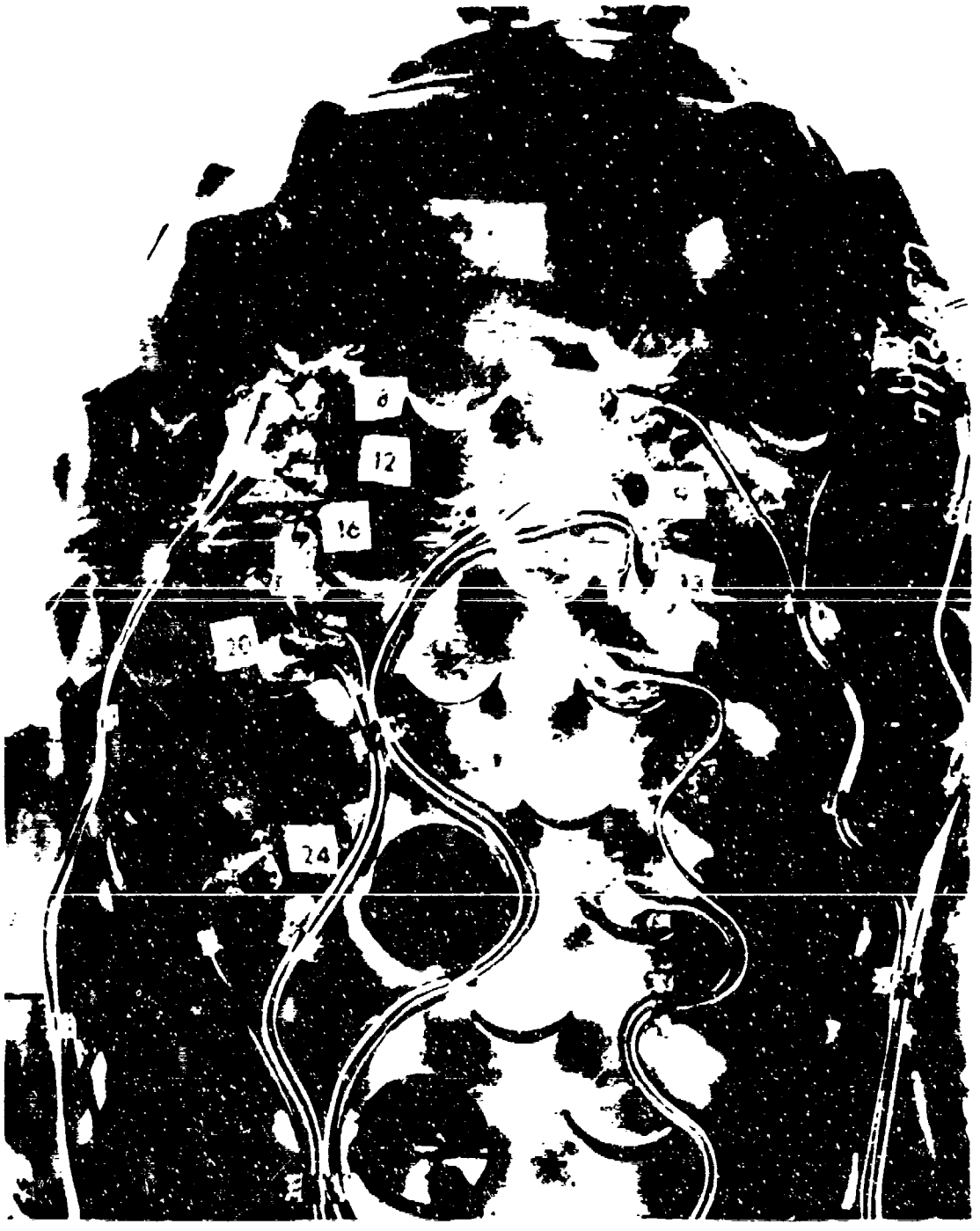

Figure 23. Combustor Liner Instrumentation at 164 and 196 Degrees CWALF.

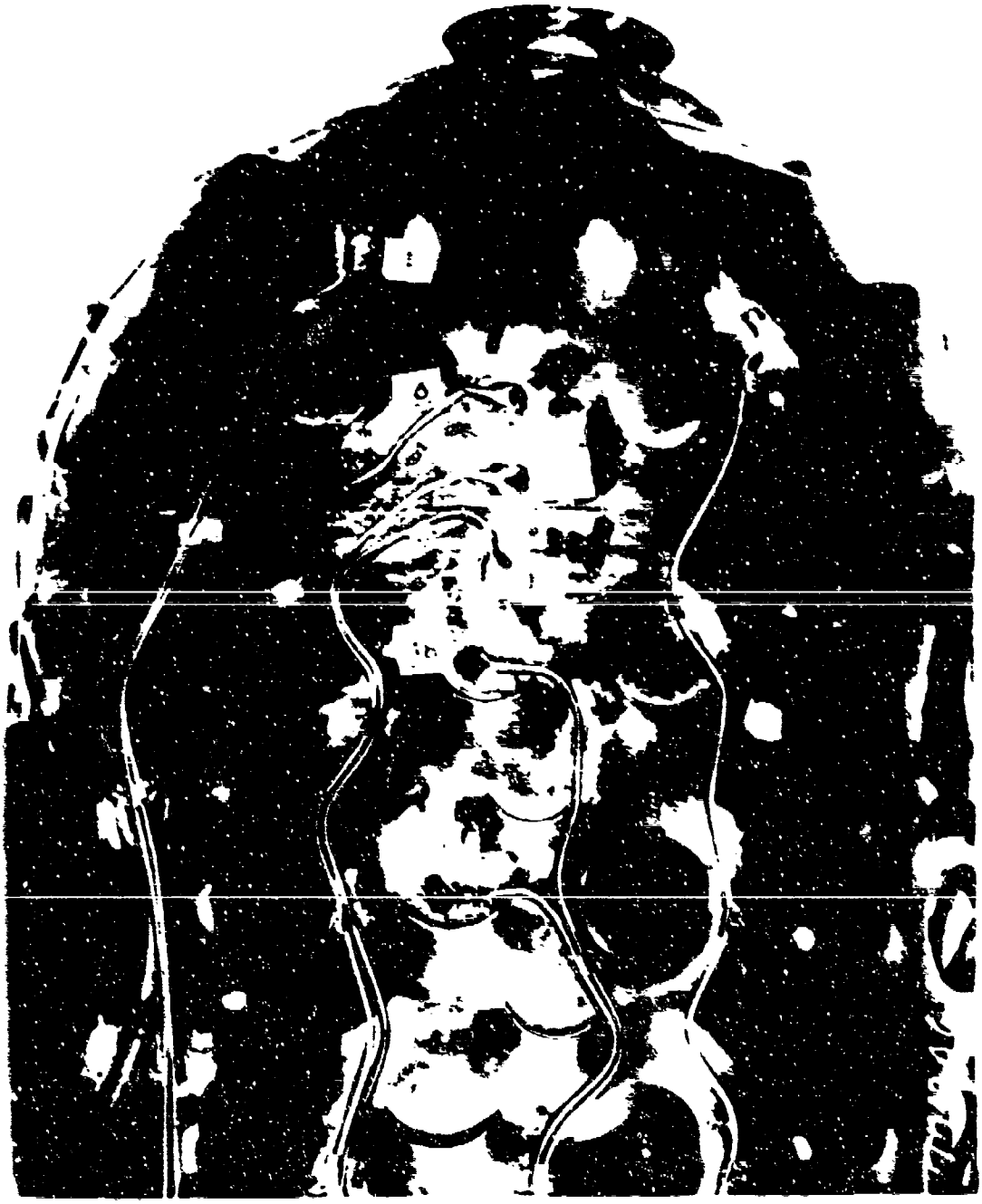

Figure 24. Combustor Liner Instrumentation at 300 Degrees CWALF.

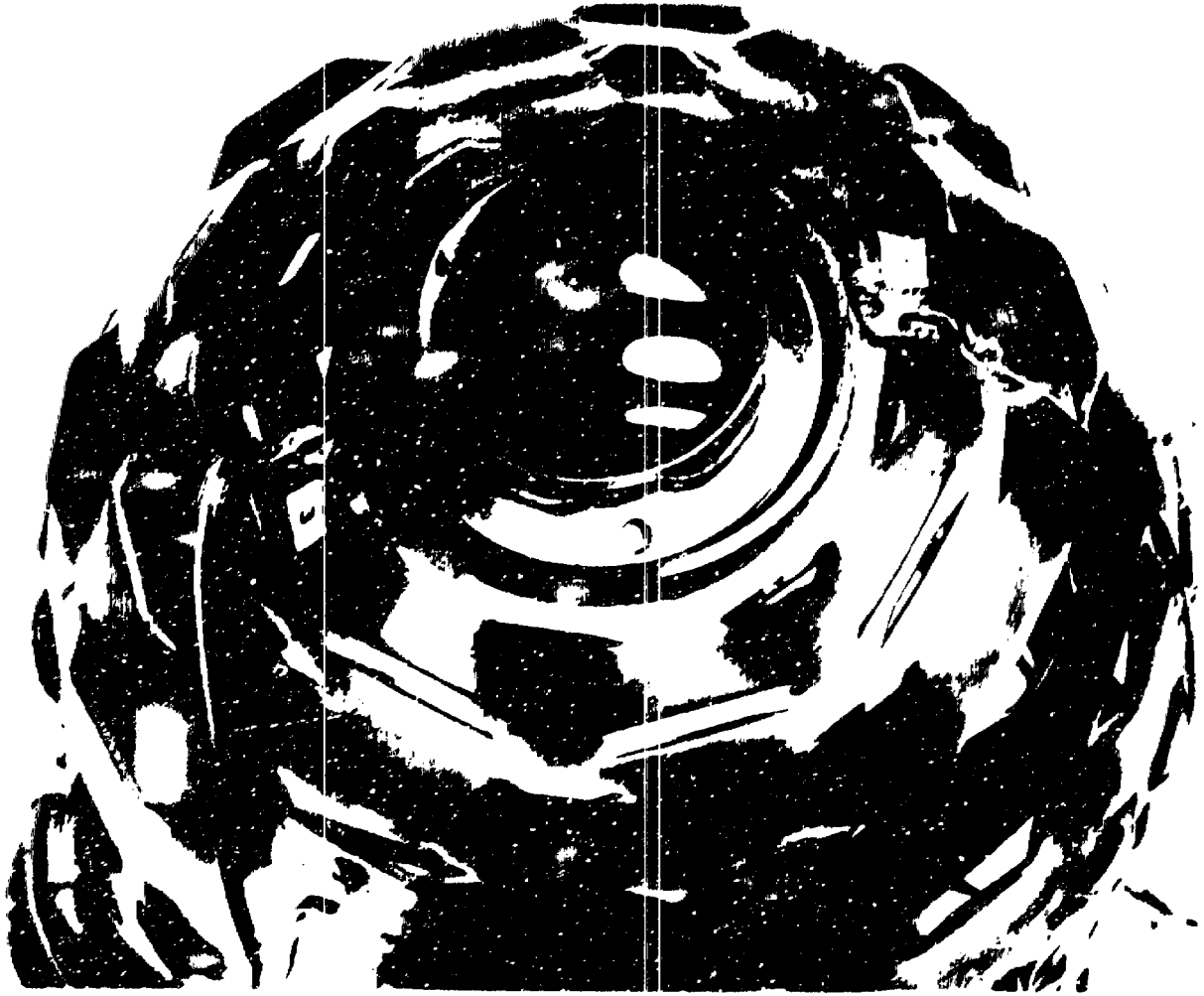

Figure 25. Combustor Dome Instrumentation.

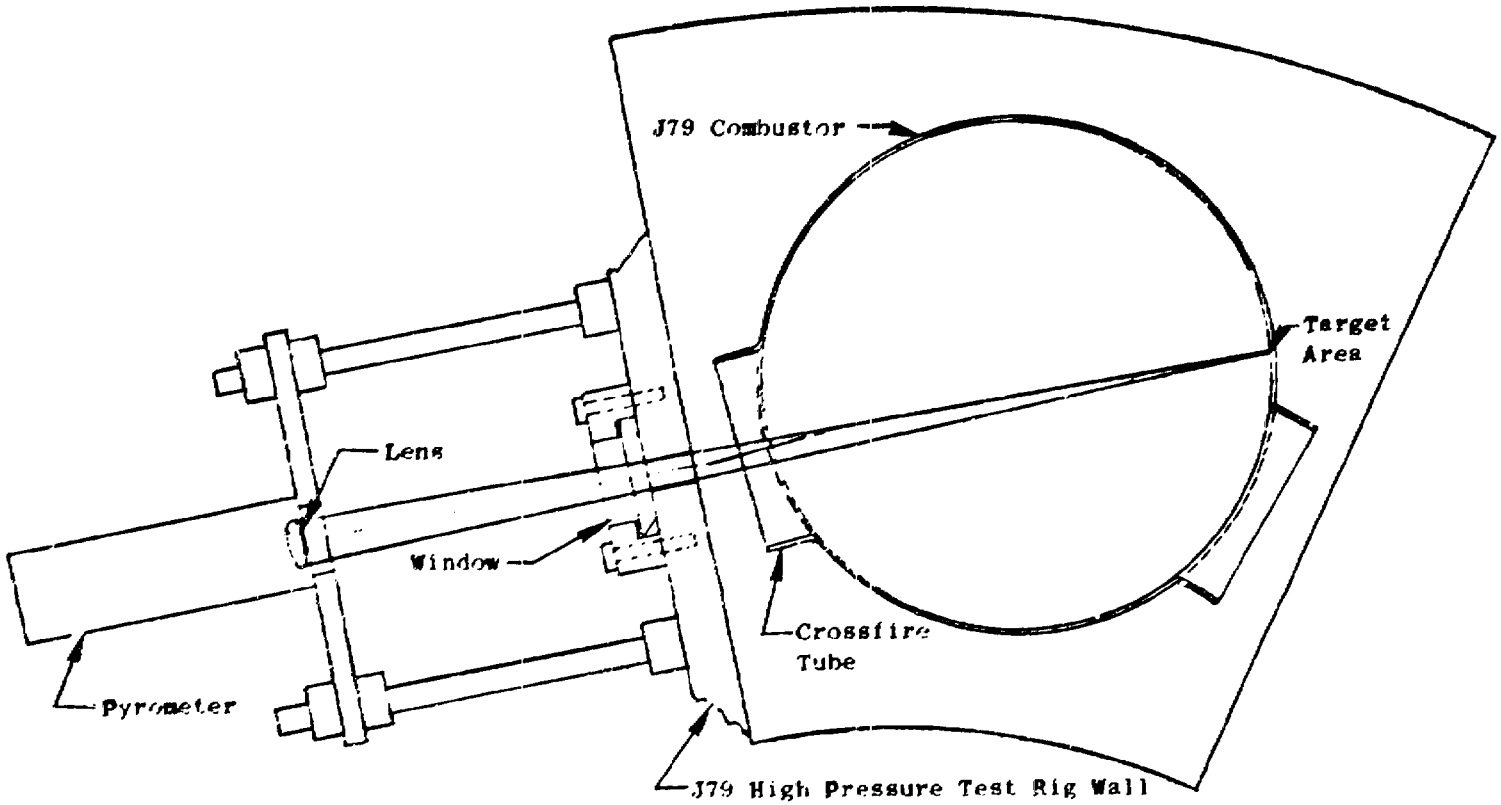

Figure 26. Optical Pyrometer Setup in High Pressure Test Rig.

sapphire window which is transparent to radiation of even longer wavelengths. The sapphire window was swept clean by a small flow of filtered air. The pyrometer was calibrated by viewing a resistance-heated-carbon backbody furnace through the same optical system used in the combustor test. The furnace temperature was measured with a disappearing-filament optical pyrometer.

3. High Pressure Test Procedures

A total of 14 high pressure rig tests were run: one for each test fuel plus a repeat test with fuel No. 1 to establish test variability. Two different fuel nozzles and combustors were alternated in the tests, so that while one set was undergoing test, the other set was being cleaned, calibrated, and re-instrumented as needed.

Each test was conducted to the ten-point test schedule shown in Table 12. On Point No. 1, minimum lightoff and lean blowout limits at idle inlet conditions were determined. On Points No. 2 through 10, steady-state operating, performance, and emissions measurements were obtained at simulated engine idle, cruise, takeoff, and dash operating conditions. At each of these simulated engine operating conditions, data were recorded at two nominal fuel-air ratios: 80 and 100 percent of the engine cycle value corrected for the test fuel heating value. However, if the 80 percent fuel-air ratio point indicated that the 100 percent fuel-air ratio point would locally exceed the gas temperature limits of the exit thermocouple rakes, a lower fuel-air ratio point was substituted. This limit was usually exceeded at simulated takeoff conditions, so a 60 percent fuel-air ratio point was usually substituted for the 100 percent point.

Test Points 2 through 10 were changed every thirty minutes (nominally) in each test in order to subject the combustor to approximately the same 4.5 hour carbon deposition cycle with each fuel. At the completion of each test, the combustor was removed for visual inspection and photographic documentation of the carbon accumulation. Pre- and post-test airflow calibrations of the combustors were also periodically conducted to determine if the carbon accumulation and/or thermal cycling had caused any change in effective airflow area, but no discernable changes were ever found.

B. Cold-Day Ground Start/Altitude Relight Tests

Low-pressure/temperature single can combustor rig tests were conducted at simulated J79 engine ground cranking and altitude windmilling operating conditions to determine the cold-day ground start and altitude relight characteristics of each of the test fuels. The apparatus and procedures which were utilized are described in the following sections.

1. Low Pressure Test Rig Description

These tests were conducted in the Building 301 Combustion Laboratory at the Evendale Plant. This facility has capabilities for testing small combustor rigs over a wide range of simulated ground start and altitude relight conditions. Liquid nitrogen heat exchangers are used to obtain low fuel and air temperatures, and steam ejectors in the exhaust ducting are used to obtain low combustor inlet pressures.

Table 12. High Pressure Test-Point Schedule.

Test Point Number[1]	W_3 Total Airflow, kg/s	Combustor Airflow, kg/s	P_3 Inlet Total Pressure, MPa	T_3 Inlet Total Temperature, K	V_r Reference Velocity, m/s	W_f[2] Fuel Flow Rate, g/s	f[2] Fuel-Air Ratio, g/kg	Comments
1	1.83	1.33	0.269	421	24.2	Determine Ignition and Lean Blowout Fuel Flow		Idle Inlet Conditions
2	1.83	1.33	0.269	421	24.2	11.9	[illegible]	
3	1.83	1.33	0.269	421	24.2	14.6	9.4	True Idle Condition
4	3.02	2.46	0.471	559	27.2	26.9	10.9	
5	3.02	2.46	0.471	559	27.2	33.5	13.6	True Subsonic Cruise (0.9[illegible]/11.7 km
6	7.[illegible]	6.28	1.359	66[illegible]	28.6	1[illegible].7	16.6	
7	7.[illegible]	6.28	1.359	66[illegible]	28.6	125.9[3]	20.0[3]	True Takeoff
8	6.[illegible]	[illegible]	1.191	78[illegible]	33.5	7[illegible].4	12.9	
9	6.[illegible]	[illegible]	1.191	78[illegible]	33.[illegible]	9[illegible].9	16.5	Simulated Supersonic Dash (2.[illegible] [illegible] km
10	1.83	1.33	0.269	421	24.2	14.4	9.4	True Idle Condition

(1) Each steady-state test point 1-10 to be maintained 30 minutes so total test time is 4.[illegible] hours.

(2) Based on [illegible] fuel. For other fuels, adjust for heating value.

(3) Adjust (reduce) if necessary to exit rake peak temperature limit.

The low-pressure, single-can J79 combustor rig used in these tests is shown in Figure 27. The combustor housing is made from actual engine parts and the rig exactly duplicates a one-tenth segment of the engine combustion system flow path. Combustor inlet temperatures and pressure are measured with probes in the plenum chamber. The combustor assembly is installed from the rear of the combustor housing which bolts up to a segment of an engine combustor transition duct. An array of thermocouples is located in the transition duct to sense ignition and blowout. This rig has no provisions for turbine cooling air extraction.

Air obtained from the central supply system was dried at the facility to a dew point of about 240 K and metered with a standard ASME orifice. Fuel flow rates were measured with calibrated turbine meters corrected for the density and viscosity of each test fuel at the measured supply temperature. All temperature, pressure, and flow data were read on direct indicating instruments (manometers, potentiometers, etc.) and hand logged by the test operator.

2. Cold-Day Ground Start Procedure

The first part of the test with each fuel was structured to evaluate cold-day ground starting characteristics. The test point schedule is shown in Table 13. The airflow rate (0.318 kg/s) and combustor inlet pressure (ambient) were set to simulate typical engine ground starting conditions (1000 rpm). Fuel and air temperature were lowered from ambient to 239 K minimum (JP-8 freeze point) in steps to simulate progressively colder days. At each temperature step, minimum ignition and lean blowout fuel flow rates were determined. Maximum fuel flow rate was taken as 7.56 g/s/can, which is well above the current engine minimum fuel flow rate (4.22 g/s/can). The test sequence was as follows:

1) With inlet conditions set, energize the igniter and slowly open the fuel control valve until lightoff is obtained. Record lightoff fuel flow rate. Deenergize igniter.

2) Slowly decrease fuel flow rate to blowout. Record lean blowout fuel flow rate.

3) Decrease fuel and air inlet temperatures in 5 to 8 K increments and repeat Steps 1 and 2.

When the minimum temperature limit was established, the second portion of the test was begun: altitude relight.

3. Altitude Relight Test Procedure

The second portion of the test with each fuel was structured to evaluate altitude relight and stability characteristics. The test schedule is also shown in Table 13. Investigations were carried out at four airflow rates (0.23, 0.41, 0.50, and 0.91 kg/s) selected to span the J79 engine altitude relight requirement map (Figure 12). Air temperature was selected from the windmilling data and ranged from 244 K to ambient. Fuel temperature was matched to the air temperature. The test sequence was structured to determine:

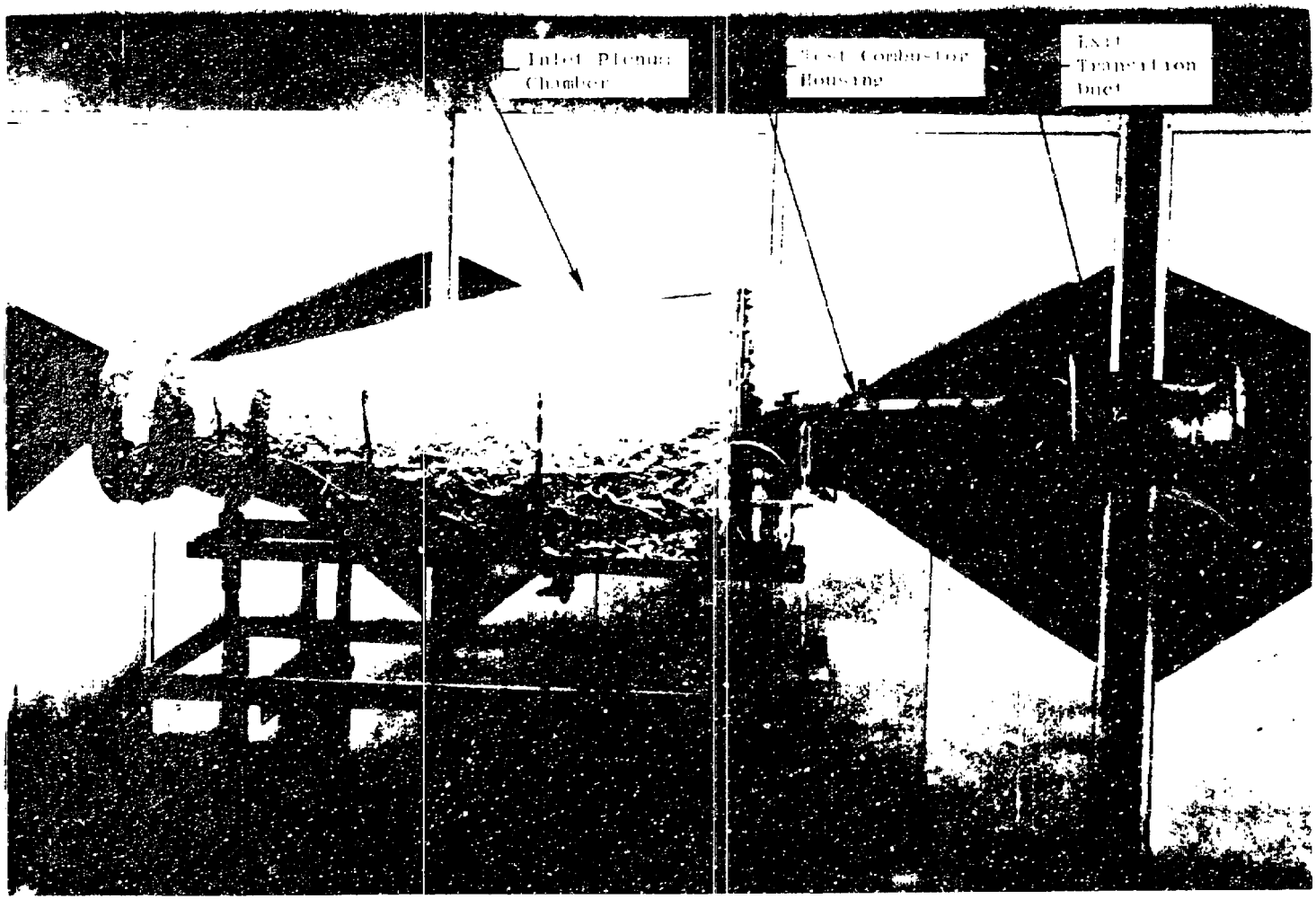

Figure 27. Low Pressure J79 Combustor Test Rig.

Table 13. Low Pressure Test Point Schedule.

Test Point Number	Simulated Flight Altitude, km	Simulated Flight Mach Number	W_c, Combustor Airflow, kg/s	P_3, Air Inlet Pressure, kPa	T_3, Air Inlet Temperature, K	T_f, Fuel Temperature, K	W_f, Fuel Flow, g/s	Comments(1)
1.1.1	0	0	0.318	101	277	277	0-7.56	Determine W_f at LO
1.1.2	0	0	0.318	101	277	277	0-7.56	Determine W_f at LBO
1.2.1	0	0	0.318	101	272	272	0-7.56	Determine W_f at LO
1.2.2	0	0	0.318	101	272	272	0-7.56	Determine W_f at LBO
1.3.1	0	0	0.318	101	266	266	0-7.56	Determine W_f at LO
1.3.2	0	0	0.318	101	266	266	0-7.56	Determine W_f at LBO
	Continue 1.X.X Sequence Until Ground Start T_3 Limit is Determined, or T_3 = 239 K							
2.1.0	15.2	0.89	0.227	24.1	244	244	4.22	Starting point for Series
2.1.1	--	--	0.227	--	244	244	4.22	Determine P_3 min. at LO
2.1.2	--	--	0.227	--	244	244	4.22	Determine P_3 min. at PBO
2.1.3	--	--	0.227	--	244	244	0-7.56	Determine W_f min. at LO
2.1.4	--	--	0.227	--	244	244	0-7.56	Determine W_f min. at LBO
2.2.0	15.2	1.08	0.408	41.4	277	277	4.22	Same sequence as 2.1 to determine altitude LO, LBO, and PBO limits.
2.3.0	15.2	1.14	0.500	62.0	Amb.	Amb.	4.22	
2.4.0	15.2	1.22	0.901	68.9	Amb.	Amb.	4.22	

(1) LO = Lightoff (Increasing W_f or P_3)

LBO = Lean Blowout (Decreasing W_f)

PBO = Pressure Blowout (Decreasing P_3)

1) The maximum relight and blowout pressure altitudes with current engine minimum fuel flow rates (4.22 g/s/can).

2) The minimum relight and lean blowout fuel flow rates at the relight altitudes determined in (1).

The test sequence was as follows:

1) With 15.2 km (50,000 ft) altitude conditions set, energize the igniter, set fuel flow rate at 4.22 g/s, then increase combustor inlet pressure (reduce altitude and flight Mach number) until ignition occurs. Deenergize the igniter and record maximum relight altitude conditions.

2) With fuel flow rate at 4.22 g/s, slowly reduce combustor inlet pressure until blowout occurs. Record maximum pressure altitude blowout conditions.

3) Energize igniter and increase fuel flow until lightoff. Deenergize igniter and record minimum lightoff fuel flow rate at maximum relight altitude.

4) Slowly reduce fuel flow rate until blowout. Record lean blowout fuel flow rate at maximum relight altitude conditions.

5) Repeat Steps 1 through 4 at each airflow setting.

The J79-17A combustion system has excellent relight characteristics, so the facility minimum pressure capability (about 40 kPa, corresponding to an altitude of over 18 km) was often encountered before a pressure blowout limit was reached.

C. Fuel Nozzle Fouling Tests

Tests with each of the fuels were conducted to determine the relative tendency to cause fuel nozzle fouling, which might be in the form of valve sticking, metering slot plugging, or carbon buildup in spin chambers and orifices. The J79 fuel nozzle was known to have a long, trouble-free service life and to be quite tolerant of fuel property variation. It was anticipated; therefore, that the test conditions would need to be extra severe to produce any significant fouling in a short test.

The tests were conducted in the Building 304-1/2 Combustion Laboratory using the simple test rig shown in Figure 28. In this setup, hot fuel is flowed through the fuel nozzle which is immersed in a high velocity hot gas stream. Initially selected test conditions were:

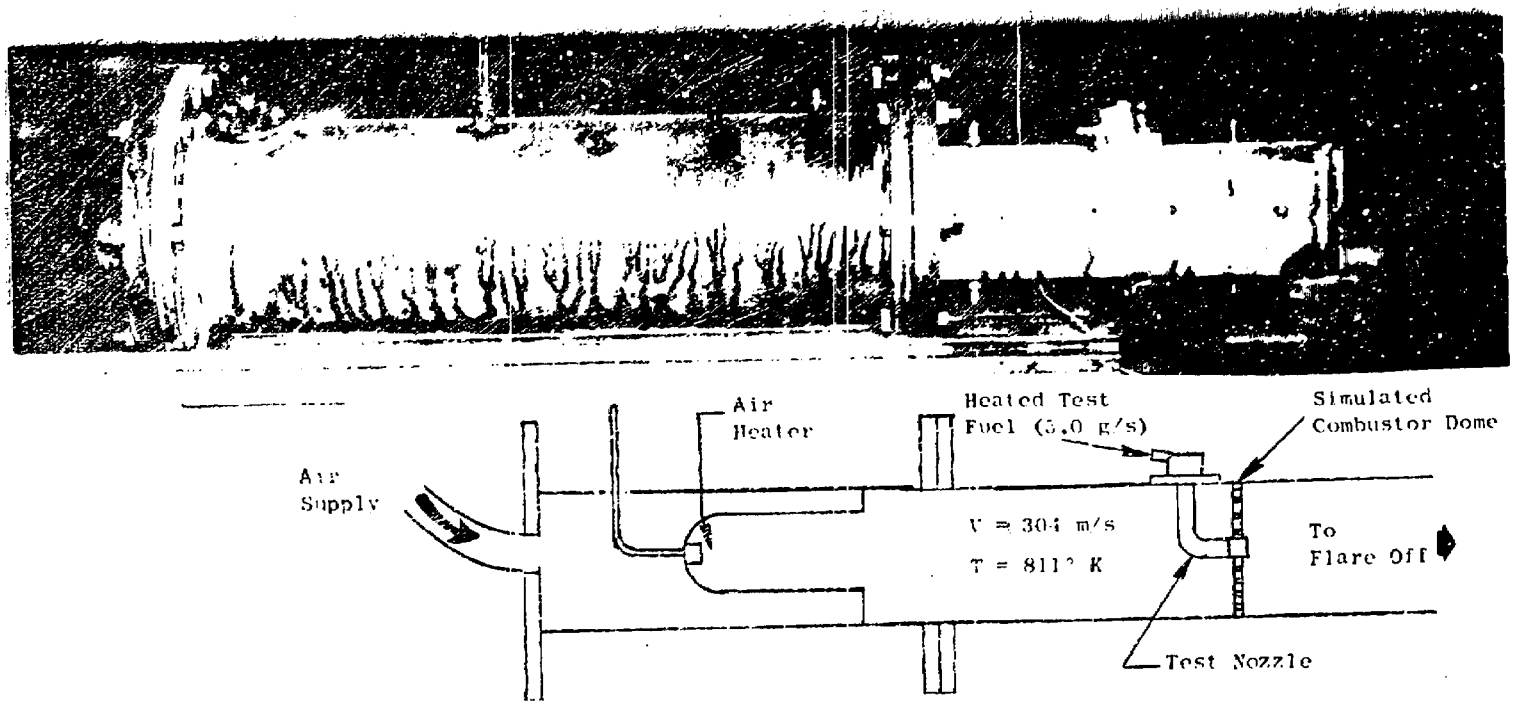

Figure 28. Fuel Nozzle Fouling Test Setup.

Gas Temperature	811 K
Gas Velocity at Fuel Nozzle Stem	304 m/s
Gas Pressure Drop Across Fuel Nozzle Air Shroud	13.8 kPa
Fuel Flow Rate	5.04 g/s
Fuel Temperature	436 K
Run Time	300 minutes (total)

Both the gas temperature (and velocity) and the fuel temperature were significantly higher than are normally encountered in J79 engine use, and this elevation was expected to accelerate the fouling tendency. Moreover, the fuel flow rate was much lower than ever encountered at high temperature engine conditions and this depression was expected to further aggravate the fouling tendency. At this low flow rate only the primary nozzle was flowing.

The fuel nozzles were cleaned before each test, then run for 300 minutes, with a shutdown at 100 minutes for an intermediate flow calibration. Fuel temperature was increased to 478K after the second test because no fouling had been detected. Also, some changes in nozzle flow divider valve configuration were made in later tests; these changes are described in Section VI-A-9.

D. Test Fuel Handling Procedures

Special procedures were followed in all of the tests to ensure that the test fuels were not contaminated or mistakenly identified. Hand valves were installed in the fuel lines near each of the test rigs for obtaining fuel samples while a test was in progress.

The fuels were delivered in tank trailers, as needed, and transferred into three isolated, underground storage tanks of 40-m^3 capacity each. These tanks had previously contained only clean, light distillates. Nevertheless, to assure their suitability for this program, they were first emptied as far as possible, using the permanently installed unloading pumps. The manhole covers were then removed, and the few inches of remaining liquid were pumped out using a portable pump. The tanks were then inspected and found to be in good condition with only a light, adherent coating of rust on all interior surfaces. These surfaces were washed down with a small quantity of the next test fuel, and this was then removed with the portable pump. After replacing each manhole cover, the test fuel was transferred into the tank, and a sign identifying the test fuel was placed on the switch controlling the tank unloading pump. This procedure was repeated for each of the first 12 test fuels. The thirteenth test fuel, the diesel, was handled in a similar manner except that it was stored in a tank trailer parked near the underground storage tanks.

As fuel was needed for the high pressure tests, it was transferred from the appropriate tank, using a 4 m^3 stainless steel tank trailer. This tank also was drained and flushed with the next test fuel before being loaded. After filling, it was marked with the proper fuel number, hauled to the test site, and parked adjacent to the test cell. The tank drain valve was connected directly to the cell system by a flexible hose, after flushing the hose with a suitable volume of test fuel. In the test cell immediately before the line entered the test rig, a valved line was teed off for drawing samples. This location was selected because it insured that the fuel actually used in the test was being sampled.

For the tests planned, it was not intended to change fuels during a test, so the fuel sampling procedure consisted of drawing a sample just before the first data point was taken and again after the last data point was taken. In each case, the sample container was rinsed twice with a small portion of the fuel being sampled, before actually taking the sample.

Similar sampling procedures were followed in both the altitude relight and the fuel nozzle fouling tests. For both of these tests, fuel was transferred from the trailer to clean drums which were clearly marked and moved to the test sites. These drums were in good condition and had previously contained only clean materials, such as calibrating fluid. Before filling, they were drained, inspected, and rinsed with the next test fuel.

Pretest samples taken at the test sites were returned to Wright-Patterson Air Force Base for verification of significant characteristics, to determine whether fuel quality had been compromised during storage or handling at the several test sites. Analyses included density, viscosity, surface tension, and vapor pressure. These analyses were performed by Monsanto Research Corporation.

A compilation of these data is shown on Table 14. From a comparison of the properties of the original samples with those of samples returned from the several test sites, it is apparent that no significant change in fuel properties occurred. Therefore, it was concluded that fuel handling procedures were satisfactory, and analysis of samples of the remaining test fuels was considered unwarranted.

Table 14. Fuel Verification Analyses.

(All Properties at 311K)

Sample Source	Fuel No.	Density, kg/m^3	Viscosity, mm^2/s	Surface Tension, mN/m	Vapor Pressure kPa
Original	1	744.0	0.816	22.17	17.1
Relight Test	1	744.0	-	21.4	16.5
Relight Test	1	743.5	-	22.6	16.3
Fouling Test	1	744.0	-	22.3	15.9
Fouling Test	1	743.9	-	21.8	16.1
Perf./Emission Test	1	745.3	0.825	-	-
Perf./Emission Test	1	744.8	0.823	-	-
Original	2	791.4	1.555	24.80	2.7
Relight Test	2	791.6	-	25.1	2.5
Fouling Test	2	791.8	-	25.0	2.3
Fouling Test	2	791.2	-	25.5	2.5
Perf./Emission Test	2	791.1	1.530	-	-
Original	3	793.2	1.721	24.87	2.4
Fouling Test	3	793.7	-	25.0	1.5
Fouling Test	3	793.1	-	25.2	1.5
Relight Test	3	793.3	-	25.5	2.6
Perf./Emission Test	3	793.5	1.708	-	-

E. Data Analysis Procedures

Generally standard data reduction and presentation techniques were employed Key parameters and calculation procedures are indicated in Table 11 and Appendix A. Some additional special procedures are described in the following sections.

1. Fuel Property Correlation Procedures

Analyses of the experimental test results were conducted to: (1) correlate the performance and emission parameters with combustor operating conditions; (2) as appropriate, correct the measured rig data to true standard day engine operating conditions; and, (3) correlate the corrected data with the appropriate fuel properties from Section III. To illustrate the procedure, the CO emission data is outlined below.

Inspection of the CO emission data for the first two high pressure tests (JP-4 fuel, Table A-1) showed that as in Reference 7 the data were in the form.

$$EI_{CO} = k_\theta \left(\frac{V_r}{24.1}\right) \left(\frac{0.248}{P_3}\right)^{k_1} \left[\exp\left(\frac{421 - T_3}{k_2}\right)\right] = k_\theta \, S_{CO} \qquad (5)$$

where the combustor operating parameters (V_r, P_3, and T_3) have been normalized to engine operating conditions at idle. Multiple regression techniques were employed to determine the constants k_θ, k_1, and k_2. A very good correlation was found, as shown in Figure 32. Additional analyses showed that in general k_θ was slightly fuel dependent, but k_1 and k_2 essentially not. The CO emission operating or severity parameter was then taken to be:

$$S_{CO} = \left(\frac{V_r}{24.1}\right) \left(\frac{0.248}{P_3}\right)^{0.7} \left[\exp\left(\frac{421 - T_3}{150}\right)\right] \qquad (6)$$

which is tabulated in Table A-2, and was used as shown in Table A-3 to correct measured test data to true engine operating conditions by the relationship:

$$EI_{CO\ engine} = EI_{CO\ test} \left(\frac{S_{CO\ engine}}{S_{CO\ test}}\right) \qquad (7)$$

The correction was usually very small except at dash operating conditions (75 percent density in rig tests) as shown in Table A-3. Corrections were then tabulated (Table 15, for example) and plotted against appropriate fuel properties (Figures 33 and 34, for example). Equations for the effect of fuel hydrogen content on CO emissions shown in Figure 33 are the result of regression analyses, and show, for example, that

$$EI_{CO,\ cruise} = 14.8 \left(\frac{H}{14.5}\right)^{-1.38} \quad g/kg$$

with a correlation coefficient (r) of (-0.753).

2. Combustor Life Prediction Procedures

Field experience shows that the J79 combustor is life-limited by low cycle fatigue crack propagation from the ends of the punched louvers on the inner liner. From the measured metal temperature rises, the stresses that are calculated, including stress concentration factors at these cracks, are well above the yield strength of the material, resulting in plastic yielding on each cycle. Since the metal temperatures are in the range where creep can occur below the yield stress, additional plastic deformation occurs beyond that which corresponds to relaxation to the yield stress. This total plastic deformation correlates reasonably well with low cycle fatigue life in many applications.

The J79 combustor, developed before 1960, has a relatively short life and is less amenable to detailed analysis than are more recent combustor designs. The punched louvers of the J79 combustor liner have cracks already initiated at the ends of the punch when the part is new. This crack results in a severe stress concentration region at which crack propagation proceeds. Also, the thermal gradients in the vicinity of the ends of the louver punch are very high because of the presence of the fresh introduction of film air at this point creating a sudden transition from hot metal to highly cooled metal. Total life is influenced by changing stress levels as the cracks propagate and changing metal temperatures due to metal distortion.

Table 15. Summary of CO Emission Test Results.

Fuel Number	CO Emission Index, g/kg			
	Idle	Cruise	Takeoff	Dash
1	68.2	16.5	5.7	2.4
1R	63.8	14.2	4.8	2.6
2	73.2	17.3	5.8	2.9
3	71.2	15.8	4.2	2.2
4	72.4	18.9	4.8	2.5
5	73.4	16.1	4.7	2.6
6	72.6	21.5	8.2	3.2
7	75.5	18.5	3.6	1.5
8	75.9	20.5	3.4	1.7
9	69.7	18.0	3.7	1.9
10	66.2	17.7	4.5	3.7
11	63.4	15.1	3.1	1.6
12	57.0	13.7	4.3	2.7
13	68.0	17.0	3.0	1.5

Cyclic test of simple louver specimens in the presence of thermal gradients have been conducted to provide basic data for estimating the life of punched louver combustors. In these tests, the crack propagated in approximately direct proportion to the number of thermal exposure cycles. Based on these louver specimen findings and low cycle fatigue material properties, the design curve shown in Figure 29 is in use at General Electric for the J79 combustor liner, for either fatigue life to initial cracking or for crack propagation rate. From this curve it can be estimated that a 45 K change in liner temperature results in about a factor of two change in life.

Definitive experience from J79 engines for combustor life effects with different fuels or with different metal temperatures does not exist. Difference in life of about 25 percent has been observed between Navy (JP-5) and Air Force (JP-4) operational experience. It is believed that differences in operational usage are as large an influence on life as is the fuel difference and may, therefore, mask any attempt to attribute this observed life difference to the fuel type alone. However, a 25 percent life reduction is predicted by the trends shown in Figure 29 for a metal temperature change of 20 K, and based on the data in Reference 5, this is approximately the metal temperature change expected for a change in hydrogen content of 14.5 to 13.8 percent.

The aft combustor liner has much longer life than does the inner liner and it is not affected by fuel type. It was noted in Reference 6 that the metal temperatures in the aft portion of the outer or rear liner were not affected by the luminosity changes of fuels that did affect the upstream inner liner. These data were not actually presented in Reference 6, so they are presented here in Figure 30. Temperature measurements were not taken in this aft liner region in this present program because of this experience, and no difference in aft liner life with fuel changes is predicted.

3. Turbine Life Prediction Procedures

If alternate fuels created substantial changes in temperature pattern factor or temperature profile in the combustor exit gases, changes in turbine component life would be predicted. However, as discussed in Section VI-A-6 no changes were found in these parameters. As indicated above in Figure 30, the aft liner temperatures which are well away from the high flame luminosity were unaffected by the same fuel changes that affected significantly the forward liner; therefore, the stator vanes in the turbine

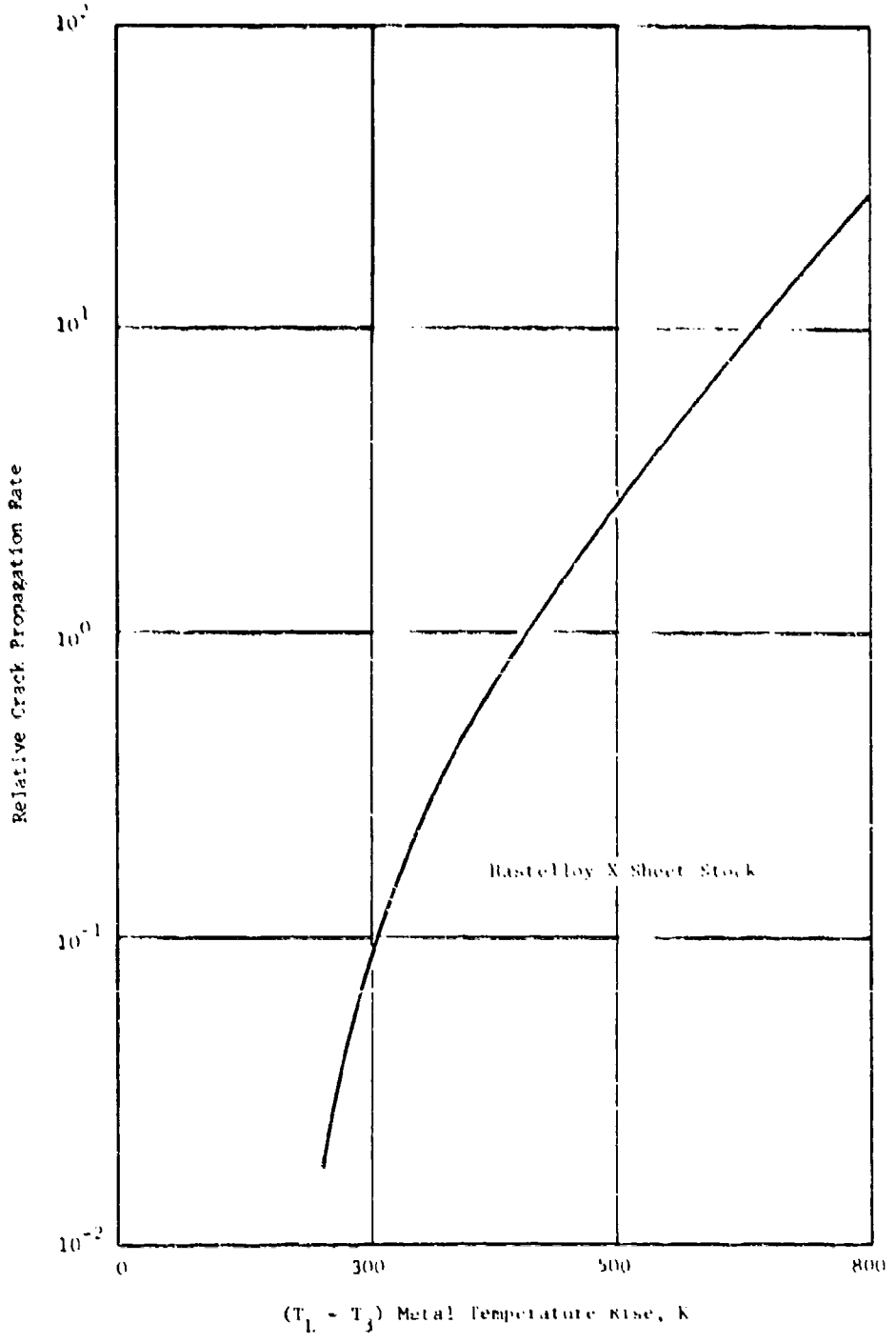

Figure 29. Effect of Temperature Gradient on Crack Propagation Rate.

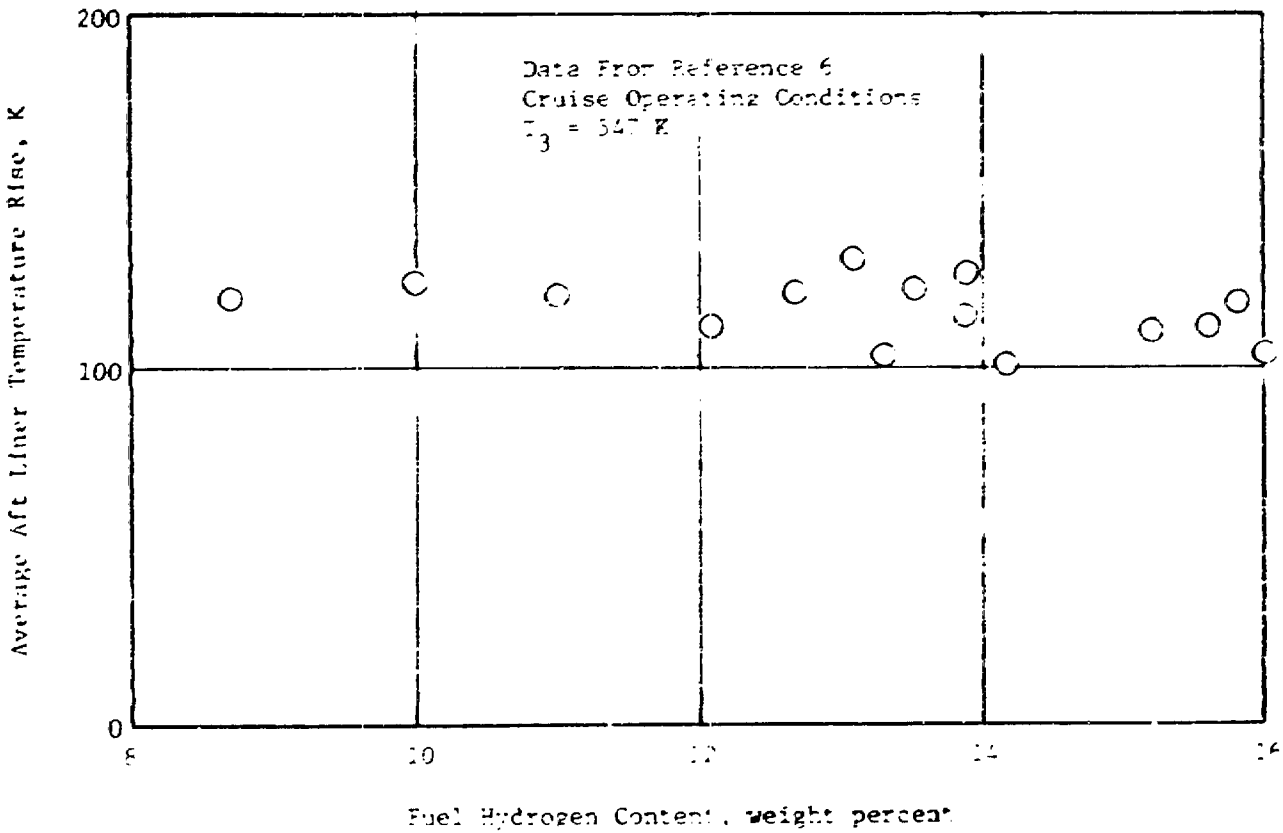

Figure 30. Effect of Fuel Hydrogen Content on Aft Liner Temperature.

diaphragm which are even further away from these flame luminosity effects are also expected to be negligibly affected. Figure 31 illustrates the very small view the stator leading edge has of the luminous flame region. This small view factor results in negligible effects in the J79 engine. However, in other engines with annular combustors and shorter combustors, large view factors exist and flame luminosity may in some cases become significant to the vane leading edge temperature.

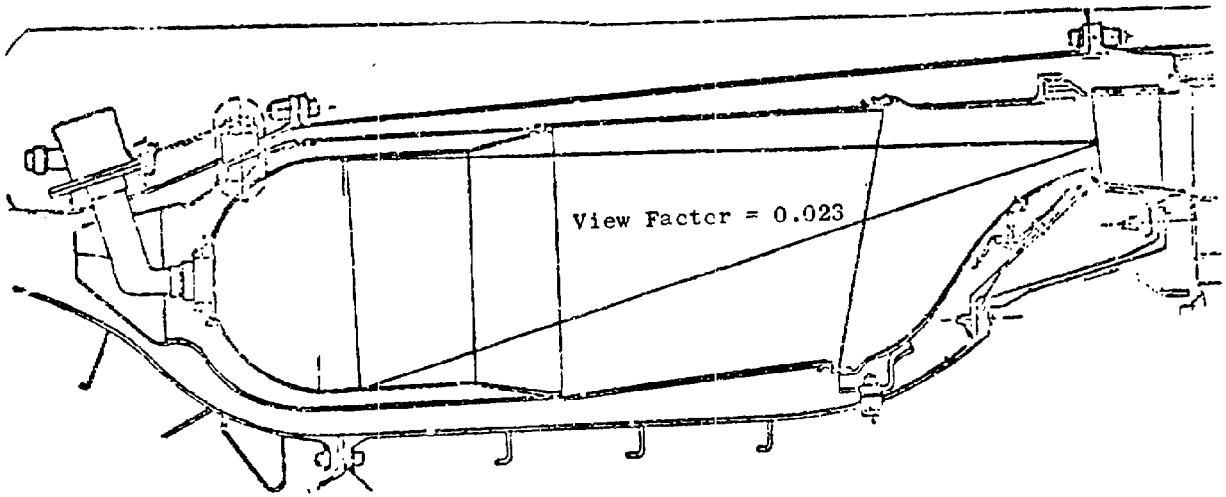

Figure 31. Turbine Nozzle Diaphragm View Factor.

SECTION VI

RESULTS AND DISCUSSION

All planned test series (44 total) were completed and no major problems were encountered. In general, results were well ordered and consistent with published data insofar as comparisons could be made. Detailed test results, which are listed in Appendices A through E, are summarized and discussed in the following section. Engine system life prediction analyses based on these results are then presented in Section VI-B. Further, an overall assessment of these tests and analyses is presented in Section VI-C.

A. Experimental Test Results

Fourteen high-pressure rig tests were conducted to obtain the performance/emissions/durability data. These data are listed in Appendices A and B and summarized in Sections VI-A-1 through VI-A-7. Fourteen low pressure rig tests were conducted in parallel to obtain the ground start and altitude relight data. These data are listed in Appendix C and summarized in Sections VI-A-7 and 8. Also in parallel, 18 fuel nozzle fouling tests were conducted to obtain the data listed in Appendix D and summarized in Section VI-A-9.

1. CO and HC Emissions

Carbon monoxide (CO) and unburned hydrocarbons (HC) are both products of incomplete combustion, and are, therefore, generally highest at low power operating conditions (idle and cruise). Figure 32 shows the strong effect of combustor operating conditions on CO emission levels with JP-4 fuel. At idle operating conditions, the CO emission index is about 64 g/kg which corresponds to a combustion inefficiency of about 1.5 percent and is in good agreement with engine measurements. At cruise, takeoff, and dash operating conditions, the CO emission levels are approximately 29, 7, and 3 percent, respectively, of the idle CO emission level, which indicates the strong effect of combustor inlet temperature and pressure on combustion reaction rates, and hence, on combustion efficiency and CO emission levels. These pressure and temperature effects, determined by multiple regression curve-fit techniques of these data, are in good agreement with previous results (Reference 7). Within these test limits, no effect of fuel-air ratio is evident. Moreover, very good repeatability between the two combustor assemblies and test runs is indicated.

Carbon monoxide emission results very similar to those shown in Figure 32 were obtained with each of the other fuels, and all of the results are listed in Table 15. The effect of fuel hydrogen content on CO emission levels at each of the power levels is shown in Figure 33. At takeoff and dash operating conditions CO levels are very low and virtually independent of fuel hydrogen content, and any other fuel property. At cruise operating conditions a significant fuel hydrogen effect (negative 1.38 exponent) is indicated, but no effect of other fuel properties (aromatic type or base fuel) is evident. At idle operating conditions, a relatively weaker fuel hydrogen effect (negative 0.47 exponent) is indicated, but the correlation is poor and other fuel property

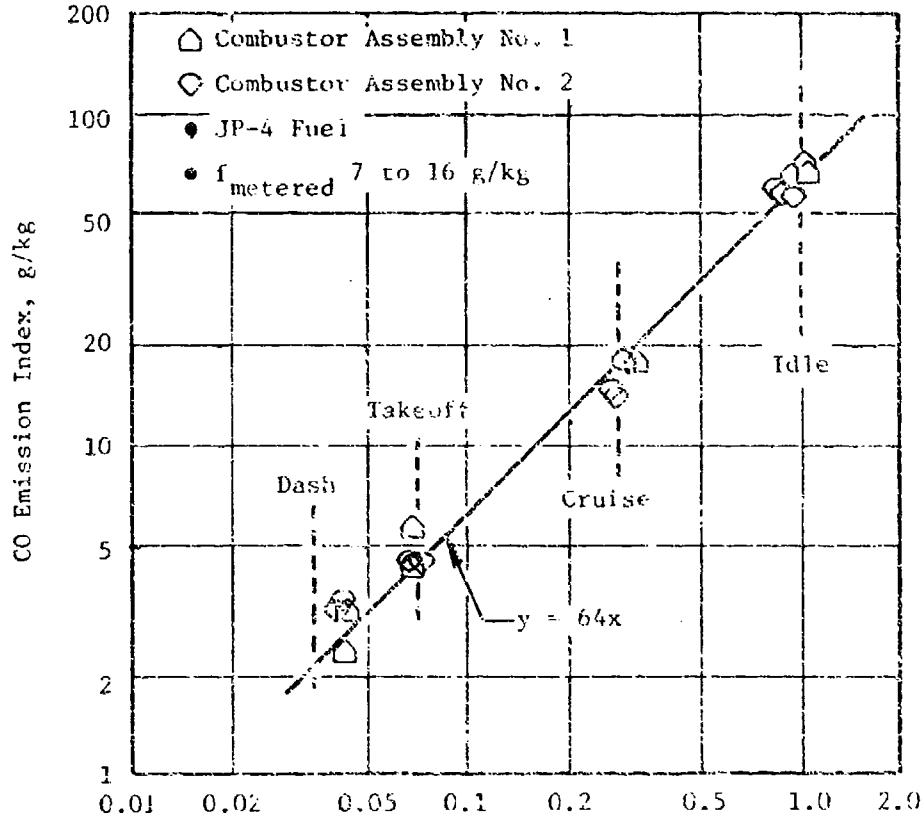

$$S_{co} = \left(\frac{V_r}{24.2}\right)\left(\frac{0.248}{P_3}\right)^{0.7}\left[\exp\left(\frac{421-T_3}{150}\right)\right], \text{ m/s, MPa, K}$$

Figure 32. Effect of Operating Conditions on CO Emission Levels.

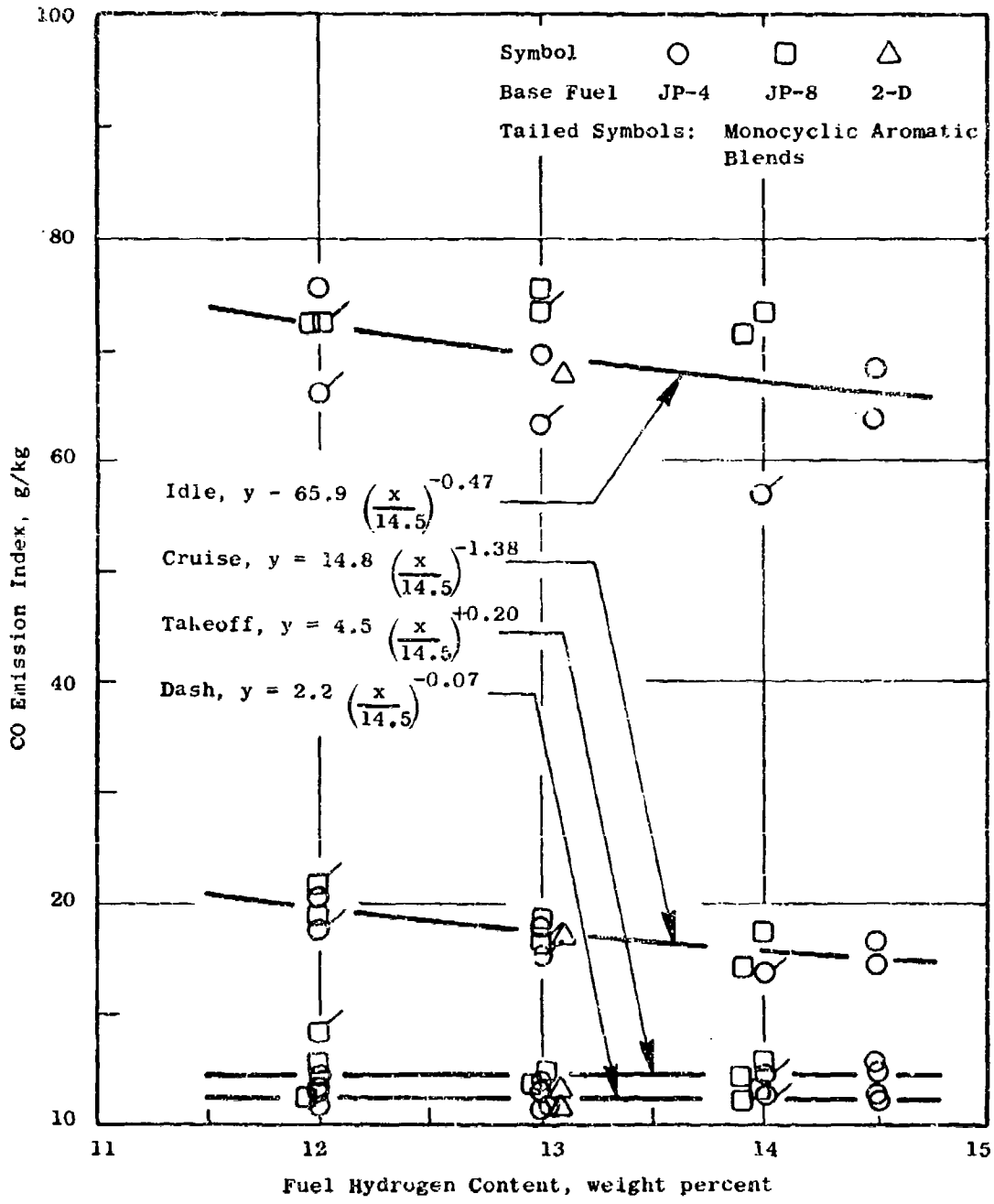

Figure 33. Effect of Fuel Hydrogen Content on CO Emission Levels.

effects are evident. In particular, the lowest idle CO levels are obtained with the JP-4/monocyclic aromatic blends, suggesting a volatility or atomization effect. Figure 34 shows these same idle CO data plotted (without regard to hydrogen content) against relative spray droplet size (from Table 7) or fuel 10 percent recovery temperature (from Table 3), the latter being one of the more commonly used indicators of fuel volatility. It appears that either of these parameters correlates the idle CO data better than does hydrogen content. Both of these properties can be expected to affect idle emissions, but for these tests it is difficult to judge which property is most important since, for these fuels at least, they turn out to be highly interrelated (mathematically compounded). There is some indication in Figure 34 that for the JP-4-based fuels, the volatility parameter better correlates the results than does the droplet size parameter.

Hydrocarbon emission levels generally have been found to follow the same trends as do CO emissions, but to be more sensitive to combustor operating conditions and to exhibit more variability. Both of these trends were observed in the present tests and are illustrated in Figure 35, where HC emission levels are plotted against CO emission levels for the idle and cruise test points and all fuels. At idle the HC index is about 25 g/kg (2.3 percent inefficiency). At cruise the levels are an order of magnitude lower, and at takeoff and dash conditions the levels were very low. There is considerable scatter in the cruise and idle data, but the regression curve fit exponent (1.79) is in good agreement with past experience (about 1.5 to 3.0). Table 16 summarizes the HC results for all fuels and operating conditions. The idle and cruise data are plotted against fuel hydrogen content in Figure 36. The idle data are further plotted against fuel volatility and relative spray droplet size in Figure 37. Neither of these plots indicates any clear fuel property effect on the HC emission levels.

2. NO_x Emissions

Oxides of nitrogen (NO_x) may form from oxidation of nitrogen which originated either in the air or in the fuel. Current jet engine fuels and all of the fuels used in this program contained negligible amounts of bound nitrogen, but in the future, alternate sources and/or processing economics may result in significant quantities of bound nitrogen in aircraft fuels. The following discussion is therefore applicable only to the "thermal" NO_x production characteristics of current and advanced fuels. Fuels containing significant quantities of bound nitrogen have been investigated in other programs, and typical results are contained in References 8, 9, and 10.

In contrast to CO and HC emissions, which are products of incomplete combustion and are, therefore, generally significant only at low power conditions, "thermal" NO_x is an equilibrium product of high temperature combustion, and is therefore highest at high power operating conditions. Figure 38 shows the strong effect of combustor operating conditions on NO_x emission levels with JP-4 fuel. The data for both combustor assemblies correlate well with a combustor operating severity parameter determined by curve fit techniques as described in Section V-E-1. This correlation shows the significant effects of inlet pressure, temperature, humidity, velocity, and fuel-air ratio. At takeoff conditions, the NO_x emission index is about 10.5 g/kg, which is in good agreement with several engine measurements. At dash, cruise, and idle operating conditions, the NO_x levels are approximately 166, 42, and 24 percent, respectively, of the takeoff NO_x level. Very similar results were obtained in each of the tests; the results

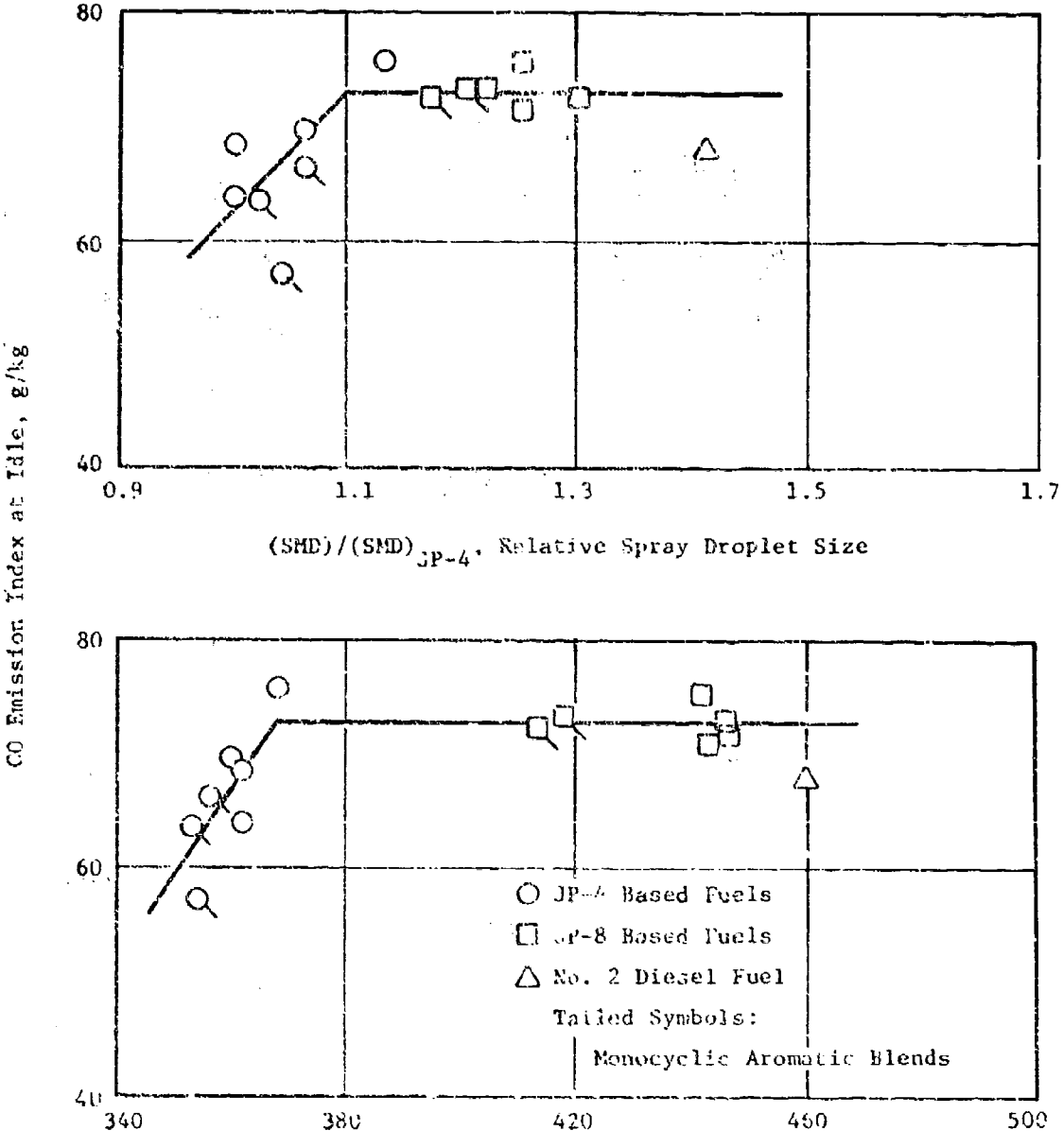

Figure 34. Effect of Fuel Atomization and Volatility on Idle CO Emission Levels.

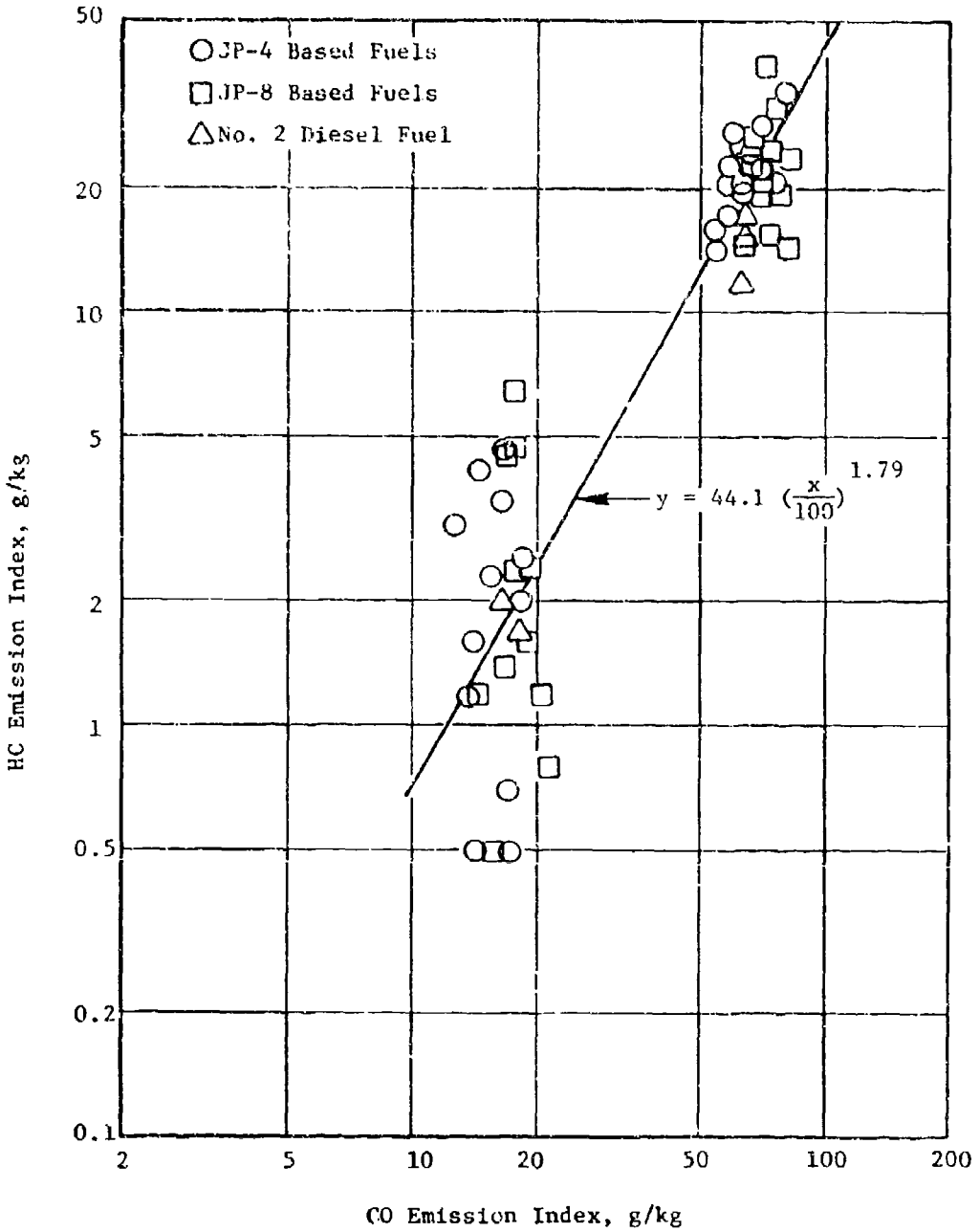

Figure 35. Variation of HC Emission Levels with CO Emission Levels.

Table 16. Summary of HC Emission Test Results.

Fuel Number	HC Emission Index, g/kg			
	Idle	Cruise	Takeoff	Dash
1	23.6	0.5	0.1	0.1
1R	22.6	0.5	0.1	0.1
2	20.4	2.4	2.4	0
3	25.3	0.5	0.1	0
4	15.1	1.0	0.6	0.1
5	23.6	0.5	0	0
6	22.6	0.8	0.3	0.1
7	33.9	2.2	0.9	0.3
8	35.1	-	1.8	0.4
9	30.5	2.6	1.5	0.4
10	22.4	1.9	1.2	0.4
11	26.8	2.2	1.2	0.4
12	17.3	1.5	1.1	0.5
13	15.5	1.5	0.5	0.1

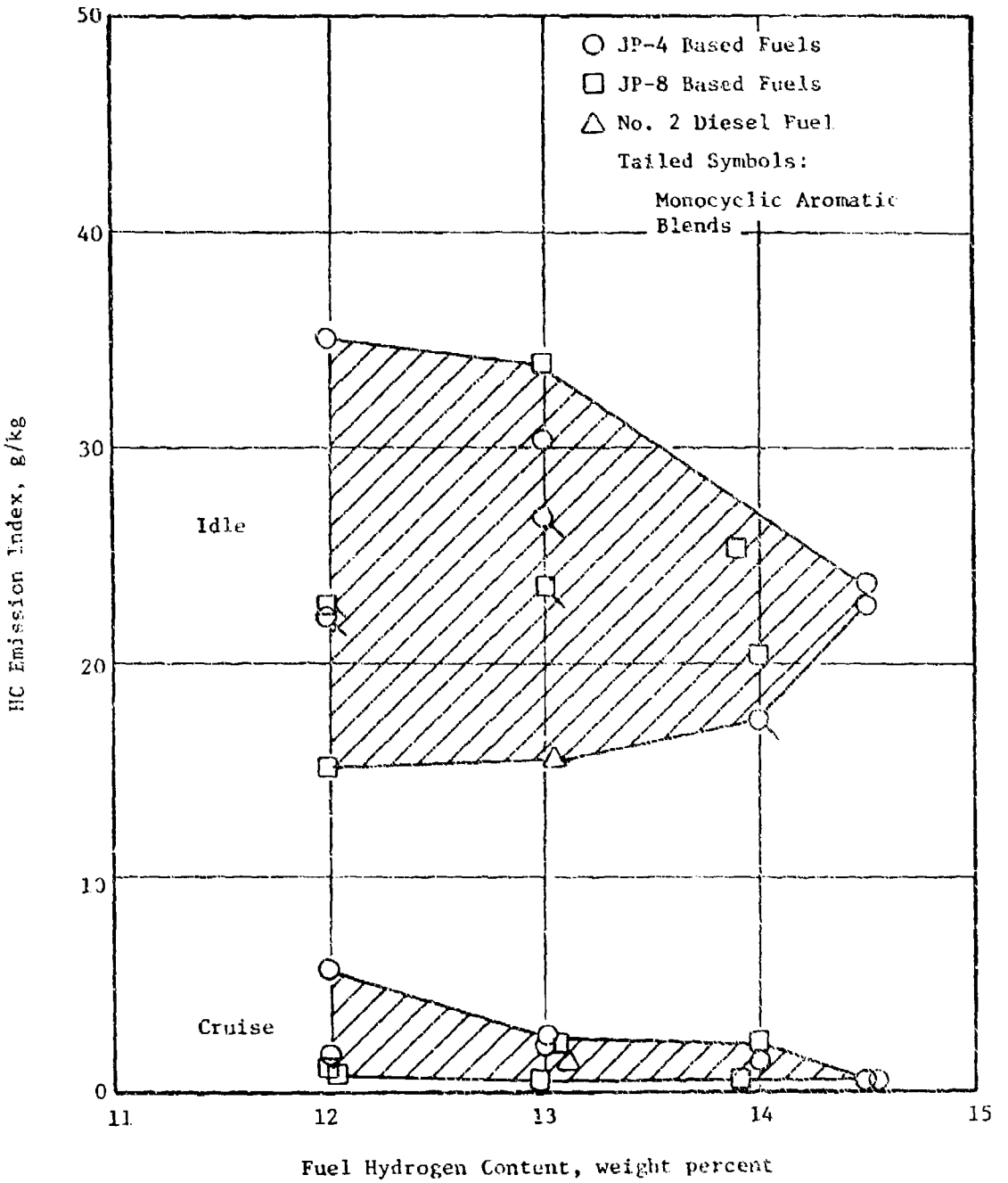

Figure 36. Effect of Fuel Hydrogen Content on HC Emission Levels.

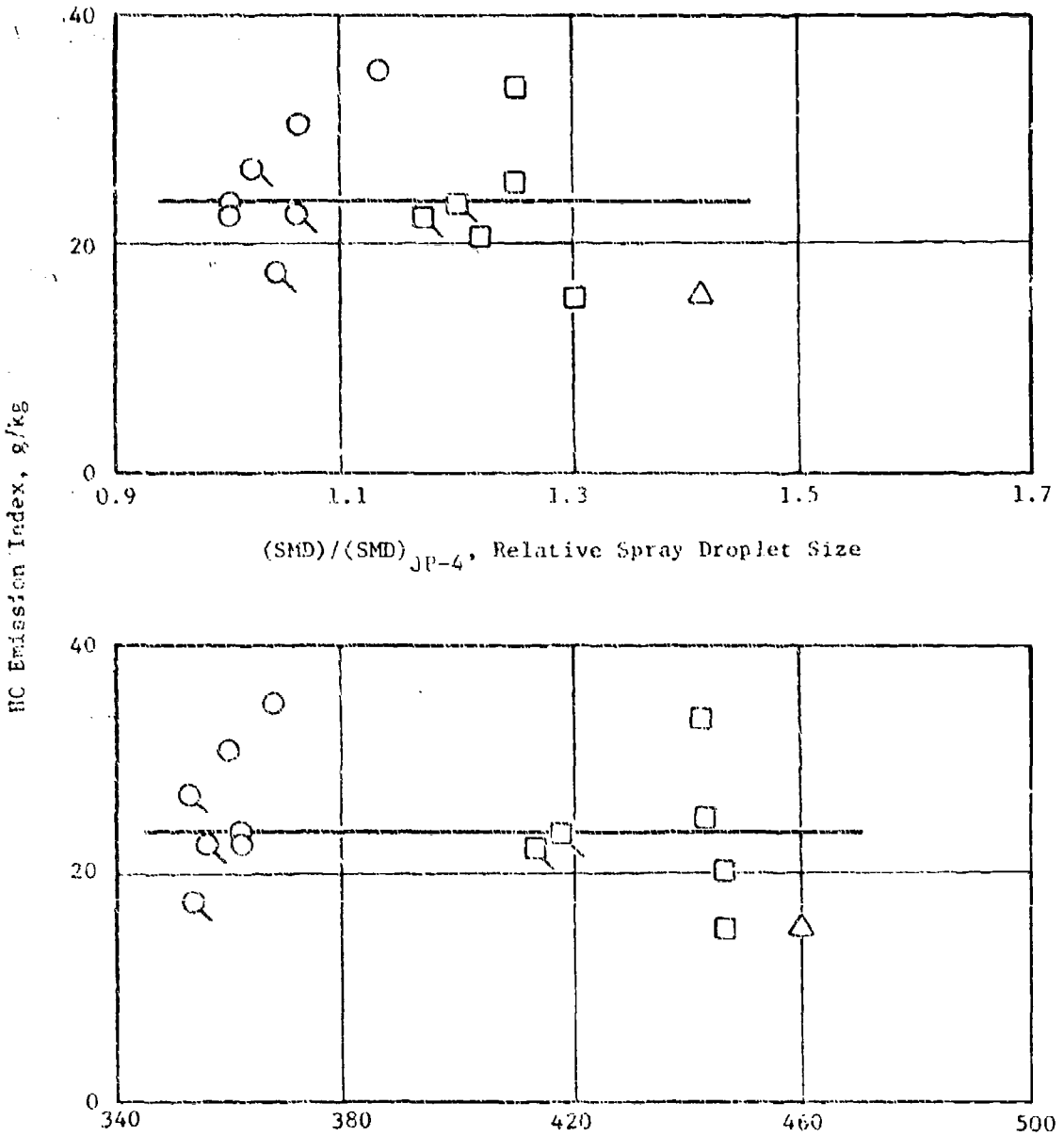

Figure 37. Effect of Fuel Atomization and Volatility on Idle HC Emission Levels.

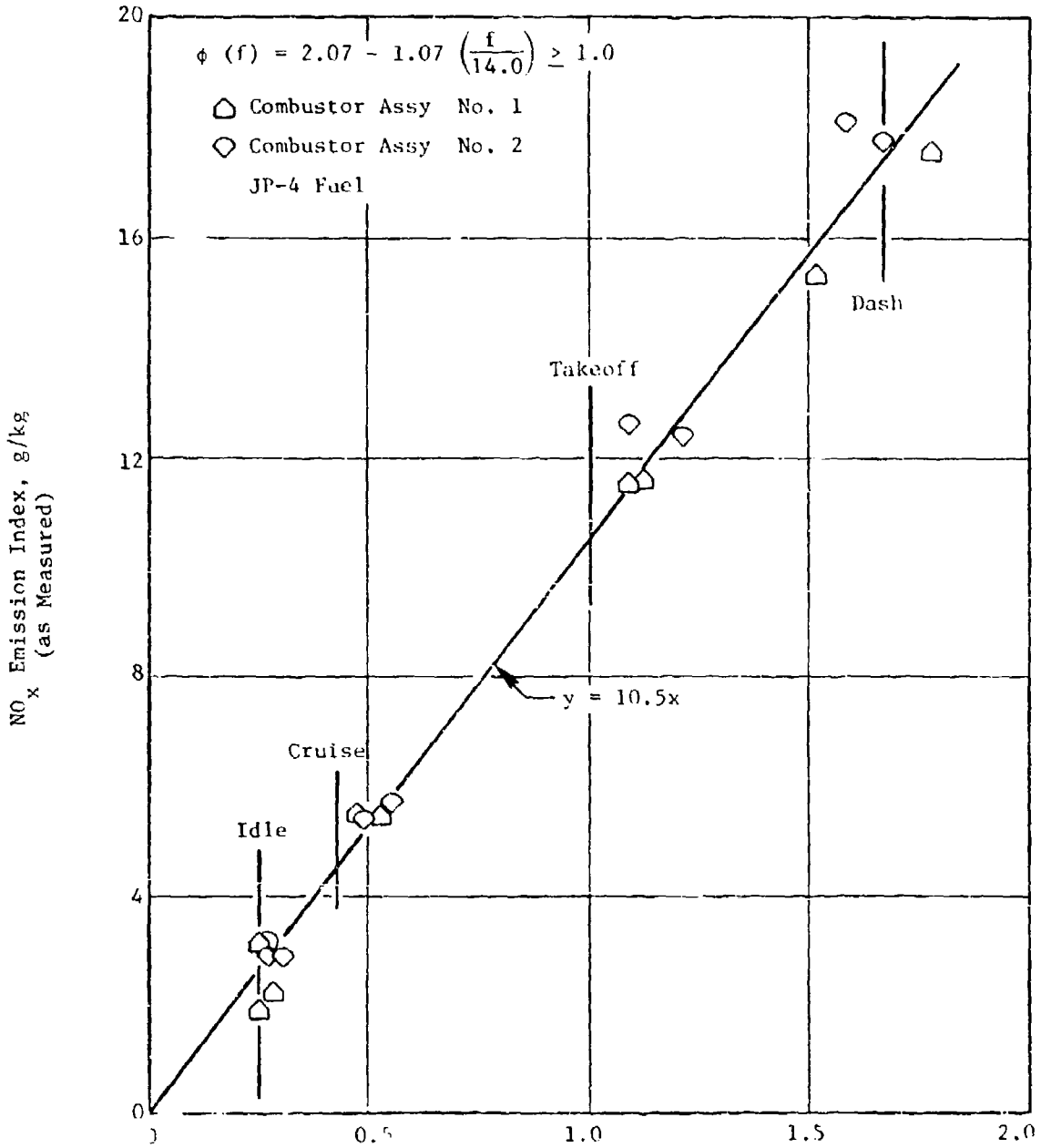

$$SNO_x = \left(\frac{28.6}{V_r}\right)\left(\frac{P_3}{1.359}\right)^{0.37} [\phi\ (f)] \left[\exp\left(\frac{T_3 - 664}{192} + \frac{6.29 - h_3}{53.2}\right)\right]$$

Figure 38. Effect of Operating Conditions on NO_x Emission Levels.

are summarized in Table 17 and Figure 39. At idle and cruise operating conditions, virtually no effect of fuel properties is evident, and at the high power operating conditions (takeoff and dash), NO_x levels decreased with fuel hydrogen content. This dependence on fuel hydrogen content can be predicted for diffusion flame processes such as this because of the flame temperature dependence on fuel hydrogen content and, in turn, the effect of flame temperature on NO_x formation rates. Figure 40 shows the effect of flame temperature (from Table 7) on the NO_x emission levels at takeoff.

3. Smoke Emissions

Smoke, like CO and HC, is a product of incomplete combustion, but combustors with virtually 100 percent combustion efficiency can produce highly visible exhaust plumes, because the soot particle sizes are of the same order as the visible light wave lengths. The J79-17A combustion system produces highly visible exhaust plumes, particularly when fueled with the fuels of lower hydrogen content (Reference 6).

The effect of combustor operating conditions on smoke levels with JP-4 fuel is shown in Figure 41. No simple operating parameter could be derived from the data, so smoke number is merely plotted against combustor fuel-air ratio and keyed as to inlet conditions. Within the test range, there is virtually no fuel-air ratio effect, and the repeatability between combustor assemblies is quite good. At true idle, cruise, and 75 percent density dash operating conditions, the smoke levels are approximately 29, 74, and 65 percent, respectively, of the smoke level at true takeoff operating conditions. At full density dash operating conditions smoke levels might be expected to be somewhat higher at the combustor exit plane and then be partially consumed in the afterburning process. Because of the uncertainty of the extent of these two opposing processes, no corrections were made. However, in Table 18 all of the data have been corrected to engine outlet fuel-air ratio according to the procedure outlined in Appendix E to account for turbine cooling air dilution of the main combustor products. When this correction is applied, the engine smoke number at takeoff with JP-4 fuel (~55) is in good agreement with engine measurements (~62). Also shown in Table 18 are corresponding smoke emission indices, calculated from the smoke number by the procedure described in Appendix E.

In Figures 42 and 43, the effects of fuel hydrogen content on engine smoke number and smoke emission index are illustrated. At low power conditions (idle and cruise) very good correlations are indicated, with no discernable effect of any other fuel property. In particular, these data were studied to determine if any effect of aromatic type could be found, since some investigations have concluded that bicyclic aromatics have a greater adverse effect on flame radiation and smoke than do monocyclic aromatics in the same volumetric concentration. No effect of aromatic type is evident in these low power data, and if there is any effect in the high power data it is less than the data variability.

Table 17. Summary of NO_x Emission Test Results.

Fuel Number	NO_x Emission Index, g/kg[1]			
	Idle	Cruise	Takeoff	Dash
1	2.44	4.29	10.10	16.79
1R	2.70	4.71	11.01	18.26
2	2.82	4.81	11.07	18.28
3	2.79	4.86	11.32	18.76
4	2.73	4.95	11.89	19.88
5	2.98	5.08	11.67	19.26
6	2.44	4.69	11.76	19.91
7	2.47	4.41	10.50	17.52
8	1.96	4.28	11.54	19.92
9	2.22	4.42	11.32	19.27
10	2.72	4.70	10.91	18.06
11	2.31	4.51	11.43	19.40
12	2.41	4.44	10.80	18.13
13	2.62	4.78	11.52	19.29

[1] Corrected to ambient humidity of 6.3 g/kg

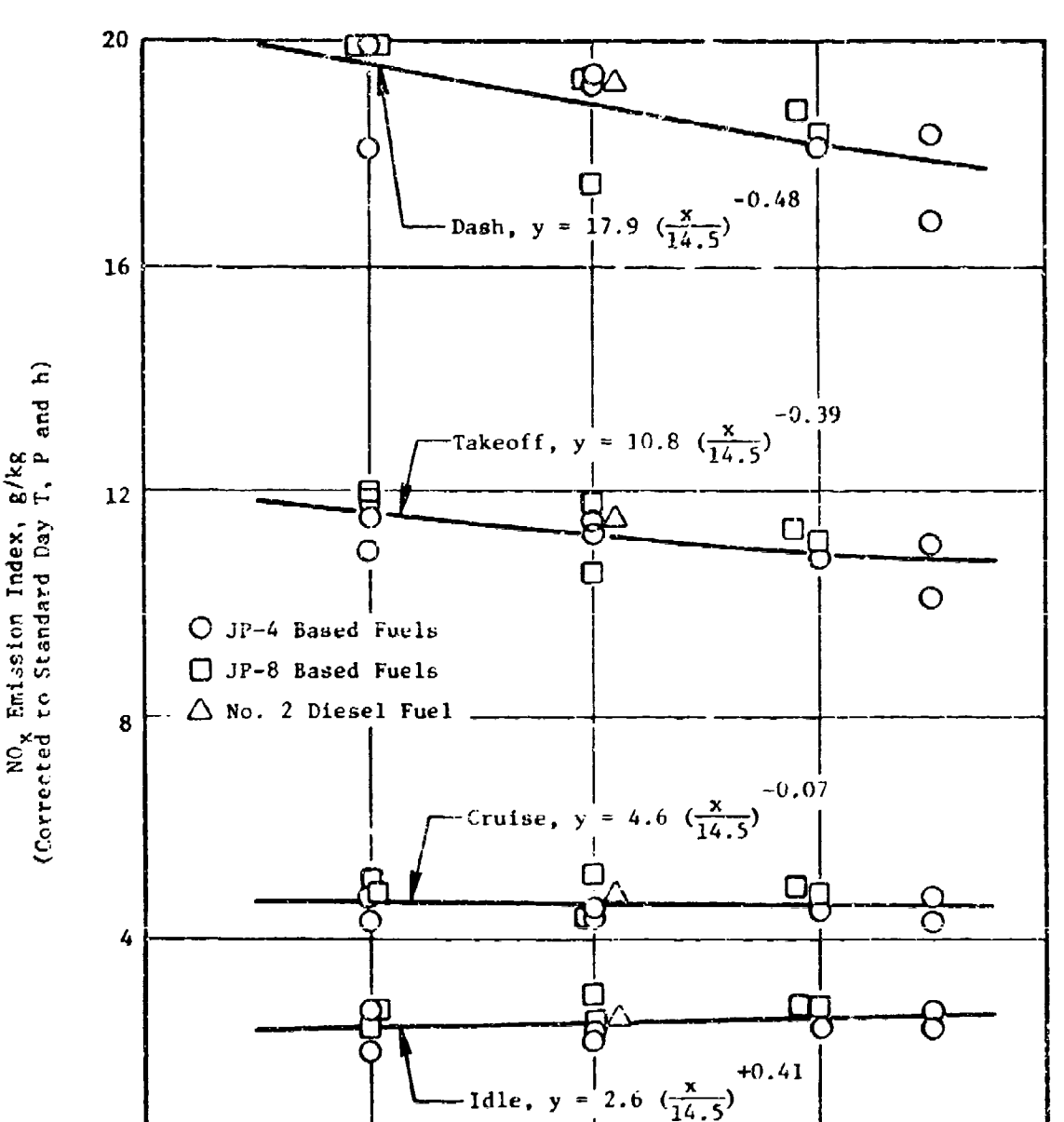

Figure 39. Effect of Fuel Hydrogen Content on NO_x Emission Levels.

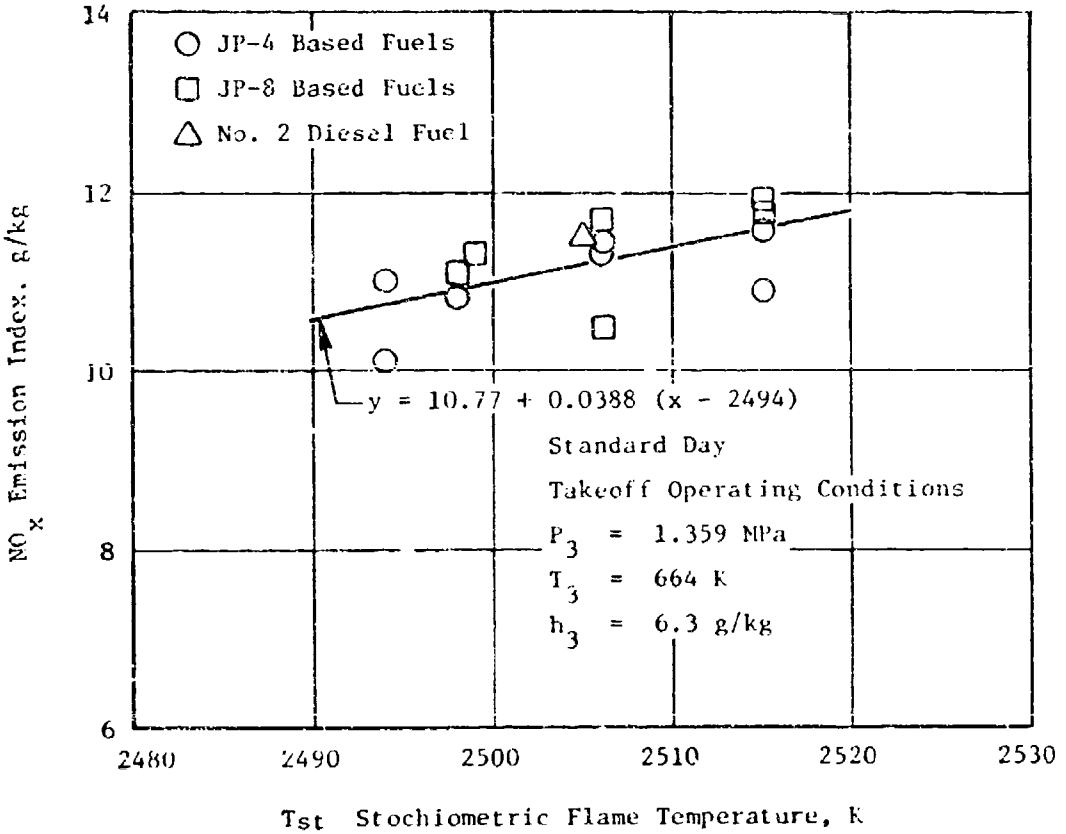

Figure 40. Effect of Flame Temperature on NO_x Emission Levels.

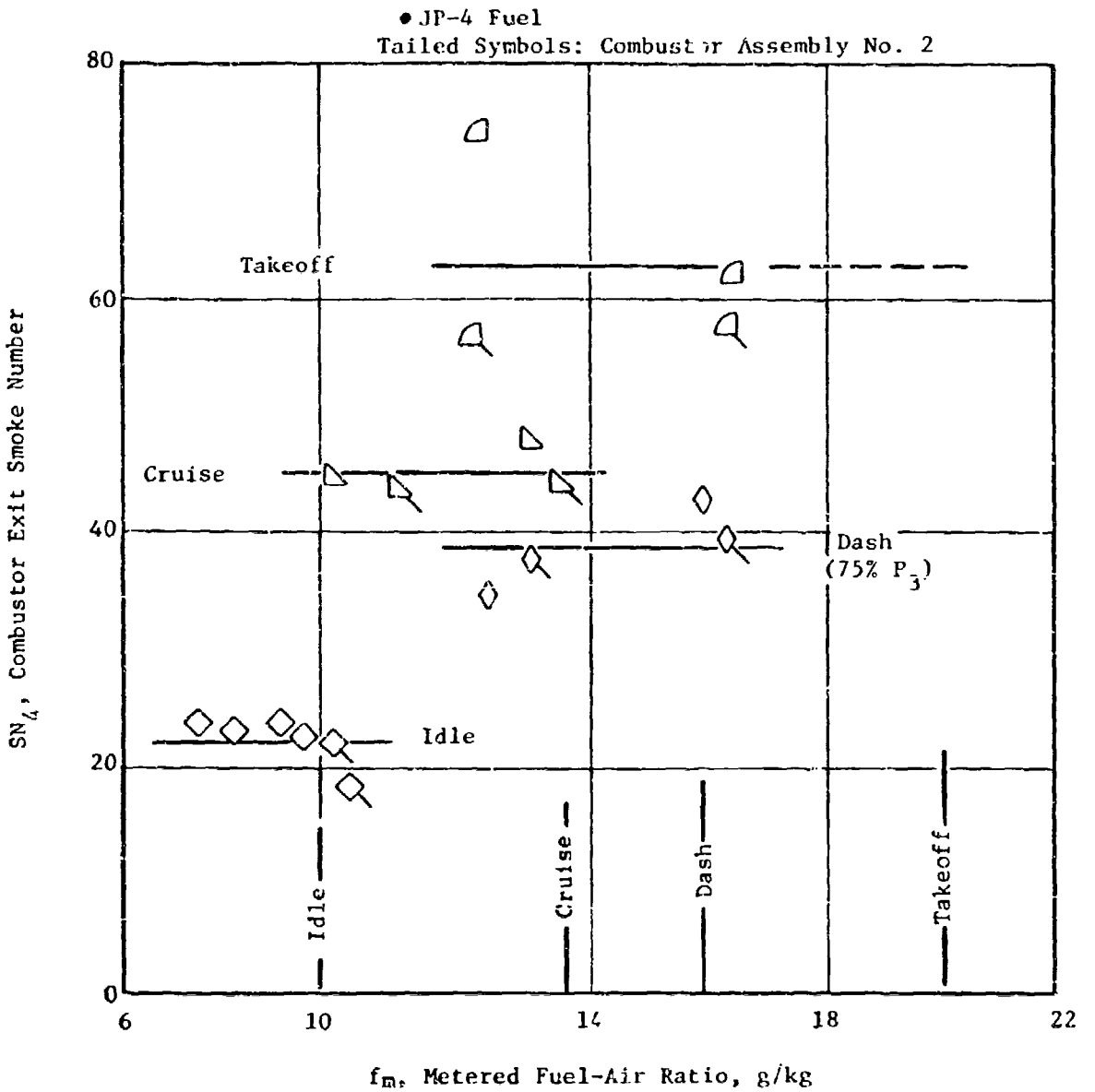

Figure 41. Effect of Operating Conditions on Rig Smoke Emission Levels.

Table 18. Summary of Smoke Emission Test Results.

Fuel Number	SN_8, Smoke Number at Engine Exit				EI_s, Smoke Emission Index, g/kg			
	Idle	Cruise	Takeoff	Dash	Idle	Cruise	Takeoff	Dash
1	17.1	41.4	55.2	36.0	0.20	0.58	1.02	0.34
1R	14.0	37.8	51.5	33.6	0.16	0.45	0.82	0.29
2	28.5	50.1	61.8	38.0	0.38	0.93	1.52	0.39
3	24.1	47.6	53.1	33.3	0.27	0.75	0.91	0.29
4	51.1	77.3	75.8	51.8	1.40	4.43	3.38	0.83
5	38.2	61.6	66.9	40.2	0.70	1.73	1.98	0.43
6	56.0	78.8	72.1	44.4	1.81	4.68	2.68	0.52
7	51.3	69.9	85.6	59.2	1.38	2.90	5.00	1.81
8	52.4	76.6	88.9	74.6	1.50	4.29	6.08	3.26
9	43.5	71.6	73.1	75.2	0.87	3.20	2.38	3.36
10	58.7	77.3	67.1	80.0	2.16	4.49	1.67	4.47
11	43.8	68.3	62.7	47.5	0.89	2.70	1.29	0.65
12	27.4	53.2	63.9	47.1	0.34	1.08	1.38	0.64
13	40.9	61.2	69.4	51.1	0.75	1.73	1.92	0.81

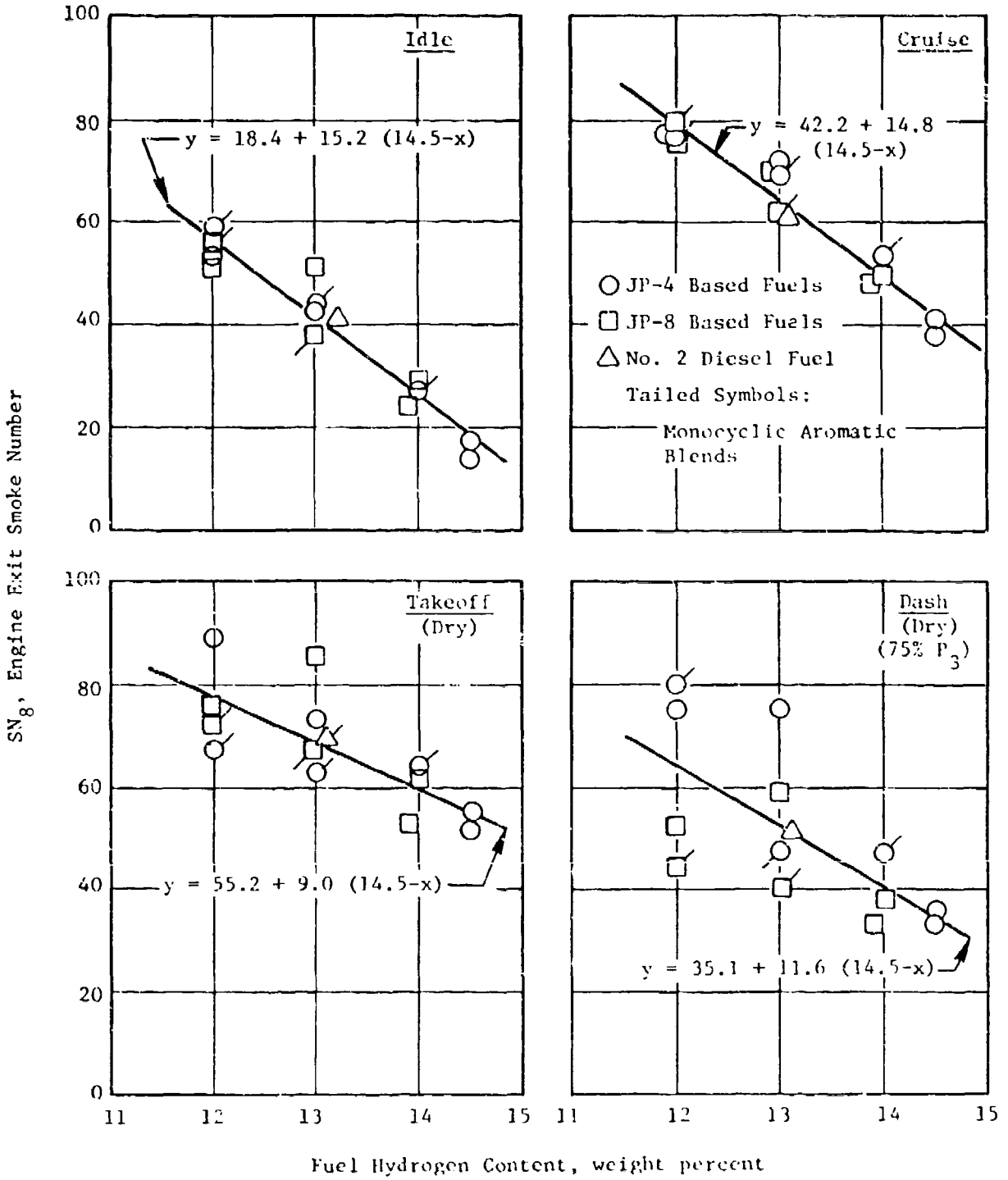

Figure 42. Effect of Fuel Hydrogen Content on Smoke Emission Levels.

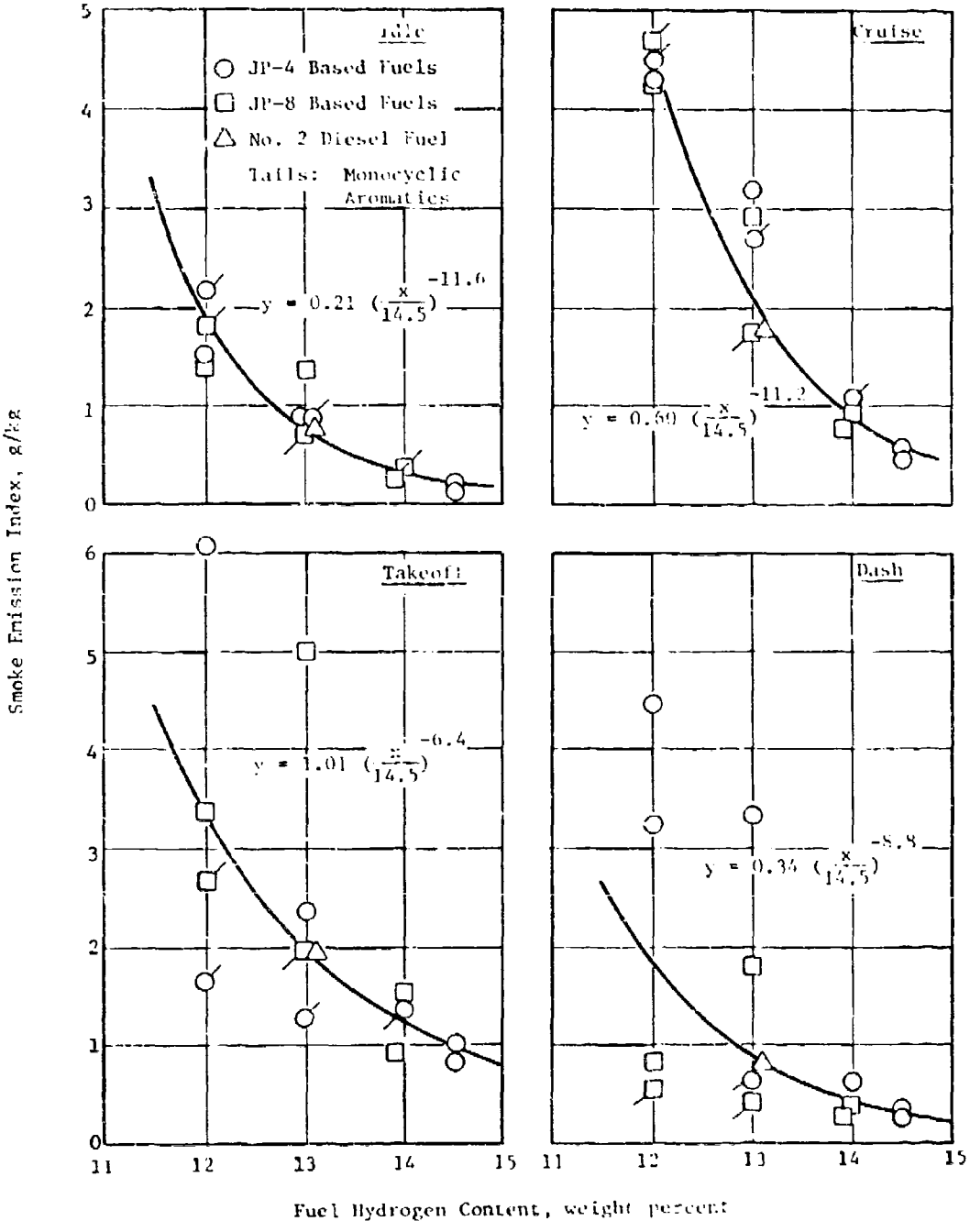

Figure 43. Effect of Fuel Hydrogen Content on Soot Emission Index.

4. Carbon Deposition and Emission

As discussed in Section V-A-2, each high pressure combustor test was run with procedures established to provide information as to the relative carbon deposition tendencies of each fuel. Each test began with a clean combustor and fuel nozzle, and was run to approximately the same total time (4.5 hours). At the completion of each test, visual ratings of the relative carboning tendencies were made which are summarized in Table 19. Photographs, which are included in Appendix B, were also made, in order to document the carbon deposition tendencies. Figures 44 and 45 illustrate the approximate extremes in carbon deposition which were found. As shown, some carbon deposition was found in all tests, with the greatest accumulations on and around the fuel nozzle air shroud face. The variations between fuels were, however, fairly subtle, and no massive "clinker"-type deposits were found. Figure 46 shows the variation in visual rating with fuel hydrogen content. The tendency for deposits to decrease with increasing fuel hydrogen content is evident, but there is considerable scatter in the data - which was not unexpected in these relatively short tests.

In an effort to better quantify the relative carbon forming tendencies, cycle-averaged large carbon particle emission samples were collected with the procedure described in Section V-A-2. It was expected that these measurements might provide a better measure of the carbon formation tendencies than would the post-test combustor inspections since periodic shedding is known to occur (Reference 6), particularly in the first few hours of test (Reference 11). Results of these analyses are also listed in Table 19, and the variation with fuel hydrogen content is illustrated in Figure 47. A strong effect of fuel hydrogen content is indicated, but the data scatter is too great to identify any other fuel property effects.

5. Liner Temperature and Flame Radiation

Inner liner temperature measurements were obtained in the high pressure combustor tests at the locations described in Section V-A-2; detailed data are listed in Appendix A. Figure 48 shows typical spatial variations in measured liner temperature rise ($T_L - T_3$). Peak temperatures always occurred at the 60 degree position and either at the fourth or fifth thermocouple row. The effect of combustor operating conditions or average and peak inner liner temperatures with JP-4 fuel is shown in Figure 49. Strong effect of combustor inlet temperature (and pressure), a negligible effect of fuel-air ratio, and good repeatability between combustor assemblies are all indicated. Similar results were obtained with each of the other fuels, and results are summarized in Table 20. Rises in both peak and average inner liner temperature at all four engine power levels correlate very well with fuel hydrogen content, as shown in Figure 50. At each power level, peak temperature rise is about 50 percent higher than the average temperature rise, and the peak temperatures are much more sensitive to fuel hydrogen content than are average temperatures. These liner temperature levels and trends are in good agreement with those in Reference 6, and also with those in Reference 10, as shown in Figure 51. The dimensionless liner temperature parameter $(T_{L,\,max.} - T_{L,\,max.,\,JP-4})/T_{L,\,max.,\,JP-4} - T_3)$ was shown in Reference 10 to correlate a wide variety of data involving rich combustion systems with pressure-atomizing fuel injection systems designed by three different engine manufacturers. With the addition of the current data

Table 19. Summary of Carbon Deposition and Emission Test Results.

Fuel Number	Visual Rating of Carbon Deposition on Liner/Fuel Nozzle		Test Cycle Averaged Large Carbon Particle Emission Rate, g Carbon/kg Gas
	First[1] Rater	Second[2] Rater	
1	B	2	35.1
1R	A	8	20.1
2	A	1	3.4
3	A	7	14.9
4	A	13	21.1
5	B	4	99.0
6	A	3	44.0
7	A	6	15.3
8	–	–	81.6
9	A	9	–
10	W	11	407.8
11	W	12	342.5
12	A	5	28.0
13	W	10	40.9

(1) A = Average, B = Better (Cleaner) than Average, W = Worse (Dirtier) than Average.

(2) Ranked 1 (Cleanest) to 13 (Dirtiest).

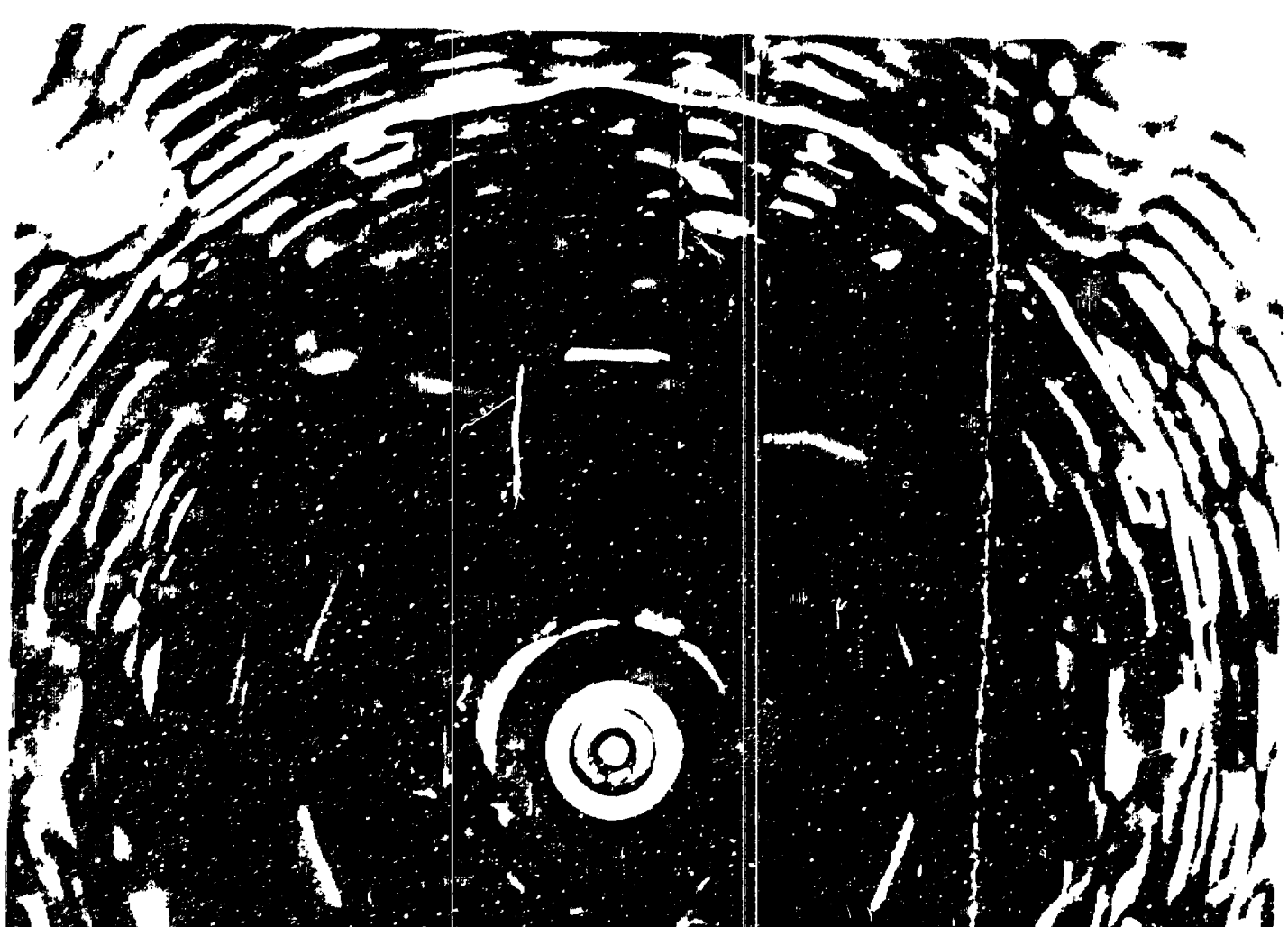

Figure 44. Combustor Post-Test Condition with Relatively Low Carbon Deposition (Fuel No. 2).

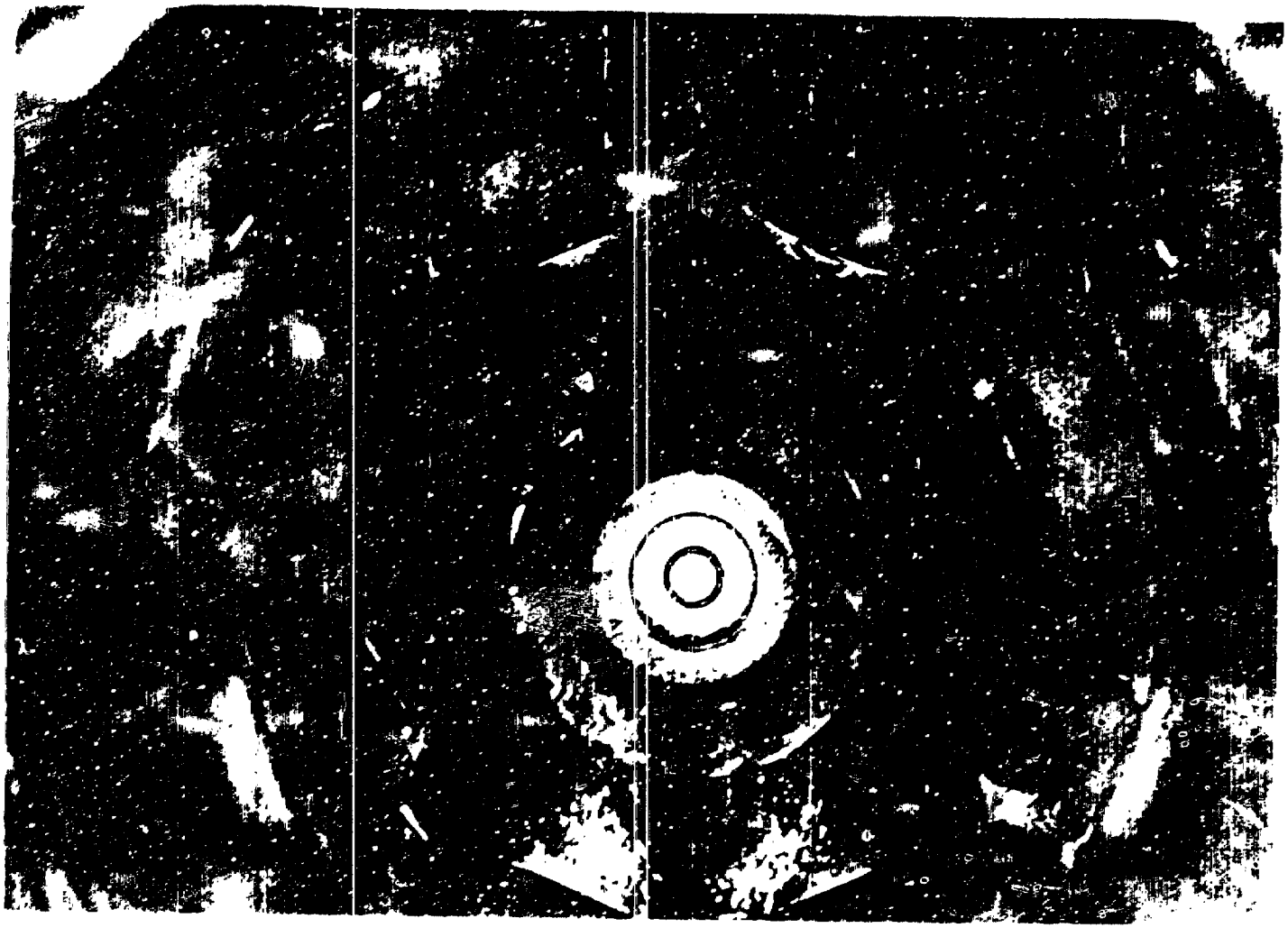

Figure 45. Combustor Postrest Condition with Relatively High Carbon Deposition (Run No. 4).

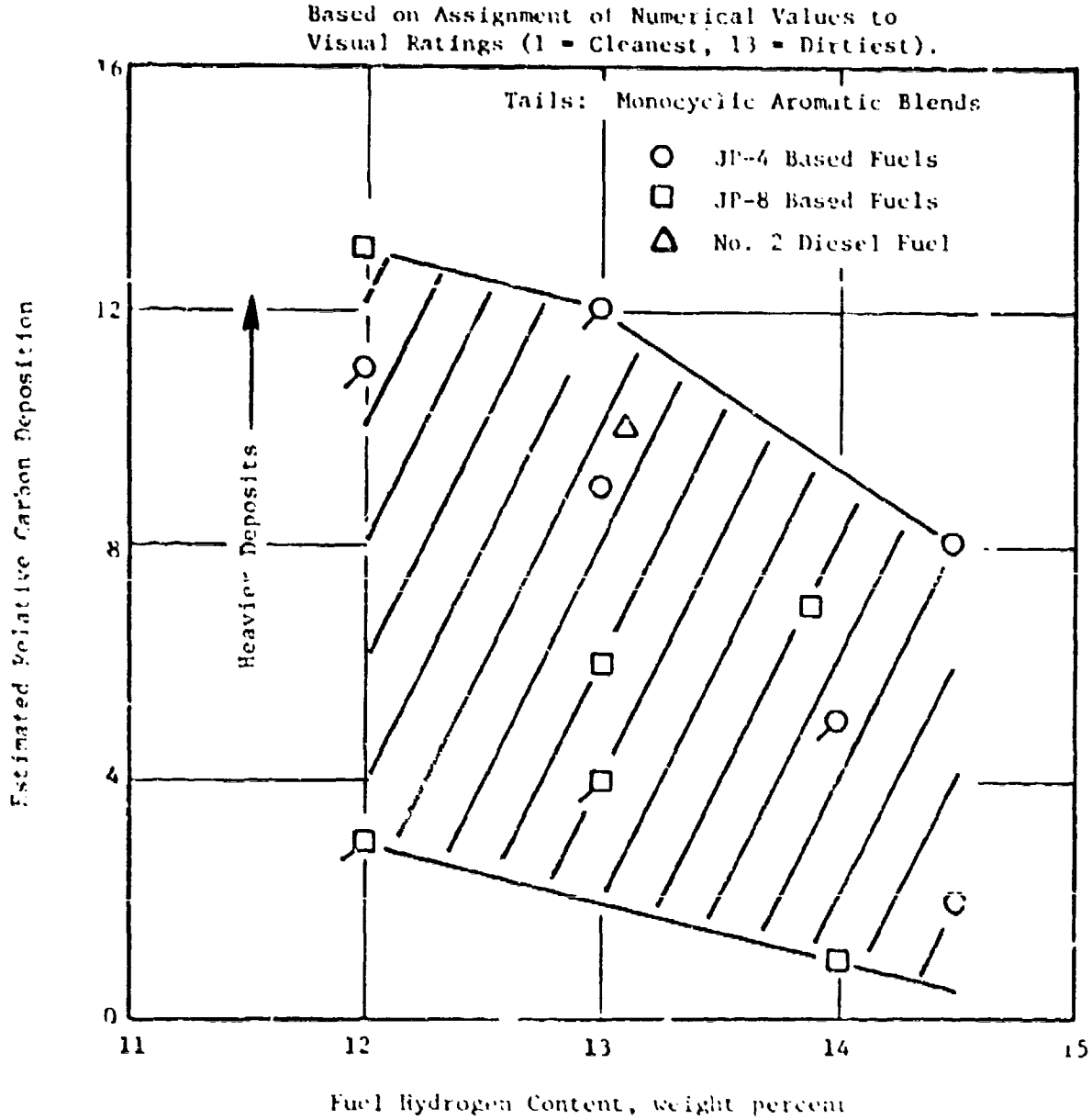

Figure 46. Effect of Fuel Hydrogen Content on Combustor Carbon Deposition.

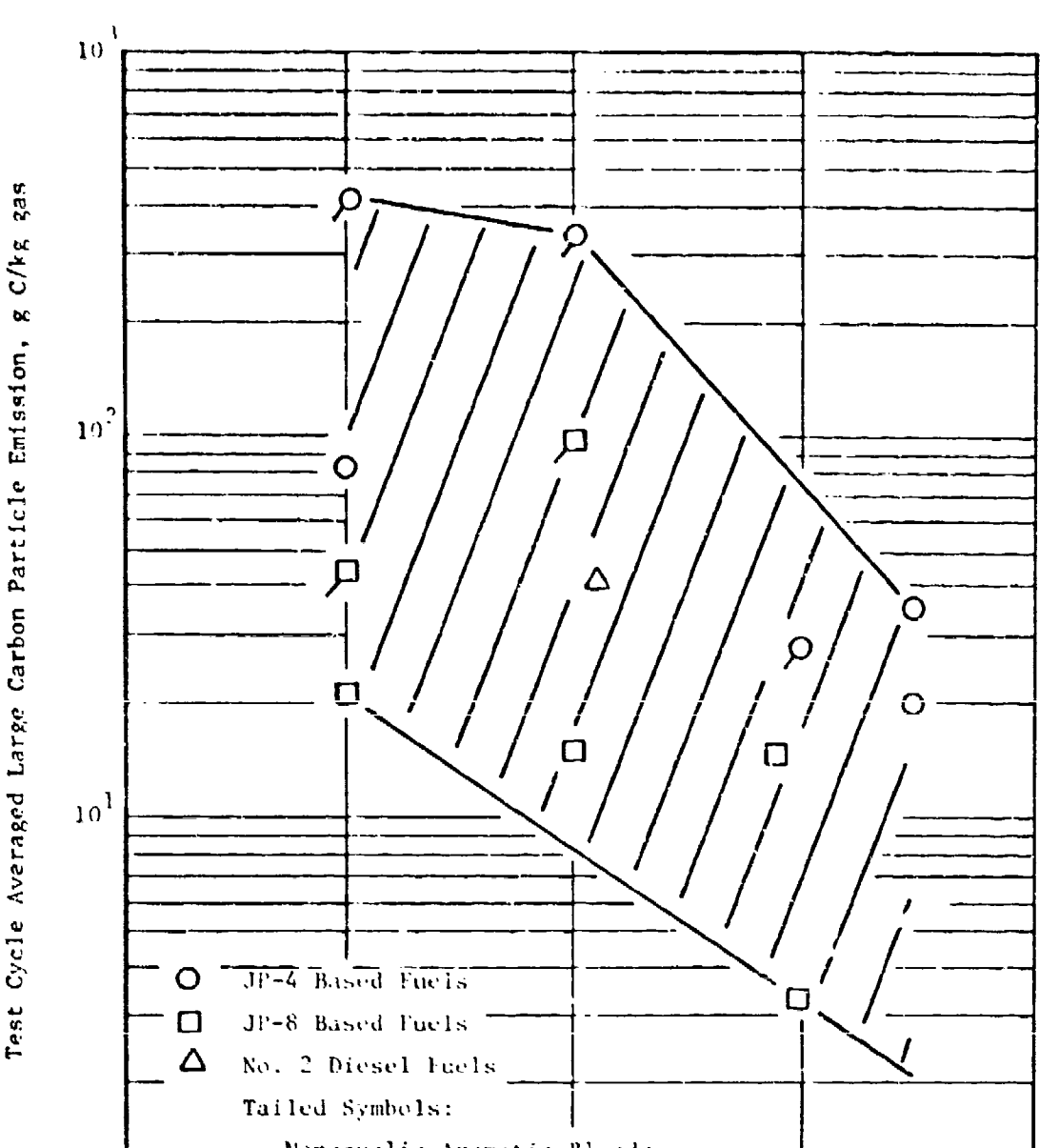

Figure 47. Effect of Fuel Hydrogen Content on Large Carbon Particle Emission.

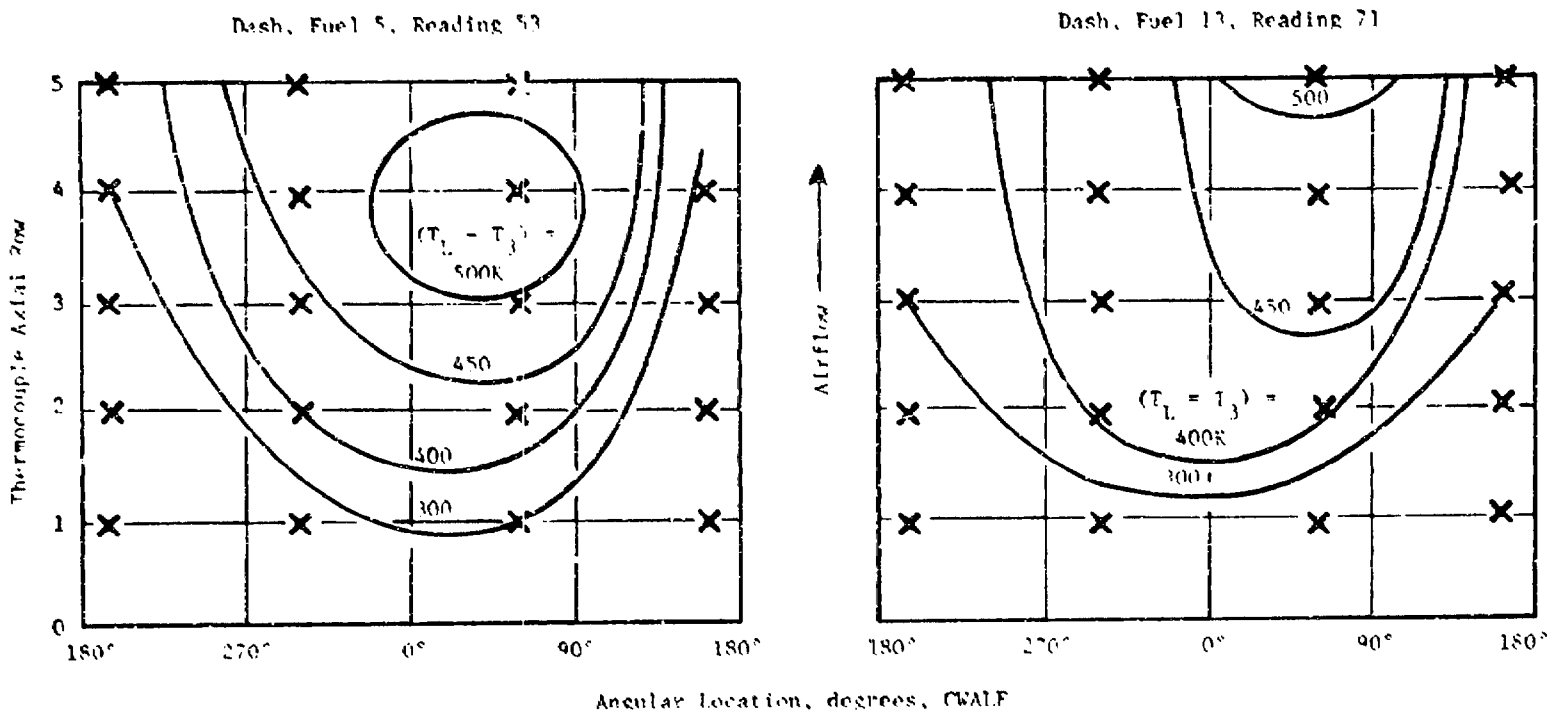

Figure 48. Typical Inner Liner Temperature Distributions.

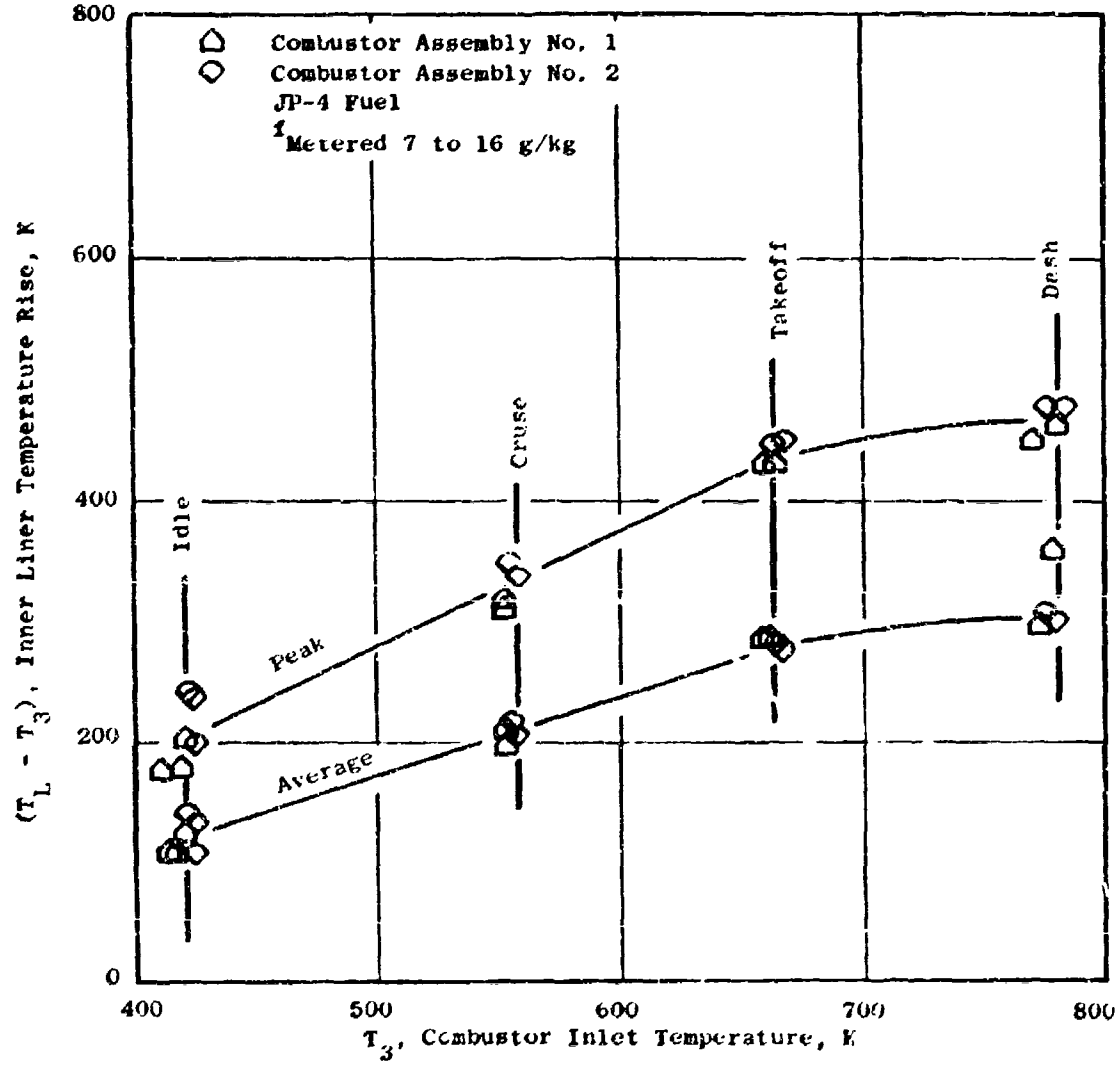

Figure 49. Effect of Operating Conditions on Inner Liner Temperature Rise.

Table 20. Summary of Liner Temperature Test Results.

- Based on 24 Inner Liner Thermocouples (Figure 21)

Fuel Number	$(T_{L,\ max.} - T_3)$, Peak Temperature Rise, K				$(T_{L,\ avg} - T_3)$, Average Temperature Rise, K			
	Idle	Cruise	Takeoff	Dash	Idle	Cruise	Takeoff	Dash
1	180	315	425	450	115	210	280	332
1R	212	340	440	475	132	208	273	302
2	210	340	428	465	130	223	293	285
3	210	340	430	495	129	215	282	305
4	265	428	502	545	150	268	284	295
5	245	395	482	515	139	224	250	250
6	305	420	482	528	160	250	282	293
7	260	365	446	476	158	245	288	302
8	370	440	478	506	205	265	277	282
9	314	409	471	495	170	239	275	305
10	345	420	480	520	180	270	293	292
11	295	410	465	495	175	255	302	317
12	224	342	450	480	145	245	306	320
13	310	410	482	500	165	265	317	340

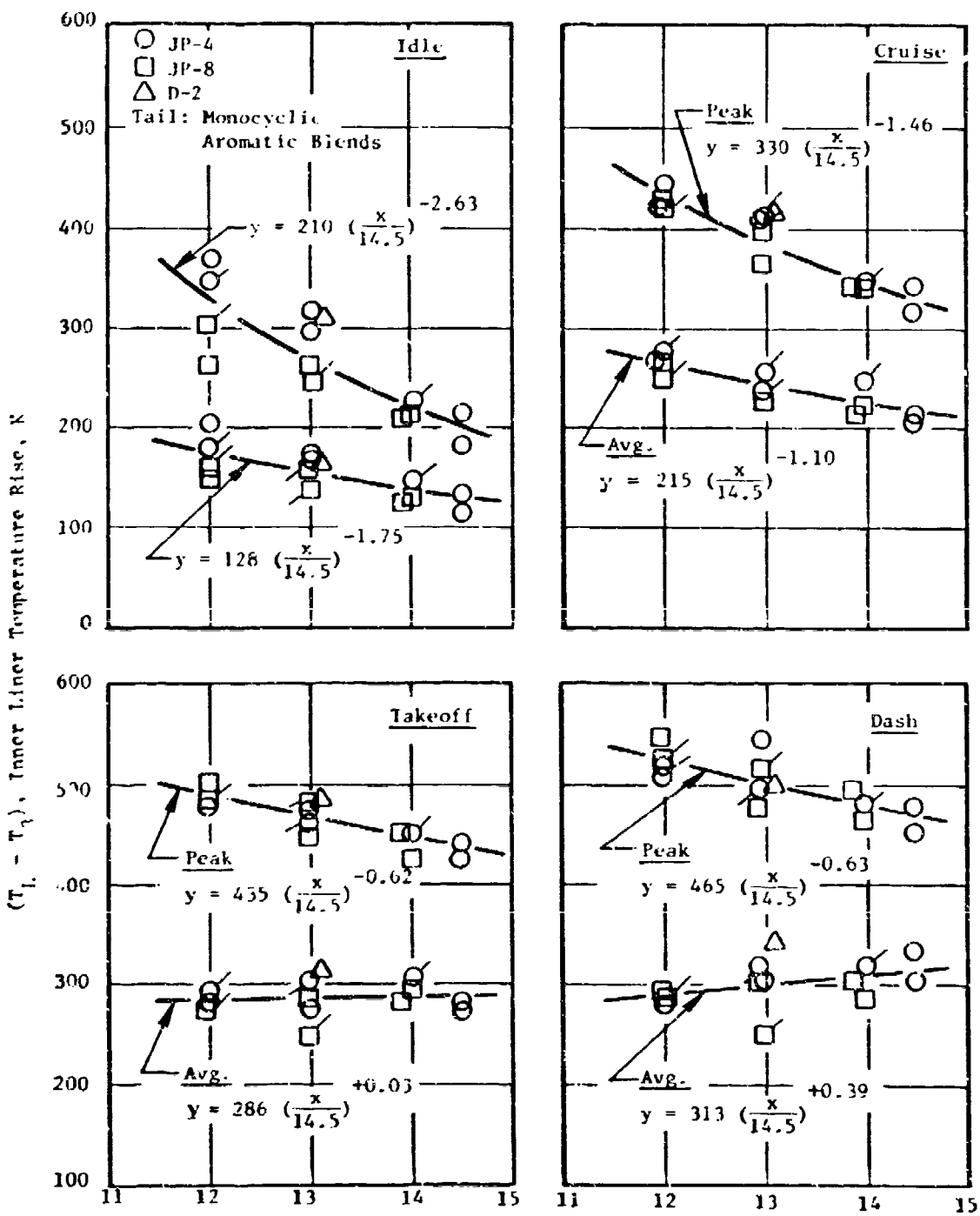

Figure 50. Effect of Fuel Hydrogen Content on Inner Liner Temperature Rise.

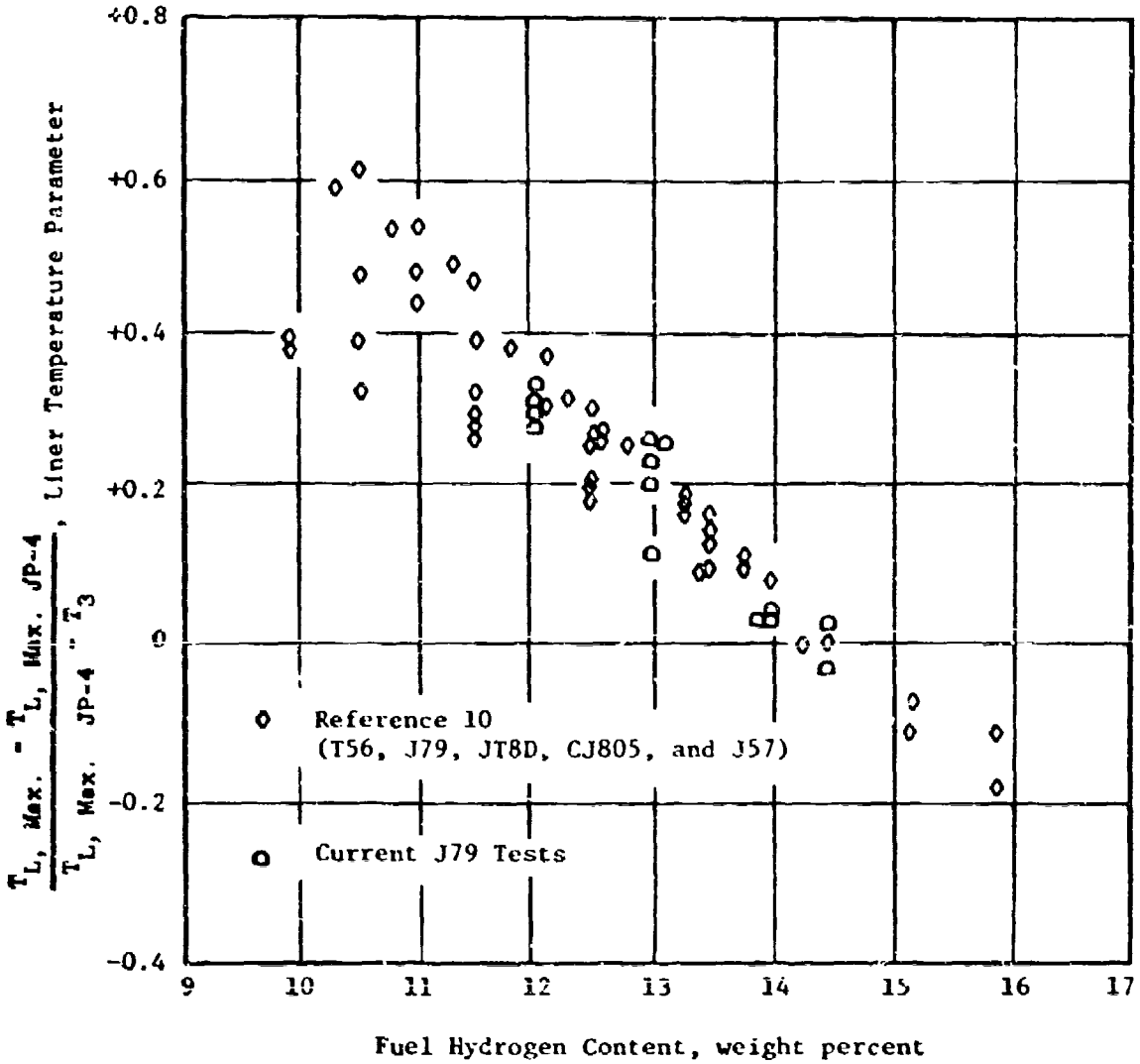

Figure 51. Effect of Fuel Hydrogen Content on Liner Temperature Parameter at Cruise Operating Conditions.

to this correlation, it appears that fuel hydrogen content has been shown to be the only important fuel parameter with respect to liner temperature trends, and (by inference) probably the only important fuel parameter with respect to flame radiation and smoke emissions.

Flame radiation measurements at the cross-fire port plane were obtained with the apparatus and procedures described in Section V-A-2; detailed data are listed in Appendix A. Figure 52 shows the effect of combustor operating conditions on flame radiation with JP-4 fuel. The operating parameter shown was obtained by multiple regression curve fit of these data. An exponential effect of inlet pressure and temperature, with a weak inverse power effect of fuel-air ratio, correlate the data. The inverse fuel-air ratio effect is interpreted to be associated with axial lengthening and/or downstream movement of the intense flame zone with increasing fuel-air ratio. Good measurement repeatability is indicated in these two JP-4 fuel tests, but in later tests some problems were encountered in processing the pyrometer signal, maintaining pyrometer alignment and viewing window cleanliness. Overall results are summarized in Table 21, and effects of fuel hydrogen content are illustrated in Figure 53. The effect of hydrogen content seems to increase with inlet pressure and temperature. The reduced hydrogen content fuel data are, however, judged to be not accurate enough to determine if other fuel properties are important but, on the surface at least, Figure 53 indicates a tendency for bicyclic aromatic blends to produce higher flame radiation than monocyclic aromatic blends with the same low hydrogen content. It seems that if this effect were real, it would also show up in the liner temperature and smoke data.

6. Combustor Exit Profile and Pattern Factor

Combustor exit temperature distributions were measured in the high pressure tests using the fixed thermocouple rake array described in Section V-A-2. Detailed data are listed in Appendix A, and typical results are shown in Figure 54. Both average and peak radial temperature profiles always tended to be inboard peaked, and some small but consistent differences between the profiles of the two different combustor assemblies were observed. Combustor assembly Number 1 tended to produce somewhat lower average profiles but higher peak profiles. The effect of combustor operating conditions on pattern factor, shown in Figure 55, also differed somewhat between the two assemblies. Combustor assembly Number 1 tended to be less sensitive to operating conditions than assembly Number 2. Pattern factor and average profile peak factor for all tests are summarized in Table 22. Overall, pattern factor was about 0.05 higher and average profile peak factor was about 0.02 lower for combustor assembly Number 1. No significant fuel effect was expected, and as shown in Figure 56, if there is one it is small relative to this combustor geometry difference.

7. Cold-Day Ground Starting and Idle Stability

Fourteen cold-day ground start tests were conducted in the low pressure rig using procedures described in Section V-B-2. Detailed test results are listed in Appendix C. Typical results are illustrated in Figure 57. In each test, 1000 rpm engine motoring conditions were simulated, and lean lightoff and lean blowout limits were determined as a function of ambient (fuel and air) temperature in steps from test cell ambient down to 239 K (-30° F). As shown in Figure 57,

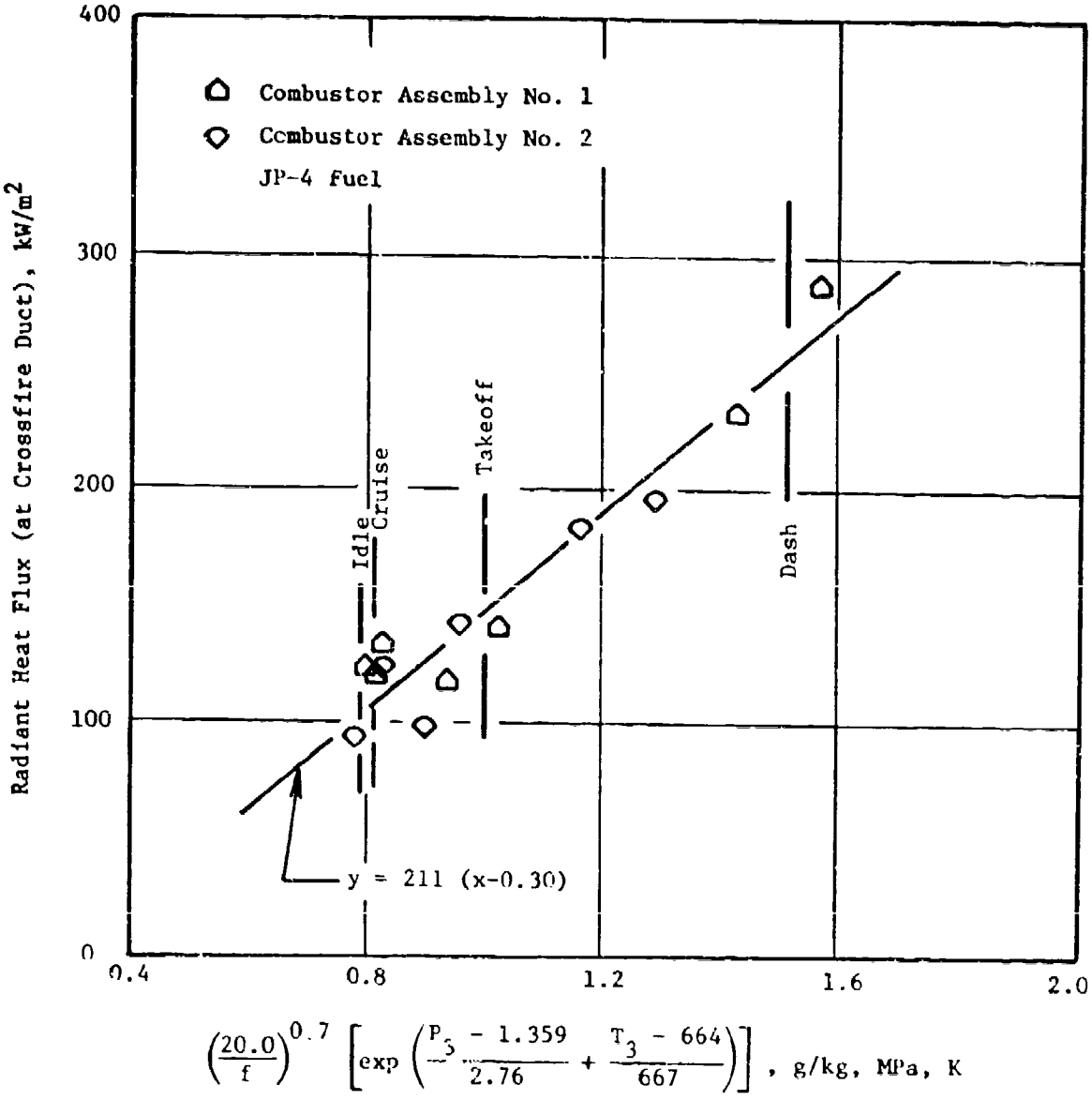

$$\left(\frac{20.0}{f}\right)^{0.7}\left[\exp\left(\frac{P_3 - 1.359}{2.76} + \frac{T_3 - 664}{667}\right)\right], \text{ g/kg, MPa, K}$$

Figure 52. Effect of Combustor Operating Conditions on Flame Radiation.

Table 21. Summary of Radiant Heat Flux Test Results.

Fuel Number	Radiant Heat Flux, kW/m^2			
	Idle	Cruise	Takeoff	Dash
1	108.3	113.0	152.6	260.2
1R	99.1	103.8	142.4	247.3
2	119.1	124.0	164.1	273.0
3	111.1	115.6	152.7	253.6
4	201.0	212.5	306.4	562.0
5	113.6	119.7	169.5	304.9
6	116.9	121.8	162.5	273.2
7	173.8	184.5	272.4	511.4
8	-	-	395.0	595.0
9	140.2	148.3	214.2	393.6
10	183.4	192.2	265.2	463.6
11	110.0	114.0	190.0	-
12	-	-	-	-
13	-	-	-	-

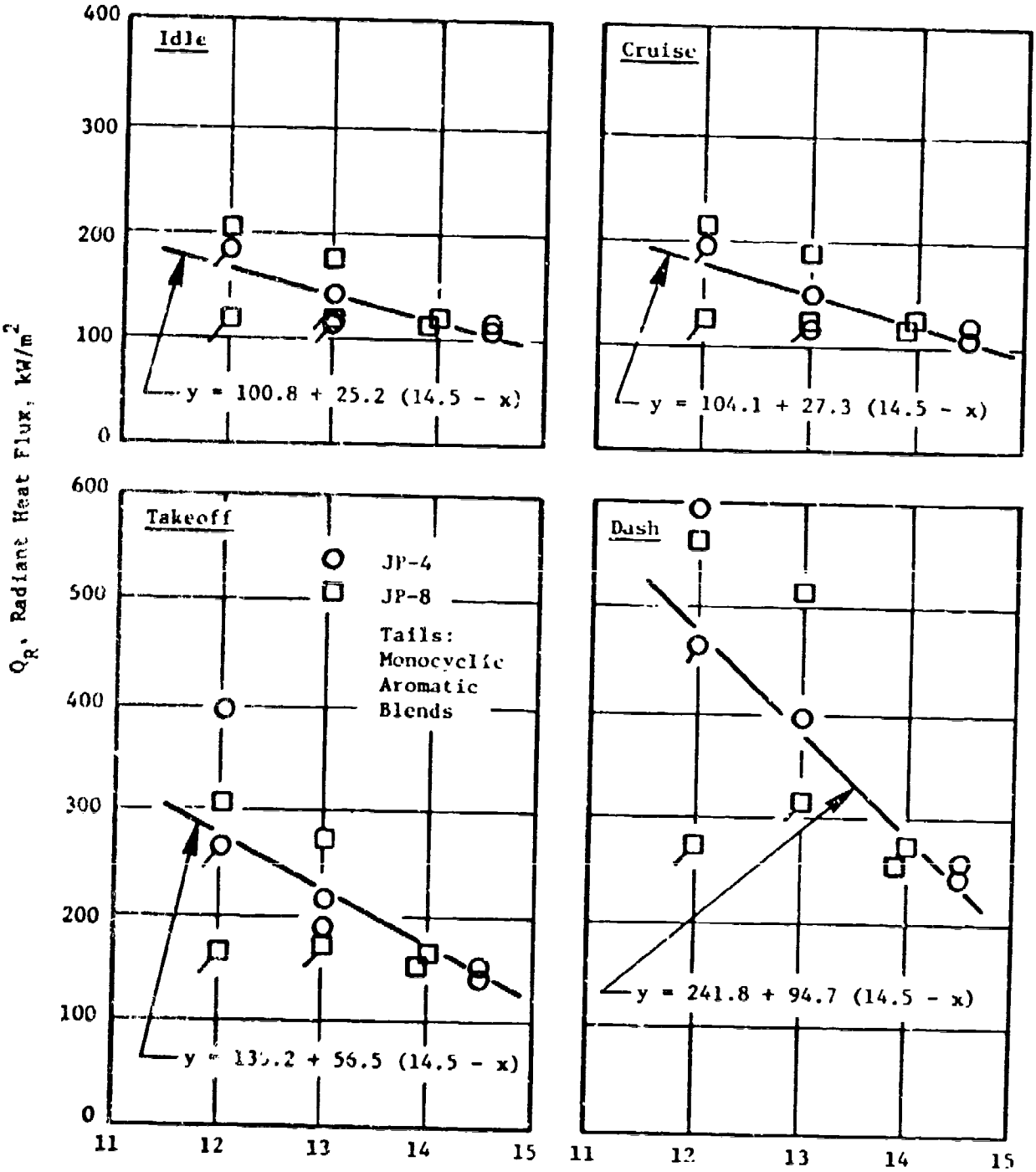

Figure 53. Effect of Fuel Hydrogen Content on Flame Radiation.

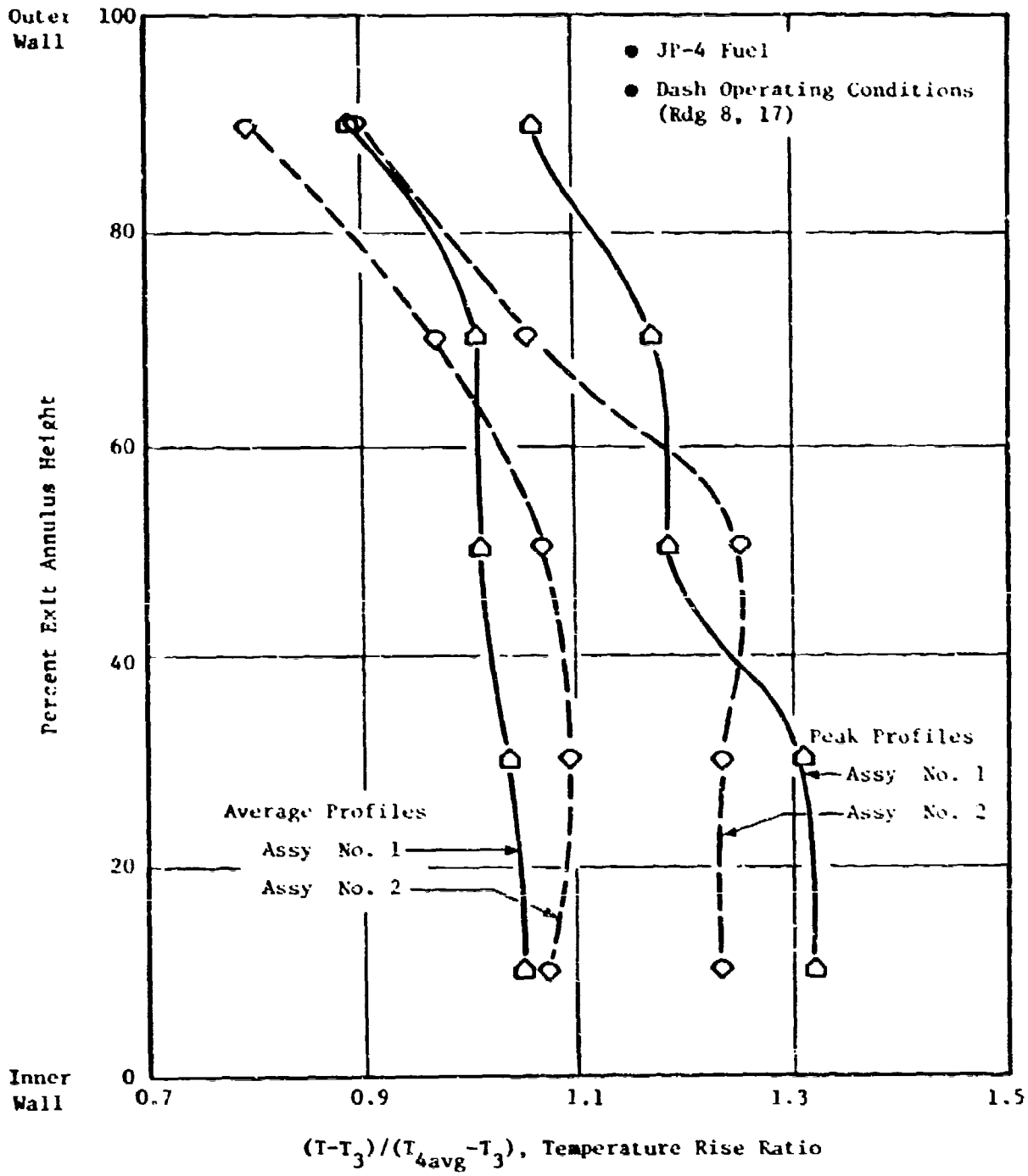

Figure 54. Typical Combustor Exit Temperature Profiles.

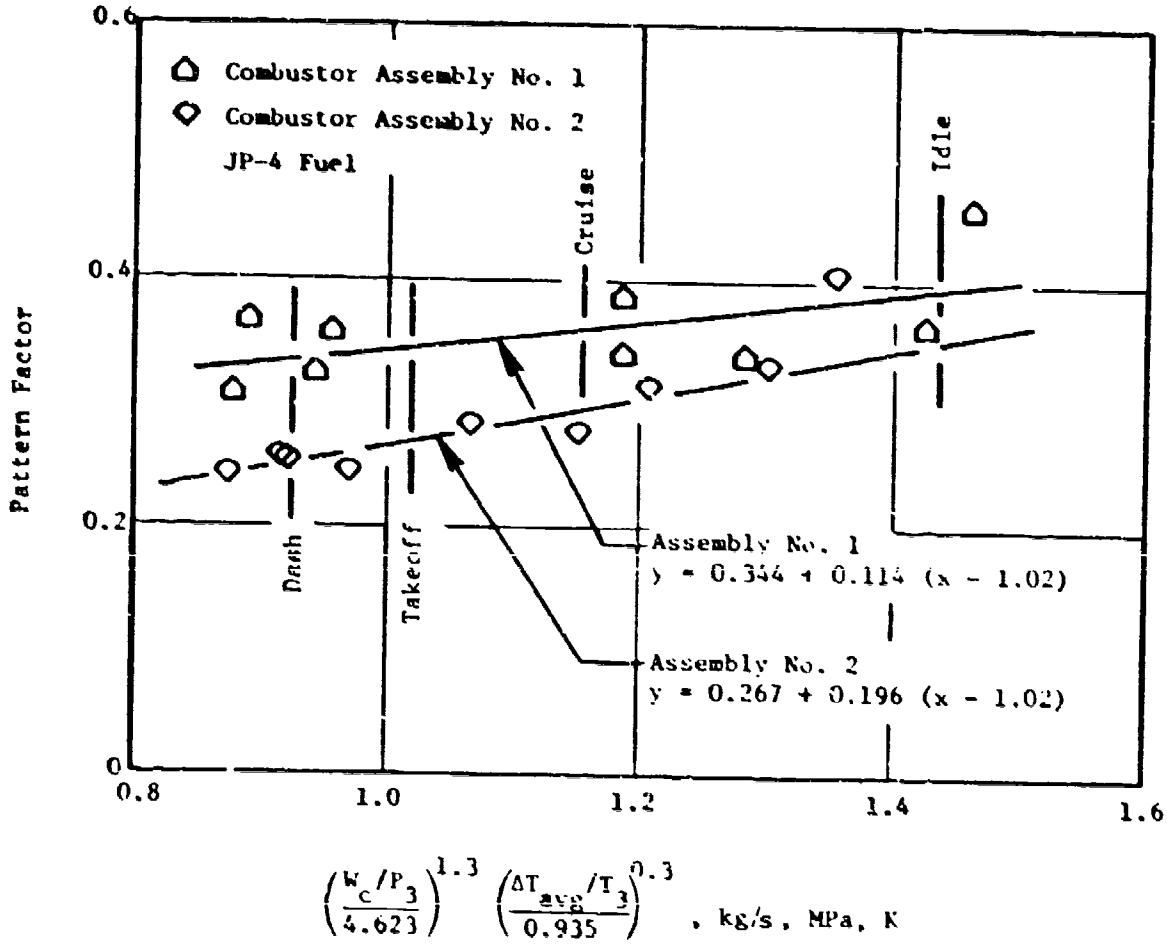

Figure 55. Effect of Combustor Operating Conditions on Pattern Factor.

Table 22. Summary of Pattern Factor and Radial Profile Test Results.

Fuel Number	Combustor Assy Number	Pattern Factor $(T_{4max} - T_{4avg})/(T_{4avg} - T_3)$				Profile Factor $(T_{4Imm\ max} - T_3)/(T_{4avg} - T_3)$			
		Idle	Cruise	Takeoff	Dash	Idle	Cruise	Takeoff	Dash
1	1	0.391	0.359	0.344	0.333	1.124	1.073	1.110	1.050
1R	2	0.349	0.293	0.267	0.2[illegible]	1.136	1.125	1.107	1.093
2	1	0.345	0.332	0.326	0.321	1.116	1.093	1.105	1.108
3	2	0.407	0.328	0.290	0.264	1.089	1.096	1.106	1.098
4	1	0.353	0.305	0.282	0.266	1.156	1.123	1.096	1.073
5	2	0.379	0.302	0.264	0.239	1.123	1.123	1.112	1.106
6	1	0.388	0.323	0.291	0.269	1.125	1.098	1.099	1.084
7	2	0.360	0.265	0.219	0.187	1.103	1.098	1.121	1.112
8	2	0.304	0.258	0.235	0.220	1.139	1.139	1.144	1.127
9	2	0.296	0.232	0.201	0.179	1.109	1.102	1.130	1.105
10	1	0.403	0.298	0.247	0.212	1.136	1.112	1.126	1.114
11	2	0.323	0.278	0.257	0.242	1.164	1.161	1.161	1.156
12	1	0.440	0.320	0.263	0.223	1.161	1.128	1.107	1.091
13	2	0.272	0.240	0.225	0.215	1.112	1.114	1.135	1.117
Avg	1	0.387	0.323	0.292	0.271	1.136	1.105	1.107	1.087
Avg	2	0.336	0.275	0.245	0.224	1.122	1.120	1.127	1.114
Avg	1 & 2	0.358	0.296	0.265	0.244	1.128	1.113	1.118	1.103

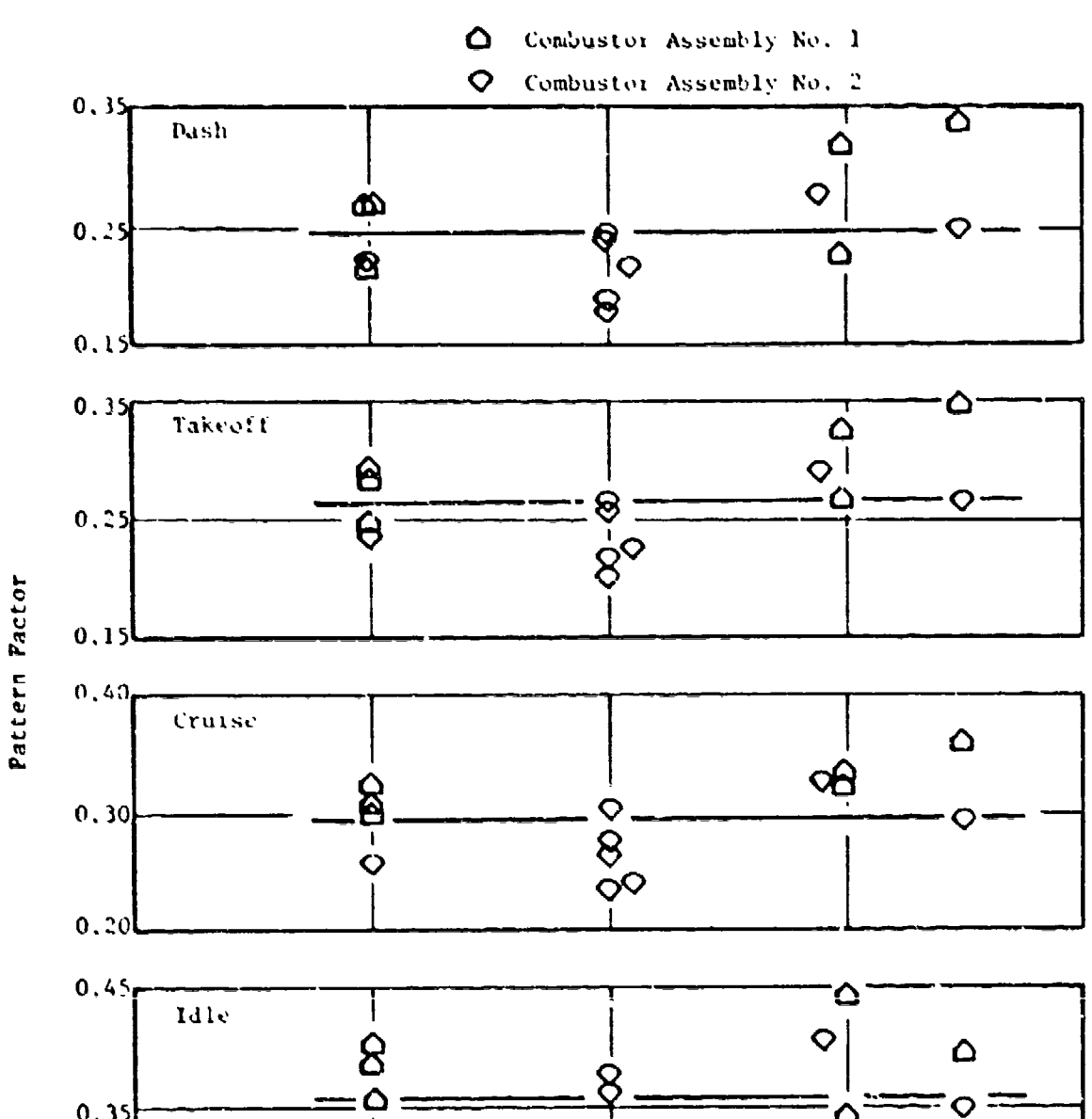

Figure 56. Effect of Fuel Hydrogen Content on Pattern Factor.

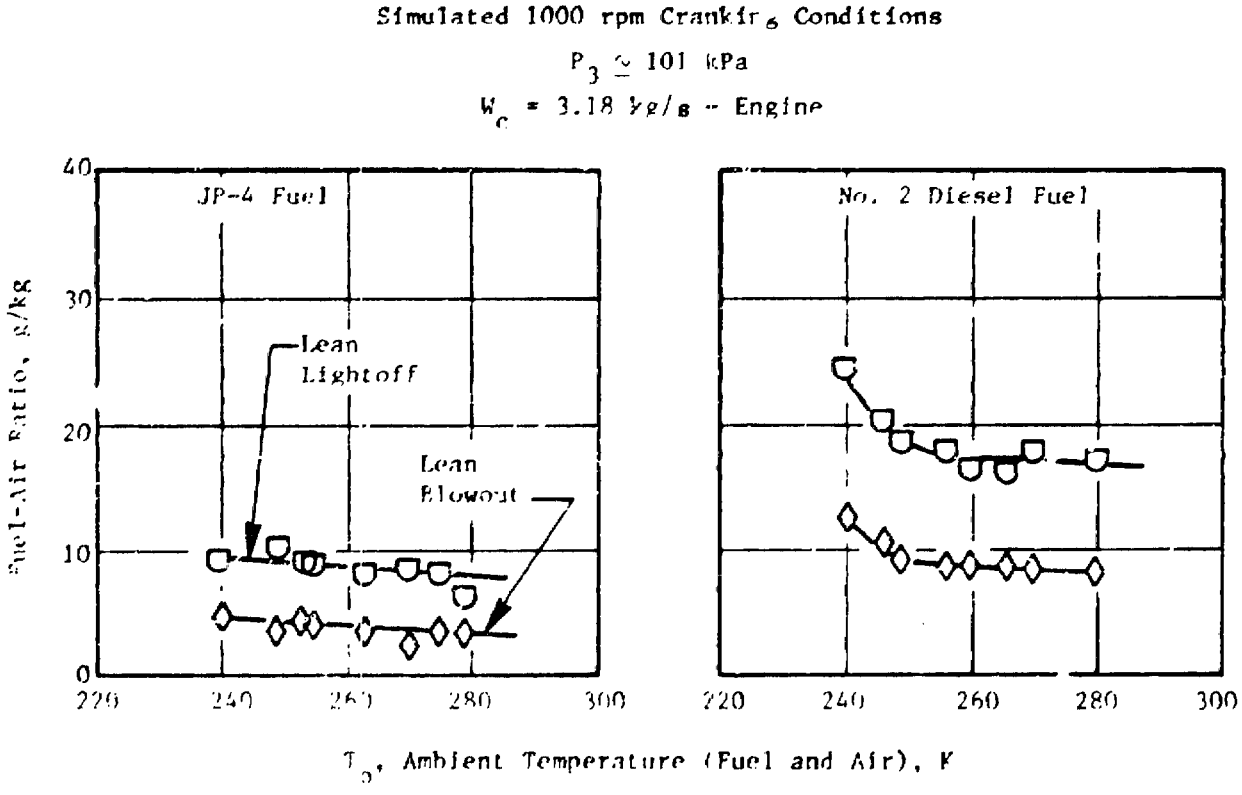

Figure 57. Typical Ground Start Characteristics.

even with the most viscous fuel (No. 13, D-2) lightoffs were obtained down to 239K, but the fuel-air ratios required were fuel-type- and temperature-dependent. Lean blowout fuel-air ratios were usually about half of what the ratios were for lightoff, with similar fuel-type and temperature dependence. Results for all fuels are summarized in Table 23. Effects of fuel properties on lean lightoff fuel-air ratio are illustrated in Figure 58. As discussed in Section VI-A-1, volatility and atomization characteristics of these fuels are highly correlated, but the volatility parameter somewhat better correlated the idle CO emissions. These cold-day start data do, however, correlate very well with relative spray droplet size. No effect of hydrogen content or aromatic type is evident.

Lean lightoff and blowout limits were also measured at idle operating conditions for all of the test fuels, as part of the high pressure test series. These data are summarized in Table 24. As shown, lean blowout fuel-air ratios were less than 2.6 g/kg with all fuels, and lightoff fuel-air ratios ranged from 3.9 to 8.6 g/kg, the variation being attributed to data scatter rather than to any fuel property effect. At these inlet conditions, lightoff and blowout are probably more dependent on fuel nozzle size (spray development) and dome airflow than upon any of the fuel properties.

8. Altitude Relight

Fourteen altitude relight tests were conducted in the low pressure rig using procedures described in Section V-B-2. Detailed results are listed in Appendix C and summarized in Table 25.

Overall, very good altitude relight characteristics were found, with very minor fuel effects. Lightoffs were generally readily obtained at the 15.2 km altitude/minimum engine fuel flow rate conditions, and pressure blowout limits were beyond the facility capability. Over 90 percent of the 110 lightoff attempts were successful, and most of the unsuccessful attempts were outside the estimated current engine limits (Figure 12).

In Table 25(a), combustor conditions are tabulated for the estimated J79-17A engine altitude relight limits shown in Figure 12. Relight results (success) of the present tests are then listed in Table 25(b). For each of the JP-4- or JP-8-based fuels, the present results are in good agreement with the engine estimates. Lightoffs were readily obtained at the two intermediate airflow rates. They were generally obtained at the two extreme airflow rates, but some increased fuel flow rates were occasionally required. The lowest airflow rate (left-hand side of the relight map) is outside the estimated engine start limits with JP-5 or JP-8 fuel. As expected, therefore, in these tests most of the relight difficulties were in this operating region probably because of (1) low fuel and air temperature, and (2) very low combustor pressure drop.

In sharp contrast to the highly successful JP-4/JP-8-based fuel relight success, the diesel fuel was very difficult to light, apparently due to its higher viscosity. After this diesel fuel finding, a brief repeat of the JP-4 fuel test was conducted which repeated the earlier results very well. It appears that significantly higher spark energy and/or better fuel atomization are needed with diesel-type fuels.

Table 23. Summary of Ground Start Test Results[1].

Fuel Number	Fuel-Air Ratio, g/kg			
	Standard Day (288.2 K)		Cold Day[2] (239.0 K)	
	Lean Lightoff	Lean Blowout	Lean Lightoff	Lean Blowout
1	8	3	9	5
1R	9	4	9	4
2	13	5	16	5
3	15	5	14	5
4	13	5	19	7
5	10	6	14	7
6	13	4	14	7
7	18	8	19	11
8	16	8	15	8
9	12	10	15	11
10	13	7	14	7
11	16	11	15	12
12	13	10	15	10
13	17	8	24	12

(1) Simulated 1000 rpm Cranking Conditions
P_3 = 101 kPa
W_c = 3.18 kg/s per engine

(2) All fuels light-off to 239 K (at least)

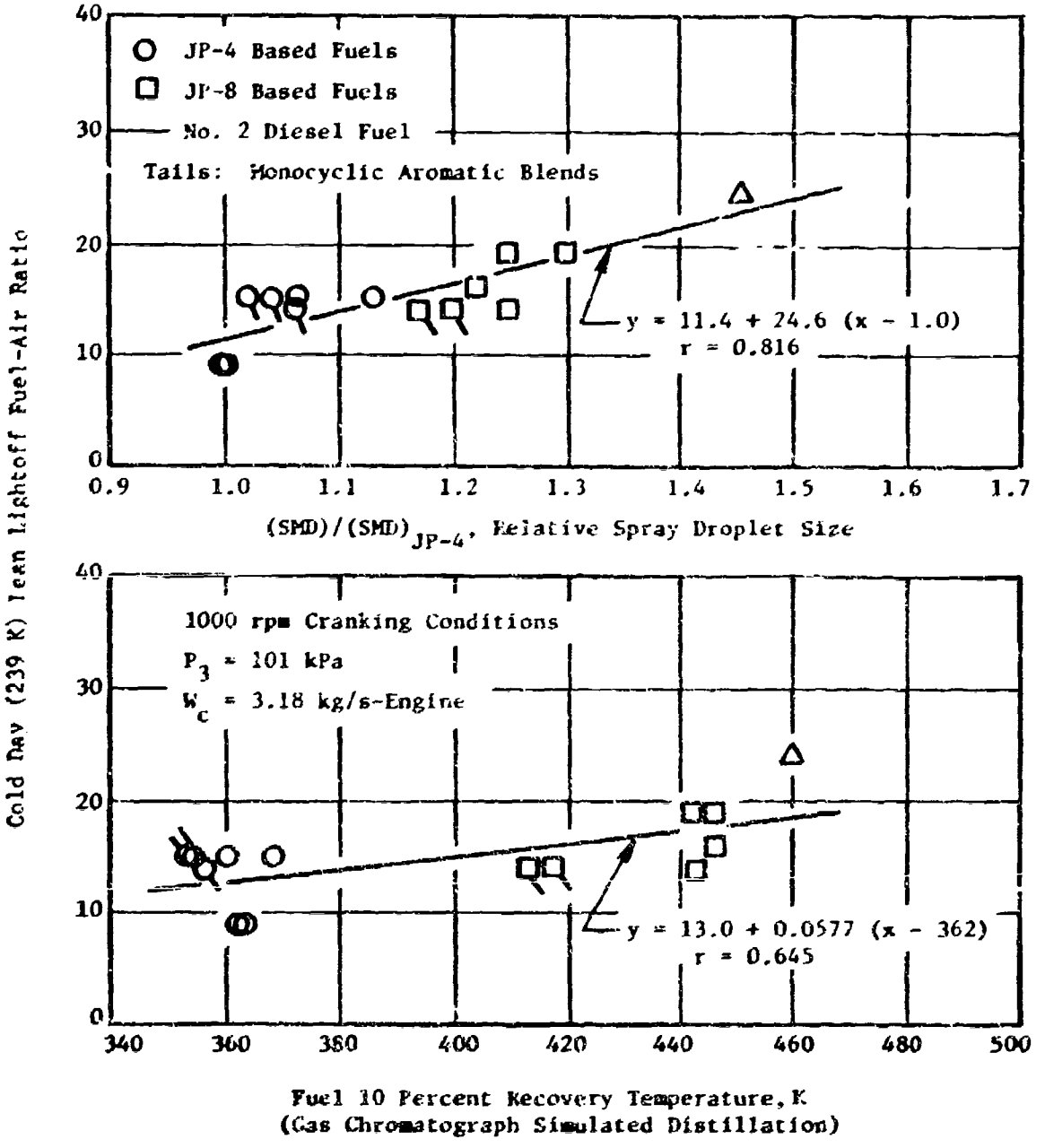

Figure 58. Effect of Fuel Atomization and Volatility on Cold Day Ground Start.

Table 24. Summary of Idle Stability Test Results.

(Simulated Ground Idle Combustor Operating Conditions)

	Lightoff		Lean Blowout	
Fuel Number	W_f, Fuel Flow, g/s/can	f, Fuel-Air Ratio, g/kg	W_f, Fuel Flow, g/s/can	f, Fuel-Air Ratio, g/kg
1	8.0	5.1	All Blowout Fuel Flows Too Low to Measure	All Blowout Fuel-Air Ratios Less than 2.6 g/kg
1R	8.1	5.5		
2	9.3	6.3		
3	6.3	4.3		
4	9.4	5.6		
5	9.3	5.6		
6	7.6	4.9		
7	7.6	4.8		
8	7.2	4.6		
9	6.6	4.3		
10	12.7	8.6		
11	6.1	3.9		
12	8.6	5.5		
13	12.9	8.5		

Table 25. Summary of Altitude Relight Test Results.

(a) Combustor Conditions at Estimated J79-17A Engine Current Start Limits (Figure 12).

W_c, kg/s	2.27		4.08		4.99		9.07	
Fuel	JP-4	JP-5/JP-8	JP-4	JP-5/JP-8	JP-4	JP-5/JP-8	JP-4	JP-5/JP-8
Alt., km	9.5	-	11.9	8.5	14.6	9.4	18.0	13.4
M_o	0.57	-	0.92	0.73	1.10	0.85	1.29	1.18
P_3, kPa	34.5	-	42.7	48.3	48.3	51.7	56.5	84.8
T_3, K	244	-	292	275	367	289	467	403

(b) Rig Test Relight Success at Engine Limit Conditions*.

Fuel	2.27 kg/s		4.08 kg/s		4.99 kg/s		9.07 kg/s	
Number	JP-4	JP-5	JP-4	JP-5	JP-4	JP-5	JP-4	JP-5
1	Yes		Yes		Yes		-	
1R	Yes		Yes		Yes		Yes(1)	
2	Yes		Yes		Yes		Yes(1)	
3	No	-	Yes		Yes		Yes	
4	Yes(1)		Yes		Yes		Yes(2)	
5	Yes		Yes		Yes		Yes	
6	Yes		Yes		Yes		Yes	
7	Yes(2)		Yes		Yes		Yes	
8	Yes		Yes		Yes		Yes	
9	Yes		Yes		Yes		-	Yes
10	No	-	Yes		Yes		Yes	
11	No	-	Yes(3)		Yes		-	Yes
12	Yes		Yes(3)		Yes		No	No
13	No	-	No	No	No	No	No	No

* W_f = 4.22 g/s/can at relight unless footnoted.

(1) ~20% increase in W_f required for lightoff

(2) ~40% increase in W_f required for lightoff

(3) ~80% increase in W_f required for lightoff

Table 25. Summary of Altitude Relight Test Results (Concluded).

(c) Rig Test Altitude Pressure Blowout Limits

W_f = 4.22 g/s/can

Fuel Number	W_c = 2.27 kg/s (engine)		W_c = 4.08 kg/s (engine)		W_c = 4.99 kg/s (engine)		W_c = 9.07 kg/s (engine)	
	Alt., km	M_o	Alt., km	M_o	Alt., km	M_o	Alt., km	M_o
1								
1R	>16.4	>0.95	>17.1	>1.15	>16.3	>1.17	>17.2	>1.26
2	>16.4	>0.95	>17.1	>1.15	>16.3	>1.17	>17.2	>1.26
3	>16.4	>0.95	>17.1	>1.15	>16.3	>1.17	>17.2	>1.26
4	>16.4	>0.95	>17.1	>1.15	>16.3	>1.17	>17.2	>1.26
5	>16.4	>0.95	>17.1	>1.15	>16.3	>1.17	>17.2	>1.26
6	16.4	0.95	>17.1	>1.15	>16.3	>1.17	>17.2	>1.26
7	14.0	0.88	>17.1	>1.15	>16.3	>1.17	>17.2	>1.26
8	>16.4	>0.95	>17.1	>1.15	>16.3	>1.17	>17.2	>1.26
9	>16.4	>0.95	>17.1	>1.15	>16.3	>1.17	>17.2	>1.26
10	--	--	>17.1	>1.15	>16.3	>1.17	>17.2	>1.26
11	--	--	>17.1	>1.15	>16.3	>1.17	>17.2	>1.26
12	>16.4	>0.95	--	--	>16.3	>1.17	>17.2	>1.26
13	--	--	--	--	--	--	--	--

For each of the test conditions where successful altitude relights were obtained, pressure (altitude) blowout limits were determined; the results are shown in Table 25(c). These investigations showed even less fuel-type sensitivity than did the relights. In only two of the 44 attempts were the limits found to be within the facility capability (approximately 17 km altitude). The two cases where limits were reached were on the left side of the windmilling map using JP-8-based fuel blends (Fuels 6 and 7).

9. Fuel Nozzle Fouling

Eighteen fuel nozzle fouling tests were conducted; they are described in Section V-C. The principal results were periodic fuel flow calibrations, which are listed in Appendix D. The test procedure was altered three times in this series in an attempt to define more clearly the relative fouling tendencies of all the fuels, in short tests. Normally, fuel nozzle fouling occurs only after long use, which would require long-time tests and large fuel quantities to duplicate, but these were beyond the scope of this program. The test procedure changes made in this series were:

1) After inconclusive tests with Fuels 1 and 2 (no significant flow calibration deterioration), the fuel temperature was increased (from 436 to 478 K) to accelerate the fouling tendency.

2) After tests with Fuels 1, 2, and 3 at the higher temperature, flow calibration deterioration at the second calibration point (0.86 MPa fuel nozzle pressure drop) was found and determined to be due to secondary orifice flow divider valve leakage (which was never designed to be leakproof or to operate on primary-only at these severe test conditions). Blocked secondary flow divider valve configurations elmiminated this extraneous fouling, and therefore, were used in tests of Fuels 1 through 6.

3) Another type of extraneous fouling occurred in the later blocked valve tests (accumulated carbon from the valve cavity deposited in passages that could neither be inspected nor adequately cleaned between runs). Therefore, a new standard fuel nozzle was used in each of the last seven tests (Fuels 7-13), and only deterioration at the first calibration point (0.522 MPa pressure drop where only the primary orifice flows) was analyzed.

A summary of the primary orifice flow calibration data for all of the tests is presented in Table 26, and the standard fuel nozzle data is plotted against fuel thermal stability rating (from Table 6) in Figure 59. At least in those short tests, no significant fuel effect is evident. Thus, as expected, the J79 fuel nozzle is probably quite tolerant to fuel property changes within the range covered, and much more sophisticated long-term tests would be needed to detect fuel differences.

Table 26. Summary of Fuel Nozzle Fouling Test Results.

Fuel Number	Estimated Fuel Breakpoint, K	Posttest Primary Flow Rate / Pretest Primary Flow Rate[1]	
		Standard Fuel Nozzle (Dual Orifice)	Special Fuel Nozzle (Blocked Secondary Orifice)
1	533	1.166	0.985
2	576	0.950	1.000
3	576	1.000	0.984
4	553	--	0.906
5	558	--	0.954
6	548	--	0.531
7	573	0.987	--
8	538	0.991	--
9	523	0.994	--
10	553	0.991	--
11	548	0.991	--
12	543	0.952	--
13	--	0.994	--

(1) Five (5)-hour test
Fuel temperature 478 K
Air temperature 811 K
Air velocity 304 m/s
Fuel flow rate 5.0 g/s

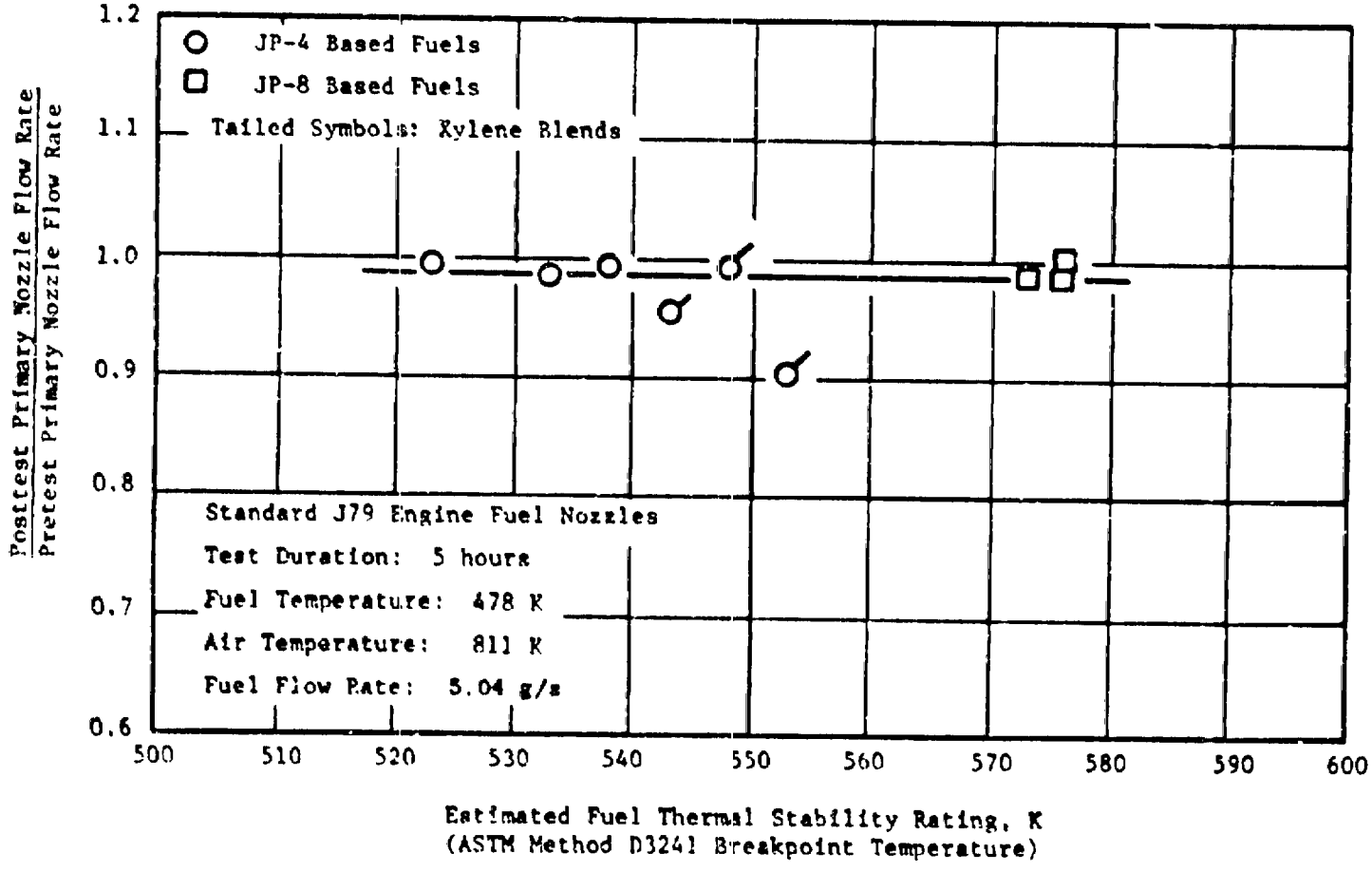

Figure 58. Effect of Fuel Thermal Stability Rating on Fuel Nozzle Fouling Tendency.

B. Engine System Life Predictions

Life prediction analyses were performed using the procedures described in Sections V-E-2/3 and test data presented in Section VI-A. In particular, the liner temperature data contained in Section VI-A-5 and the combustor exit temperature data contained in Section VI-A-6 were considered.

1. Combustor Life Predictions

The maximum liner temperature occurred near the plane of the cross-fire tubes, and at the takeoff conditions they ranged from approximately 1090 to 1165K for the fuels investigated in this program. These maximum temperatures correspond to peak metal temperature rises ($T_{L,\ max} - T_3$) of about 425 to 500K. These data, together with the crack propagation cyclic life curve shown in Figure 29, are the basis for the predicted inner liner relative life curve shown in Figure 60. The predicted decrease in life is due to two factors: the increased effective stress because of larger temperature gradients, and the decay in material properties at the higher temperature level. The relative predicted life for several fuels is approximately as follows:

Fuel Hydrogen Content, Weight, Percent	Relative J79-17A Combustor Life
14.5 (current JP-4)	1.00
14.0 (current JP-8)	0.78
13.0 (ERBS fuel, Ref. 1)	0.52
12.0 (minimum, this program)	0.35

2. Turbine Life Predictions

As discussed in Section V-E-3, flame radiation changes are not predicted to affect turbine nozzle diaphragm temperatures because of the small viewing angle. Profile or pattern factor changes would be expected to directly affect turbine temperatures, but as was anticipated, no fuel effects on combustor outlet temperature distribution were observed. The J79-17A turbine life is therefore not expected to be affected by fuel property changes investigated in this program.

C. Assessment of Results

The data and analyses presented in the previous section provide a summary of the effects of fuel property variations on the performance, emission, and durability characteristics of the J79-17A combustion system, based on single combustor/fuel nozzle rig tests. The data are generally well ordered and in good agreement with previous data, where comparisons could be made. Therefore, these data are thought to be a valuable addition to the USAF data bank. However, since these are all rig results, some direct verification by engine tests is recommended.

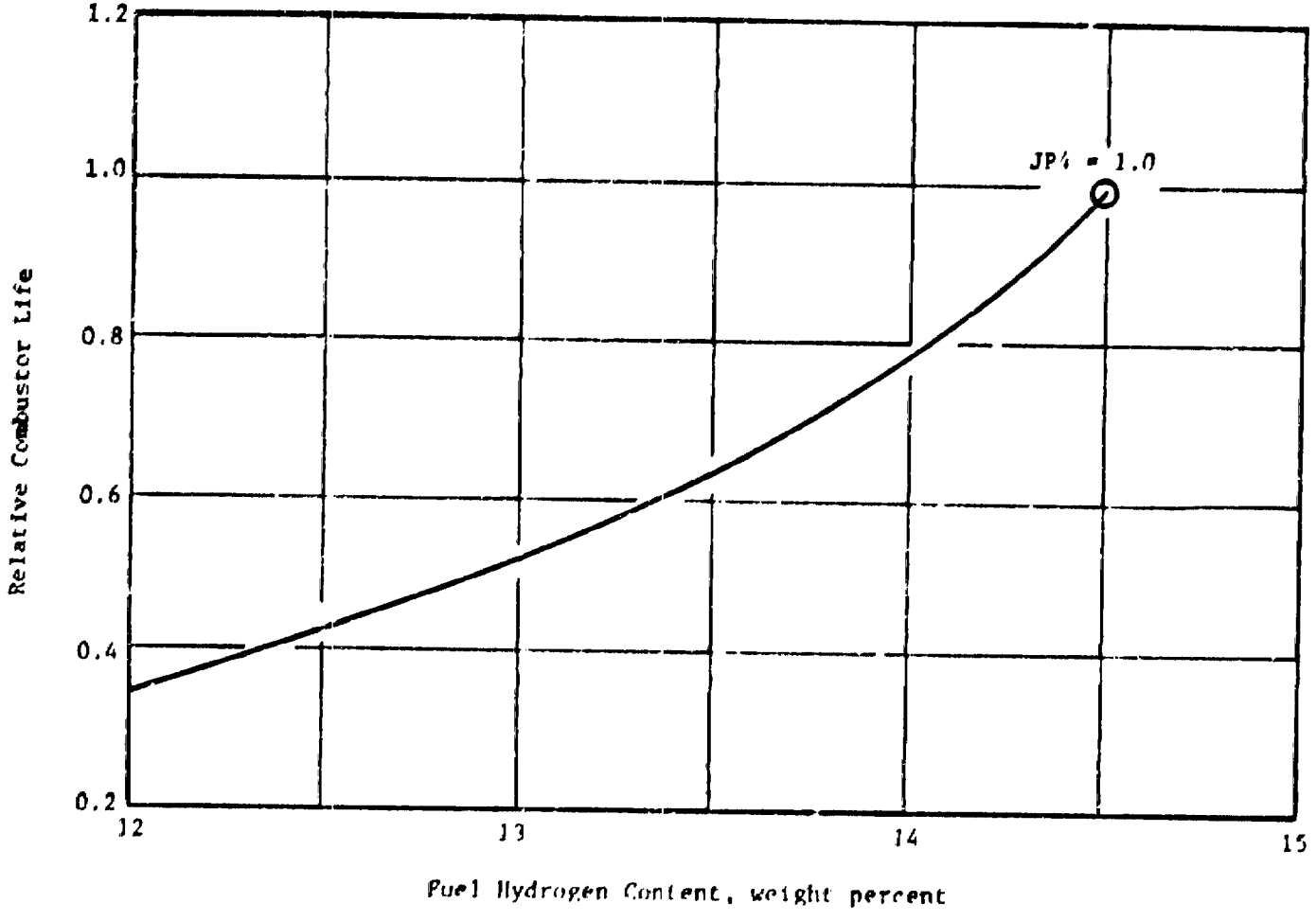

Figure 60. Predicted Effect of Fuel Hydrogen Content on Combustor Life.

These data show that fuel hydrogen content is a key fuel property, particularly with respect to high power performance e 'ssions and durability. Smoke, flame radiation, liner temperature (and hence, combustor life), carbon deposition, and NO_x emissions were all found to be dependent upon fuel hydrogen content, with no discernable effect from any other fuel property. Hence, fuel hydrogen content is a key fuel property at high engine power operating conditions (takeoff, subsonic cruise and supersonic dash). At low power conditions, fuel hydrogen content tends to become unimportant, but fuel volatility and viscosity are important, since they affect fuel atomization and evaporation char.cteristics. The J79-17A combustion system has excellent cold-day ground start and altitude relight characteristics, but these data indicate that conversion from JP-4 to JP-8 as the primary USAF fuel will result in noticeable reductions in these starting capabilities. The high energy ignition system which is standard equipment for the JP-5 fueled US Navy J79-10 engine might be considered for USAF use with JP-8 fuel. Further, these data indicate that a more viscous fuel, such as No. 2 diesel, would very seriously reduce the starting capability of the J79-17A engine. Both ignition system and fuel injection changes would probably be required to cope with this great a fuel change.

The J79-17A fuel nozzle appears to be quite tolerant of fuel property changes with respect to fouling. This was expected both from the service history and the design geometry (relatively large metering ports and loose tolerances). The short but severe tests conducted in this program tend to support this background, but were not very conclusive. It appears that one of the concerns regarding future fuel characteristics is the extent to which the thermal stability ratings will change, and the extent to which engine fuel supply/ injection system performance will be affected. Additional studies in this area are, therefore, needed.

SECTION VII

CONCLUSIONS AND RECOMMENDATIONS

Based on the J79-17A combustion system experiments and analyses conducted in this program, the following conclusions and recommendations are made:

A. Conclusions

1) Fuel hydrogen content strongly affected smoke, carbon deposition, liner temperature, flame radiation and moderately affected NO_x emissions. Hydrogen content is, therefore, probably the single most important fuel property, particularly with respect to high power performance and emission characteristics and combustor durability (life).

2) Fuel volatility (as indicated by initial boiling range) and viscosity effects became evident at low power operating conditions. Cold day starting and altitude relight capability are highly dependent upon these properties.

3) Within the range tested, neither aromatic type (monocyclic or bicyclic) nor final boiling range produced any direct effect on emissions or combustor performance.

4) None of the fuel properties produced any measurable effect on combustor exit temperature distribution (profile and pattern factor), idle stability, fuel nozzle fouling tendency, or turbine life.

5) More sophisticated long-term tests are needed to determine the effects of fuel thermal stability on fuel supply/injection system components.

B. Recommendations

1) J79-17A engine tests with selected fuels are recommended to verify the trends established in these single combustor/fuel nozzle rig tests.

2) Additional single combustor/fuel nozzle rig tests with the low-smoke/long-life J79 combustor design are recommended. These data would show the effect of combustor design features on fuel property sensitivity within the same engine envelope/operating range.

3) Efforts to determine the factors which affect fuel thermal stability and its relationship to engine fuel supply/injection system performance are recommended.

APPENDIX A

HIGH PRESSURE TEST DATA

Table A-1 presents a summary of the key reduced data from the high pressure performance and emission tests. Table A-2 presents additional measured and calculated parameters for these tests.

Table A-3 presents the measured and corrected CO emission test data at the four engine operating conditions. The procedure for correcting the measured data to engine conditions by the ratio of the severity parameters is also shown. As can be seen, the corrections are all relatively small except at dash operating conditions where the test pressure was reduced. Measured and corrected hydrocarbon emission data are similarly presented in Table A-4.

The NO_x emissions data were correlated as shown in Table A-5. A linear regression curve fit of the test data points for each fuel was performed (see Figure 38) from which the quoted engine emission indices were calculated. Small differences in measured and corrected indices are primarily due to the humidity correction.

Table A-6 presents the smoke data analysis. As discussed in Section VI-A-3 no operating condition severity parameter for smoke could be readily found, so the data presented are as measured, except that they have been corrected to engine Station 8 fuel-air ratio conditions as described in Appendix E.

Table A-7 presents the detailed liner temperature measurements. The data are presented as liner temperature rise ($T_{liner} - T_3$). The thermocouple locations indicated correspond to those shown in Figure 21. Average liner temperature rise is also listed. With only two exceptions, the maximum always occurred on Thermocouple 19 or 23 and is listed in Table A-1.

Table A-8 presents a summary of the flame radiation data analysis. Linear regression curve fits of the data (see Figure 52) were performed from which the quoted engine flame radiation levels were calculated.

Table A-9 presents a summary of the pattern factor data analyses. Again, linear regression curve fits of the data (see Figure 55) were performed from which the quoted engine pattern factor levels were calculated. Table A-10 presents the detailed combustor exit temperature profile data for all tests.

Table A-1. [illegible]

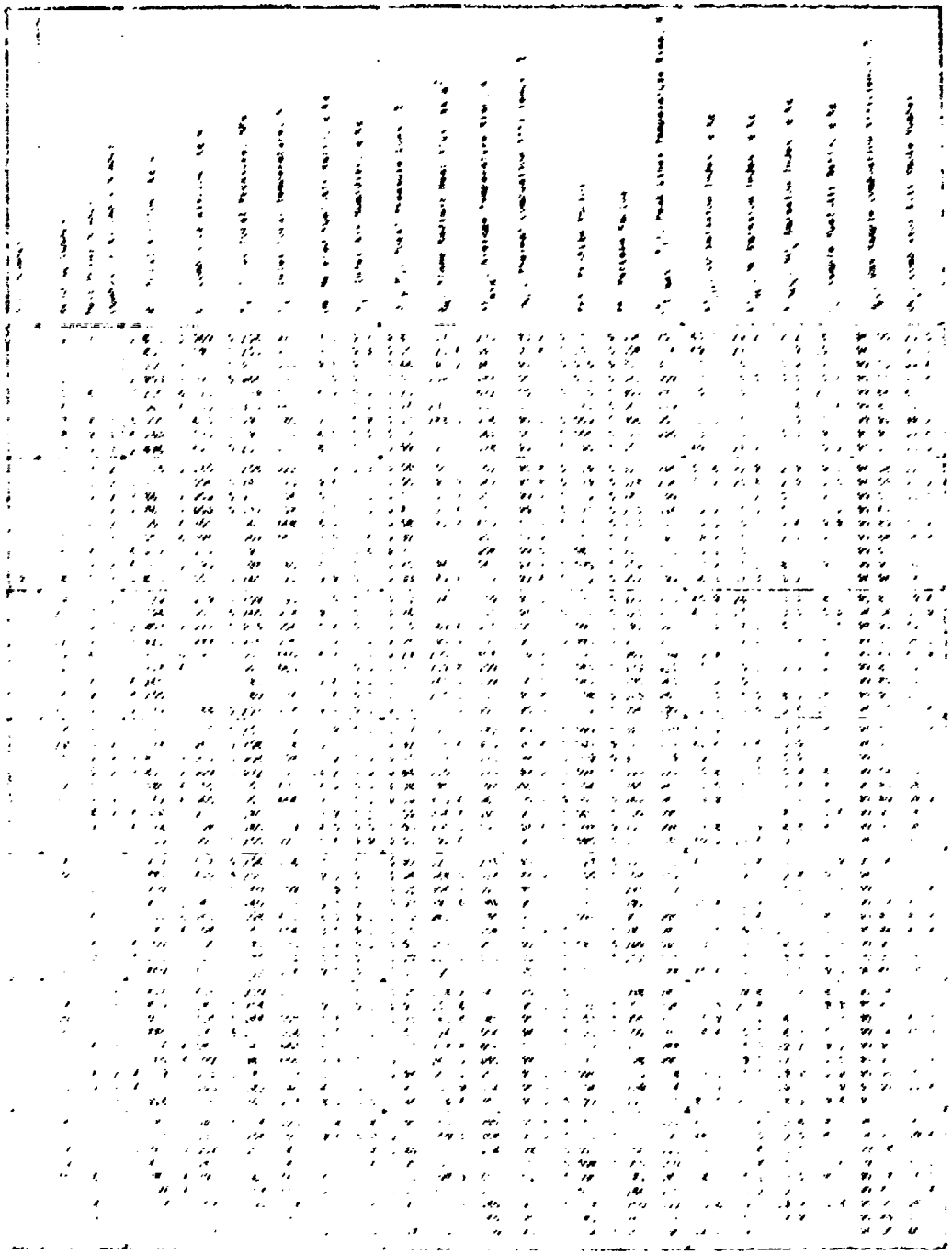

[illegible]

Table A-1. Basic High Pressure Test Data (Concluded).

Table A-2. Supplementary High Pressure Test Data.

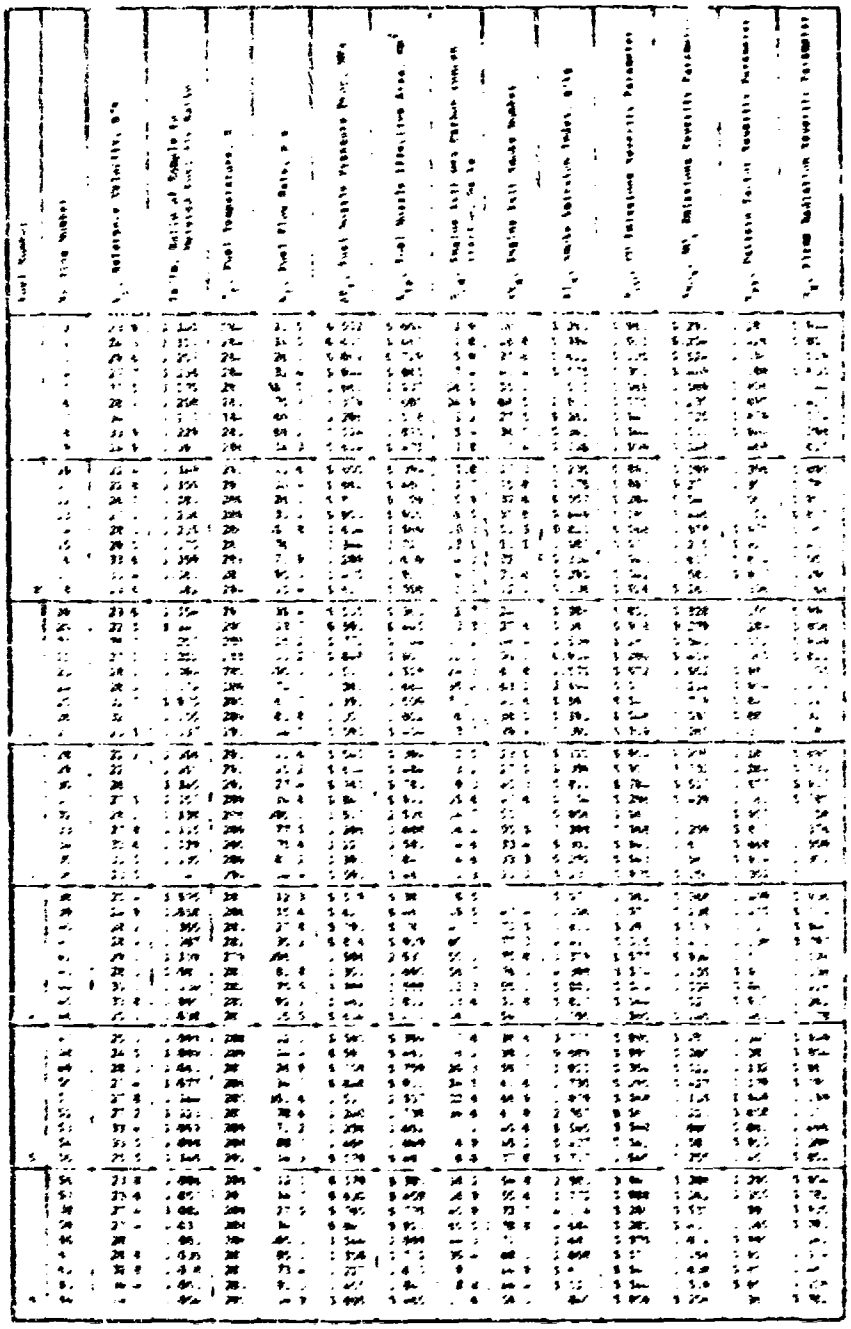

Table A-2. Supplementary High Pressure Test Data (Concluded).

Table A-3. CO Emission Test Data Correlation.

(a) Data Correction to Engine Condition:

$$EI_{CO,\ engine} = \left(EI_{CO,\ test}\right)\left(\frac{S_{CO,\ engine}}{S_{CO,\ test}}\right)$$

where:

$$S_{CO} = \left(\frac{V_r}{24.2}\right)\left(\frac{0.248}{P_3}\right)^{0.7}\left[\exp\left(\frac{421 - T_3}{150}\right)\right]$$

Fuel Number	EI_{CO}, test, g/kg (as measured, Table A-1 at test points 3, 5, 6 and 9)				EI_{CO}, engine, g/kg corrected to S_{CO} = 1.000, 0.286, 0.0710 and 0.0345			
	Idle (3)	Cruise (5)	Takeoff (6)	Dash (9)	Idle (1.000)	Cruise (0.286)	Takeoff (0.0710)	Dash (0.0345)
1	69.2	17.4	5.5	3.1	68.2	16.5	5.7	2.4
1R	57.2	14.2	4.3	3.2	63.8	14.2	4.8	2.6
2	67.2	17.5	5.9	3.5	73.2	17.3	5.8	2.9
3	64.7	15.8	4.0	2.8	71.2	15.8	4.2	2.2
4	77.5	20.8	5.2	3.2	72.4	18.9	4.8	2.5
5	73.0	16.6	4.2	3.2	73.4	16.1	4.7	2.6
6	68.1	21.4	8.1	4.1	72.6	21.5	8.2	3.2
7	69.8	19.2	3.5	2.1	75.5	18.5	3.6	1.5
8	76.5	22.1	3.6	2.2	75.9	20.5	3.4	1.7
9	66.6	18.2	3.7	2.3	69.7	18.0	3.7	1.9
10	61.5	16.0	4.4	3.6	66.2	17.7	4.5	3.7
11	61.1	15.6	3.1	1.9	63.4	15.1	3.1	1.6
12	53.9	14.1	4.2	3.4	57.0	13.7	4.3	2.7
13	62.9	18.0	3.0	2.1	68.0	17.0	3.0	1.5

(b) Data Correlation with Fuel Hydrogen Content:

$$EI_{CO} = b\left(\frac{H}{14.5}\right)^{m}$$

Engine Power Level	Idle	Cruise	Takeoff	Dash
b, Intercept	65.93	14.85	4.48	2.25
m, Slope	-0.470	-1.384	0.198	-0.070
r, Correlation Coefficient	-0.414	-0.753	+0.051	-0.017

Table A-4. HC Emission Test Data Correlation.

$$EI_{HC,\ engine} = \left(EI_{HC,\ test}\right)\left(\frac{S_{CO,\ engine}}{S_{CO,\ test}}\right)^{1.79}$$

where:

$$S_{CO} = \left(\frac{V_r}{24.2}\right)\left(\frac{0.248}{P_3}\right)^{0.7}\left[\exp\left(\frac{421 - T_3}{150}\right)\right]$$

Fuel Number	$EI_{HC,\ Test}$, g/kg (as measured, Table A-1 at points 3, 5, 6, 9 & 10)				$EI_{HC,\ Engine}$, g/kg (corrected to S_{CO} = 1.000, 0.286, 0.0710, 0.0345)			
	Idle (3&10)	Cruise (5)	Takeoff (6)	Dash (9)	Idle (1.000)	Cruise (0.286)	Takeoff (0.0710)	Dash (0.0345)
1	25.5	0.5	0.1	0.1	23.6	0.5	0.1	0.1
1R	19.1	0.5	0.1	0.1	22.6	0.5	0.1	0.1
2	18.2	2.4	1.7	0.0	20.4	2.4	2.4	0.0
3	22.6	0.5	0.1	0.0	25.3	0.5	0.1	0.0
4	16.9	1.2	0.6	0.1	15.1	1.0	0.6	0.1
5	24.3	0.5	0.0	0.0	23.6	0.5	0.0	0.0
6	20.5	0.8	0.3	0.1	22.6	0.8	0.3	0.1
7	31.7	2.4	0.9	0.5	33.9	2.2	0.9	0.3
8	34.3	-	2.0	0.7	35.1	-	1.8	0.4
9	28.4	2.6	1.5	0.5	30.5	2.6	1.5	0.4
10	19.6	2.0	1.2	0.5	22.4	1.9	1.2	0.4
11	25.7	2.3	1.2	0.6	26.8	2.2	1.2	0.4
12	17.6	1.6	1.0	0.7	17.3	1.5	1.1	0.5
13	13.5	1.7	0.5	0.2	15.5	1.5	0.5	0.1

Table A-5. NO_x Emission Test Data Correlation.

(a) Correlation with Combustor Operating Conditions:

$$EI_{NO_x} = m\, S_{NO_x} + b$$

where:

$$S_{NO_x} = \left(\frac{28.6}{\theta_T}\right)\left(\frac{P_3}{1.359}\right)^{0.37} \underbrace{\left[2.07 - 1.07\left(\frac{f_4}{14.3}\right)\right]}_{\geq 1.0} \left\{\exp\left[\left(\frac{T_3 - 664}{192}\right) + \left(\frac{6.20 - h}{53.2}\right)\right]\right\}$$

Fuel Number	Number of Data Points	m, slope g/kg	b, Intercept g/kg	r, correlation coefficient
1	9	10.07	+0.02	0.994
1R	9	10.93	+0.08	0.998
2	8	10.86	+0.21	0.994
3	9	11.21	+0.10	0.991
4	9	12.05	-0.16	0.996
5	8	11.44	+0.23	0.990
6	9	12.27	-0.52	0.994
7	8	10.58	-0.07	0.996
8	9	12.61	-1.07	0.996
9	7	11.97	-0.65	0.994
10	9	10.78	+0.33	0.991
11	9	12.01	-0.56	0.994
12	9	11.04	-0.24	0.991
13	9	11.70	-0.18	0.996

EI_{NO_x}, engine, g/kg (calculated from operating conditions correlation at S_{NO_x} = 0.240, 0.424, 1.000, and 1.664)			
Idle (0.240)	Cruise (0.424)	Takeoff (1.000)	Dash (1.664)
2.44	4.29	10.10	16.79
2.70	4.71	11.01	18.26
2.82	4.81	11.07	18.28
2.79	4.86	11.32	18.76
2.73	4.95	11.89	19.88
2.98	5.08	11.67	19.26
2.44	4.69	11.76	19.91
2.47	4.41	10.50	17.52
1.96	4.28	11.54	19.92
2.22	4.42	11.32	19.27
2.72	4.70	10.91	18.06
2.31	4.51	11.43	19.40
2.41	4.44	10.80	18.13
2.62	4.78	11.52	19.29

(b) Data Correlation with Fuel Hydrogen Content:

$$EI_{NO_x} = b\left(\frac{H}{14.5}\right)^m$$

Engine Power Level	Idle	Cruise	Takeoff	Dash
b, Intercept	2.63	4.60	10.77	17.87
m, Slope	+0.407	-0.072	-0.386	-0.475
r, Correlation Coefficient	+0.255	-0.093	-0.591	-0.643

Table A-6. Smoke Emission Test Data Correlation.

(a) Data correction to engine conditions:

Fuel Number	SN_4 (as measured, Table A-1, at test points 3, 5, 6, 9 and 10)				SN_8 (as corrected to f_8, Table A-2, at test points 3, 5, 6, 9 and 10)			
	Idle (3&10)	Cruise (5)	Takeoff (6)	Dash (9)	Idle (3&10)	Cruise (5)	Takeoff (6)	Dash (9)
1	23.3	47.8	62.3	42.6	17.1	41.4	55.2	36.0
1R	19.6	44.2	57.8	39.2	14.0	37.8	51.5	33.6
2	34.2	56.3	67.9	43.5	28.5	50.1	61.8	38.0
3	29.0	53.1	58.4	38.5	24.1	47.6	53.1	33.3
4	54.6	82.1	80.8	56.4	51.1	77.3	75.8	51.8
5	43.0	65.9	42.2	44.8	38.2	61.6	66.9	40.2
6	59.9	82.4	76.5	47.5	56.0	78.8	72.1	44.4
7	55.9	74.8	87.4	64.1	51.3	69.9	85.6	59.2
8	56.0	81.0	90.8	80.0	52.4	76.6	88.9	74.6
9	45.9	76.0	75.2	79.1	43.5	71.6	73.1	75.2
10	63.0	82.0	68.9	85.1	58.7	77.3	67.1	80.0
11	47.4	72.4	64.2	52.0	43.8	68.8	62.7	47.5
12	32.4	58.4	65.2	51.6	27.4	53.2	63.9	47.1
13	48.0	67.4	70.3	56.6	40.9	61.2	69.4	51.1

(b) Data correlation with Fuel Hydrogen Content:

$$SN_8 = b + m\ (14.5 - H)$$

Engine Power Level	Idle	Cruise	Takeoff	Dash
b, Intercept	18.41	42.24	55.51	35.12
m, Slope	15.23	14.83	8.95	11.59
r, Correlation Coefficient	0.960	0.966	0.744	0.676

Table A-7. Detailed Liner Temperature Data.

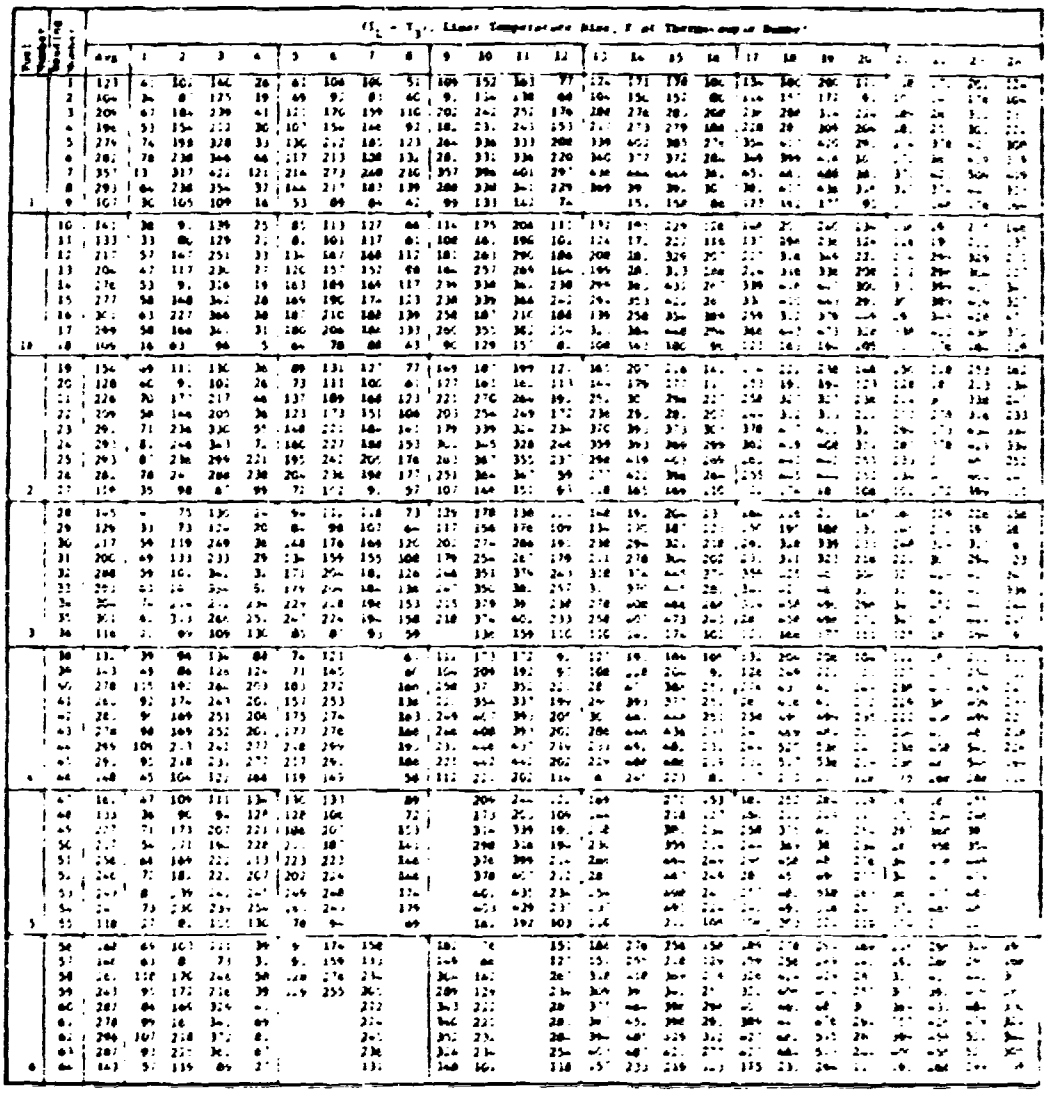

Table A-7. Detailed Liner Temperature Data (Concluded).

Table A-8. Flame Radiation Data Correlation.

(a) Correlation with Combustor Operating Conditions:

$$\dot{q}_R = m\, S_R + b$$

where

$$S_R = \left(\frac{20.0}{f_m}\right)^{0.7} \left| \exp\left[\left(\frac{P_3 - 1.359}{2.76}\right) + \left(\frac{T_3 - 664}{667}\right)\right]\right|$$

Fuel Number	Number of Data Points	m, Slope, kW/m²	b, Intercept, kW/m²	r, Correlation Coefficient*	Q_r, Radiant Heat Flux, kW/m² (Calculated From Operating Conditions Correlation at S_r = 0.788, 0.811, 1.000 and 1.514)			
					Idle (0.788)	Cruise (0.811)	Takeoff (1.000)	Dash (1.514)
1	7	209	- 57	0.970	106.2	113.0	152.6	260.2
1R	7	204	- 62	0.955	99.1	103.8	142.4	247.3
2	9	212	- 48	0.960	119.1	124.0	164.1	273.0
3	9	196	- 44	0.988	111.1	115.6	152.7	253.6
4	9	497	-191	0.795	201.1	212.5	306.4	562.0
5	9	264	- 94	0.943	113.6	119.7	169.5	304.9
6	9	215	- 53	0.913	116.9	121.8	162.5	273.2
7	9	465	-193	0.952	173.8	184.5	272.4	511.4
8	2	400	+ 6	-	-	-	395	595
9	9	349	-135	0.924	140.2	145.3	214.2	393.6
10	7	356	-121	0.972	183.4	192.2	265.2	483.6
11	2	400	-197	-	110	114	190	-
12	-	-	-	-	-	-	-	-
13	-	-	-	-	-	-	-	-

(b) Data Correlation with Fuel Hydrogen Content:

$$\dot{q}_R = b + m\,(14.5 - H)$$

Engine Power Level	Idle	Cruise	Takeoff	Dash
b, Intercept	100.8	105.3	155.2	241.8
m, slope	25.2	26.8	56.5	94.7
r, correlation coefficient	0.676	0.672	0.696	0.714

Table A-9. Pattern Factor Correlation.

(a) Correlation with Combustor Operating Conditions:

$$PF = m\, S_{PF} + b$$

where

$$S_{PF} = \left(\frac{W_c/P_3}{4.623}\right)^{1.3} \left(\frac{\Delta T_{avg}/T_3}{0.9348}\right)^{0.3}$$

Fuel Number	Number of Data Points	m, Slope	b, Intercept	r, Correlation Coefficient	PF, Pattern Factor (Calculated From Operating Conditions Correlation at S_{PF} = 1.436, 1.154, 1.018 and 0.924)			
					Idle (1.436)	Cruise (1.154)	Takeoff (1.018)	Dash (0.924)
1	9	0.1142	0.2274	0.603	0.391	0.359	0.344	0.333
1R	8	0.1955	0.0678	0.953	0.349	0.293	0.267	0.248
2	9	0.0462	0.2784	0.336	0.345	0.332	0.326	0.321
3	8	0.2778	0.0077	0.983	0.407	0.328	0.290	0.264
4	9	0.1656	0.1107	0.925	0.353	0.305	0.282	0.266
5	8	0.2747	-0.0151	0.928	0.378	0.302	0.264	0.238
6	8	0.2327	0.0547	0.896	0.366	0.323	0.291	0.268
7	9	0.3564	-0.1225	0.975	0.360	0.269	0.219	0.187
8	9	0.1638	0.0655	0.924	0.304	0.258	0.235	0.220
9	9	0.2284	-0.0317	0.914	0.296	0.232	0.201	0.179
10	9	0.3731	-0.1379	0.978	0.403	0.298	0.247	0.212
11	9	0.1579	0.0959	0.885	0.323	0.278	0.257	0.242
12	9	0.4227	-0.1674	0.946	0.440	0.320	0.263	0.225
13	9	0.1110	0.1121	0.625	0.272	0.240	0.228	0.219

(b) Correlation with Combustor Assembly (no fuel effect found):

Engine Power Level	Idle	Cruise	Takeoff	Dash
Assembly No. 1 (Fuels 1, 2, 4, 6, 10, & 12)				
$\overline{PF}$, Mean Pattern Factor	0.3587	0.3228	0.2922	0.2707
σ_{PF}, Standard Deviation	0.0346	0.0216	0.0320	0.0493
Assembly No. 2 (Fuels 1R, 3, 5, 7, 8, 9, 11, & 13)				
$\overline{PF}$, Mean Pattern Factor	0.3562	0.2745	0.2248	0.2242
σ_{PF}, Standard Deviation	0.0655	0.0324	0.0296	0.0268

Table A-10. Combustor Exit Temperature Profile Data.

Fuel Number	Reading Number	Temperature Rise Ratio, $\Delta T_{Local}/\Delta T_{Avg}$									
		Average Profile					Peak Profile				
		1 (Outer)	2	3	4	5 (Inner)	1 (Outer)	2	3	4	5 (Inner)
2											
2R											
"											
3											
4											
5											
6											

Table A-10. Combustor Exit Temperature Profile Data (Concluded).

Port Number	Reading Number	Temperature Rise Ratio, $\Delta T_{Local}/\Delta T_{Avg}$									
		Average Profile					Peak Profile				
		1 (Outer)	2	3	4	5 (Inner)	1 (Outer)	2	3	4	5 (Inner)
13											
12											
11											
10											
9											
8											
7											

APPENDIX B

CARBON DEPOSITION DATA

Before and after each high pressure combustor test, the combustor liner and fuel nozzle were visually inspected and flow-calibrated. No significant change in flow calibration or fuel spray quality was ever detected. After each test, which began with a c m fuel nozzle and combustor liner, carbon deposition was observed, visually rated (see Table IV), and photographically documented. These post-test photos of the general fuel nozzle tip and inner liner dome condition are presented in Figures B-1 through B-13. Photos were not obtained for Test 8 in order to expedite testing. Closeup photos of the fuel nozzle tip condition are presented in Figures B-14 through B-26.

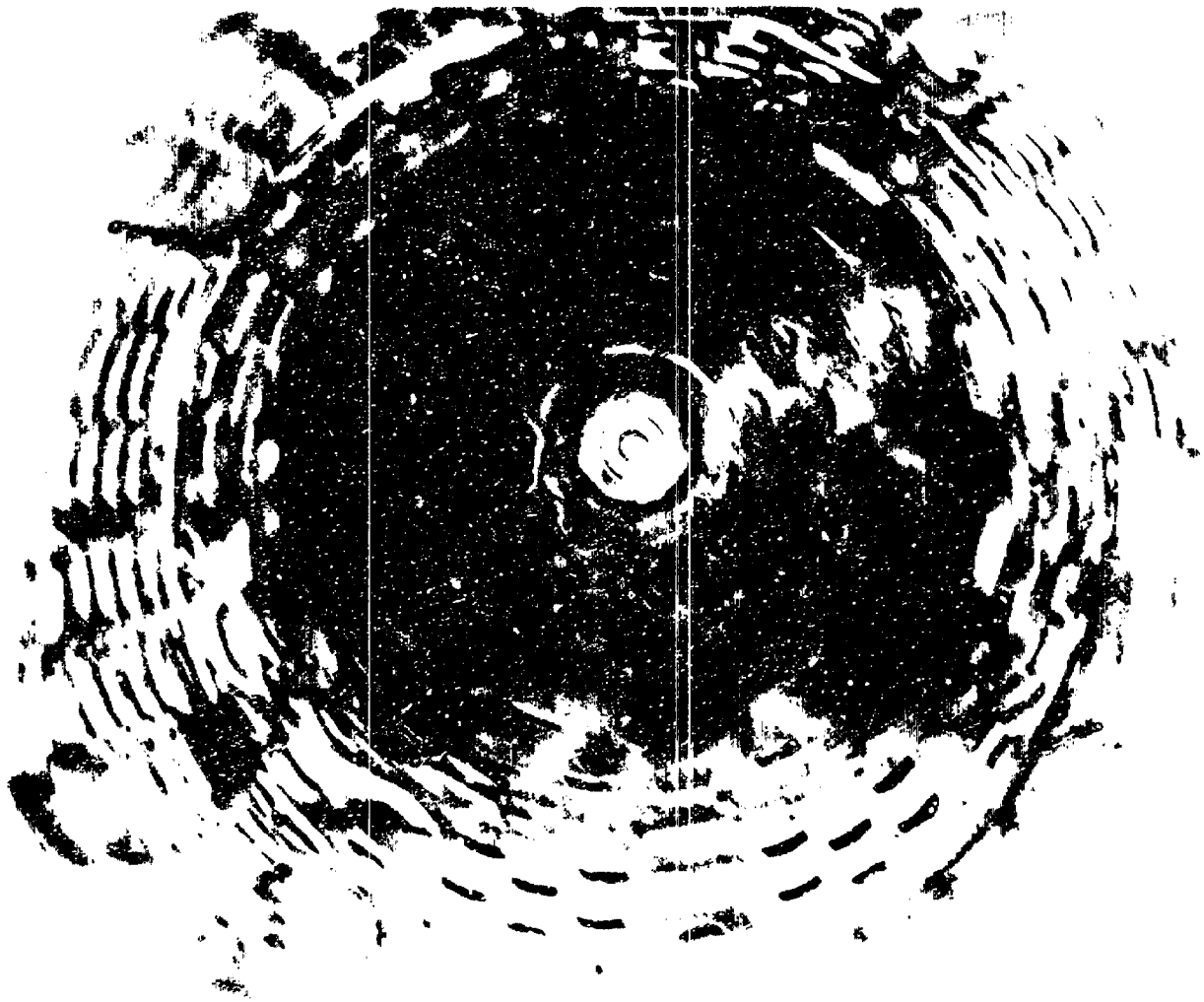

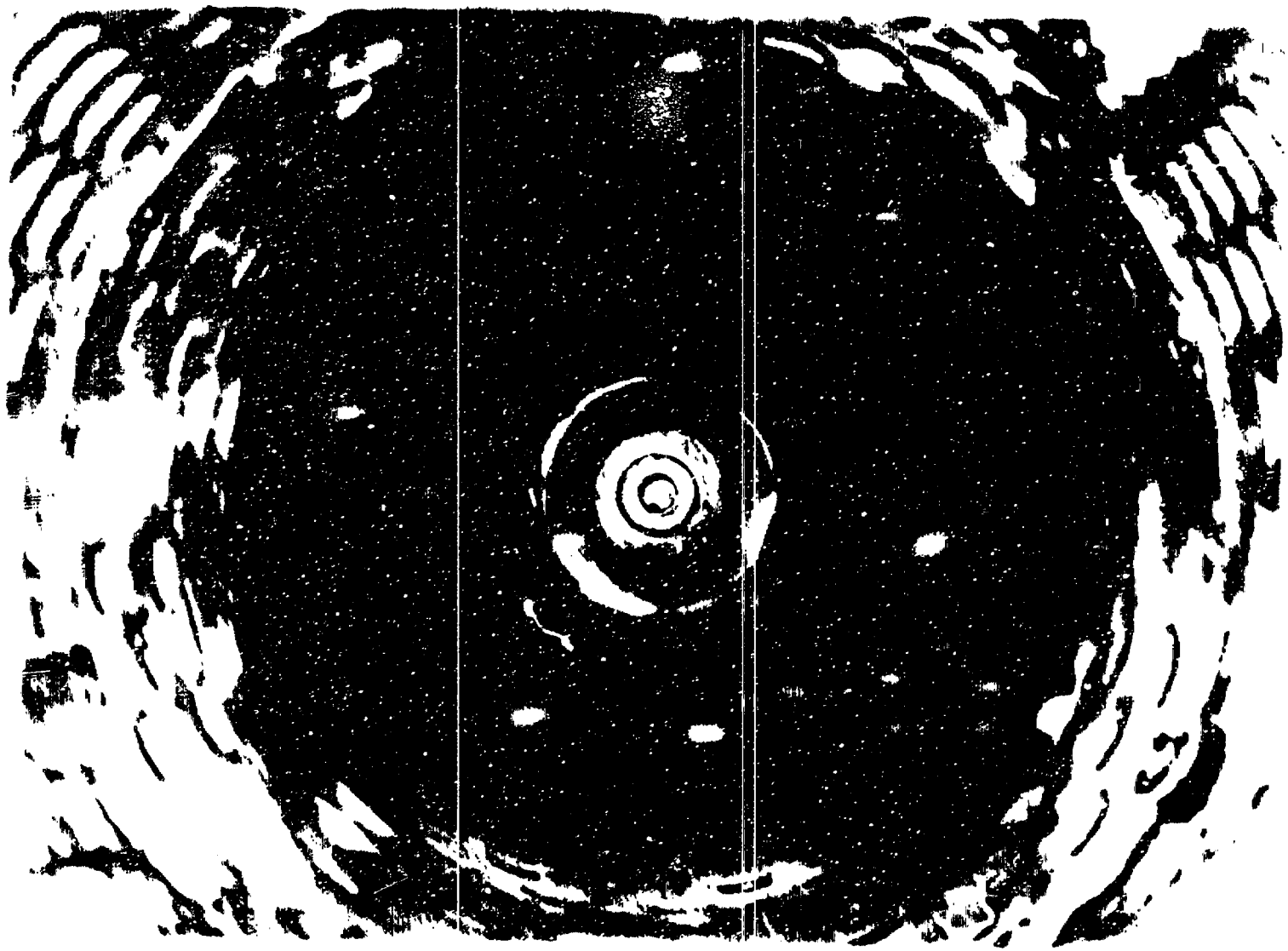

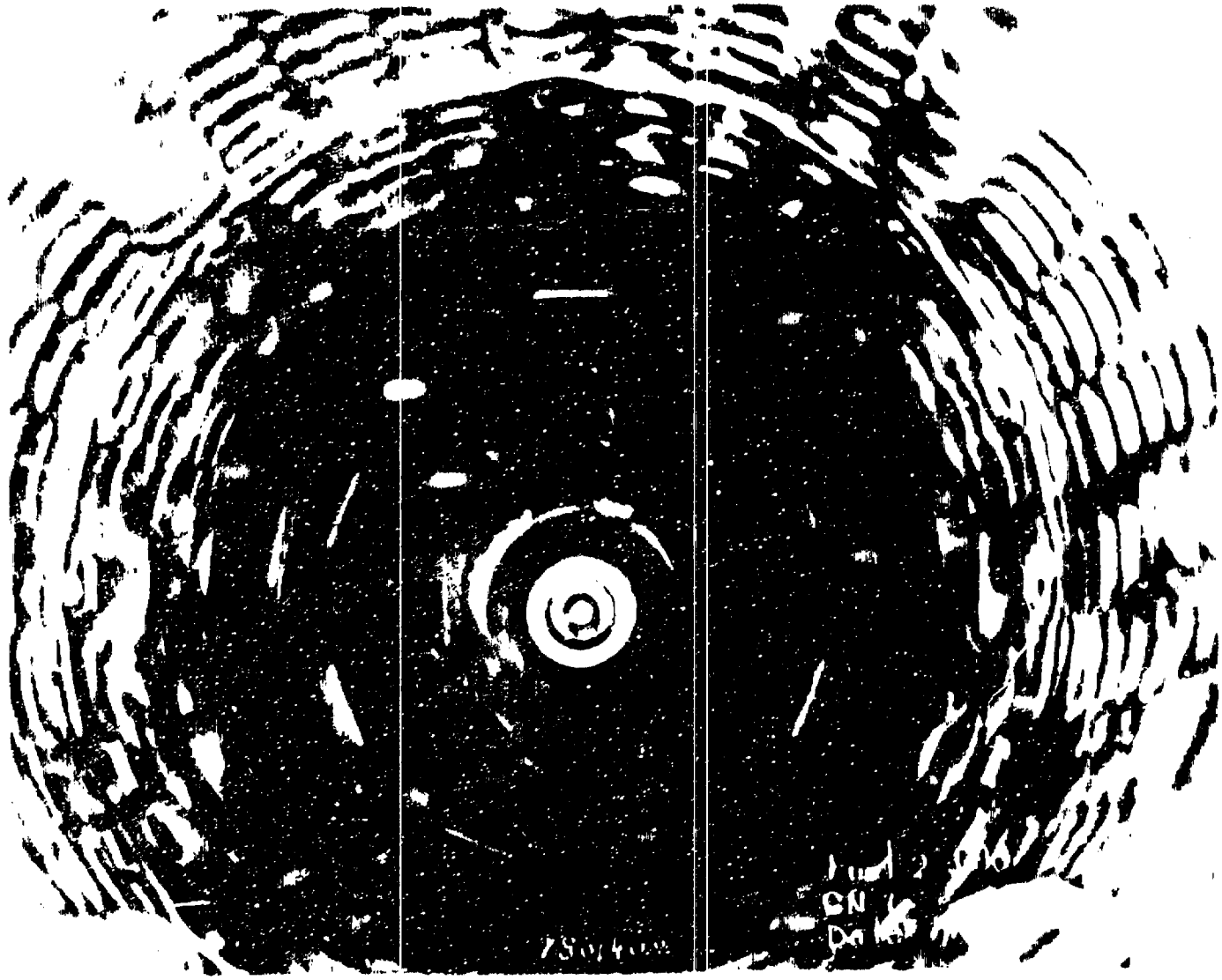

Figure B-1. Postfire Photograph of Liner After Test of Fuel 2.

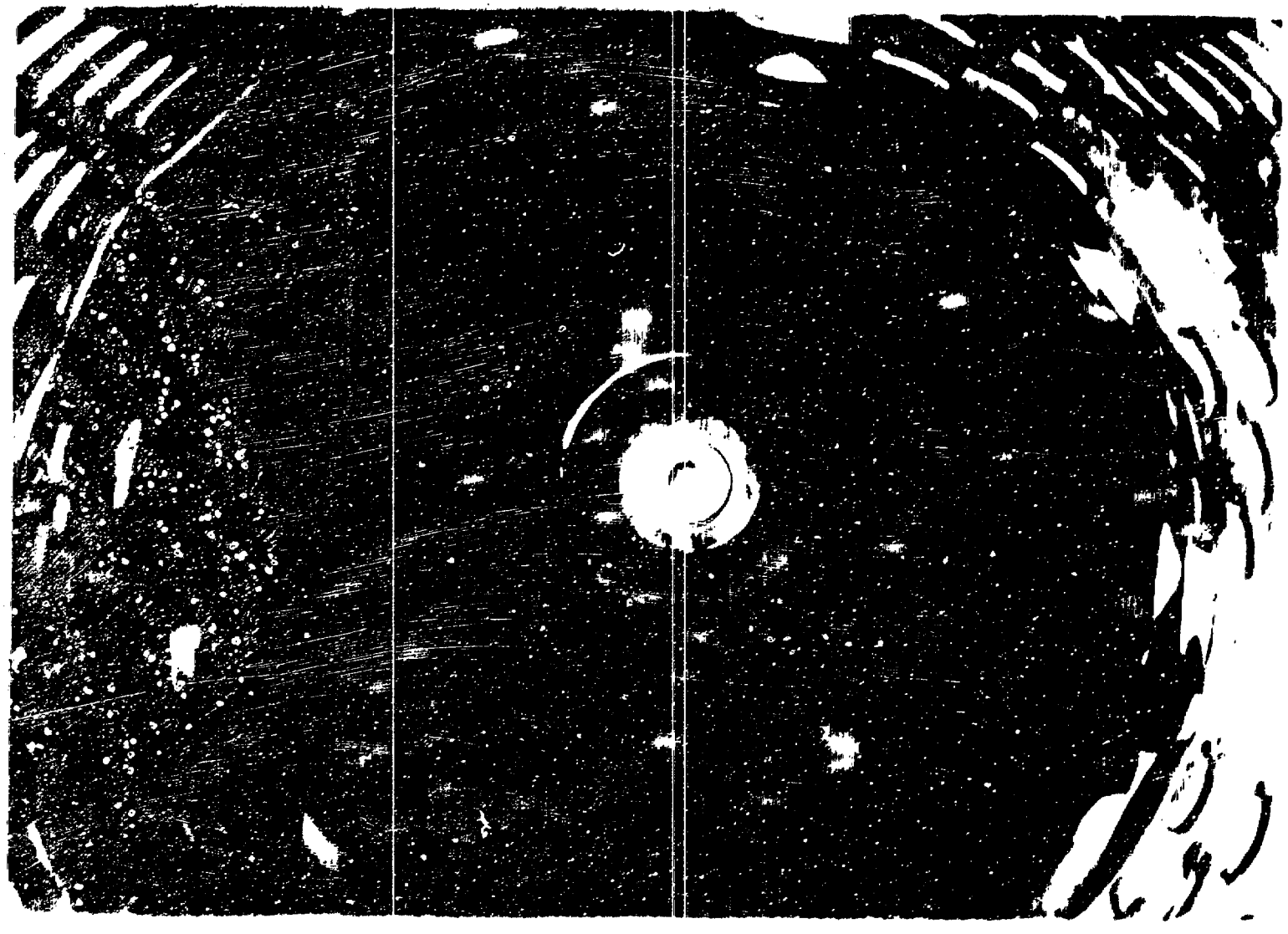

Figure E-4. Post-test Photograph of Liner After Test of Fuel 3.

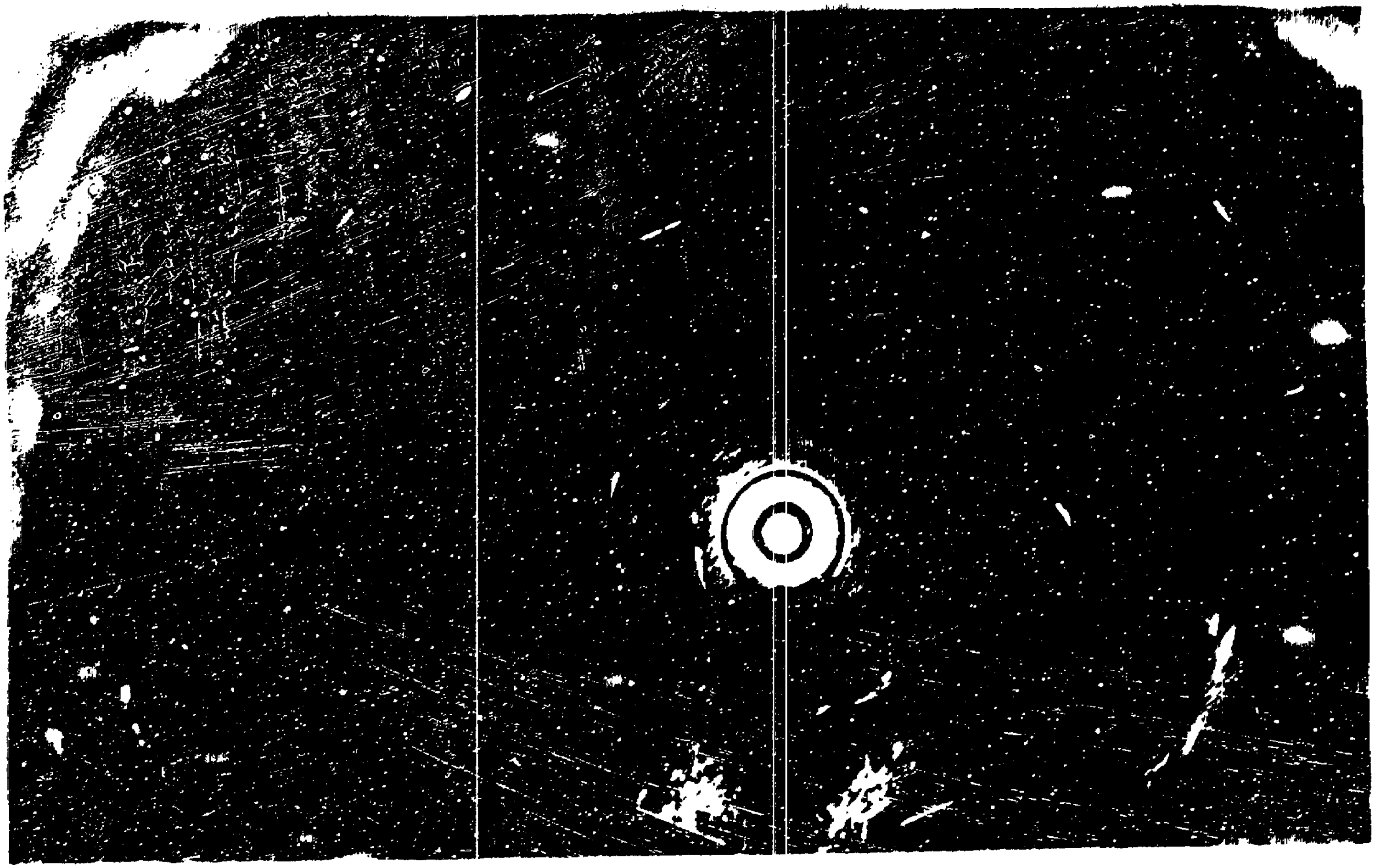

Figure 8-5. Posttest Photograph of Liner After Test of Fuel 4.

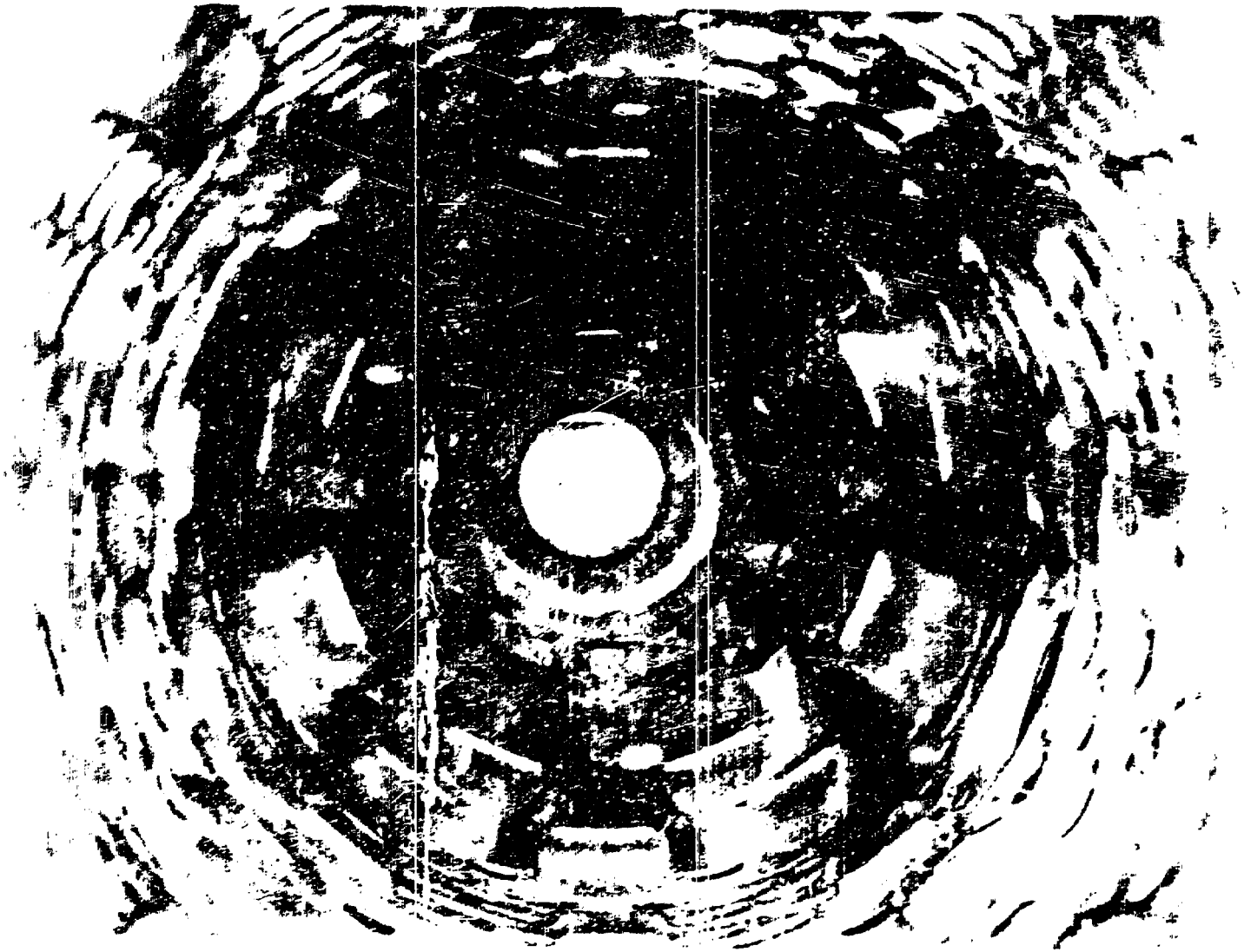

Figure B-6. Posttest Photograph of Liner After Test of Fuel 5.

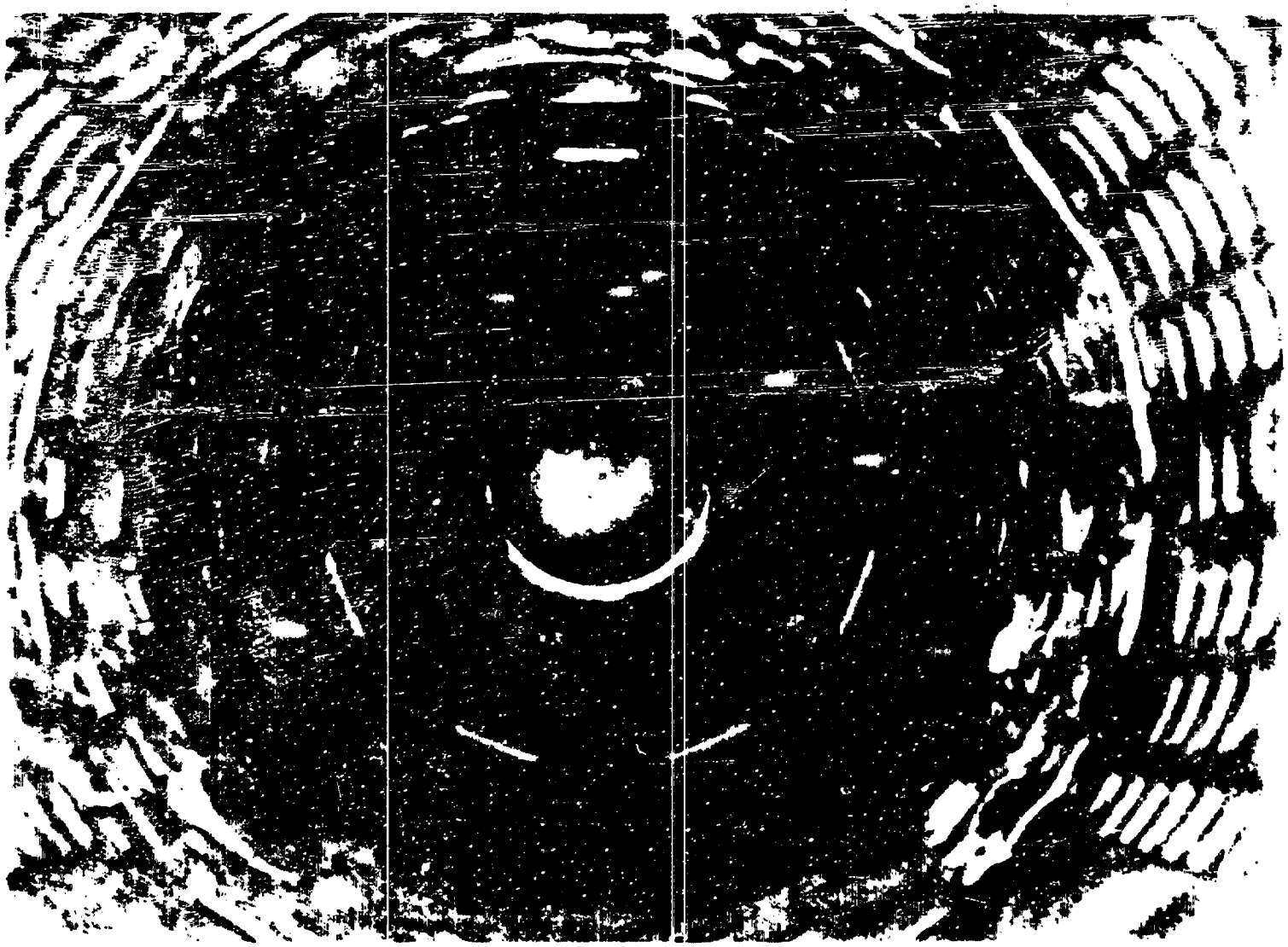

Figure B-7. Posttest Photograph of Liner After Test of Shot 6.

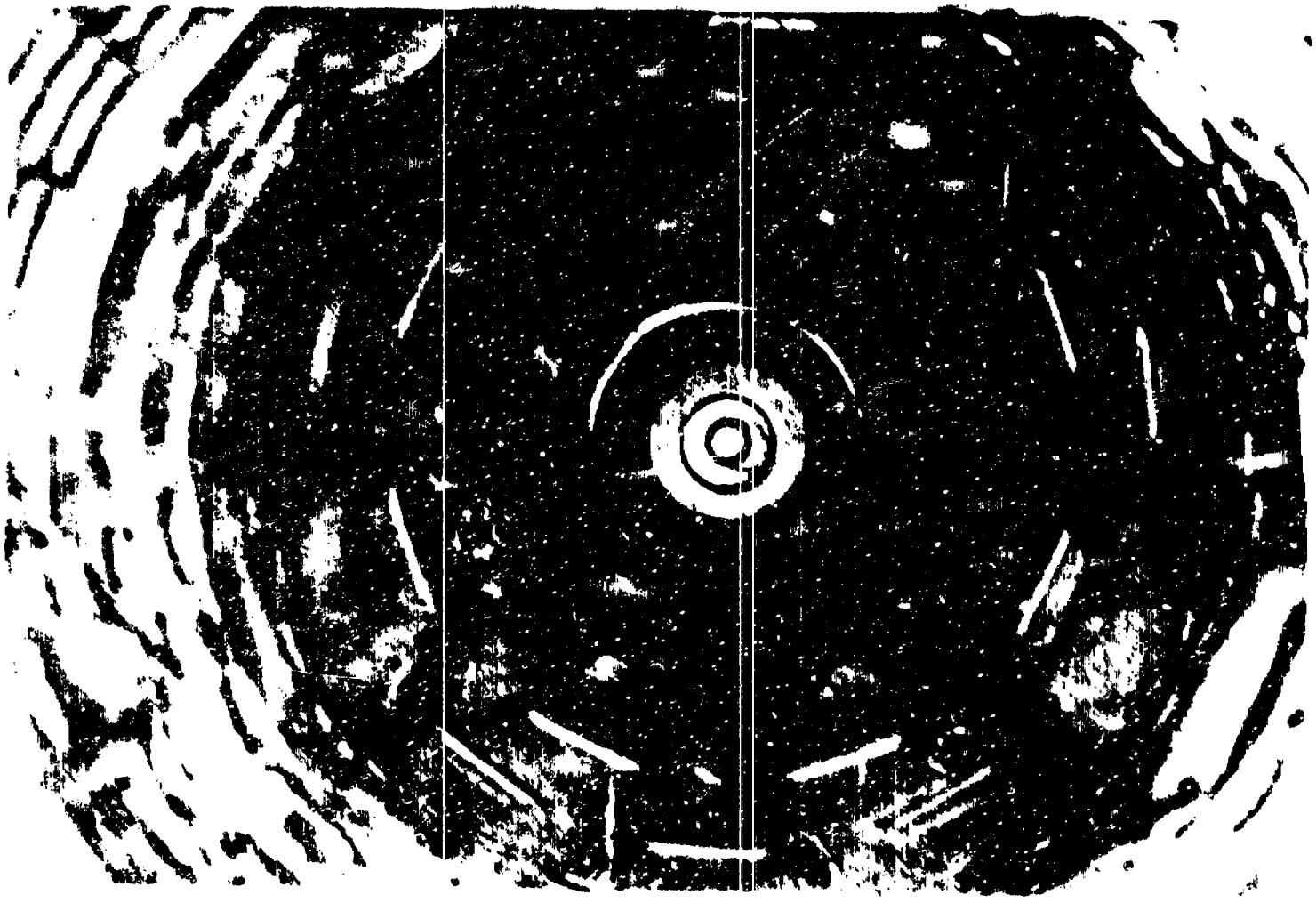

Figure B-8. Post-Test Photograph of Liner After Test of Fuel 7.

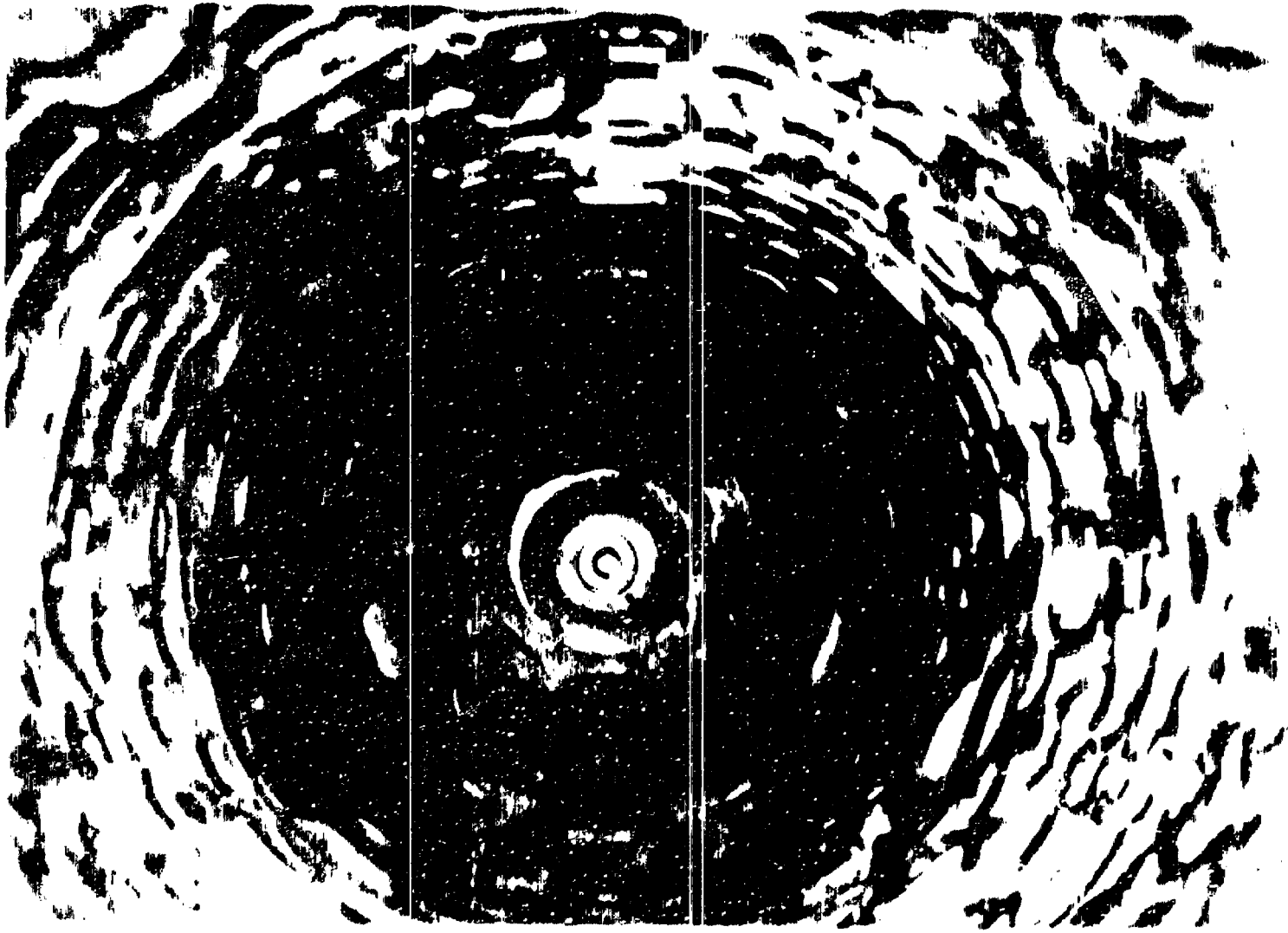

Figure F-9. Posttest Photograph of Cloth After Test of Fuel 9.

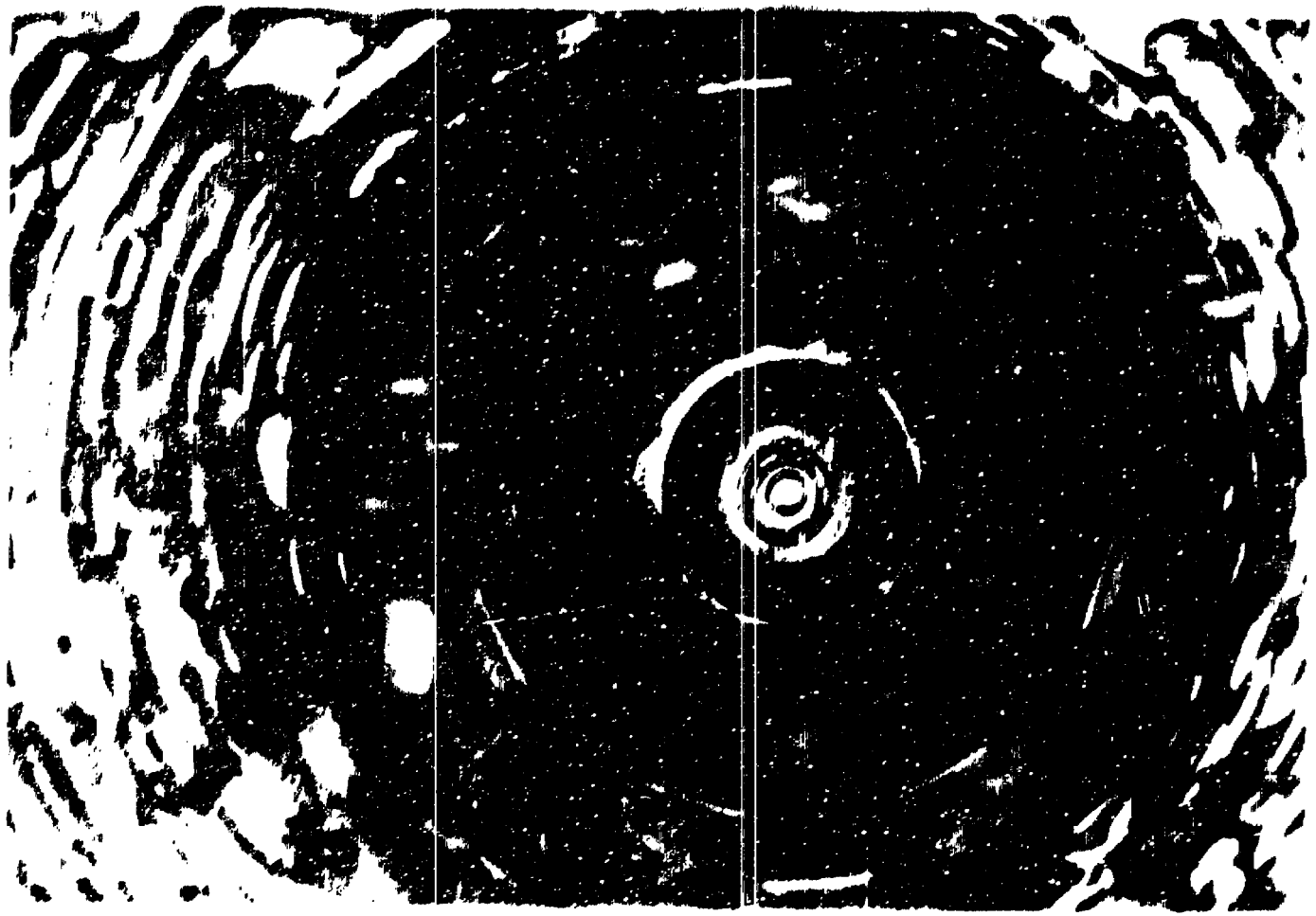

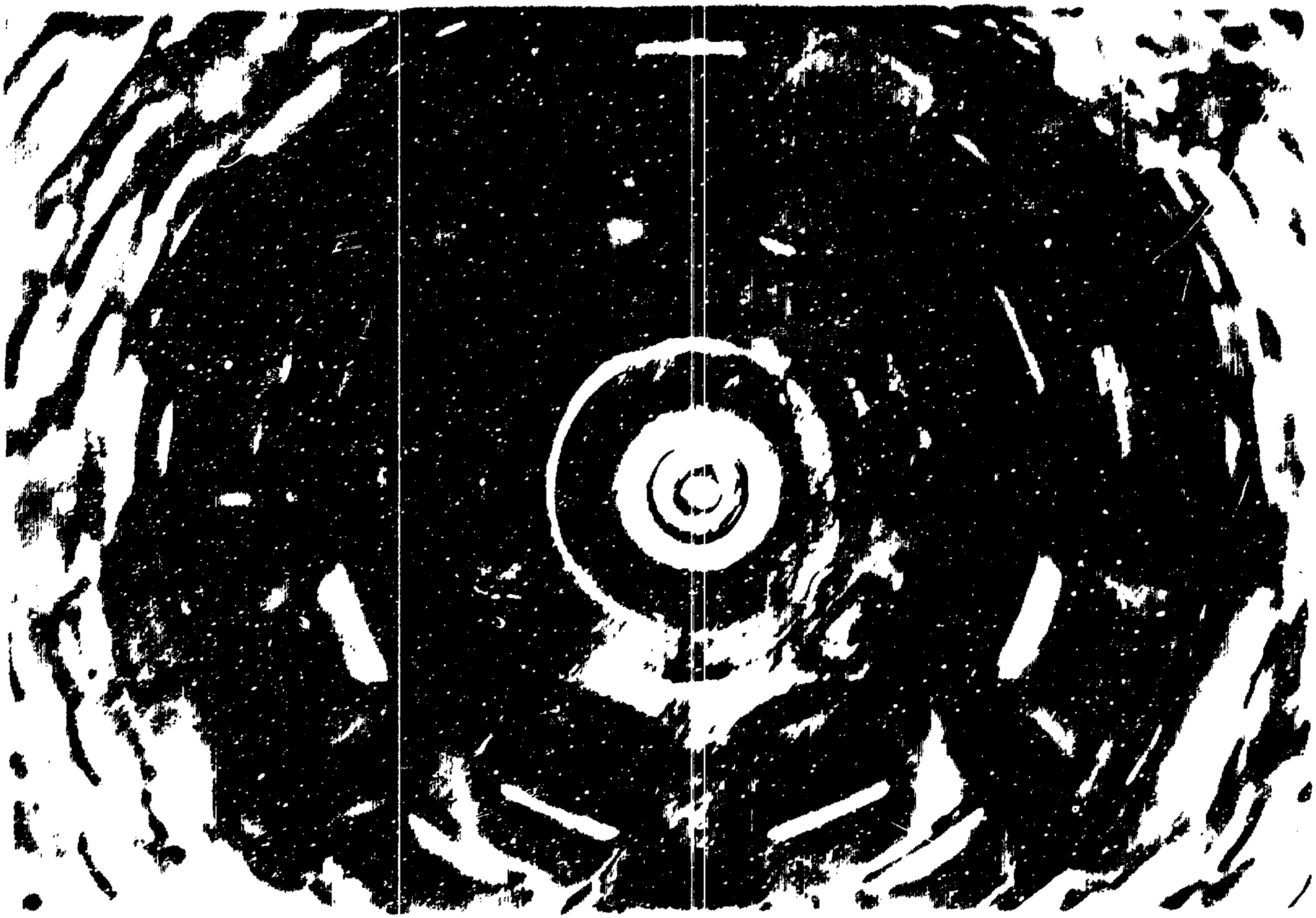

[illegible]

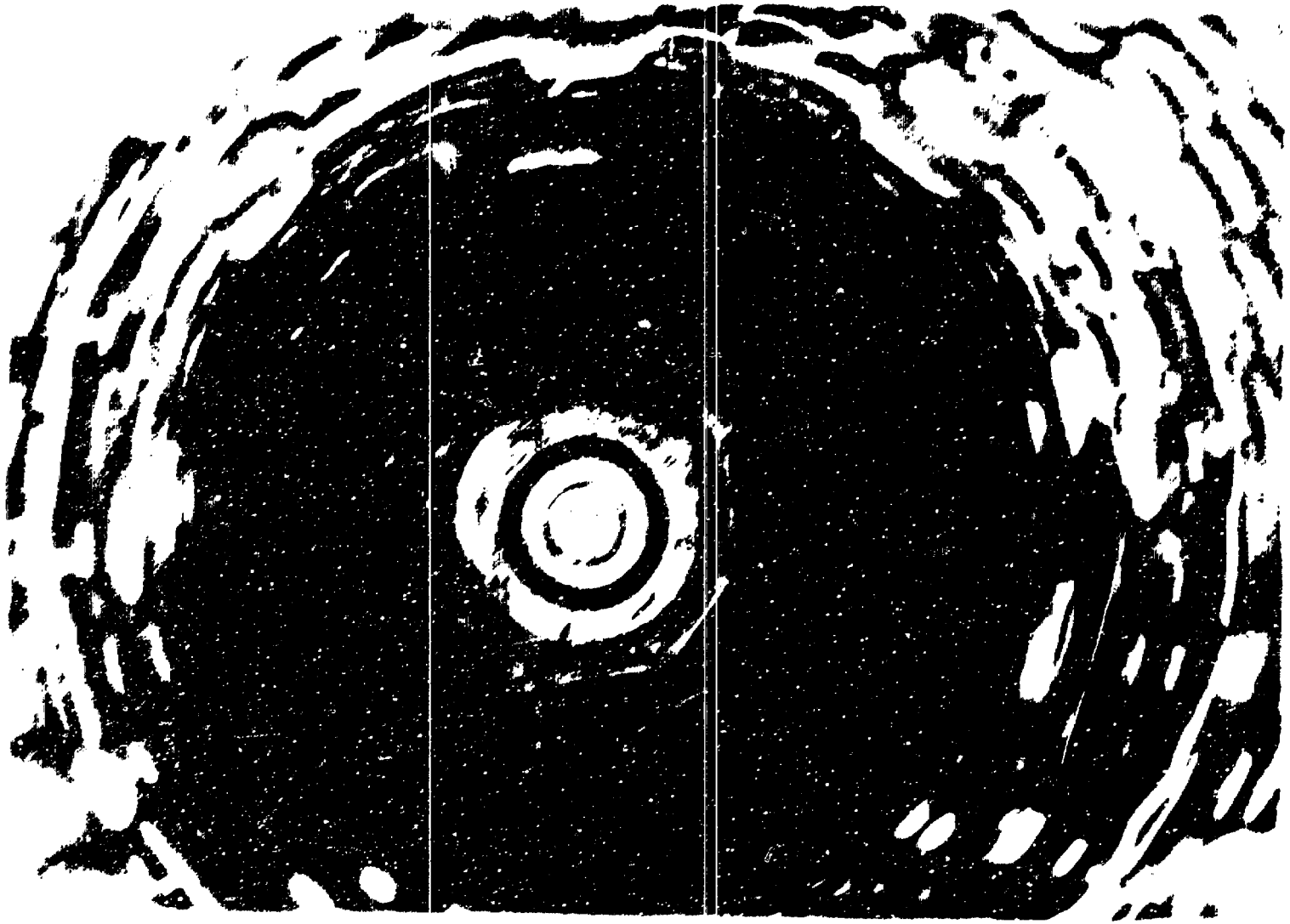

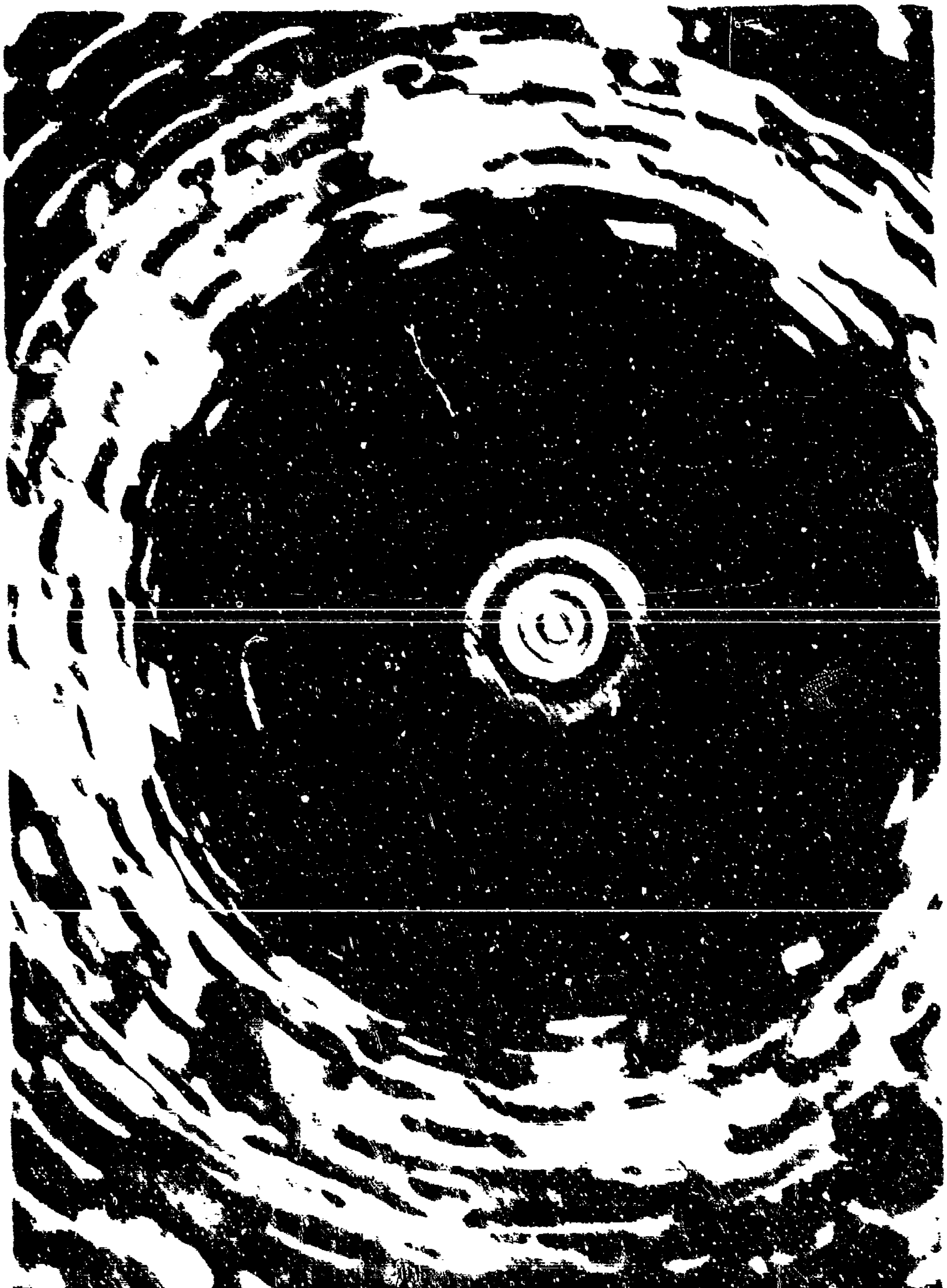

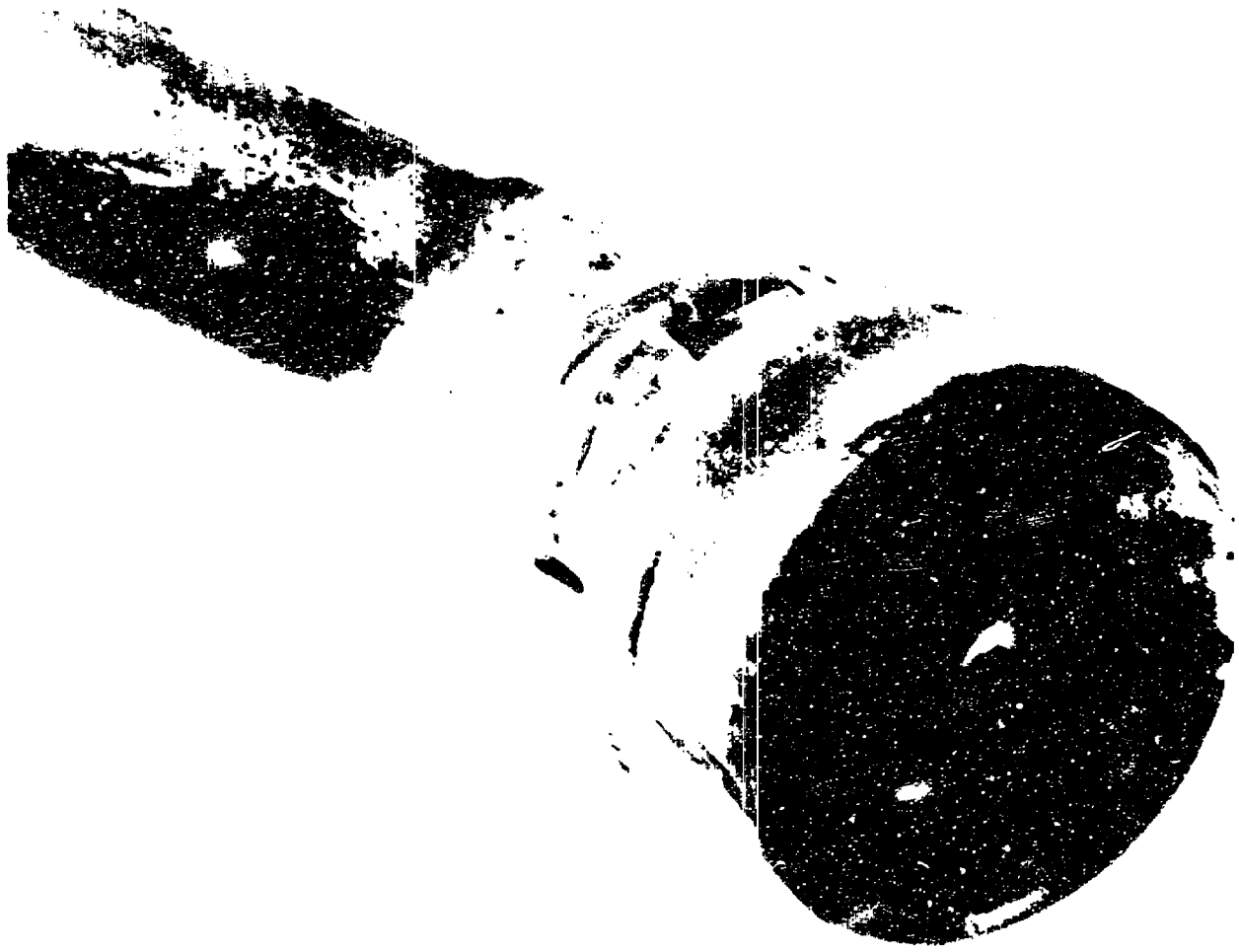

Figure B-14. Postlest Photograph of Fuel Nozzle After Test of Fuel 1.

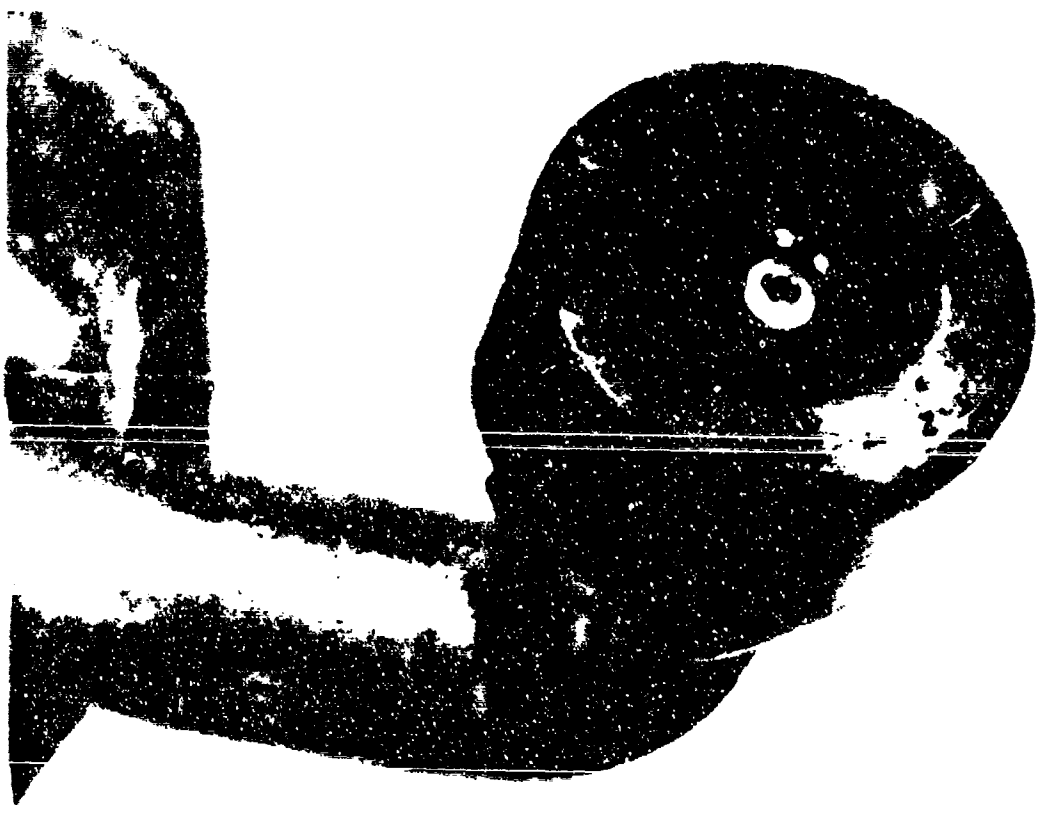

Figure B-15. Posttest Photograph of Fwd Nozzle After Test of Fwd IR.

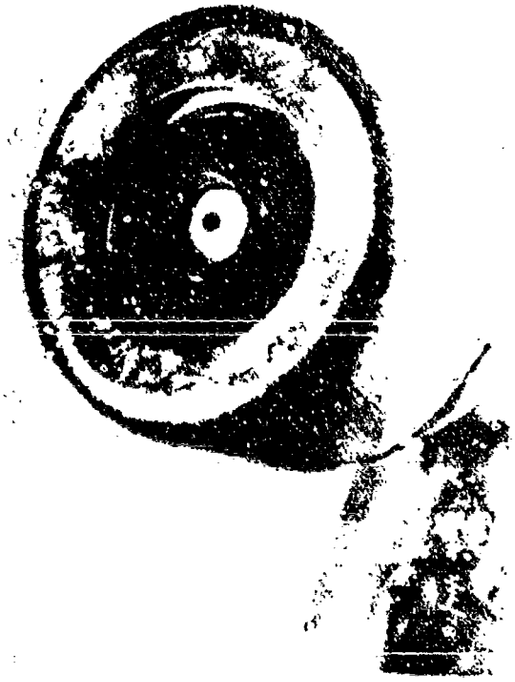

Figure B-16. Posttest Photograph of Jet Nozzle After Test of Jet 2.

Figure B-17. Posttest Photograph of Fuel Nozzle After Test of Fuel 5.

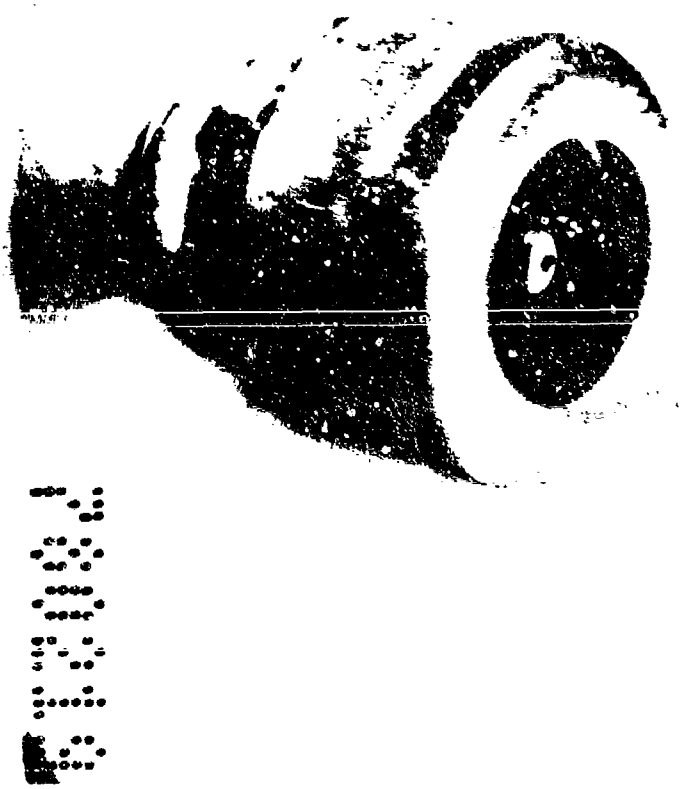

Figure B-18. Posttest Photograph of Fuel Nozzle After Test of Fuel 4.

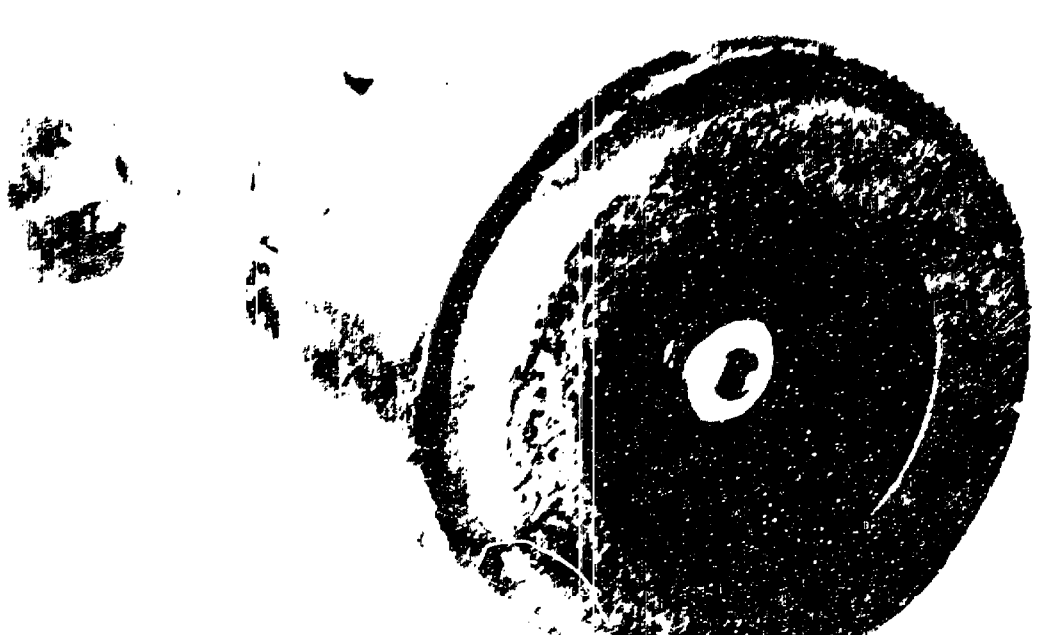

Figure B-19. Posttest Photograph of Fuel Nozzle After Test of Fuel 5.

Figure B-20. Posttest Photograph of Fuel Nozzle After Test of Fuel 6.

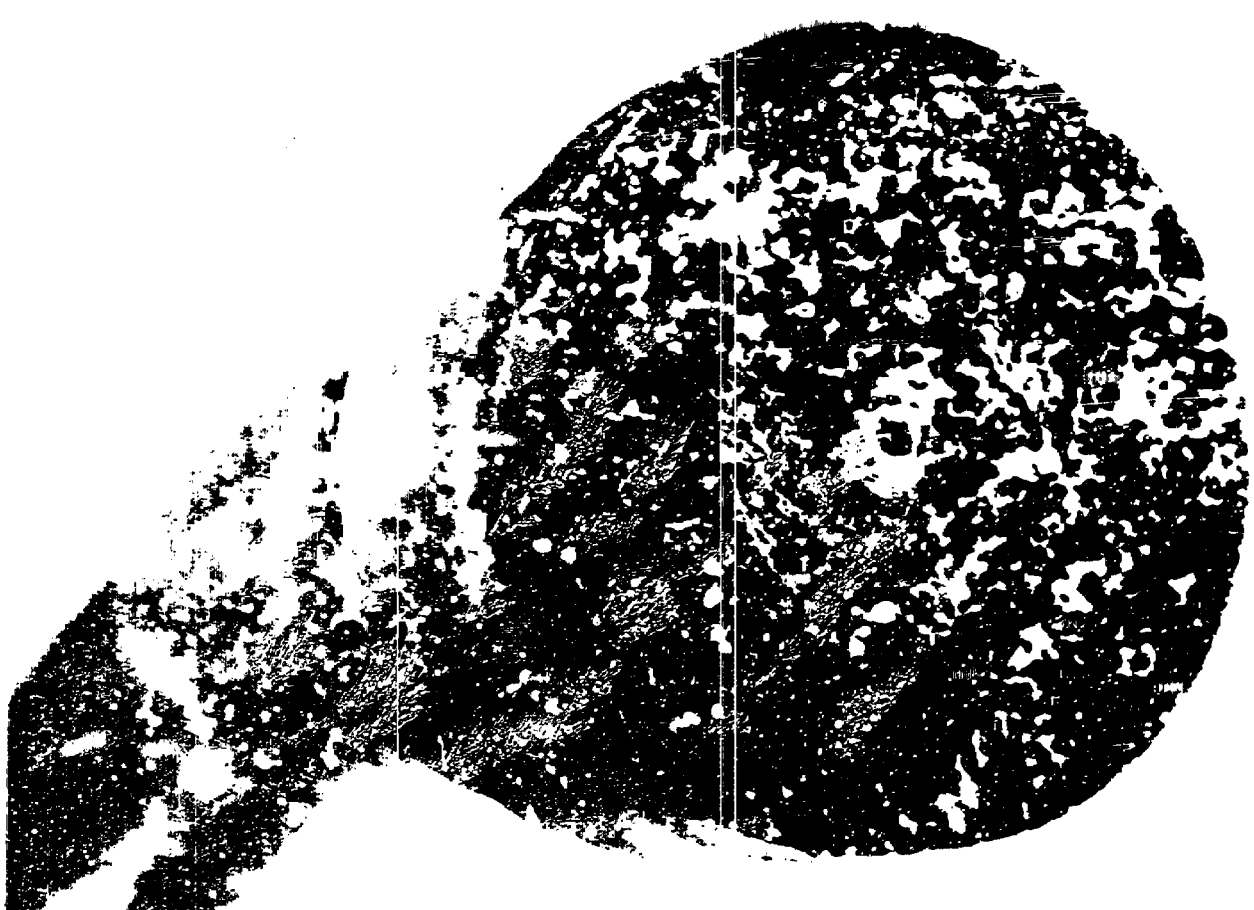

Figure B-21. Posttest Photograph of Fuel Nozzle After Test of Fuel 7.

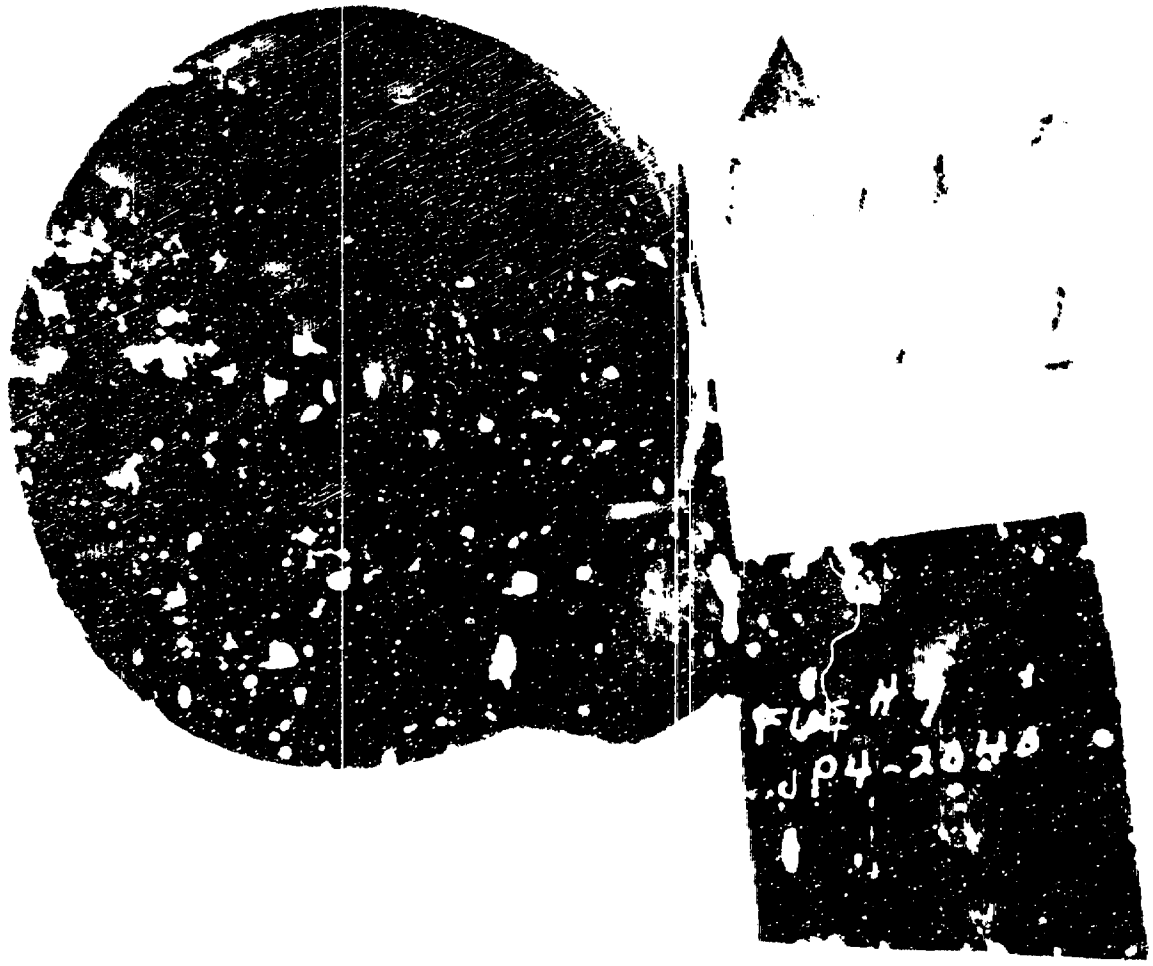

Figure B-22. Posttest Photograph of Fuel Nozzle After Test of Fuel 6.

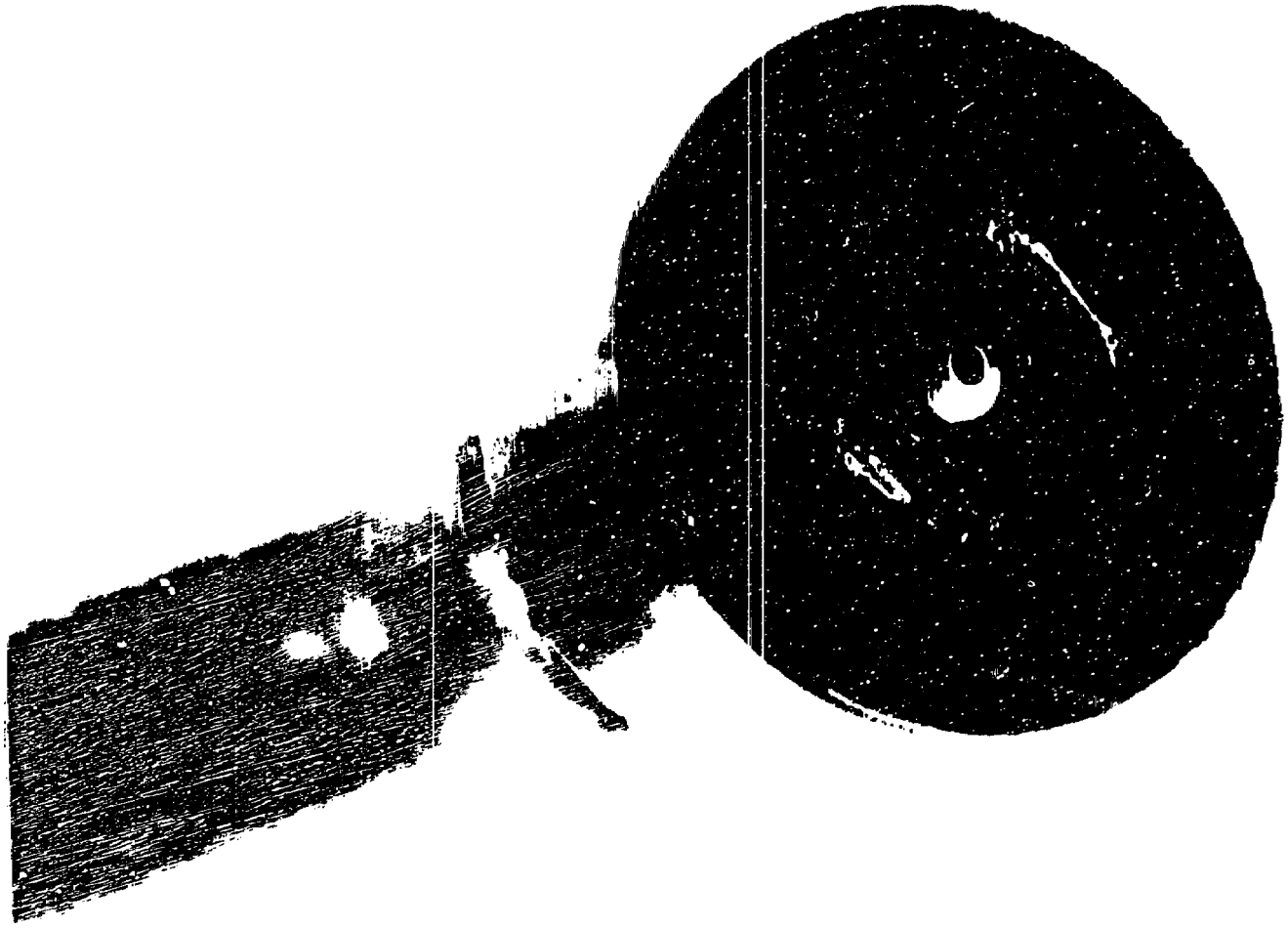

Figure B-23. Posttest Photograph of Fuel Nozzle After Test of Fuel 10.

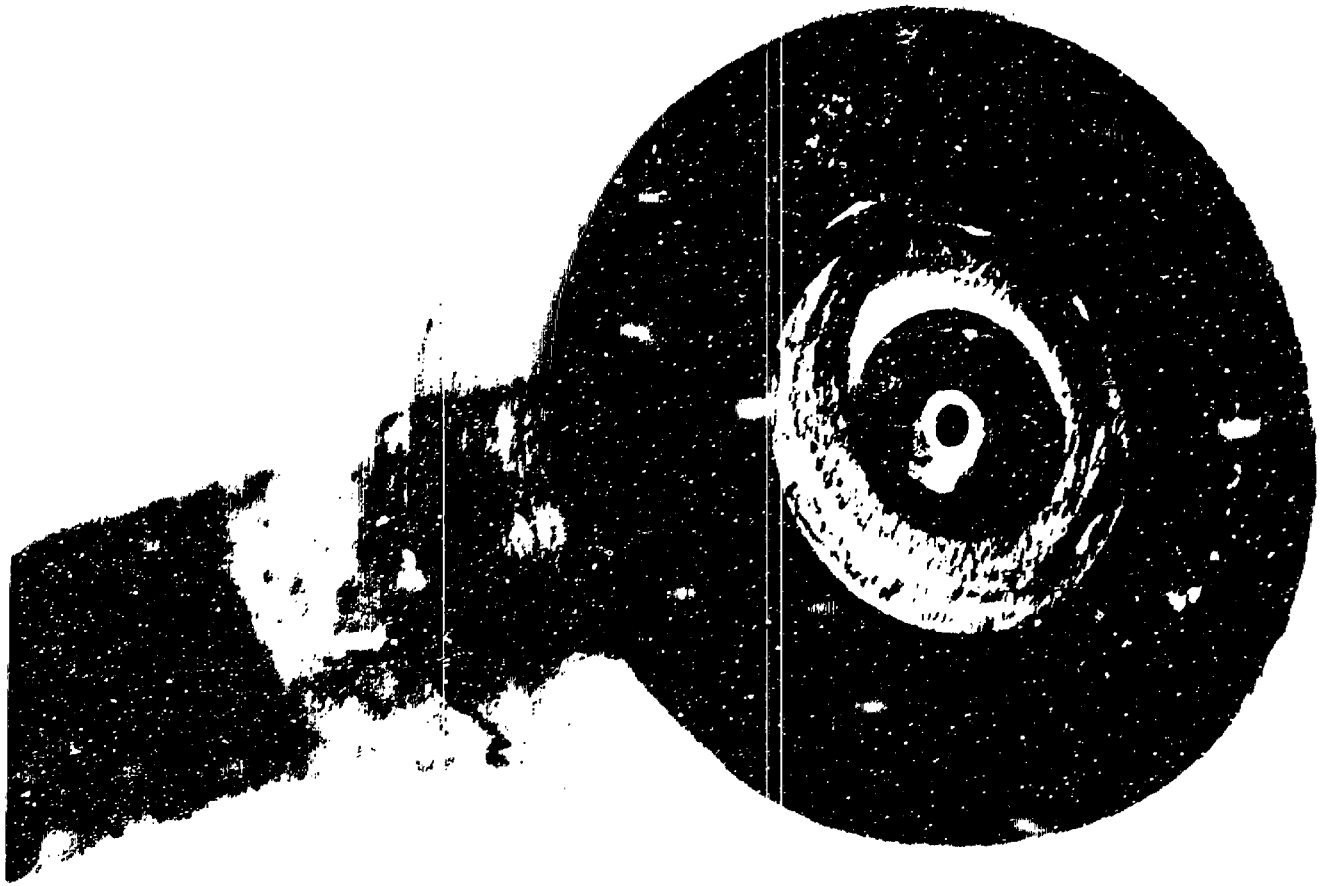

Figure B-24. Posttest Photograph of Fuel Nozzle After Test of Fuel II.

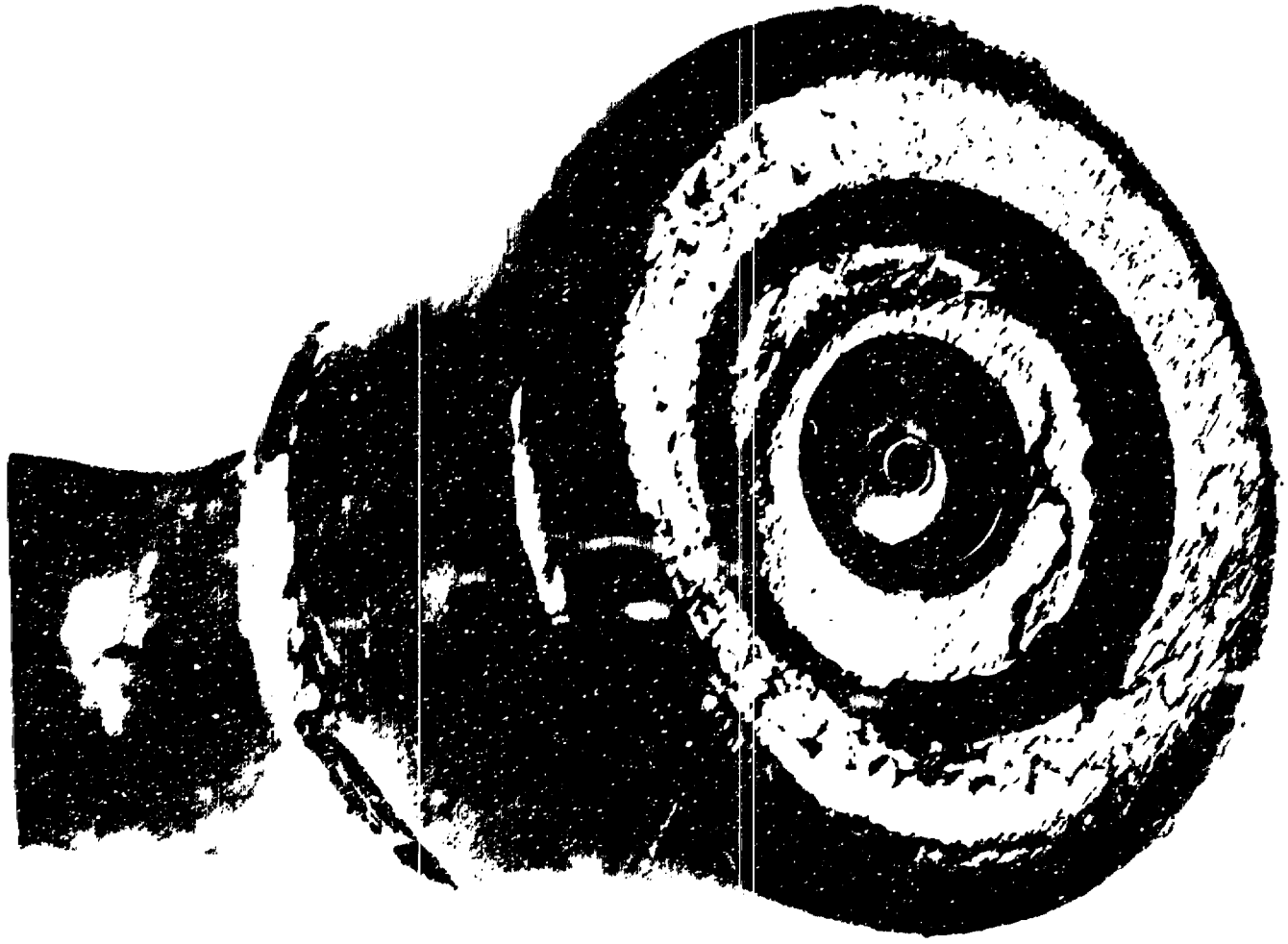

Figure B-25. Post test Photograph of Fuel Nozzle After Test of Fuel 17.

Figure B-26. Posttest Photograph of Fuel Nozzle After Test of Fuel 15.

APPENDIX C

LOW PRESSURE TEST DATA

Two types of test were conducted in the low pressure combustor test rig: altitude relight tests and cold-day ground start tests. Apparatus and procedures which were used are described in Section V-B.

Detailed results of the altitude relight tests are presented in tables C-1 through C-7. The combustor operating conditions are listed from which the simulated flight conditions were determined, and in the remarks column, the type of data point is indicated (LIGHT = maximum altitude relight capability at normal minimum fuel flow rate, PBO = pressure blowout, LLO = lean lightoff, LBO = lean blowout).

Detailed results of the cold-day ground start tests are listed in tables C-8 through C-11. At each combustor operating condition shown, lean lightoff and lean blowout fuel-air ratios were determined which are listed. All lightoff attempts were successful, so each test was terminated only after the planned minimum temperature (239K) was reached.

Table C-1. Altitude Relight Test Results, Fuel Number 1.

Fuel Number	Simulated Flight Condition Alt km	M_F -	Combustor Operating Conditions T_F K	T_3 K	P_3 kPa	W_a (engine) kg/s	$\frac{\Delta P}{P}$ %	$\frac{PT}{V}$ MPa-K m/s	W_f (engine) g/s	f g/kg	Remarks Light	PBO	LLO	LBO
1	15.2	0.89	247.7	241.7	23.9	2.267	5.66	0.326	42.2	18.6	Yes			
	18.3+	1.06	247.7	241.7	21.5	2.267	-	0.262	42.2	18.6		X		
	18.3+	1.06	241.5	239.8	21.5	2.267	6.35	0.262	21.4	9.3			X	
	18.3+	1.06	241.5	239.8	21.5	2.267	-	0.262	4.3	1.9				
	15.2	1.08	281.9	279.7	41.3	4.082	7.89	0.536	42.2	10.3	Yes			
	18.3+	1.16	281.9	279.7	30.6	4.082	-	0.295	42.2	10.3		X		
	18.3+	1.16	279.8	279.5	30.6	4.082	10.65	0.295	18.3	4.5			X	
	18.3+	1.16	279.8	279.5	30.6	4.082	-	0.295	3.8	0.9				X
	6.4	0.71	286.7	279.8	62.0	4.990	5.35	0.989	42.2	8.5	Yes			
	18.3+	1.19	286.7	279.8	35.7	4.990	-	0.328	42.2	8.5		X		
	18.3+	1.19	291.9	297.8	35.7	4.990	9.30	0.328	15.8	3.2			X	
	18.3+	1.19	291.9	297.8	35.7	4.990	-	0.328	4.0	0.8				-
1F	15.2	0.89	244.6	244.7	24.1	2.268	5.58	0.328	42.2	18.6	Yes			
	18.3+	1.06	244.6	244.7	21.6	2.268	-	0.265	42.2	18.6		X		
	18.3+	1.06	245.9	244.7	22.0	2.268	6.11	0.274	19.2	8.5			X	
	18.3+	1.06	245.9	244.7	22.0	2.268	-	0.274	2.5	1.1				X
	15.2	1.08	277.7	278.1	41.5	4.082	7.31	0.542	42.2	10.3	Yes			
	18.3+	1.16	277.7	278.1	30.5	4.082	-	0.312	42.2	10.3		X		
	18.3+	1.16	278.2	278.4	30.9	4.082	9.53	0.319	19.9	4.9			X	
	18.3+	1.16	278.2	278.4	30.9	4.082	-	0.319	9.5	2.3				X
	6.4	0.71	297.8	302.4	62.1	4.990	5.23	0.990	42.2	8.4	Yes			
	18.3+	1.19	297.8	302.4	35.4	4.990	-	0.322	42.2	8.4		X		
	18.3+	1.19	297.3	302.4	35.6	4.990	9.16	0.326	19.3	3.9			X	
	18.3+	1.19	297.3	302.4	35.6	4.990	-	0.326	2.5	0.5				X
	19.3+	1.29	291.8	291.8	68.9	9.072	13.28	0.647	42.2	4.7	Yes			
	18.3+	1.29	291.8	291.8	58.8	9.072	-	0.425	42.2	4.7		FL		
	18.3+	1.29	291.7	291.7	58.8	9.072	19.30	0.425	50.4	5.5			HIGH	
	18.3+	1.29	291.7	291.7	58.8	9.072	-	0.425	11.3	1.2				X

FL = Facility Limit, No Blowout

HIGH = Light @ W_f >42.2 g/s

Table C-2. Altitude Relight Test Results, Fuel Numbers 2 and 3.

FUEL NO.	SIMULATED FLIGHT CONDITION ALT	SIMULATED FLIGHT CONDITION M_p	COMBUSTOR OPERATING CONDITIONS T_F	T_3	P_3	W_c (engine)	$\frac{\Delta P}{P}$	$\frac{PT}{V}$	W_f (engine)	f	REMARKS Light	PBO	LLO	LBO
	km	-	K	K	kPa	kg/s	%	MPa-K / m/s	g/s	g/kg				
2	6.8	0.44	244.0	243.8	46.7	2.268	3.21	1.236	42.2	18.6	YES			
	18.3+	1.06	244.0	243.8	21.0	2.268	--	0.250	42.2	18.6		X		
	18.3+	1.06	243.5	244.1	24.0	2.268	6.23	0.328	44.4	20.5			HIGH	
	18.3+	1.06	242.5	244.1	24.0	2.268	--	0.328	16.9	7.5				X
	15.2	1.08	277.2	277.9	40.1	4.082	8.12	0.506	42.2	10.3	YES			
	18.3+	1.16	277.2	277.9	28.8	4.082	--	0.261	42.2	10.3		X		
	18.3+	1.16	278.0	277.9	30.1	4.082	10.82	0.285	41.5	10.2			X	
	18.3+	1.16	278.0	277.9	30.1	4.082	--	0.285	10.5	2.6				X
	6.6	0.72	290.3	292.9	60.9	4.990	5.27	0.953	42.2	8.4	YES			
	18.3+	1.19	290.3	292.9	33.9	4.990	--	0.295	42.2	8.4		X		
	18.3+	1.19	288.9	292.8	34.2	4.990	9.31	0.301	30.2	6.1			X	
	18.3+	1.19	288.9	292.8	34.2	4.990	--	0.301	7.6	1.5				X
	18.3+	1.29	292.1	289.4	67.7	9.072	13.16	0.648	42.2	4.7	YES			
	18.3+	1.29	292.1	289.4	51.5	9.072	--	0.375	42.2	4.7		X		
	18.3+	1.29	291.7	289.3	54.5	9.072	16.33	0.421	47.3	5.2			HIGH	
	18.3+	1.29	291.7	289.3	54.5	9.072	--	0.421	7.4	0.8				X
3	15.2	0.89	244.4	243.5	24.1	2.267	5.98	0.329	42.2	18.6	NO			
	6.1	0.42	247.0	244.0	50.6	2.267	2.85	1.449	44.5	19.6			HIGH	
	18.3+	1.06	247.0	244.0	19.6	2.267	7.36	0.217	44.5	19.6		X		
	6.1	0.42	247.0	244.0	50.6	2.267	--	1.449	31.5	13.9				X
	15.2	1.08	275.3	279.4	41.6	4.082	7.84	0.543	42.2	10.3	YES			
	18.3+	1.16	275.3	279.4	30.6	4.082	--	0.295	42.2	10.3		X		
	18.3+	1.16	272.0	279.6	31.1	4.082	10.48	0.304	45.1	11.1			HIGH	
	18.3+	1.16	272.0	279.6	31.1	4.082	--	0.304	13.2	3.2				X
	6.4	0.71	295.0	285.2	62.0	4.989	5.22	0.988	42.2	8.5	YES			
	18.3+	1.19	295.0	285.2	34.2	4.989	--	0.301	42.2	8.5		X		
	18.3+	1.19	295.0	285.5	34.5	4.989	9.36	0.306	42.2	8.5			X	
	18.3+	1.19	295.0	285.5	34.5	4.989	--	0.306	12.6	2.5				X
	18.3+	1.29	293.6	272.4	69.0	9.072	14.39	0.674	42.2	4.7	YES			
	18.3+	1.29	293.4	272.4	52.5	9.072	--	0.390	42.2	4.7		FL		
	18.3+	1.29	293.0	272.3	61.4	9.072	16.16	0.534	45.1	5.0			HIGH	
	18.3+	1.29	293.0	272.3	61.4	9.072	--	0.534	11.3	1.3				X

FL = Facility Limit, No Blowout

Table C-3. Altitude Relight Test Results, Fuel Numbers 4 and 5.

Fuel Number	Simulated Flight Condition		Combustor Operating Conditions								Remarks			
	Alt.	M_P	T_F	T_3	P_3	W_c (engine)	$\frac{\Delta P}{P}$	$\frac{PT}{V}$	W_f (engine)	f	Light	PBO	LLO	LEO
	km	-	K	K	kPa	kg/s	%	MPa-k/m/s	g/s	g/kg				
4	15.2	0.89	243.8	244.7	24.06	2.267	3.52	0.328	42.2	18.6	No			
	10.1	0.59	247.0	244.7	31.92	2.267	7.02	0.577	48.5	21.4			HIGH	
	18.3+	1.06	247.0	244.7	21.78	2.267	-	0.269	48.5	21.4		X		
	10.1	0.59	247.0	244.7	31.92	2.267	7.02	0.577	20.8	9.2				X
	9.2	0.76	276.4	279.4	44.82	4.082	6.80	0.631	42.2	10.3	Yes			
	18.3+	1.16	276.4	279.4	31.65	4.082	-	0.315	42.2	10.3		X		
	18.3+	1.16	278.4	279.7	32.34	4.082	9.43	0.329	42.2	10.3			X	
	18.3+	1.16	278.4	279.7	32.34	4.082	-	0.329	10.1	2.5				X
	9.4	0.84	296.2	284.1	51.92	4.989	7.62	0.693	42.2	8.5	Yes			
	18.3+	1.19	296.2	284.1	35.37	4.989	-	0.322	42.2	8.5		X		
	18.3+	1.19	297.0	276.7	35.37	4.989	11.86	0.322	42.2	8.5			X	
	18.3+	1.19	297.0	276.7	35.37	4.989	-	0.322	42.2	8.5				X
	18.3+	1.29	281.5	282.0	68.88	9.072	13.28	0.671	42.2	4.7	No HIGH			
	18.3+	1.29	289.8	283.3	68.88	9.072	13.28	0.671	56.6	6.2		FL		
	18.3+	1.29	289.8	283.3	54.12	9.072	16.90	0.414	42.2	4.7				
	18.3+	1.29	289.8	283.3	68.88	9.072	-	0.671	21.2	2.3				X
5	15.2	0.89	243.5	245.9	24.06	2.267	6.03	0.328	42.2	18.6	Yes			
	18.3+	1.06	243.5	245.9	19.65	2.267	-	0.218	42.2	18.6		X		
	18.3+	1.06	243.5	245.9	22.75	2.267	6.03	0.293	42.2	18.6			X	
	18.3+	1.06	243.5	245.9	22.75	2.267	-	0.293	19.7	8.7				X
	9.2	0.76	277.3	277.8	44.68	4.082	5.23	0.627	42.2	10.3	Yes			
	18.3+	1.16	277.3	277.8	32.54	4.082	-	0.333	42.2	10.3		X		
	18.3+	1.16	275.9	278.1	32.34	4.082	7.23	0.329	41.6	10.2			X	
	18.3+	1.16	275.9	278.1	32.34	4.082	-	0.329	18.3	4.5				X
	9.5	0.85	288.7	310.0	51.71	4.989	6.79	0.688	42.2	8.5	Yes			
	18.3+	1.19	288.7	310.0	35.58	4.989	-	0.326	42.2	8.5		X		
	18.3+	1.19	292.6	310.4	35.58	4.989	9.86	0.326	42.8	8.6			X	
	18.3+	1.19	292.6	310.4	35.58	4.989	-	0.326	16.1	3.2				X
	18.3+	1.29	293.9	303.1	68.88	9.072	16.22	0.671	42.2	4.7	Yes			
	18.3+	1.29	293.9	303.1	53.92	9.072	20.72	0.411	42.2	4.7		FL		
	18.3+	1.29	295.0	302.6	53.85	9.072	20.75	0.410	43.1	4.8			HIGH	
	18.3+	1.29	295.0	302.6	53.85	9.072	-	0.410	11.3	1.3				X

FL = Facility Limit, No Blowout

Table C-4. Altitude Relight Test Results, Fuel Numbers 6 and 7.

Fuel Number	Simulated Flight Condition		Combustor Operating Conditions								Remarks			
	Alt.	M_T	T_2	T_3	P_3	W_c (engine)	$\frac{\Delta P}{P}$	$\frac{PT}{V}$	W_f (engine)	f				
	km	-	K	K	kPa	kg/s	%	MPa-K / m/s	g/s	g/kg	Ignition	PBO	LLO	LBO
6	19.2	0.89	243.9	243.4	24.34	2.267	6.58	0.335	42.2	18.6	Yes			
	18.3+	1.06	244.8	242.9	22.34	2.267	-	0.282	42.2	18.6		X		
	18.3+	1.06	244.8	242.9	22.68	2.267	7.06	0.291	42.2	18.6			X	
	18.3+	1.06	244.8	242.9	22.68	2.267	-	0.291	13.7	6.0				X
	9.2	0.76	278.8	278.2	45.02	4.082	5.53	0.637	42.2	10.3	Yes			
	18.3+	1.16	278.8	278.2	31.23	4.082	-	0.307	42.2	10.3		X		
	18.3+	1.16	278.4	278.5	31.51	4.082	7.98	0.312	42.2	10.3			X	
	18.3+	1.16	278.4	278.5	31.51	4.082	-	0.312	11.3	2.8				X
	9.4	0.84	290.5	292.6	51.85	4.989	7.08	0.691	42.2	8.5	Yes			
	18.3+	1.19	290.5	292.6	35.65	4.989	-	0.327	42.2	8.5		X		
	18.3+	1.19	292.0	292.8	35.92	4.989	10.22	0.332	42.2	8.5			X	
	18.3+	1.19	292.0	292.8	35.92	4.989	-	0.332	4.4	0.9				X
	18.3+	1.29	292.6	293.9	69.09	9.072	16.18	0.675	42.2	4.7	Yes			
	18.3+	1.29	292.6	293.9	53.43	9.072	-	0.404	42.2	4.7		FL		
	18.3+	1.29	294.3	294.5	55.02	9.072	20.30	0.428	42.2	4.7			X	
	18.3+	1.29	294.3	294.5	55.02	9.072	-	0.428	11.3	1.3				X
7	14.0	0.85	242.0	245.7	24.55	2.267	6.68	0.351	58.0	23.6	HIGH			
	18.3+	1.06	245.4	245.2	23.13	2.267	-	0.303	58.0	23.6		HIGH		
	14.0	0.85	245.2	244.9	24.55	2.267	4.96	0.341	84.2	28.3			HIGH	
	14.0	0.85	246.5	241.2	24.55	2.267	-	0.341	31.5	13.9				X
	9.6	0.76	278.4	276.8	44.80	4.082	6.60	0.631	42.2	10.3	Yes			
	18.3+	1.16	278.9	276.6	20.08	4.082	-	0.127	42.2	10.3		X		
	18.3+	1.16	279.3	278.4	21.43	4.082	23.20	0.144	42.2	10.3			X	
	18.3+	1.16	279.8	277.4	21.43	4.082	-	0.144	12.0	2.9				X
	9.4	0.84	297.8	309.8	51.81	4.989	7.97	0.690	42.2	8.5	Yes			
	18.3+	1.19	300.4	309.7	29.08	4.989	-	0.104	42.2	8.5		X		
	18.3+	1.19	301.5	309.2	33.64	4.989	29.98	0.144	42.2	8.5			X	
	18.3+	1.19	300.6	309.4	23.64	4.989	-	0.144	12.6	2.5				X
	18.3+	1.29	300.8	305.5	68.95	9.071	13.75	0.672	42.2	4.6	Yes			
	18.3+	1.29	301.5	307.1	37.18	9.071	-	0.196	42.2	4.6		FL		
	18.3+	1.29	302.0	309.4	39.99	9.071	38.53	0.226	79.5	8.8			HIGH	
	18.3+	1.29	302.3	309.0	39.99	9.071	-	0.226	16.4	1.8				X

FL = Facility Limit, No Blowout

Table C-5. Altitude Relight Test Results, Fuel Numbers 8 and 9.

Fuel Number	Simulated Flight Condition: Alt. km	Simulated Flight Condition: M_∞ -	Combustor Operating Conditions: T_2 K	T_3 K	P_3 kPa	W_c (engine) kg/s	$\frac{\Delta P}{P}$ %	$\frac{PT}{V}$ MPa-K/s	W_f (engine) g/s	f g/kg	Remarks: Light	PBO	LLO	LBO
8	11.5	0.69	245.5	246.0	27.40	2.267	4.54	0.425	42.2	18.6	Yes			
	18.3+	1.06	247.6	245.4	13.78	2.267	-	0.188	42.2	13.6		FL		
	11.3	0.67	244.3	242.5	28.28	2.267	4.62	0.453	42.2	18.6			X	
	11.3	0.67	247.0	247.3	28.26	2.267	-	0.453	30.0	13.2				X
	9.2	0.76	276.2	277.7	44.81	4.082	5.66	0.631	42.2	10.3	Yes			
	18.3+	1.16	277.8	277.4	18.29	4.082	-	0.105	42.2	10.3		FL		
	18.3+	1.16	280.3	277.6	21.17	4.082	23.76	0.141	42.2	10.3			X	
	18.3+	1.16	278.9	276.8	21.17	4.082	-	0.141	17.6	4.3				X
	9.5	0.85	309.3	324.3	51.61	4.990	6.84	0.685	42.2	8.5	Yes			
	18.3+	1.19	308.9	323.1	22.18	4.990	-	0.127	42.2	8.5		FL		
	18.3+	1.19	311.2	321.4	21.51	4.990	37.87	0.119	11.3	2.3			X	
	18.3+	1.19	310.9	322.3	21.51	4.990	-	0.119	~0	~0				X
	18.3+	1.29	308.4	310.7	68.99	9.070	11.22	0.674	42.2	4.6	Yes			
	18.3+	1.29	308.4	309.4	35.73	9.070	-	0.181	42.2	4.6		FL		
	18.3+	1.29	308.4	309.1	35.63	9.070	48.00	0.180	42.2	4.6			X	
	18.3+	1.29	308.4	308.9	35.63	9.070	-	0.180	20.2	2.2				X
9	14.4	0.88	244.3	244.3	24.35	2.270	4.70	0.335	42.2	18.6	Yes			
	18.3+	1.06	249.0	246.3	14.46	2.270	-	0.118	42.2	18.6		FL		
	18.3+	1.06	244.8	243.0	23.05	2.270	9.26	0.300	42.2	18.6			X	
	18.3+	1.06	247.6	244.0	23.05	2.270	-	0.300	16.8	7.4				X
	9.1	0.76	280.3	278.4	45.11	4.080	4.95	0.640	42.2	10.3	Yes			
	18.3+	1.16	277.3	279.1	19.20	4.080	-	0.116	42.2	10.3		FL		
	9.1	0.76	278.7	277.8	45.11	4.080	4.95	0.640	42.2	10.3			X	
	9.1	0.76	281.2	281.2	45.11	4.080	-	0.640	~0	~0				X
	9.4	0.84	303.9	306.7	51.85	4.990	6.45	0.691	42.2	8.5	Yes			
	18.3+	1.19	305.0	309.1	22.92	4.990	-	0.133	42.2	8.5		FL		
	18.3+	1.19	304.8	308.9	21.83	4.990	35.14	0.122	41.6	8.3			X	
	18.3+	1.19	305.6	308.9	21.83	4.990	-	0.122	16.4	3.3				X
	18.3+	1.29	295.0	306.3	68.95	9.070	13.96	0.672	75.6	8.3	HIGH			
	18.3+	1.29	300.4	306.4	37.96	9.070	-	0.204	42.2	4.6		FL		
	18.3+	1.29	306.3	300.6	76.91	9.070	11.36	0.837	42.2	4.6			X	
	18.3+	1.29	295.4	306.3	68.95	9.070	-	0.672	30.0	3.3				X

FL = Facility Limit, No Blowout

Table C-6. Altitude Relight Test Results, Fuels 10 and 11.

FUEL NO.	SIMULATED FLIGHT CONDITION ALT. km	M_p -	COMBUSTOR OPERATING CONDITIONS T_F K	T_3 K	P_3 kPa	W_c (engine) kg/s	$\frac{\Delta P}{P}$ %	$\frac{PT}{V}$ kPa-K/m/s	W_f (engine) g/s	f g/kg	REMARKS Light	PBO	LLO	LBO
10	14.4	0.88	248.2	274.5	24.3	2.27	4.88	.330	75.6	33.3	NO			
	0	0	247.2	244.4	92.7	2.27	1.72	4.855	42.2	18.6	NO			
	0	0	243.7	244.3	92.7	2.27	1.72	4.855	75.6	33.3	HIGH			
	0	0	243.7	244.3	92.7	2.27	--	4.855	29.0	12.7				X
	9.2	0.77	277.0	279.5	44.77	4.08	5.04	.630	42.2	10.3	YES			
	18.3+	1.16	280.4	279.3	23.94	4.08	--	.180	42.2	10.3		X		
	18.3+	1.16	278.6	278.2	35.12	4.08	8.32	.388	42.2	10.3			X	
	18.3+	1.16	278.4	277.6	35.12	4.08	--	.388	20.8	5.1				X
	9.4	0.83	308.7	311.7	51.61	4.99	5.93	.685	42.2	8.5	YES			
	18.3+	1.19	300.6	311.5	26.65	4.99	--	.183	42.2	8.5		X		
	18.3+	1.19	301.1	310.6	27.84	4.99	19.65	.199	42.2	8.5			X	
	18.3+	1.19	300.6	311.0	27.84	4.99	--	.199	20.8	4.2				X
	18.3+	1.29	299.1	306.3	68.92	9.07	12.03	.672	42.2	4.6	YES			
	18.3+	1.29	299.7	299.7	38.51	9.07	--	.210	42.2	4.6		X		
	18.3+	1.29	299.1	305.5	42.16	9.07	30.90	.251	42.2	4.6			X	
	18.3+	1.29	299.3	305.9	42.16	9.07	--	.251	24.6	2.7				X
11	15.2	0.89	244.4	245.0	24.11	2.27	5.10	.329	75.6	33.3	NO			
	0	0	244.4	245.0	93.70	2.27	0.32	4.97	42.2	18.6	NO			
	0	0	242.2	244.7	93.70	2.27	0.32	4.97	75.6	33.3	HIGH			
	0	0	242.2	244.7	93.70	2.27	--	4.97	31.5	13.9				X
	9.2	0.76	279.8	277.6	44.77	4.08	5.05	.631	75.6	18.5	HIGH			
	18.3+	1.16	275.9	277.1	22.5	4.08	--	.159	42.2	10.3		X		
	17	0.43	277.8	277.1	89.6	4.08	1.11	2.526	46.6	8.6			HIGH	
	17	0.43	277.8	276.2	89.6	4.08	--	2.526	35.3	11.4				X
	9.4	0.82	301.4	320.3	51.7	4.99	6.24	.685	75.6	15.1	HIGH			
	18.3+	1.19	303.0	321.0	26	4.99	--	.185	42.2	8.5		X		
	18.3+	1.19	300.6	313.0	2	4.99	23.86	.169	38.4	7.7			X	
	18.3+	1.19	300.6	313.0	2	4.99	--	.169	19.5	3.9				X
	18.3+	1.29	303.2	305.9	68.8	9.07	0.87	.670	75.6	8.3	HIGH			
	18.3+	1.29	305.9	305.2	39.2	9.07	--	2.175	42.2	4.7		X		
	18.3+	1.29	304.3	305.9	70.1	9.07	0.84	.695	44.7	4.9			HIGH	
	18.3+	1.29	304.8	305.7	70.1	9.07	--	.695	32.6	3.6				X

Table C-7. Altitude Relight Test Results, Fuels 12 and 13.

FUEL NO.	SIMULATED FLIGHT CONDITION		COMBUSTOR OPERATING CONDITIONS								REMARKS			
	ALT	H_p	T_F	T_3	P_3	W_C (engine)	$\frac{\Delta P}{P}$	$\frac{PT}{V}$	W_f (engine)	f				
	km	-	K	K	kPa	kg/s	%	MPa-K/m/s	g/s	g/kg	Light	PBO	LLO	LBO
12	15.2	0.89	246.5	244.8	24.01	2.27	4.97	.326	75.6	33.3	NO			
	10.1	0.59	246.5	245.4	31.56	2.27	1.89	.563	42.2	18.6	YES			
	18.3+	1.06	241.3	242.2	14.97	2.27	--	.127	42.2	18.6		FL		
	10.1	0.59	244.8	242.7	31.56	2.27	--	.563	25.2	11.1				X
	9.2	0.76	277.8	279.0	44.8	4.08	1.10	.631	42.2	10.4	NO			
	9.2	0.76	278.2	279.0	44.8	4.08	--	.631	75.6	18.5	HIGH			
	9.2	0.76	278.4	278.7	44.8	4.08	--	.631	53.6	13.1				X
	9.5	0.85	299.8	315.3	1.38	4.99	5.90	.679	42.2	8.5	YES			
	18.3+	1.19	303.2	315.4	22.25	4.99	--	.127	42.2	8.5		FL		
	18.3+	1.19	304.8	315.4	22.42	4.99	29.63	.129	40.95	8.2			X	
	18.3+	1.19	304.3	315.4	22.42	4.99	--	.129	27.72	5.6				X
	18.3+	1.29	307.6	314.4	68.95	9.07	14.73	0.674	75.6	8.3	NO			
	0	0	307.6	314.4	97.60	9.07	6.59	1.347	75.6	8.3	NO			
13	14.0	0.89	249.0	243.7	24.6	2.27	4.24	.342	75.6	33.3	NO			
	0	0	244.6	242.8	93.8	2.27	0.40	2.823	75.6	33.3	HIGH			
	0	0	245.9	242.6	93.8	2.27	--	2.823	37.8	16.6				X
	9.2	0.76	275.9	277.0	44.9	4.08	4.98	.633	75.6	18.5	NO			
	1.1	0.42	276.7	277.8	94.4	4.08	1.13	2.804	75.6	18.5	HIGH			
	1.1	0.42	277.0	277.3	94.4	4.08	--	2.804	29.6	7.2				X
	8.7	0.84	302.8	316.3	51.6	4.99	6.49	.684	75.6	15.1	NO			
	1.4	0.50	305.3	316.6	95.5	4.99	1.82	2.346	75.6	15.1	HIGH			
	1.4	0.50	305.3	316.6	95.5	4.99	--	2.346	31.5	6.3				X
	18.3+	1.29	301.5	318.3	69.0	9.07	0.97	.673	75.6	8.3	NO			
	0	0	301.7	318.3	103.4	9.07	0.46	1.513	75.6	8.3	NO			

Table C-8. Ground Start Test Results, Fuels 1 Through 3.

Fuel No.	Combustor Operating Conditions					Lean Blowout		Lean Lightoff	
	T_F	T_3	P_3	W_c (Engine)	$\frac{\Delta P}{P}$	W_f (Engine)	f	W_f	f
	K	K	kPa	kg/s	%	g/s	g/kg	g/s	g/kg
1	278.6	278.6	100.0	3.175	0.79	11.2	3.5	20.8	6.5
	275.0	274.0	100.0	3.175	0.79	11.3	3.6	25.6	8.1
	270.4	267.3	100.0	3.175	0.77	7.3	2.3	27.6	8.7
	262.6	260.2	100.1	3.175	0.72	11.2	3.5	26.1	8.2
	254.9	254.5	100.0	3.175	0.67	13.1	4.1	27.5	8.7
	252.7	246.5	100.0	3.175	0.70	13.9	4.4	28.9	9.1
	249.0	243.4	100.0	3.175	0.67	11.2	3.5	32.8	10.3
	239.8	237.2	100.0	3.175	0.67	15.6	4.9	29.4	9.3
1R	261.2	260.9	101.0	3.175	0.76	13.6	4.3	22.9	7.2
	254.4	256.9	101.0	3.175	0.76	12.1	3.8	28.6	9.0
	251.0	248.6	101.0	3.175	0.71	12.0	3.8	28.4	8.9
	241.2	243.6	101.1	3.175	0.64	10.1	3.2	31.9	10.0
	239.0	239.0	101.1	3.175	0.64	13.9	4.4	27.6	8.7
2	299.7	294.8	99.6	3.175	0.94	8.7	2.7	41.3	13.0
	278.4	278.1	99.6	3.175	0.80	14.2	4.5	39.1	12.3
	268.7	267.8	99.5	3.175	0.88	12.5	3.9	37.8	11.9
	260.4	258.8	99.5	3.175	0.73	15.8	5.0	44.0	13.9
	255.6	255.4	99.5	3.175	0.83	17.6	5.5	47.8	15.1
	248.7	248.7	99.5	3.175	0.80	17.6	5.5	47.9	15.1
	244.0	243.7	99.5	3.175	0.83	11.3	3.6	53.9	17.0
	240.7	238.1	99.4	3.175	0.78	15.4	4.9	52.5	16.5
3	297.0	300.4	98.3	3.175	1.01	7.3	2.3	39.7	12.5
	278.2	275.4	98.2	3.175	0.86	25.8	8.1	60.2	19.0
	266.5	265.4	98.1	3.175	0.86	19.5	6.1	62.0	19.5
	261.5	261.8	98.1	3.175	0.89	19.5	6.1	54.8	17.3
	255.4	254.6	98.0	3.175	1.04	18.8	5.9	52.3	16.5
	249.8	249.3	98.0	3.175	0.91	16.3	5.1	46.6	14.7
	244.3	243.6	98.0	3.175	0.99	16.4	5.2	45.4	14.3
	243.2	239.4	98.0	3.175	0.94	15.4	4.8	45.4	14.3

Table C-9. Ground Start Test Results, Fuels 4 Through 7.

Fuel No.	Combustor Operating Conditions					Lean Blowout		Lean Lightoff	
	T_F	T_3	P_3	W_c (engine)	$\frac{\Delta P}{P}$	W_f (engine)	f	W_f	f
	K	K	kPa	kg/s	%	g/s	g/kg	g/s	g/kg
4	277.4	278.0	102.5	3.175	0.66	14.5	4.6	40.6	12.8
	272.9	272.0	102.6	3.175	0.73	17.4	5.5	41.8	13.2
	268.5	267.0	102.5	3.175	0.68	17.6	5.5	44.1	13.9
	261.5	261.2	102.5	3.175	0.61	15.8	5.0	42.7	13.4
	254.0	255.8	102.5	3.175	0.74	20.7	6.5	46.4	14.6
	250.9	249.3	102.5	3.175	0.60	18.6	5.9	47.9	15.1
	244.8	242.8	102.5	3.175	0.51	18.8	5.9	52.3	16.5
	238.5	237.5	102.4	3.175	0.49	20.8	6.6	59.1	18.6
5	277.0	277.4	102.0	3.175	0.71	18.3	5.8	34.0	10.7
	272.5	272.2	102.0	3.175	0.73	18.3	5.8	33.1	10.4
	265.9	267.5	102.0	3.175	0.61	18.8	5.9	36.5	11.5
	262.1	260.4	102.0	3.175	0.81	18.3	5.8	38.4	12.1
	254.7	256.0	102.0	3.175	0.76	19.5	6.1	40.1	12.6
	250.9	248.3	102.0	3.175	0.61	19.8	6.2	44.0	13.9
	244.8	245.0	102.0	3.175	0.54	21.0	6.6	45.4	14.3
	238.6	237.8	101.9	3.175	0.55	20.9	6.6	44.0	13.9
6	275.8	277.4	101.7	3.175	0.67	20.2	6.4	42.7	13.5
	273.7	272.3	101.7	3.175	0.67	11.3	3.6	37.8	11.9
	267.2	265.5	101.7	3.175	0.73	10.7	3.4	43.2	13.6
	263.5	260.7	101.7	3.175	0.64	7.6	2.4	39.1	12.3
	255.8	256.3	101.7	3.175	0.64	14.5	4.6	41.5	13.1
	251.3	249.0	101.7	3.175	0.62	12.0	3.8	42.2	13.3
	246.7	243.2	101.7	3.175	0.61	10.7	3.4	42.2	13.3
	240.2	239.0	101.7	3.175	0.64	20.8	6.6	44.1	13.9
7	280.0	276.6	99.4	3.175	0.61	26.8	8.4	57.2	18.0
	272.0	272.0	99.4	3.175	0.60	28.9	9.1	52.9	16.7
	263.9	265.4	99.4	3.175	0.60	28.4	8.9	60.2	19.0
	262.3	263.1	99.4	3.175	0.58	30.2	9.5	59.1	18.6
	258.1	254.6	99.5	3.175	0.56	28.9	9.1	56.6	17.8
	249.8	248.5	99.5	3.175	0.70	32.8	10.3	59.0	18.6
	245.8	243.4	99.7	3.175	0.64	37.0	11.7	61.7	19.4
	239.3	240.1	99.8	3.175	0.65	36.3	11.4	61.2	19.3

Table C-10. Ground Start Test Results, Fuels 8 Through 11.

Fuel No.	Combustor Operating Conditions					Lean Blowout		Lean Lightoff	
	T_F	T_3	P_3	W_c (engine)	$\frac{\Delta P}{P}$	W_f (engine)	f	W_f	f
	K	K	kPa	kg/s	%	g/s	g/kg	g/s	g/kg
8	277.0	278.7	100.2	3.175	0.67	25.7	8.1	48.9	15.7
	270.6	272.2	100.2	3.175	0.66	26.2	8.2	52.7	16.6
	268.4	266.6	100.2	3.175	0.61	27.5	8.7	49.1	15.5
	260.9	262.0	100.2	3.175	0.62	27.0	8.5	52.3	16.5
	257.0	252.8	100.2	3.175	0.68	27.0	8.5	47.3	14.9
	252.6	250.9	100.4	3.175	0.45	15.0	4.7	40.3	12.7
	246.5	245.2	100.2	3.175	0.52	20.8	6.6	44.7	14.1
	248.7	242.4	100.2	3.175	0.50	23.9	7.5	46.4	14.6
9	275.4	277.2	100.2	3.18	0.79	30.2	9.5	37.8	11.9
	272.0	270.9	100.2	3.18	0.81	31.2	9.8	34.6	10.9
	268.2	267.5	101.2	3.18	0.76	31.2	9.8	36.5	11.5
	263.0	258.7	101.3	3.18	0.52	32.0	10.0	37.8	11.9
	256.4	255.7	100.3	3.18	0.52	32.0	10.0	37.2	11.7
	251.5	249.8	101.5	3.18	0.62	32.6	10.2	41.0	12.9
	246.3	245.3	101.6	3.18	0.44	32.6	10.2	40.3	12.7
	239.9	238.6	101.6	3.18	0.44	34.0	10.7	48.5	15.2
10	278.4	276.9	100.9	3.18	0.49	23.3	7.3	42.8	13.4
	271.1	272.5	101.0	3.18	0.32	19.5	6.1	42.5	13.3
	262.6	261.4	101.0	3.18	0.30	20.2	6.4	40.1	12.6
	252.5	255.5	100.8	3.18	0.62	22.7	7.1	42.2	13.2
	249.6	248.5	100.8	3.18	0.50	19.5	6.1	40.3	12.6
	243.7	243.8	100.9	3.18	0.40	21.4	6.7	42.6	13.4
	248.3	238.6	100.9	3.18	0.41	21.4	6.7	43.2	13.6
11	277.5	277.5	102.1	3.18	0.57	34.7	11.0	52.3	16.5
	274.4	271.4	100.6	3.18	0.59	34.7	11.0	47.9	15.1
	266.1	266.4	100.6	3.18	0.53	34.7	11.0	50.4	15.9
	262.0	260.3	100.6	3.18	0.53	35.7	11.2	46.5	14.7
	257.5	256.8	100.6	3.18	0.52	36.3	11.4	47.9	15.1
	248.1	250.1	100.7	3.18	0.57	38.7	12.0	49.1	15.4
	247.0	239.4	100.7	3.18	0.56	39.7	12.5	53.6	16.9
	245.7	245.1	100.6	3.18	0.80	36.4	11.5	48.5	15.3

Table C-11. Ground Start Test Results, Fuels 12 and 13.

Fuel No.	Combustor Operating Conditions					Lean Blowout		Lean Lightoff	
	T_F	T_3	P_3	W_c (engine)	$\frac{\Delta P}{P}$	W_f (engine)	f	W_f	f
	K	K	kPa	kg/s	%	g/s	g/kg	g/s	g/kg
12	277.3	277.2	100.1	3.18	0.60	33.9	10.7	42.2	13.3
	270.4	271.6	100.1	3.18	0.56	30.1	9.5	41.3	13.0
	266.4	267.0	100.1	3.18	0.64	30.2	9.5	40.2	12.6
	262.0	259.5	100.2	3.18	0.47	34.6	10.9	40.3	12.7
	255.4	254.7	100.1	3.18	0.58	25.8	8.1	38.4	12.1
	252.6	250.0	100.1	3.18	0.52	29.0	9.1	41.0	12.9
	245.7	245.6	100.1	3.18	0.54	32.8	10.3	45.4	14.3
	254.4	237.9	100.2	3.18	0.66	32.1	10.1	47.2	14.9
13	279.8	278.8	100.0	3.18	0.60	25.2	7.9	54.1	17.0
	270.0	273.9	100.2	3.18	0.60	25.3	8.0	56.0	17.6
	268.7	266.3	100.6	3.18	0.57	26.4	8.3	51.0	16.0
	259.7	260.6	100.8	3.18	0.58	26.7	8.4	51.4	16.1
	255.6	255.4	100.8	3.18	0.60	27.0	8.5	55.4	17.4
	249.3	251.4	100.8	3.18	0.75	28.9	9.1	57.9	18.2
	246.8	246.0	100.8	3.18	0.72	32.7	10.3	63.0	19.8
	243.7	240.3	100.6	3.18	0.74	39.6	12.4	76.8	24.1

APPENDIX D

FUEL NOZZLE FOULING TEST

Fuel nozzle fouling tests were conducted in a small flame-tunnel rig using apparatus and procedures described in Section V-C. Primary results were periodic bench flow calibrations of the fuel nozzles to detect metering orifice plugging and/or flow divider valve seizure. These results were supplemented with visual inspection of the fuel nozzle tip and flow divider valve components. As described in Section VI-A-9, two types of fuel nozzle configuration were tested. Blocked flow divider valve configuration periodic flow calibration results are listed in Table D-1. Standard fuel nozzle actual periodic flow calibration results are listed in Table D-2, which have been normalized in Table D-3.

Table D-1. Fuel Nozzle Fouling Test Results with Blocked Secondary Orifice Valve.

Fuel Temperature 478 K

Test Fuel Number	Fuel Nozzle Serial Number	Test Time, Minutes	Fuel Flow Rate, g/s at ΔP_f = 0.352 MPa	Fuel Flow Rate / Pretest Fuel Flow Rate
1	76520	0	8.57	--
		100	8.44	0.985
		300	8.44	0.985
2	80417	0	8.27	--
		100	8.27	1.000
		300	8.27	1.000
3	76520	0	8.19	--
		100	8.20	1.001
		300	8.06	0.984
4	106575	0	8.69	--
		100	8.57	0.986
		300	7.87	0.906
5	76520	0	9.05	--
		100	8.95	0.98
		300	8.63	0.954
6	80417*	0	9.13	--
		100	8.04	0.881
		300	4.85	0.531

* Suspect fuel nozzle was not fully cleaned before test.

Table D-2. Fuel Nozzle Fouling Test Results with Standard Dual Orifice Fuel Nozzle.

Test Fuel Number	Fuel Nozzle Serial Number	Fuel Temperature, K	Test Time, Minutes	Fuel Flow Rate (g/s) at ΔP_f (MPa)						
				0.552	0.862	2.068	3.447	2.068	0.862	0.552
1	80417	436	0	8.59	27.2	139.6	257.9	140.2	26.5	8.53
		436	100	8.61	27.1	140.5	261.4	145.9	26.8	8.56
		436	300	8.56	26.3	139.2	256.7	139.0	25.3	8.39
2	76520	436	0	8.43	28.2	145.9	256.7	145.9	28.1	8.32
		436	100	8.42	26.5	143.3	254.1	144.8	27.8	10.45
		436	300	8.32	27.0	143.6	253.9	144.4	27.7	8.28
1	76520	478	0	8.34	27.2	139.4	254.0	139.4	27.2	8.33
		478	100	8.44	22.0	135.8	245.2	135.8	26.3	8.69
		478	300	9.73	16.0	122.2	221.1	122.7	25.6	8.04
2	158578	478	0	8.35	26.2	137.5	252.8	138.1	28.3	8.61
		478	100	8.13	22.2	134.2	245.1	134.8	27.7	8.95
		478	300	7.94	21.7	134.[illegible]	245.1	134.8	27.6	8.57
3	106575	478	0	8.57	27.7	140.9	250.2	140.9	27.5	8.49
		478	100	8.79	26.3	139.5	252.[illegible]	139.5	27.6	8.42
		478	300	8.57	23.4	131.9	245.1	133.3	25.7	8.42
7	122372	478	0	8.91	28.1	138.8	249.0	138.3	29.0	9.03
		478	100	8.92	24.3	135.8	245.1	135.8	28.5	8.98
		478	300	8.79	21.5	134.6	240.0	134.6	28.7	8.79
8	82575	478	0	8.56	30.0	140.8	259.2	140.8	30.3	9.23
		478	100	8.03	26.8	130.7	241.3	135.7	31.2	9.93
		478	300	8.48	26.0	108.6	183.6	110.5	28.1	9.41
9	132823	478	0	8.72	25.1	134.6	242.8	134.6	24.7	8.66
		478	100	8.85	22.8	132.4	245.1	134.4	23.8	8.67
		478	300	8.67	19.3	122.0	219.9	125.4	24.4	8.54
10	35922	478	0	9.42	29.0	135.8	245.2	134.6	28.9	9.80
		478	100	8.79	28.1	119.4	222.6	125.[illegible]	29.4	10.68
		478	300	8.49	21.7	112.1	215.7	123.5	26.5	9.95
11	131471	47[illegible]	0	8.14	27.2	140.9	251.5	140.9	27.5	8.15
		478	100	8.13	23.6	117.8	216.7	126.0	26.7	8.13
		478	300	8.06	23.8	110.9	190.5	110.4	25.2	8.06
12	23878	478		8.85	27.6	134.6	245.2	133.2	28.2	9.16
		478	100	8.50	22.9	127.3	233.3	129.8	15.1	10.39
		478	300	8.42	24.3	115.9	206.9	119.7	24.6	10.77
13	87960	478	[illegible]	8.20	26.6	131.9	247.7	131.9	27.5	8.46
		478	100	8.32	24.2	127.5	38.8	127.5	27.0	8.47
			300	8.15	22.3	129.5	237.8	129.5	26.3	8.[illegible]

Table D-3. Normalized Fuel Nozzle Fouling Test Results with Standard Dual Orifice Fuel Nozzle.

Test Fuel Number	Fuel Nozzle Serial Number	Fuel Temperature, K	Test Time, Minutes	(Fuel Flow Rate)/(Pretest Fuel Flow Rate) at ΔP_f (MPa)						
				0.552	0.862	2.068	3.447	2.068	0.862	0.552
1	80417	436	100	1.001	0.995	1.006	1.014	1.040	1.014	1.003
		436	300	0.996	0.968	0.997	0.995	0.991	0.957	0.984
2	76520	436	100	0.999	0.938	0.982	0.990	0.992	0.991	1.256
		436	300	0.987	0.955	0.984	0.989	0.990	0.987	0.995
1	76520	478	100	1.012	0.810	0.975	0.965	0.975	0.968	1.044
		478	300	1.166	0.588	0.877	0.871	0.881	0.940	0.965
2	158578	478	100	0.973	0.846	0.976	0.970	0.976	0.987	1.040
		478	300	0.950	0.827	0.979	0.920	0.976	0.973	0.996
3	106575	478	100	1.026	0.950	0.990	1.000	0.990	1.005	0.991
		478	300	1.000	0.845	0.936	0.979	0.946	0.936	0.991
7	122372	478	100	1.001	0.865	0.982	0.984	0.982	0.980	0.994
		478	300	0.987	0.765	0.973	0.964	0.973	0.989	0.974
8	82575	478	100	0.938	0.894	0.928	0.931	0.964	1.031	1.076
		478	300	0.991	0.865	0.771	0.708	0.785	0.927	1.020
9	132823	478	100	1.014	0.910	0.984	1.009	0.999	0.964	1.001
		478	300	0.994	0.771	0.906	0.906	0.932	0.990	0.987
10	35922	478	100	0.933	0.967	0.879	0.908	0.929	1.017	1.090
		478	300	0.901	0.746	0.826	0.880	0.918	0.917	1.015
11	131471	478	100	0.998	0.866	0.836	0.862	0.894	0.970	0.998
		478	300	0.991	0.870	0.787	0.758	0.784	0.915	0.990
12	23878	478	100	0.962	0.831	0.946	0.952	0.974	0.957	1.135
		478	300	0.952	0.881	0.861	0.844	0.900	0.872	1.176
13	87960	478	100	1.014	0.910	0.967	0.964	0.967	0.979	1.001
		478	300	0.994	0.839	0.982	0.960	0.982	0.957	0.965

APPENDIX E

SMOKE DATA CALCULATION

In this program, combustor component rig tests were conducted in which smoke emission levels were measured at the combustor exit plane by the method specified in Reference 4. The result is a Smoke Number (SN) which expresses the opacity of filter paper that has been stained by the exhaust gases. SN is therefore, not a true thermodynamic property of the exhaust gas. A relationship between SN and carbon weight fraction (X_c), which is a thermodynamic property, is presented in Reference 12. This relationship is reproduced in Figure E-1.

When combustor exhaust gases are diluted by turbine cooling air as they are in the J79 engine, both SN and X_c are reduced. Smoke emission index (EI_s) g carbon/kg fuel, however, remains constant. EI_s is calculated by the relationship:

$$EI_s = (x_{ci}) \left(\frac{1000 + f_i}{f_i}\right) (10^{-3})$$

where:

i = engine station where sample is taken

f = fuel-air weight ratio (g fuel/kg air)

Therefore, engine smoke level, which would be measured at engine Plane 8, can be calculated from combustor rig measurements, taken at simulated engine Plane 4, by the following procedure:

1. Measure (SN_4) and f_4) at simulated engine test conditions
2. $SN_4 \rightarrow X_{c4}$ (from Figure E1)
3. $EI_s = (X_{c4}) \left(\frac{1000 + f_4}{f_4}\right) (10^{-3})$
4. Cycle data $\rightarrow f_8$ at simulated engine test condition
5. $X_{c8} = EI_s \left(\frac{f_8}{1000 + f_8}\right)(10^3)$
6. $X_{c8} \rightarrow SN_8$ (from Figure E-1)

For the J79-17A engine, $f_8/f_4 = 0.838$ at non-afterburning operating conditions. In the test data summary, SN_4, X_{c8}, EI_s, and SN_8 are all tabulated in Tables A1 and A2 for possible future use.

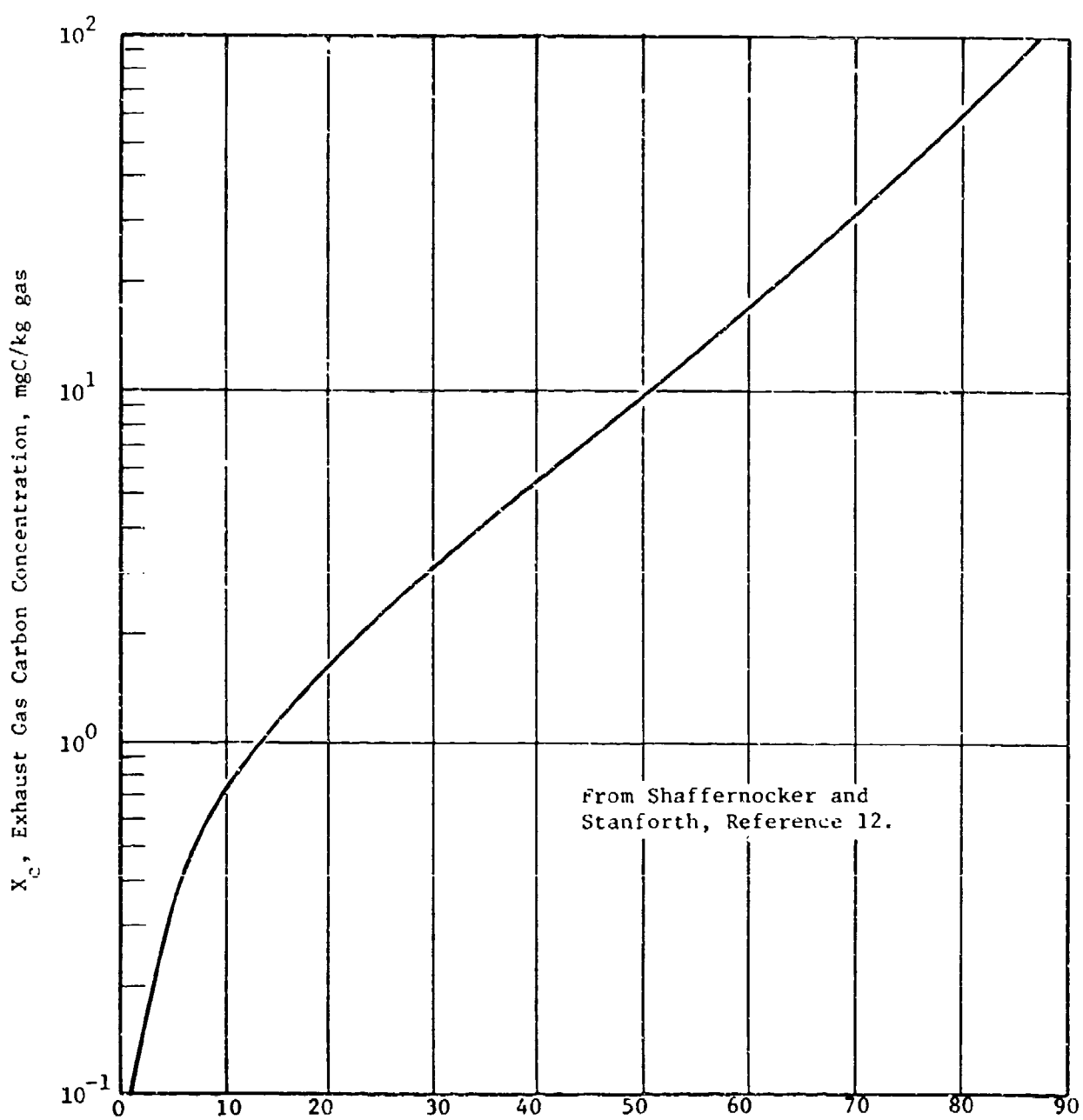

Figure E-1. Experimental Relationship Between Smoke Number and Exhaust Gas Carbon Concentration.

APPENDIX F

NOMENCLATURE

SYMBOL		UNITS
A	Area	cm^2, mm^2
CO	Carbon monoxide	-
CO_2	Carbon dioxide	-
CWALF	Clockwise aft looking forward	-
EI	Pollutant emission index	g pollutant/kg fuel
FBP	Final boiling point	K
H	Fuel hydrogen content (weight %)	wt %
HC	Hydrocarbon	-
IBP	Initial boiling point	K
JFTOT	Jet Fuel Thermal Oxidation Tester	-
NO_x	Total oxides of nitrogen (=NO+NO_2)	-
Q	Heat of combustion	MJ/kg
S	Combustor operating severity parameter	-
SMD	Sauter mean diameter	-
SN	Smoke number (by ARP #1256)	-
T	Temperature	K
V	Velocity	m/s
W	Mass flow rate	g/s, kg/s
X	Exhaust gas pollutant concentration	mg pollutant/kg air
b	Curve fit equation intercept	-
f	Fuel-air ratio	g fuel/kg air
h	Absolute humidity	g H_2O/kg air
k	Arbitrary constant	-

SYMBOL		UNITS
m	Curve fit equation slope	-
n	Hydrogen-to-carbon atom ratio	-
$\dot{q}$	Heat flux	kW/m^2
r	Curve fit correlation coefficient	-
x	Independent variable	-
y	Dependent variable	-
ΔP	Pressure drop	mPa
ΔT	Temperature rise	K
η	Combustion efficiency	%
ν	Viscosity	mm^2/s
ρ	Density	kg/m^3
σ	Surface tension	mN/m
$\phi(f)$	Fuel-air ratio function (Figure 38)	-

SUBSCRIPTS

3	Compressor exit station (Combustor inlet)
4	Combustor exit station
8	Engine exit station
c	Combustor
e	Effective
f	Fuel
m	Metered
r	Reference
st	Stoichiometric
L	Liner (metal)
gs	Gas sample
TC	Thermal (Thermocouple)
s	Sample
avg	Average
max	Maximum
OGV	Outer guide vane
TND	Turbine nozzle diaphragm
Imm.max	Immersion Maximum

REFERENCES

1. Longwell, J.P., "Jet Aircraft Hydrocarbon Fuels Technology", NASA CP-2033, January 1978.

2. Colley, W.D., et al, "Development of Emissions Measurement Technique for Afterburning Turbine Engines: Supplement 2 - Afterburner Plume Computer Program User's Manual", Air Force Aero Propulsion Laboratory, AFAPL-TR-75-52, Supplement 2", October 1975.

3. Jasuja, A.K., "Atomization of Crude and Residual Fuel Oils", ASME Paper 78-GT-83, April 1978.

4. "Aircraft Gas Turbine Engine Exhaust Smoke Measurement", Aerospace Recommended Practice 1179, SAE, 1970.

5. "Procedure for the Continuous Sampling and Measurement of Gaseous Emissions from Aircraft Turbine Engines", Aerospace Recommended Practice 1256, SAE, 1971.

6. Macaulay, R.W., and Shayeson, M.W., "Effects of Fuel Properties on Liner Temperatures and Carbon Deposition in the CJ805 Combustor for Long Life Applications", ASME Paper 61-WA-304, November 1961.

7. Gleason, C.C., Rogers, D.W., and Bahr, D.W., "Experimental Clean Combustor Program Phase II Final Report", NASA CR-134971, August 1976.

8. Gleason, C.C., and Bahr, D.W., "Experimental Clean Combustor Program Alternate Fuels Addendum, Phase II Final Report", NASA CR-134972, January 1976.

9. Moses, C.A., and Naegeli, D.W., "Effects of High Availability Fuels on Combustor Properties", AFAPL-101, January 1978.

10. Blazowski, W.S., and Jackson, T.A., "Evaluation of Future Jet Fuel Combustion Characteristics", AFAPL-TR-77-93, July 1978.

11. Russell, R.J., and Witton, J.J., "An Investigation of Turbine Erosion by Combustor Generated Carbon in a Lightweight Marine Gas Turbine", ASME Paper 78-GT-96, April 1978.

12. Shaffernocker, W.M., and Stanforth, C.M., "Smoke Measurement Techniques", SAE 680346, April 1968.

*U.S.Government Printing Office: 1979 — 657-084/245